Numerical Study of Convective Fluid Flow in Porous and Non-porous Media

Gilbert Makanda

Submitted in fulfillment of the academic
requirements for the degree of

DOCTOR OF PHILOSOPHY

in the

School of Mathematics, Statistics and Computer Science
University of KwaZulu-Natal
Pietermaritzburg

2015

Declaration

The work described in this thesis was carried out in the School of Mathematics, Statistics and Computer Science, University of KwaZulu-Natal Pietermaritzburg, from May 2011 to August 2015 under the supervision of Professor Precious Sibanda.

This thesis presents original work by the author and has not been submitted in any form for any degree or diploma to any university or institution of learning. Where use has been made of the work of others it is duly acknowledged.

August, 2015.

Student: _____ _____

Gilbert Makanda Date

Supervisor: _____ _____

Prof. Precious Sibanda Date

Acknowledgements

I would like to thank my supervisor Professor Precious Sibanda. Through his guidance I have learnt the research methods used in the application of mathematics in fluid flow. His efforts in making me an independent mathematician are greatly appreciated.

I would also want to thank Professor Sandile Motsa, Dr Zodwa G Makukula, Dr Sachin Shaw, Dr Mahesha Narayana, Dr Peri Kameswaran and Dr Faiz Awad for their support in the development of this work. I specifically want to thank Professor Sandile Motsa for the guidance in mathematical programming in Matlab, Maple and Mathematica. I would also want to thank the organizers of the annual workshops in numerical methods held in the School of Mathematics, Statistics and Computer Science at the University of KwaZulu Natal.

I would also want to thank Professor Daniel Makinde for the support that he gave me during the study period. I have learnt a lot from his wide experience in the reasearch area of fluid mechanics.

I would like to thank my friends in the area of fluid mechanics Dr Gift Muchatibaya and Dr George Buzuzi, for their support during the study period. I would also like to thank Mr John Farmer for the support that he gave me.

I would also want to thank my wife Maudy Makanda for her continuous support.

Abstract

Most practical problems can be modeled by ordinary or partial differential equations. Most of the problems that describe real world situations are highly nonlinear and it is not always possible to obtain exact solutions. Situations arising in fluid flow present theoretically challenging problems. However, not all equations from these problems can be solved analytically, we therefore use numerical methods to solve them. Most research works in fluid flow use less accurate methods such as finite differences, finite element and finite volume. Some common numerical methods lack stability and accuracy, and for this reason improved numerical methods that are accurate, robust and computationally efficient are required. Most traditionally used methods are rigorous and pose great challenges in implementing them.

In this study we explored the use of new and improved methods which were used to solve mathematical models in fluid flow. These methods are the `bvp4c` algorithm, the Runge-Kutta-Fehlberg integration scheme with the shooting method, the successive linearization method, the spectral relaxation method, the quasi-linearization method and the bivariate quasi-linearization method. The study was carried out in the form of published papers on six new problems in fluid flow. The new and improved methods were used in all chapters of this study. The thesis consists of an introduction that gives a review of the common methods in use and provide evidence in the literature that show the accuracy of spectral methods. In Chapter 2 a detailed review of methods used in the thesis was presented. We also presented the general implementaion of these methods for application in other contexts. In Chapter 3, we investigated radiation effects of magnetohydrodynamic Newtonian fluid flow over an exponentially stretching sheet. In Chapter 4, we studied natural convection from a downward pointing cone in a viscoelastic fluid embedded in porous medium. In Chapter 5, we investigated the problem of diffusion of chemically reactive species in Casson fluid from an unsteady stretching surface in a porous medium in the presence of a magnetic field. In Chapter 6, we studied the effects of radiation on magnetohydrodynamic fluid flow in Casson fluid from a horizontal circular cylinder with partial slip in non-Darcy porous medium with viscous dissipation. In Chapter 7, we studied the effect of radiation on free convection from a spinning cone in Casson fluid with partial slip, cross diffusion and viscous

dissipation. In Chapter 8, the double diffusion mixed convection Casson fluid flow over a horizontal plate is studied and incorporates Soret effects and viscous dissipation with thermal solutal dispersion.

In this study we concluded that the new spectral methods are highly accurate, robust and computationally efficient in solving nonlinear differential equations. These methods are recommended for use in highly nonlinear differential equations in fluid flow. The methods can be used in similar situations in other contexts. The problems presented in this study are new and developed from existing studies whose results have been improved.

List of Tables

List of Figures

Nomenclature

Symbol	Meaning	Symbol	Meaning
A	Unsteadiness parameter	k_0	Non-Newtonian parameter
B	Magnetic flux density	k_p	Darcian drag force coefficient
Bi	Biot number	$\bar{K}$	Permeability coefficient in porous media
C	Fluid solute concentration	K	Radiation parameter
C_f	Skin friction coefficient	k^*	Mean radiative absorption coefficient
C_p	Specific heat capacity	L	Characteristic length
C_w	Wall concentration	M	Magnetic parameter
C_∞	Free stream concentration	Nu	Nusselt number
D	Solutal diffusivity	Nu_x	Local Nusselt number
Da	Darcy number	Pr	Prandtl number
D_f	Dufour number	Pr^*	Modified Prandtl number
D_y	y-component solutal dispersion	P_y	Yield stress in Casson fluid
Ec	Eckert number	q_r	Radiative heat flux
f_w	suction/blowing parameter	q_w	Wall heat flux
Gb	Gebhart number	R^*	Non-dimensional cone radius
Gr	Grashof number	R	Chemical reaction parameter
Gr^*	Modified Grashof number	Re	Reynolds number
J_w	Wall mass flux	Re_x	Local Reynolds number
k	Thermal conductivity	r	Radius of the cone/circle
k_1	Chemical reaction rate		

Sc	Schmidt number	T_m	Mean fluid temperature
S_{co}	Solutal slip factor	T_w	Wall fluid temperature
S_f	Velocity slip factor	T_∞	Free stream fluid temperature
S_g	Rotational slip factor	u	fluid velocity in the x direction
Sh	Sherwood number	U_0	Characteristic fluid velocity
Sh_x	Local Sherwood number	U_w	Fluid wall velocity
Sr	Soret number	v	fluid velocity in the y direction
S_T	Thermal slip factor	V_w	Wall suction/blowing velocity
T	Fluid temperature	w/∞	surface/free stream subscripts

Greek symbols

Symbol	**Meaning**	**Symbol**	**Meaning**
α	Thermal diffusivity	Λ	Viscoelastic parameter
α_y	y-component thermal dispersion	μ	Dynamic viscosity
β	Casson parameter	ν	Kinematic viscosity
β_T	Coefficient of thermal expansion	ρ	Fluid density
β_C	Coefficient of solutal expansion	σ	Electrical conductivity
ϵ	Spin parameter	σ^*	Stefan-Boltzmann constant
γ	Permeability parameter	τ_w	Wall shear stress
γ_0	Thermal-dispersion parameter	ζ_0	Solutal-dispersion parameter
λ	Thermal convection parameter	θ^*	Half angle of cone vertex
Λ^*	Forchheimer parameter	ψ	Stream function
ξ	Transverse coordinate	ω	velocity component in z direction

Abbreviations

ADE	Advection-Dispersion Equation
ADM	Adomian Decomposition Method
BQLM	Bivariate Quasi-linearization Method
BSQLM	Bivariate Spectral Quasi-linearization Method
CFD	Computational Fluid Dynamics
CWDFD	Chebyshev Wavelet Finite Difference Method

DG	Discontinuous Garlekin
DTM	Differential Transform Method
FEM	Finite Element Method
FV	Finite Volume
FEM	Finite Element Method
FVEM	Finite Volume Element Method
FDM	Finite Difference Method
FCM	Finite Cover Method
GFEM	Generalized Finite Element Method
IMEX RK	Implicit Explicit Runge-Kutta
IRK	Implicit Runge-Kutta
LSHF	Linear Surface Heat Flux
LST	Linear Surface Temperature
MHD	Magnetohydrodynamic
ODE	Ordinary Differential Equations
PDE	Partial Differential Equations
QLM	Quasi-linearization Method
RK	Runge-Kutta
RKN	Runge-Kutta-Nystrom
SFD	Staggered-grid Finite Difference Method
SLM	Successive Linearization Method
SLLM	Spectral Local Linearization Method
SOR	Successive Over Relaxation
SPM	Spectral Perturbation Method
SRM	Spectral Relaxation Method
VIM	Variational Iteration Method
WG	Weak Garlekin
XFEM	Extended Finite Element Method

Contents

Preface

The work presented here has been published, or accepted for publication as follows;

Chapter 3;

Kameswaran, P. K., Narayana, M., **Makanda, G.**, Sibanda, P. (2012a) On radiation effects on hydromagnetic Newtonian liquid due to an exponential stretching sheet, *Boundary Value Problems*, **2012**, **doi**:1186/1687/2770/2012/105

Chapter 4;

Makanda, G., Makinde, O. D., Sibanda, P. (2013) Natural convection of viscoelastic fluid from a cone embedded in a porous medium with viscous dissipation, *Mathematical Problems in Engineering*, **2013**, Article ID 934712, 11 pages, **doi**: 10.1155/2013/934712

Chapter 5;

Makanda, G., Shaw, S., Sibanda, P. (2015a) Diffusion of chemically reactive species in Casson fluid over an unsteady stretching surface in porous medium with viscous dissipation, *Mathematical Problems in Engineering*, **2014**, Article ID 724596, 10 pages, **doi**: 10.1155/2014/724596

Chapter 6;

Makanda, G., Shaw, S., Sibanda, P. (2015b) Effects of radiation on MHD free convection of Casson fluid from a horizontal circular cylinder with partial slip in non-Darcy porous medium with viscous dissipation, *Boundary Value Problems*, **2015**, **doi**:1186/s13661/015/0333/5

Chapter 7;

Makanda, G., Shaw, S., Sibanda, P. (2015c) Effects of radiation on free convection from a spinning cone with partial slip in non-Darcy porous medium with cross diffusion and viscous dissipation, (under review: Open Physics)

Chapter 8;

Shaw, S., **Makanda, G.**, Sibanda, P. (2015) Effects of double dispersion on Casson fluid flow with viscous dissipation and convective boundary condition, (under review: Mathematical Prolems in Engineering)

1

Introduction

Various types of equations arise when modelling physical situations and a substantial body of mathematical research is devoted to their study (Suli and Mayers, 2003). In science and engineering many problems can be described by differential equations but these are not so easy to solve analytically, due to their nonlinearity and complexity. Even for ordinary differential equations, exact solutions may be unobtainable. As a result numerical methods are used (Griffiths and Higham, 2010; Laburta et al., 2015) and this has been greatly facilitated by the use of fast computers. In physics, geology, astrophysics, mechanics, and geophysics, models for problems often include partial differential equations, presenting even greater challenges (Langtangen, 2003). In this regard, the numerical approach is more recent than analytic approaches, and was facilitated by the introduction of computational mechanics, which influenced the development of techniques for numerical solutions (Evans et al., 2000). A challenge in numerical methods is that computing equivalent expressions in different ways may take different times to execute (Householder, 1953). We need to investigate new and alternative numerical methods that can possibly solve these systems accurately with less computation time.

1.1. Numerical methods for differential equations in fluid flow

In transport processes, problems such as contaminant or tracer transport in porous media have been frequently modelled by advection-dispersion equations (ADE). In such cases, applying analytical methods such as the inverse Laplace transform have brought little success and so numerical methods have been used (Wang and Zhan, 2015). These numerical methods have proved effective in a wide range of problems where strong nonlinearity arises, such as seepage with free surfaces (Zheng et al., 2015), and in diffusion problems in fuel cells (Ferreira et al., 2015). Numerical algorithms and computer simulations have simplified different approaches in numerical methods for solving these fluid flow problems (Hysing, 2012). In particular, discretization methods have been developed.

1.1.1 Discretization methods

Discretization methods are based on approximating derivatives of function expressions. These approximations are forward, backward and central differences. Discretization methods include the finite element method (FEM), finite volume (FV) and finite difference method (FDM). Further developments include the finite cover method (FCM), the generalized finite element method (GFEM), mixed finite element methods and the extended finite element method (XFEM) (Chen and Li, 2015), as well as spectral and discontinuous Garlekin methods (Wang et al., 2014). As judged by the number of commercial computational fluid dynamics codes, the three most frequently used discretization methods are the finite difference method (2%), finite element method (15%) and finite volume method (80%). The remaining 3% consist mostly of spectral, boundary element, vorticity type and lattice-Boltzmann methods (Veress and Rohacs, 2012).

The finite difference method approximates the given equation at a finite number of points. If the points can be placed on a regular grid, the approximation is simple and yields symmetric matrices (Seibold, 2008). Finite difference methods have been used for a variety of problems; for example predator-prey models (Dimitrov and Kojouharov, 2007), singular two-point boundary value problems (Kumar, 2003), simulations of stably stratified fluid

flows (Bodmar et al., 2012), and fluid structure coupling problems (Sugiyama et al., 2011). They have also been applied to simulations of the Navier-Stokes equations and constitutive equations of viscoelastic fluids (Zou et al., 2014) and stochastic modelling of the Black-Scholes model (Goncalves and Grossinho, 2014) and in time fractional nonlinear reaction-diffusion equations (Sungu and Demir, 2014).

While the finite difference method (FDM) may be considered easy to understand (Gong et al., 2014), conflict may arise between three desired properties. It is not possible to simultaneously optimize all three attributes of a numerical method namely: stability, accuracy of the solutions and efficiency of the algorithm (Poochinapan et al., 2014). In this regard, Kudryavtsev (2013) noted that an important advantage of the FDM is that it uses less memory and computation time than the Garlekin method of Liu and Sen (2009). However, Cash and Singhal (1982) showed that the method requires considerable computer memory and are not highly accurate, which they see as major disadvantages. With regard to accuracy for the FDM method this depends strongly upon the mesh or grid size and its properties of stretch ratio, aspect ratio and skewness (Veress and Rohacs, 2012). Specifically, numerical experiments show that the compact finite difference method gives fifth order accuracy (Zhao and Corless, 2006). Standard numerical techniques tend to be impractical, inaccurate or slow so there is need to improve on traditional numerical methods (Cen et al., 2013). Such improvements include, for example, the work in the finite difference method, using the Chebyshev wavelet finite difference method (CWDFD) (Nasab et al., 2013; El-dabe and Ouaf, 2006), and the staggered-grid finite difference method (SFD) (Gao and Zhang, 2013).

Another discretization approach is the finite element method (FEM), which historically originated from structural mechanics (Veress and Rohacs, 2012). This method has been used with remarkable success in many fields of engineering such as solid and fluid mechanics, thermodynamics, and electromagnetism (Alves et al., 2013). Its classical formulation relies on a mesh of elements over which the polynomial approximation functions are built. Further developments include using finite element methods for the stationary Navier-Stokes problem (Wen and He, 2014); the radiative transport equation in a medium with piece-wise constant refractive index (Lehtikangas, 2015); the analysis of crack propagation in bituminous layered structures (Gajewski and Sadowski, 2014) and for a class of convection-diffusion equations

(Wu et al., 2013). Other improvements of the FEM are the extended finite element method (XFEM)

The extended finite element method (XFEM) has been found to be excellent in approximating solutions of locally non-smooth features such as jumps, kinks, high gradient, inclusions, shocks, boundary layers or cracks in solid or fluid mechanics (Toolabi et al., 2013). It emerged as a powerful procedure for analysis of crack problems, such as in Wang et al. (2014) where improvements of the finite element method made use of a combination of the weak Garlekin (WG) and the discontinuous methods. There have been further improvements of the FEM, which include the use of spectral finite element method by Zak and Krawczuk (2011). The accuracy of the FEM may be further improved by the use of hybridization of the method, as in Jeon et al. (2014). However this hybridized method then becomes too costly because of its requirement of more computation time than the original methods, although more accurate.

Classical finite differences can be expected to break down near discontinuities in a solution, in other words where the differential equations do not hold. To avert this difficulty, finite volume methods can be used (LeVeque, 2002). The finite volume method (FVM), historically attributed to McDonald in 1971, is based on the observation that the conservation laws have to be in integral form to preserve discontinuous solutions such as vortex sheets, contact discontinuities or shock waves (Veress and Rahacs 2012; Botta 2004). In the finite volume method the conservation properties of the original equation are passed along to their discrete analogues (Stokie et al., 2003). In essence, the FVM consist of partitioning the domain on which the PDE is formulated into small polygonal domains (control volumes) on which the unknown is approximated by constant values (Ion and Ion, 2011). The method does not require computation of large matrices as in the case of finite difference method (Boivin et al., 2000). Consequently, the finite volume method (FVM) is a discretization method that is well suited for numerical simulations of various types (elliptic, parabolic, or hyperbolic) of conservation laws and so it has been used extensively in several engineering fields such as fluid mechanics, heat and mass transfer or petroleum engineering (Eymad, 2000). The method also provides an efficient way to model two-phase form of incompressible fluids in geologic media, with complex geometrical structures and large variations and discontinuous changes

in the fluid velocities (Geiger et al., 2004). In particular, Zhang et al. (2012) and Manzini and Russo (2008) used the fourth order accurate finite volume method with structured adaptive mesh refinement for solving the advection-diffusion equation. Other applications of the finite volume method include work by Diaz et al. (2014) who solved the two-mode shallow water equation. Among the numerical methods suited to three-dimensional computations or unstructured meshes, the finite volume method, as being well suited to mesh refinement (Coudiere and Pierre, 2006).

Improvements in finite volume methods include their use together with finite difference and finite elements. This finite volume element (FVEM) procedure is usually easier to implement than finite element procedures and offers greater flexibility for handling complicated domain geometries (Yang, 2008). Other uses of the (FVEM) are observed in Wang (2004) where a mixed finite volume method based on rectangular mesh for a biharmonic equation is used.

All of these studies used discretization methods because analytical solutions for these problems could not be easily obtained. These methods present implementation challenges; they are rigorous and less accurate than the new spectral methods. In this thesis we do not use discretization methods; we use the new spectral methods and compare the results obtained by these discretization methods. Furthermore, we compare the effects of physical aspects on fluid flow properties obtained using discretization methods and those obtained using spectral methods.

1.1.2 The Runge-Kutta methods

Euler's method for solving differential equations was extended to a more elaborate scheme published by Runge in 1985 which was capable of greater accuracy (Butcher, 1996). Later developments were by Kutta, Heun and Nystrom (Milne, 1950), with Nystrom making corrections to fifth order methods that had been introduced by Kutta (Butcher, 2009). The Runge-Kutta method, as it is now known, has been used successfully to solve both single and systems of differential equations. The Runge-Kutta method has an order of accuracy of four (Spijker, 1996). The implicit-explicit Runge-Kutta method (IMEX RK) is a further

improvement that preserves stability (Higueras, 2014). Other refinements have reduced errors. In this regard, although error bounds for the Runge-Kutta methods are known from several works, even better error bounds than these could exist (Rivertz, 2013). The introduction of iterative schemes has brought about the reduction of computational complexity of the Runge-Kutta process (Van der Houwen and Messina, 1997). Other improvements of the Runge-Kutta method were noted in Papageorgiou and Tsitouras (1996), in which a nine stage RKN (Runge-Kutta-Nystrom) pair of algebraic equations of order eight and six were presented. Numerical techniques considered for efficient solutions of stiff initial value ordinary differential equations include the implicit Runge-Kutta (IRK) schemes (Voss and Muir, 1999). Despite these improvements, some challenges remain. For instance, such higher order methods need some fundamental evaluation at each step (Nakashima, 1984), resulting in additional computer time requirements (Chung, 2002).

In the Runge-Kutta method, one way to guarantee accuracy is to compute the solution of the boundary value problem using a unit step size and half unit step size and compare the results at data points corresponding to larger step sizes (Butcher, 2009). This requires a considerable amount of computations and must be repeated if the agreement is not enough, since this is too costly, a better procedure called Fehlberg's method is used to compute solutions using Runge-Kutta formula of higher order accuracy (Butt, 2007). This method controls the step size and is known as the Runge-Kutta-Fehlberg method. The Runge-Kutta method can have other numerical techniques embedded in them such as the shooting and Newton-Raphson methods. These methods have been widely used, for instance in Zaimi, (2012) in which the Runge-Kutta-Fehlberg with shooting technique was applied to the Blasius equation.

The application of the Runge-Kutta method in most of the literature described in this section only applied the simple fourth and fifth order Runge-Kutta methods which are less accurate than the improved Runge-Kutta methods. In this thesis we use the Runge-Kutta-Fehlberg method with shooting technique. Furthermore, we compare this method with the analytical solution demonstrating the accuracy of this method. We use this method to solve a new problem in fluid flow and compare the results obtained to those obtained by other methods.

1.1.3 The bvp4c algorithm

The Runge-Kutta computer code is the basic program for Matlab `bvp4c` solver. It is used for solving two-point boundary value problems (Shampine and Muir, 2004). The Matlab `bvp4c` solver computes the solution using a collocation method, and in so doing controls the residual error. In order to use the Matlab `bvp4c` solver, the higher order equation has to be transformed to a first order explicit form (Budd et al., 2006). Control of the size of the defect is natural in the sense of backward error analysis, although it may be easier or more natural to control the local error (Shampine, 2005). In particular the Matlab `bvp4c` makes use of the default relative error tolerance of 10^{-3} and default absolute error tolerance of 10^{-6} (Shampine, 2003). Besides its use in solving boundary value problems, the Matlab `bvp4c` solver has been used to validate other numerical solutions as observed in (Shateyi et al., 2010; Motsa and Shateyi, 2010; Narayana and Sibanda, 2012). The solver has also been extended to include a sixth order solver (Hale and Moore, 2008).

In this thesis we use the Matlab `bvp4c` due to its ability to control the step size at each time step, a characteristic which is not in earlier methods such as the finite difference. In this thesis we demonstrate the accuracy of the improved Runge-Kutta method such as the Runge-Kutta-Fehlberg method with the shooting technique. Although the method is widely used, it is worth classifying it as robust and accurate.

1.1.4 The quasi-linearization method (QLM)

Initially proposed by Bellman and Kalaba (1965), the original idea of the QLM method was to decompose the nonlinear operator as an infinite sum of Adomian polynomials (Alaidarous et al., 2013). However, computation of the Adomian polynomials is not easy with a simple equation. To offset this, other methods which eliminated the calculation of the Adomian polynomials, have been proposed (Pei and Chang, 2008). A further disadvantage of the quasi-linearization method is the instability of the method, whenever a poor initial guess is chosen (Motsa and Sibanda, 2013). To avoid this instability, Motsa and Sibanda (2013) suggested embedding the QLM algorithm within the spectral homotopy analysis method (SHAM) to obtain a sequence of integration schemes with higher order convergence. The refinement

in Yakar and Yakar (2010) of the method converged uniformly to a unique solution, semi quadratically with less restrictive assumptions. There was further generalization of the quasi-linearization method by Lakshmikantham and Shahzad (1994) and Melton and Vatsala (2008) where both showed that monotone sequences also converge to a solution quadratically.

The QLM method is known to give excellent results when applied to different nonlinear ordinary differential equations in physics such as Blasius, Duffing, Lane-Emden and Thomas-Fermi equations (El-Gebeily and O'Regan, 2007). Other applications of the QLM are in the differential equations with integral boundary conditions (Jankowski, 2003).

In this study we use the quasi-linearization method (QLM) because it is easy to implement. Direct Taylor series expansions can be applied to nonlinear terms. The resulting linearized systems are then solved by spectral methods. Furthermore, we demonstrate the accuracy of the method by comparing to other method in the preceding chapters.

1.1.5 The successive linearization method (SLM)

The successive linearization method (SLM) transforms an ordinary nonlinear differential equation into an iterative scheme made up of linear differential equations, which may then be solved by analytical or numerical methods (Motsa and Shateyi, 2012). The advantage of the SLM is that the linearized system can be solved by any method, such as the finite differences, finite elements, Runge-Kutta based shooting method or collocation methods (Motsa et al., 2013). Motsa and Sibanda (2013) used the Chebyshev spectral collocation method to solve the linearized system of differential equations for the Van der Pol and Duffing equations. The SLM was seen to give accurate results compared with others reported in the literature (Motsa et al., 2012a; Makukula et al., 2010). Successive linearization method is used in many contexts in order to improve the quality of approximations (Belkhouche and Belkhouche, 2004). One drawback of this method is that it is not easy to implement in partial differential equations.

In this study we use the successive linearization method as it is easy to implement and does not involve rigorous mathematical manipulations as in the case of finite differences. Each function in the governing equation is substituted by a power series function expression,

which is then expanded and higher powers neglected. The linearized systems are obtained after a small amount of work making it suitable for solving highly nonlinear differential equations.

1.1.6 The Keller-box method

The Keller-box method was proposed by Keller, although it is often referred to as the Preissman box scheme (Perot and Subramanian, 2007). The Keller-box method involves writing the governing equations as a system of first order differential equations (Cebeci and Smith, 1974). Derivatives of some quantities, with respect to the boundary or "normal" variable, must be introduced as unknown functions (Keller and Cebeci, 1972). The classical Keller-box method only applies to a special mesh that has line segments in one dimension, triangles in two dimension and tetrahedral in three dimension (Haque, 2010). In this method only two points are used in discretization, which can be used on a non-uniform grid without difficulty (Esfahanian and Torabi, 2006). This makes it efficient and appropriate for the solution of parabolic partial differential equations (Al-Shibani et al., 2012). The method works with both unknown functions and their derivatives at each grid point simultaneously (Esfahanian and Torabi, 2006). The Keller-box scheme is partially implicit in time and requires matrix inversion to calculate the solution (Perot and Subramanian, 2007). It is an implicit method, which is second order accurate in both space and time (Takhar et al., 1998). The method may be combined with Newton's method for linearization, as described by Cebeci and Bradshaw, (1988). The linearized system of equations can be solved by block elimination, since the system obtained has the block tri-diagonal structure (Abbasbandy, 2012).

The disadvantage of the Keller-box method is that introducing derivatives of unknown functions increases the size of the coefficient matrix, which then increases computation costs (Esfahanian and Torabi, 2006). Another drawback is that the method is difficult to apply in multi-layered flows and presents difficulties in guessing values of certain parameters (Shu and Wilks, 1995). Nevertheless, the Keller-box method has become popular for solving problems of non-similar boundary layer problems (Hamzah et al., 2008). Further applications include the solution of flow and heat transfer over a stretching sheet with Newtonian heating (Sarif et al., 2013) and radiation effects on natural convection laminar flow from a horizontal circular

cylinder (Molla et al., 2011). Further developments include using the parallel algorithm, based on the L-U decomposition (Fazio and Jannelli, 2013). The results from the Keller-box method compared well with the Homotopy analysis method (HAM) and the Adomian decomposition method (ADM).

In this thesis we do not use the Keller-box method due to the disadvantages mentioned in the literature above, instead we use the quasi-linearization method (QLM) and the bivariate quasi-linearization method (BQLM) which are more accurate and robust.

1.1.7 The shooting Method

The principle of the shooting method is converting the governing boundary value problem into an initial value problem (Holsapple et al., 2003), which can then be solved by the Euler or the Runge-Kutta methods (Islam, 2012). An appropriate initial guess is chosen to start the recursive procedure; which can present challenges (Matinfar and Ghasemi, 2013). The shooting method can be applied to two point boundary value problems with the following characteristics; n first order differential equations to be solved over an interval $[a, b]$, r boundary conditions are specified at the initial value of the independent variable, $(n-r)$ boundary conditions are specified at the terminal value of the independent variable (Ha, 2001). The shooting method is reliable and efficient without requiring any specific technique such as overflow trap, modified Newton's method or parameter mapping technique (Chang, 2010). Despite all these advantages, the shooting method becomes unwieldy and is unsuitable for higher order equations in higher dimensions unlike the cone method (Kwong, 2006). Nevertheless Hieu, (2003) studied the convergence of the shooting method and generalized the results. Oderinu and Aregbesola (2014) used the shooting method with Taylor series to allow for quick convergence. Other developments of the shooting method are seen in use together with the collocation and spline technique described in Al-Mdallal et al. (2010). Chang et al. (2007) used the lie group shooting method for quasi-boundary regularization of backward heat conduction problems.

In this study we do not implement the shooting method because the method is now well known and has been widely used in many studies. Although the method is more accurate

than the finite difference method, it is less accurate than the spectral methods.

1.1.8 Spectral methods

Spectral methods became famous in the 1970s. They have played an important role in recent investigations into numerical solutions of differential equations in regular domains. They are considered to be powerful due to their high accuracy (Tatari and Haghighi, 2014). According to Vilhena et al. (1999) spectral methods involve representing the solution to the problem as truncated series of known functions of independent variables. Spectral methods that are based on collocation methods are usually called pseudo-spectral methods (Orel and Perne, 2014), and these are widely used (Fakhar-Izadi and Dehghan, 2011). The collocation points are the zeros of the polynomial chosen for approximation (Moulla et al., 2012). For instance, in the Chebyshev collocation method, the collocation points chosen are the Gauss-Lobatto points (Makanda et al., 2013; Motsa and Shateyi, 2012; Motsa et al., 2014; Motsa and Sibanda, 2012). The Chebyshev Gauss-Lobatto nodes have also been used for the solution of the Burgers equation (Rashid et al., 2014). Recently, Legendre and Chebyshev spectral approximations have been widely used in PDEs in bounded domains (Tatari and Haghighi, 2014).

Progress has been made in solving problems in unbounded domains. In particular, Tatari and Haghighi (2014) considered Laguerre and Hermite spectral methods appropriate choices for semi-infinite and infinite domains. Specifically, a robust Christov-Galerkin spectral technique for computing interacting localized wave solutions of fourth and sixth order generalized wave equations was developed by application of spectral methods on an infinite domain (Christou and Papanicolaou, 2014). The widespread use of spectral methods has been motivated by their accuracy and efficiency in solving incompressible Navier-Stokes equations (Gottlieb and Hesthaven, 2001). A fundamental issue in this method is determining the expansion coefficient. Some approximations such as the Galerkin approximations or collocation schemes have been described by (Gottlieb and Orszag, 1977). The main advantage of the method may be considered to be that there is no need for numerical integration (Jovanovic et al., 2014). Thus, spectral methods also provide more accurate approximations with a relatively small number of unknowns, and so play increasingly important roles in

optimizing engineering design and other scientific computations (Zhou, 2014).

Applications of spectral methods include analytical solutions for neutron transport (Kadem, 2005), coupled Stokes and Darcy equations (Wang and Xu, 2014), modelling of bridges under moving vehicles (Kozar and Malic, 2013). Pozrikidis (2006) used a spectral collocation method with triangular boundary elements, for solving integral equations arising from boundary integral formulations over surfaces discretized into flat or curved triangular elements. Dlamini et al. (2013) made a comparison between the compact finite difference (CFD) method and pseudo-spectral approaches for solving similarity boundary layer problems and found that the spectral method outperformed the CFD in terms of computational speed.

Other manifestations of spectral methods include the spectral relaxation method (SRM), the spectral local linearization method (SLLM), the spectral quasi-linearization method (SQLM), the spectral perturbation method (SPM), the bivariate quasi-linearization method (BQLM) and the bivariate spectral quasi-linearization method (BSQLM). Most of these methods have been developed from the linearization methods. The spectral relaxation method (SRM) requires converting the equations into a system of first and second order differential equations (Shateyi, 2014) or arranging the equations in a particular order, placing the equations with least number of unknowns at the top of the equation list (Motsa and Makukula, 2013). The resulting system is then decoupled using ideas imported from the Gauss-Seidel method, which is normally used to solve linear algebraic systems of equations (Motsa, 2014). The decoupled system is numerically integrated using the Chebyshev pseudo spectral method (Makanda et al., 2013). Unlike other iterative schemes for solving nonlinear systems of equations, the SRM does not require any evaluation of derivatives, perturbation or linearization (Motsa, 2014). Improvements of the SRM are noted in Dlamini et al. (2012) where a multistage spectral relaxation method is proposed for solving problems of chaos control and synchronization. Thus, the SRM is an efficient, reliable, convergent, numerically stable and very easy method to implement that has a great potential as very useful tool for solving boundary layer flow problems arising from fluid dynamics applications (Motsa, 2014). The spectral local linearization method (SLLM) is based on developing a decoupled iterative scheme that is then solved chronologically using spectral methods (Motsa, 2013).

A key feature of the SLLM is that it breaks down a large coupled system of equations into a sequence of small subsystems which can be solved sequentially in a very computationally efficient manner (Motsa, 2013). Local linearization is applied before generating the iterative scheme in a manner similar to the Gauss-Seidel approach of decoupling linear algebraic equations (Motsa, 2013). The spectral quasi-linearization method (SQLM) is the QLM applied together with the Chebyshev pseudospectral method (Motsa, 2013).

In this study we implement these methods due to their accuracy, efficiency and robustness. In particular we implement the successive linearization method (SLM), the quasi-linearization method (QLM), the spectral relaxation method (SRM) and the bivariate quasi-linearization method (BQLM). From the literature mentioned above, it is clear that these methods are highly accurate as well as easy to implement.

1.1.9 The Adomian decomposition method (ADM)

The Adomian decomposition method (ADM), developed in 1984 (Adomian, 1988), is a systematic method for practical solution of linear, or nonlinear, deterministic, stochastic equations, including ordinary differential equations ODEs, partial differential equations (PDEs), integral equations, integro-differential equations (Duan et al., 2012; Biazar et al., 2004). In mathematical physics, many methods have been developed to solve differential equations, among which the Adomian decomposition method (ADM) is an efficient approximation technique used to solve initial boundary value problems (Wu et al., 2011). The advantage of the method is that it converges to exact solutions (Pue-On and Viriyapong, 2012) and needs less computations than the traditional discretization methods (Ali and Al-Saif, 2008). The method is based on decomposition of a nonlinear operator equation, as a power series expansion of a function, resulting in a polynomial. (Hendi et al., 2012). With no need for linearization, perturbation, closure approximation or discretization, all of which can result in massive numerical computations, the method can be used to solve a wide range of problems (Adomian, 1988; Somali and Gokmen, 2007). The main difficulty arises in the calculation of the values of polynomials using simple computer codes (Hendi et al, 2012). The ADM has been used by Blanco-Cocom et al. (2013) to solve the Black-Scholes equation. While Maleknejad et al. (2011) found the projection method involving the collocation method

with Legendre polynomials to be more efficient and to use less computations than the ADM. The ADM has compared favorably with other numerical methods. To elaborate, Ibijola and Adegboyegun (2012) compared it with the Picard iteration method, found that the ADM was more accurate, and so recommended that it should be used to solve differential equations. The ADM was also used by Chiniguel and Ayadi (2011) for solving the heat equation with nonlocal boundary and initial conditions, where it gave exact solutions.

In this study we do not implement ADM because it is well known and has been widely used. The ADM presents two main challenges; difficulties in calculation of the Adomian polynomials and successive application of the integral operator. These problems make it unsuitable for differential equations involving large systems of equations as it requires more computation time than spectral methods.

1.1.10 The variational iteration method (VIM)

The variational iteration method was developed by He to solve fifth order differential equations (Porshokouhi et al., 2010). The VIM changes differential equations to a recursive sequence of functions, where the limit of that sequence is considered to be the solution of partial differential equations (Hattim, 2013). The governing equation is written in terms of a linear and nonlinear operators with an appropriate correction functional (Handlovicova and Mikula, 2000; Kiymaz and Centinkaya, 2010; Matinfar et al., 2009). The correction functional is written in terms of the Lagrange multipliers (Ganji et al., 2007), which should be obtained optimally (Noor and Mohyud-Din, 2009). The successive approximation of the solution is obtained upon using the Lagrange multipliers (Mishra, 2012).

The reliability of the method and the reduction in size of computational domain give this method wide applicability (Kiymaz and Centinkaya, 2010). The variational iteration method (VIM) is combined with semi-implicit discretization in scale, which gives favorable stability and efficient computational properties (Handlovicova and Mikula, 2000). To elaborate, the excellent, and highly accurate, approximations to the nonlinear WBK (Whitham-Broer-Kaup) equations provided by the VIM have been noted by Matinfar et al. (2009). Furthermore, this method has the advantage over the Adomian decomposition of avoiding

the successive application of the integral operator (Mohyud-Din et al., 2009). The VIM's efficiency requires only four iterations to obtain highly accurate solutions for fifth order differential equations (Porshokouhi et al., 2010). The VIM is thus preferable over other numerical methods, as it is free from rounding off errors and furthermore does not require large computer memory (Salehpoor and Jafari, 2011). A comparison of the VIM with the Adomian decomposition method (ADM), homotopy analysis method (HAM) and the homotopy perturbation method (HPM) showed excellent agreement, indicating the accuracy of the VIM, as reported in Miansari et al. (2009) and Nawaz (2011). Nevertheless, the efficiency of the VIM depends on not only the identification of the parameters but also on the initial approximation of the solution, usually satisfying the boundary conditions (Geng, 2010).

The VIM has been applied to linear and nonlinear stiffness of springs (Fereidoom et al., 2010). Other applications include the work of Wu and Baleanu (2013) in which the VIM was applied to q-fractional difference equations. Yang et al. (2014) and Molliq et al. (2009) used the VIM for diffusion and wave equations. A revised VIM presented by Salepoor (2010) accelerates convergence of the system of sequences. Another improved version is reported in Geng (2012), which overcomes the restrictions of the application area of variation iterative method, and expands its scope of application.

In this study we do not use the VIM, although the method is accurate, it requires identification of certain parameters and good initial approximation. This method is well known and has been widely used.

1.1.11 The differential transform method (DTM)

The differential transform method (DTM) is one of the numerical methods for ordinary (partial) differential equations which use polynomials as the approximation to the exact solution (Hassan, 2007). The method was first proposed by Zhou (1986), who solved both linear and nonlinear initial value problems in electric circuit analysis. The semi-analytic method uses the Taylor series for the solution of the differential equation (Biazar and Mohammadi, 2010). The DTM is different from the traditional high order Taylor series methods which requires

symbolic computations of the necessary derivatives of the data function (Jafari et al., 2010). Therefore the main benefit of the method is to offer the analytical approximation and in many cases an exact solution, rapidly convergent series (Aasaraai, 2011). Thus, without linearization, discretization, or perturbation, Al-Amr (2014) considers the converging series components to be elegantly computed. Moreover, the DTM can also be used to solve higher order differential equations (Hussin et al., 2010).

Results from the DTM method have been shown to compare favorably with those from the traditional methods. Comparison of the method to the Laplace transform method is observed in (Thong-moon and Pusjuso, 2010) and the methods gave results that were in agreement. Another comparison is noted by Merdan et al. (2011) in which the method was applied to Coullet system and a good agreement of the results was reported. Furthermore, the accuracy of numerical solution obtained can be improved by taking more terms in the series (Mirzaee, 2011).

The DTM has been used in numerous applications. It was applied to boundary layer flow in nanofluid (Ebaid, 2013), nonlinear heat conduction problem (Chu and Chen, 2008), a class of stiff systems (Idress et al., 2013), the Lane-Emden equation, the white-Dwarf equation in astrophysics and Troesch's problem (Aljoufi, 2013). The DTM has also been applied to multidimensional partial differential equations (Jafari et al., 2012) and to fourth order parabolic partial differential equations (Soltanalizadeh, 2012). In addition Mukherjee and Roy (2012) applied the DTM to the Riccati equation with variable coefficients, in which they compared exact analytical solution results to numerical results obtained, and there was an excellent agreement.

1.1.12 Overview of numerical methods for fluid flow

Discretization methods have been used to solve ordinary and partial differential equations, but require more computer memory and computation time than most of the later methods. Discretization methods give rise to large matrices which need inversion, thereby increasing computation time. The accuracy of discretization methods is improved by reducing the spacing between discretization points leading to considerable computer run time. By contrast,

if the Runge-Kutta method through the Matlab `bvp4c` is incorporated it appears that accuracy is improved with less computation time than discretization methods. In this method the spacing between discretization points is automatically adjusted to achieve high accuracy and small computation time, but the issues of solving higher order and highly nonlinear equations remain unresolved.

The quasi-linearization method (QLM) is suitable for highly nonlinear ordinary and partial differential equations, all nonlinear terms in the equation are approximated by the Taylor series expansion. This reduces the rigorous processes done in discretization methods but has the shortcomings of instability whenever a poor initial approximation is chosen. This Taylor series approximation was found to be less accurate than earlier methods such as the finite volume methods. By contrast if the Adomian decomposition method (ADM), the shooting method, the variational iteration method (VIM), and the differential transform method (DTM) are incorporated it appears that accuracy is improved but solving partial differential equations by the SLM remains unresolved. The bivariate quasi-linearization method (BQLM) is suitable for solving highly nonlinear ordinary and partial differential equations in fluid flow but has shortcomings of instability whenever a poor initial guess is chosen. The choice of the number of collocation points is arbitrary, this issue and improvements of the method remains unresolved.

1.2. Background on physical properties in fluid flow

In this section we review literature on convective fluid flow in Newtonian and non-Newtonian fluids in porous and non-porous media. We consider various physical aspects which include effects of exponential stretching sheet on fluid flow, effects of radiation, magnetohydrodynamic, viscous dissipation, free or natural convection, fluid flow past various geometries, fluid flow in porous media, effects of chemical reaction on fluid flow, effects of partial slip, cross diffusion effects and double dispersion effects. Each of these aspects will be further reviewed in the preceding chapters.

1.2.1 Fluid flow on exponential stretching/shrinking sheet

When sheets are being manufactured, molten material is pulled from the slit and stretched to obtain required thickness (Pavithra and Gireesha, 2014). This situation is similar to continuous pulling of plastic sheets in the manufacturing of plastic bags. It is important to study the velocity of the stretching surface relative to the point of extrusion (Mukhopadhyay et al., 2013). The rate at which the sheet is drawn from the extrusion slit is described in a number of different ways namely; linear, continuous, unsteady and nonlinear such as exponential. In most studies it is assumed that the velocity of the stretching sheet is linearly proportional to the distance from the extrusion slit (Mandal and Mukhopadhyay, 2013). In practical applications it is argued that the velocity of stretching may not be linear (Mukhopadhyay, 2013). In light of this, it is therefore more realistic to consider an exponentially stretching sheet (Kameswaran et al., 2012). There are many other studies that considered an exponentially stretching sheets, these include the works of Das (2012), Magyari and Keller (1999), Ishak (2011) , Sajid and Hayat (2008) and Pal and Mandal (2015).

In this study we consider the fluid flow of a unique problem in which fluid flow is considered on a stretching surface. The consideration of this aspect poses a considerable challenge to the governing equations. This aspect will be considered in Chapter 3. (See also Appendix A).

1.2.2 Radiation effects in fluid flow

Radiation is the emission of energy as electromagnetic waves or as moving high energy particles that cause ionization. Energy transmitted this way may be as heat, electricity or light. When this emission is incident on fluid flow it affects certain fluid properties (Chamkha et al., 2003). To model the movement of thermal radiation, the Rosseland approximation is applied (Mustafa et al., 2015). This approximation assumes that the heat flux is proportional to the temperature change and that heat flows from the solid surface to the fluid (El-Kabeir and El-Sayed, 2012). Furthermore, it is assumed that temperature differences within the flow are small (Chamkha et al., 2003). At high temperatures, radiation effects significantly affect temperature distribution and heat transfer (Prakash and Muthtamilselvan, 2014; Das,

2011; Pal and Mandal, 2015).

The consideration of radiation effects in fluid flow give rise to a theoretically challenging problem in both ordinary and partial differential equations. The aspect of radiation effects will be considered in Chapters 3, 6 and 7. (See also Appendices A, D and E)

1.2.3 Magnetohydrodynamics

Magnetohydrodynamics (MHD) is the study of fluid flow in electrically conducting fluids with magnetic properties that affect fluid flow. Examples include plasmas, salt water, electrolytes and liquid metals. When a magnetic field is incident in an electrically conducting fluid, a current is induced. This effect polarizes the fluid and as a result the magnetic field is changed. The application of a magnetic field results in controlling the momentum and heat transfer in fluid flow (Mukhopadhyay, 2013). The inclusion of MHD terms in the momentum equation makes them challenging to solve (Khalid et al., 2015). Furthermore, changing the magnetic field parameter strongly affects the convergence of solutions (Shateyi and Marewo, 2013). There are many studies that investigated magnetohydrodynamic fluid flow; these include the work of Abbasbandy et al. (2014) considered MHD effects on the Falken-Skan fluid flow of Maxwell fluid. Prakash and Muthtamilselvan (2014) investigated the effect MHD on micropolar fluid flow.

The effect of magnetohydrodynamics will be considered in this study due to its importance in fluid flow as shown in the literature above. The MHD effect will be considered in Chapters 3, 5 and 6. (See also Appendices A, C and D)

1.2.4 Viscous dissipation

Viscous dissipation is the heat energy that is produced as a result of friction between fluid layers. In fluid flow it is sometimes important to consider the effect of viscous dissipation (Jambal et al., 2005). Viscous dissipation affects heat transfer and temperature distribution in the fluid regime (Pal and Mandal, 2015). The effect of viscous dissipation is mostly considered in non-Newtonian fluids especially power-law fluids (Shokouhmand and Soleimani,

2011). In modeling fluid flow, the dimensionless parameters that describe viscous dissipation are the Eckert number (Ec) (Eldabe et al.,2012; Makanda et al., 2012; Pal and Mandal, 2015), Gebhart number (Gb) (Kameswaran et al., 2012) and the Brinkman number (Br) (Hajipour and Dehkordi, 2012; Shokouhmand and Soleimani, 2011; Jambal et al., 2005). Some studies neglected the effects of viscous dissipation. However, many studies investigated effects of viscous dissipation; these include the works of Pal and Mandal (2015) who studied mixed convection of nanofluids with heat generation and viscous dissipation. Eldabe et al. (2012) investigated effects of viscous dissipation on a non-Newtonian fluid.

The effects of viscous dissipation will be considered in this thesis. Some studies neglected viscous dissipation which significantly affect fluid flow. The consideration of viscous dissipation will be discussed in Chapters 3, 4, 6, 7 and 8. (See also Appendices A, B, D, E and F).

1.2.5 Free or Natural convection

Natural or free convection is caused by density differences due to temperature gradient. This creates buoyant forces and fluid flow is facilitated. In fluid flow, constant fluid properties are considered except density differences (Boussinesq approximation) (Cheng, 2011). The dimensionless parameter which describes natural or free convection is called the Grashof number (Narayana et al., 2013; Rashad et al., 2014; Siddiqa et al., 2012). The Grashof number is the ratio of the buoyancy forces to the viscous forces. Fluid flow caused by free or natural convection depends on a number of factors such as the geometry, orientation, variation of temperature on the surface and thermo-physical properties of the fluid. In natural convection it is important to study the heat transfer coefficient sometimes referred to as the Nusselt number. The heat transfer rate affects the temperature distribution in the fluid regime. Many studies were conducted in free or natural convection; these include the work of Cheng (2011) who studied natural convection of a micropolar fluid, Alam et al. (2006) investigated free convection and mass transfer past a vertical plate and Hsiao (2011) considered mixed convection past a porous wedge.

The effect of natural convection in fluid flow is considered in this thesis due to its

application in a wide range of situations. The effect of natural convection will be considered in Chapters 4, 6 and 7. (See also Appendices B, D and E)

1.2.6 Fluid flow geometry

One of the most important factors of the study of fluid flow is the geometry and orientation. When modeling fluid flow the geometry over which the fluid flows affects how the fluid flows and other properties. From the literature considered in this section, the most frequent geometries are horizontal surfaces, vertical surfaces, parallel plates, inclined, circular, conical and spherical surfaces. Other unusual geometries considered in studies are wavy surfaces (Kabir, 2013), stretching surfaces (Kameswaran et al., 2012), irregular channel (Sivaraj and Kumar, 2012), vertical stretching sheet (Das, 2012), cylinders in tubes (Mitsoulis and Galazoulas, 2009) and inclined wavy surface (Cheng, 2010).

In modeling fluid flow each of the geometries presents a different mathematical expression. In this thesis we consider fluid flow on horizontal, vertical, conical and cylindrical surfaces. Studies have been done on different geometries by among others Abbas et al. (2008) who considered unsteady second grade fluid flow on an unsteady stretching sheet, Anwar et al.(2008) studied mixed convection boundary layer flow of a viscoelastic fluid over a horizontal circular cylinder, Damseh et al. (2008) studied the transient mixed convection flow of a second grade viscoelastic fluid over a vertical surface. Hayat et al.(2008) studied mixed convection in a stagnation point flow adjacent to a vertical surface in a viscoelastic fluid.

In this thesis we consider more practical geometries on which fluids flow. We consider fluid flow on a horizontal stretching surface, fluid flow past a cone, unsteady horizontal stretching surface, fluid flow past a cylinder, fluid flow past a spinning cone and fluid flow from a vertical plate. These various geometries pose a theoretical challenge on the governing equations. In this thesis we present different problems arising from these geometries and use numerical methods to solve each of them.

1.2.7 Porous media

The flow of fluid through porous media is important due to its practical application. A porous medium is a region which contains pores which offers resistance to fluid flow. The ability of the fluid to flow across a porous medium is determined by the permeability or porosity of the medium. The general mathematical model that describes a flow in porous medium is known as Darcy's law; it states that the flow rate is a function of fluid pressure, flow area and elevation (Bar-Meir, 2009). Darcy's law only applies under certain conditions, in situations in which it does not hold inertial forces are dominant. Under these conditions the fluid flow is described as non-Darcy (El-Amin et al., 2008). Examples of fluid flow in porous media include the flow of water in aquifers, fluid flow in packed beds, irrigation problems, heat storage in beds and biological systems (Khalid et al., 2015). Further applications include chemical and reservoir engineering (Aldabe et al., 2012). Many studies were performed in fluid flow in porous media, these include the works of Pal and Mandal (2015) who investigated flow of nanofluids in porous medium, Hsiao et al. (2014) studied flow of a non-Newtonian fluid in porous medium. Singh et al. (2012) studied heat transfer in a second grade fluid over an exponentially stretching sheet through porous medium.

The flow of fluids in porous media has remained problems of interest due to their wide application in industry. In this thesis we consider problems in fluid flow in porous media, these will be considered in Chapters 4, 5, 6 and 7. (See also Appendices B, C, D and E).

1.2.8 Chemical reaction effects

The flow of fluid is affected by chemical reactions that take place in it. When chemical reactions occur either energy is used or dissipated resulting in processes known as endothermic and exothermic reactions. Consequently, fluid properties are affected. In some cases chemical reactions are either destructive or constructive (Mukhopadhyay and Vajravelu, 2013). There are several studies that considered chemical reactions, these include the work of El-Kabeir and El-Sayed (2012) who studied chemical reaction in fluid flow past a cone, Das (2011), Bakr (2011) and Rashad et al. (2014). Kameswaran et al. (2013a) investigated homogeneous-heterogeneous reactions in a nanofluid flow due to a porous stretching sheet,

Shaw et al.(2013) studied homogeneous-heterogeneous reactions in a nanofluid flow due to a porous stretching sheet. In this thesis the chemical reaction effects will be considered in Chapter 5. (See also Appendix C).

1.2.9 Partial slip effects

The flow of fluid on a surface is considered to stick to the surface commonly referred to as the no-slip condition (Prabhakara and Deshpande, 2004). The solid surface is assumed to be rough, which slows down the fluid flow at the surface. The slip condition is applicable in situations where the velocity is small (Bar-Meir, 2009). Many studies in the literature considered in this thesis show that most studies assume the no-slip condition. There are some studies that considered partial slip conditions; these include among others Das (2012) who considered slip effects on a micropolar fluid over a vertical shrinking sheet. Sahoo (2009) investigated effects of partial slip in a non-Newtonian fluid. In this thesis the effects of partial slip will be considered in Chapters 6 and 7.(See Appendices D and E).

1.2.10 Cross diffusion effects

Heat and mass diffusing at the same time give rise to cross diffusion effect (Awad et al., 2011). If the difference in temperature in a molecular mass is large, then the coupled interaction is large (El-Amin, 2008). The mass transfer caused by temperature gradient is referred to as the Soret effect, while the heat transfer caused by concentration gradient is referred to as the Dufour effect (Narayana and Sibanda, 2012). In many instances in fluid flow the effects are large that they cannot be ignored (Alam et al., 2006). There are some studies that considered cross diffusion effects, these include among others Cheng (2010) who considered double diffusion fluid flow along an inclined wavy surface. Narayana et al. (2013) investigated cross diffusion effects on a vertical spinning cone. In this thesis we will consider cross diffusion effects together with partial slip and convective boundary conditions in Chapter 8. (See Appendix F)

1.2.11 Double dispersion effects

Dispersion is the distribution of material over a wide area. When heat and mass are mechanically transported from one region to the other in fluid flow, this is referred to as double dispersion. The effects of double dispersion in fluid flow have been studied by among others Loh and Vesudevan (2013) who investigated dispersion behavior in non-porous silica monolith. Hu et al. (2012) considered enhanced dispersion in supercritical fluids. Ahmed et al. (2010) investigated gas dispersion in a multi impeller bioreactor. The effect of double dispersion will be considered in Chapter 8.(See Appendix F)

1.3. Objectives

For most fluid flow problems, numerical solutions are frequently a more practical alternative to analytical solutions. However, numerical solutions may not describe all characteristics of the fluid flow adequately. In particular, discretization methods may not be suitable for solving certain nonlinear differential equations because they require more computer memory and computation time than recently developed spectral methods. Thus methods for finding numerical solutions need to be developed further, to show their accuracy, provide proof of their convergence and show that the methods are sufficiently robust for general use. In this study we will focus on using recent iterative methods, which are combined with spectral methods. To this end we will:

(i) Review

a) the Matlab `bvp4c` as the basic numerical method for boundary value problems,

b) the successive linearization method (SLM),

c) the spectral relaxation method (SRM)

d) the spectral quasi-linearization method (SQLM),

e) the local linearization method (LLM) applied with collocation to PDEs and (SQLM) applied with collocation to ODEs.

(ii) Use and evaluate the above methods to solve problems in fluid flow specifically:

a) MHD flow in a Newtonian fluid due to an exponential stretching sheet (Kameswaran et al., 2012),

b) Natural convection from a cone in a viscoelastic fluid in porous medium with viscous dissipation (Makanda et al., 2013),

c) Diffusion of chemically reactive species in Casson fluid over an unsteady stretching surface (Makanda et al. 2015a),

d) Effects of radiation on MHD free convection in a Casson fluid from a horizontal cylinder with partial slip in a non-Darcy porous medium (Makanda et al., 2015b),

e) Effects of radiation on free convection from a spinning cone with partial slip in non-Darcy porous medium with cross diffusion and viscous dissipation (Makanda et al., 2015c),

f) Effects of double dispersion on Casson fluid flow with viscous dissipation and convective boundary condition (Shaw et al., 2015)

1.4. Thesis outline

This thesis is divided into nine chapters.

In Chapter 1 we have reviewed the literature on numerical methods namely: the finite difference method (FDM), finite element method (FEM), finite volume method (FVM), the Matlab `bvp4c` solver, the successive linearization method (SLM), the quasi-linearization method (QLM), the Runge-Kutta methods, the shooting method, spectral methods, the Adomian decomposition method (ADM), the variational iteration method (VIM) and the differential transform method (DTM).

In Chapter 2 we give a detailed description of the methods that will be used in the thesis, these methods include the Matlab `bvp4c` solver, the successive linearization method (SLM), the spectral relaxation method (SRM), the spectral quasi-linearization method (SQLM) and the local linearization (LLM).

In Chapter 3 we use the Runge-Kutta method together with the shooting technique to solve a problem on radiation effects in magnetohydrodynamic Newtonian liquid due to an exponential stretching sheet.

In Chapter 4 we use successive linearization method (SLM) to solve a problem on natural convection of viscoelastic fluid from a cone embedded in porous medium with viscous dissipation.

In Chapter 5 we use the Matlab `bvp4c` algorithm and the successive linearization method (SLM) to solve a problem on diffusion of chemically reactive species in Casson fluid over an unsteady stretching surface in porous medium with viscous dissipation.

In Chapter 6 we use local linearization method (LLM) and the Matlab `bvp4c` to solve a problem on effects of radiation on MHD free convection of Casson fluid from a horizontal circular cylinder with partial slip in non-Darcy porous medium with viscous dissipation.

In Chapter 7 we use spectral relaxation method (SRM) and the Matlab `bvp4c` method to solve a problem on effects of radiation on free convection from a spinning cone with partial slip in Casson fluid in non-Darcy porous medium with cross diffusion and viscous dissipation. This is one of the few problems in which the successive linearization method is applied to four differential equations.

In Chapter 8 we use the local linearization method (LLM) to solve a problem on effects of double dispersion on Casson fluid flow with viscous dissipation and convective boundary conditions. This is one of the few problems in which the LLM is used to solve three partial

differential equations in fluid flow.

In Chapter 9, the methods are evaluated and conclusions drawn regarding their accuracy, convergence and robustness.

The next section includes appendices which consist of published papers.

References are included at the end, all the references shown were cited in the thesis.

2

Numerical methods for boundary value problems

In this chapter, we review numerical methods for solving systems of differential equations of fluid flow. The methods discussed in this chapter have been recently developed and are used to solve boundary value problems. The methods are mainly based on spectral methods which are efficient in solving boundary value problems.

The numerical methods discussed in this chapter are the only ones that will be used to solve the differential equations in the preceding chapters. We will particularly review the following methods; the Matlab `bvp4c` which will be used in Chapters 3, 5 and 8, the successive linearization method (SLM) which will be implemented in Chapters 4 and 5, the quasi-linearization method (QLM) which will be implemented in Chapters 6 and 8, spectral relaxation method (SRM) which will be used in Chapter 7 and the bivariate quasi-linearization method (BQLM) that will be implemented in Chapters 6 and 8.

2.1. Review of the Matlab bvp4c solver

Matlab provides the boundary value problem solver `bvp4c` that was developed for the solution of ordinary differential equations (Kierzenka and Shampine, 2001). The general two-point boundary value problem is

$$u'(x) = f(x, u(x), p), \tag{2.1}$$

$$g(x_L, x_R, u(x_L), u(x_R), p) = 0. \tag{2.2}$$

$$\tag{2.3}$$

Where f is continuous Lipschitz function in u and p is a vector of unknown parameters (Gokhan, 2011). The Matlab `bvp4c` solver is designed for a two-point boundary value problem where the solution sought on an interval $[a, b]$ must satisfy the boundary condition $g(u(a), u(b)) = 0$ (Shateyi et al., 2010). The most common types of BVP are those for which information is given at two points (Bogacki and Shampine, 1996). The MATLAB routine `bvp4c` is based on an adaptive Lobatto quadrature scheme (Motsa et al., 2013). The Matlab `bvp4c` solver is a residual control based adaptive mesh solver (Gokhan, 2011).

It might be necessary to give an initial guess for the solution. The quality of this guess can be critical for the performance of the solver. The Matlab `bvp4c` algorithm is based on the Runge-Kutta improved formulas that have interpolation capability (Shampine and Reichelt, 1997). A natural measure of the cost of the Runge-Kutta formula is the number of stages involved- the number of times the function $f(x, y)$ is evaluated (Bogacki and Shampine, 1996). This method will be implemented in Chapters 3, 5, 7 and 8.

2.2. Strengths and weaknesses of the bvp4c solver

The Matlab `bvp4c` solver is an adaptive solver which adjusts mesh points at each stage (Gokhan, 2011). This leads to advantages in terms of computational and storage costs (Shampine, 2003). The most challenging part of the solution of BVPs is to provide an initial

estimation to the solution (Gokhan, 2011). The quality of the initial guess can be critical to solver performance, which reduces or increase run time. The accuracy and convergence of the Matlab `bvp4c` algorithm depends on a good initial guess and work better for equations involving a few equations (Sibanda et al.,2012). One drawback is that the user must assist the solver to get the desired solution (Kierzenka and Shampine, 2001).

2.3. Successive linearization method (SLM)

We describe the successive linearization method (SLM) in general. The successive linearization (SLM) uses the Taylor series to linearize the nonlinear terms of the governing ordinary differential equations (Motsa et al., 2012a). Following the work of Motsa et al. (2012a) we consider the general nth order nonlinear ordinary differential equation, which is of the form

$$\mathcal{L}\left[u(x), u'(x), u''(x), \ldots, u^n(x)\right] + \mathcal{N}\left[u(x), u'(x), u''(x), \ldots, u^n(x)\right] = 0. \tag{2.4}$$

Where $u(x)$ is an unknown function, x is an independent variable, primes denote the derivative with respect to x. The functions $\mathcal{L}$ and $\mathcal{N}$ represent the linear and nonlinear components of the governing equation respectively. We considered $x \in [a, b]$ subject to the boundary conditions;

$$u(a) = u_a, u(b) = u_b. \tag{2.5}$$

Where u_a and u_b are given constants. The initial guess for the solution of Eq. (2.4) should satisfy the boundary conditions (2.5). For problems defined on a finite domain, it is convenient to consider polynomial functions. A suitable initial approximation, denoted by u_0 satisfies Eq. (2.5) is a straight line. Exponential functions may be used in problems defined on a semi-infinite or infinite domain. We assume that the functions $u, u', \ldots, u^n$, may be expanded in series form as

$$u(x) = u_i(x) + \sum_{m=0}^{i-1} u_m(x), \tag{2.6}$$

$$u'(x) = u_i'(x) + \sum_{m=0}^{i-1} u_m'(x), \tag{2.7}$$

$$u''(x) = u_i''(x) + \sum_{m=0}^{i-1} u_m''(x), \tag{2.8}$$

$$\vdots \quad \vdots \quad \vdots \tag{2.9}$$

$$u^{(n)}(x) = u_i^{(n)}(x) + \sum_{m=0}^{i-1} u_m^{(n)}(x). \tag{2.10}$$

Substituting Eq. (2.6)-(2.10) into Eq. (2.4) gives

$$\begin{aligned} &\mathcal{L}\left[u_i, u_i', u_i'', \ldots, u_i^n\right] + \mathcal{N}\left[\sum_{m=0}^{i-1} u_m + u_i, \sum_{m=0}^{i-1} u_m' + u_i, \sum_{m=0}^{i-1} u_m'' + u_i, \ldots, \sum_{m=0}^{i-1} u_m^n + u_i\right] \\ &\quad = -\mathcal{L}\left[\sum_{m=0}^{i-1} u_{i-1}, \sum_{m=0}^{i-1} u_{i-1}', \ldots, \sum_{m=0}^{i-1} u_{i-1}^n\right], i = 1, 2, 3 \ldots \end{aligned} \tag{2.11}$$

Where i number of successive iterations, if $u_0(x)$ is given, solving Eq. (2.11) will yield an exact solution for $U_1(x)$. Because the equation is nonlinear, the exact solution might not be easy to find. We seek an approximate solution by solving the linear part of the equation under the assumptions that u_i and its derivatives are small. This enables us to use the Taylor series method to linearize the equation. If $u_i(x)$ is a solution to Eq. (2.11), we let $u_i(x)$ denote the solution to the linearized version of Eq. (2.11). Expanding Eq. (2.11) by using the Taylor series and neglecting higher order terms gives

$$\begin{aligned} &\mathcal{L}\left[u_i, u_i', u_i'', \ldots, u_i^n\right] + a_{0,i-1}u_i^n + a_{1,i-1}u_i^{n-1} + \ldots \\ &\quad + a_{n-1,i-1}u_i' + a_{n,i-1}u_i = r_{i-1}(x)\ i = 1, 2 \ldots, \end{aligned} \tag{2.12}$$

subject to boundary conditions

$$u_i(a) = 0, u_i(b) = 0. \tag{2.13}$$

Where

$$a_{0,i-1}(x) = \frac{\partial \mathcal{N}}{\partial u_i^{(n)}} \left(u_{i-1}, u'_{i-1}, u''_{i-1}, \ldots, u^n_{i-1}\right), \tag{2.14}$$

$$a_{1,0}(x) = \frac{\partial \mathcal{N}}{\partial u_i^{(n-1)}} \left(u_{i-1}, u'_{i-1}, u''_0, \ldots, u^n_{i-1}\right), \tag{2.15}$$

$$\vdots \tag{2.16}$$

$$a_{n-1,i-1}(x) = \frac{\partial \mathcal{N}}{\partial u'_1} \left(u_{i-1}, u'_{i-1}, u''_{i-1}, \ldots, u^n_{i-1}\right), \tag{2.17}$$

$$a_{n,i-1}(x) = \frac{\partial \mathcal{N}}{\partial u_i} \left(u_{i-1}, u'_{i-1}, u''_{i-1}, \ldots, u^n_{i-1}\right), \tag{2.18}$$

$$r_{i-1}(x) = \mathcal{L}[u_{i-1}, u'_{i-1}, u''_{i-1}, \ldots, u^n_{i-1}] - \mathcal{N}[u_{i-1}, u'_{i-1}, u''_{i-1}, \ldots, u^n_{i-1}]. \tag{2.19}$$

The linearized system Eq. (2.12) can be solved by any numerical method. The successive linearization method (SLM) will be implemented in Chapters 4, 5 and 7.

2.4. Strengths and weaknesses of the successive linearization method (SLM)

The successive linearization method was compared to the analytical solution of the Lane-Emden equation and was in agreement to twenty decimal places in Motsa and Shateyi (2012). The method converges rapidly to the solution after three to four iterations (Motsa and Shateyi, 2012; Motsa et al., 2012b). The ability of the SLM to generate multiple solutions make it superior to most numerical methods which are only capable of generating one solution of nonlinear equations (Motsa et al., 2012b). The method can easily be extended to nonlinear oscillating systems and nonlinear problems with bifurcations (Motsa and Sibanda, 2012). Its implementation does not depend on small parameters unlike other traditional methods such as perturbation method (Motsa et al. 2012b). One drawback of the SLM is that when solving

fluid flow problems one should have an idea of the size of the boundary layer thickness. The determination of the number of collocation points is not straightforward.

2.5. Spectral relaxation method (SRM)

In this section we give a detailed description of the spectral relaxation method as described in Motsa et al. (2014). We consider a system of n nonlinear ordinary differential equations in n unknown functions $f_i(\eta)$, $i = 1, 2, \ldots n$ where $\eta \in [a, b]$ is the dependent variable. We define a vector $\boldsymbol{F}_i$ to be a vector of derivatives of the variable f_i with respect to η

$$\boldsymbol{F}_i(\eta) = \left[f_i^{(0)}, f_i^{(1)}, \ldots, f_i^{(m)} \right]. \tag{2.20}$$

Where $f_i^{(0)} = f_i$, $f_i^{(p)}$, is the pth derivative of f_i with respect to η and $m_i (i = 1, 2, 3 \ldots, n)$ is the highest derivative order of the variable f_i which is in the system of equations. The system can be written in terms of $\boldsymbol{F}_i$ as the sum of linear ($\mathcal{L}_i$) and nonlinear components ($\mathcal{N}_i$) as

$$\mathcal{L}_i \left[\boldsymbol{F}_1, \boldsymbol{F}_2, \ldots, \boldsymbol{F}_n \right] + \mathcal{N}_i \left[\boldsymbol{F}_1, \boldsymbol{F}_2, \ldots, \boldsymbol{F}_n \right] = \mathcal{G}_i(\eta), \ i = 1, \ldots n. \tag{2.21}$$

Where $\mathcal{G}(\eta)$ is a known function of η.

Eq. (2.21) is solved subject to two point boundary conditions which are expressed as

$$\sum_{j=1}^{m} \sum_{p=0}^{m_j - 1} \alpha_{\nu,j}^{(p)} f_j^{(p)}(a) = K_{a,\nu}, \ \nu = 1, 2, \ldots, n_a, \tag{2.22}$$

$$\sum_{j=1}^{m} \sum_{p=0}^{m_j - 1} \gamma_{\nu,j}^{(p)} f_j^{(p)}(b) = K_{b,\sigma}, \ \sigma = 1, 2, \ldots, n_b, \tag{2.23}$$

where $\alpha_{\nu,j}^{(p)}$, $\gamma_{\sigma,j}^{(p)}$ are the constant coefficients of $z_j^{(p)}$ in the boundary conditions, and η_a and η_b are the total number of prescribed boundary conditions at $\eta = a$ and $\eta = b$ respectively. Starting from the initial approximation $\boldsymbol{F}_{1,0}, \boldsymbol{F}_{2,0}, \ldots, \boldsymbol{F}_{n,0}$, the iterative method is obtained as

$$\mathcal{L}_1\left[\boldsymbol{F}_{1,r+1}, \boldsymbol{F}_{2,r}, \ldots, \boldsymbol{F}_{n,r}\right] = \mathcal{G}_1 + N_1\left[\boldsymbol{F}_{1,r}, \boldsymbol{F}_{2,r}, \ldots, \boldsymbol{F}_{n,r}\right], \tag{2.24}$$

$$\mathcal{L}_2\left[\boldsymbol{F}_{1,r+1}, \boldsymbol{F}_{2,r}, \ldots, \boldsymbol{F}_{n,r}\right] = \mathcal{G}_2 + \mathcal{N}_2\left[\boldsymbol{F}_{1,r}, \boldsymbol{F}_{2,r}, \ldots, \boldsymbol{F}_{n,r}\right], \tag{2.25}$$

$$\vdots \quad \vdots \quad \vdots \quad \vdots \quad \vdots \quad \vdots \quad \vdots \quad \vdots$$

$$\mathcal{L}_{n-1}\left[\boldsymbol{F}_{1,r+1}, \boldsymbol{F}_{2,r}, \ldots, \boldsymbol{F}_{n,r}\right] = \mathcal{G}_{n-1} + \mathcal{N}_{n-1}\left[\boldsymbol{F}_{1,r}, \boldsymbol{F}_{2,r}, \ldots, \boldsymbol{F}_{n,r}\right], \tag{2.26}$$

$$\mathcal{L}_n\left[\boldsymbol{F}_{1,r+1}, \boldsymbol{F}_{2,r}, \ldots, \boldsymbol{F}_{n,r}\right] = \mathcal{G}_n + \mathcal{N}_n\left[\boldsymbol{F}_{1,r}, \boldsymbol{F}_{2,r}, \ldots, \boldsymbol{F}_{n,r}\right]. \tag{2.27}$$

Where $\boldsymbol{F}_{i,r+1}$ and $\boldsymbol{F}_{i,r}$ are the approximation of $\boldsymbol{F}_i$ at the current and the previous iterations respectively. We state that Eqs. (2.24)-(2.27) form a system of n linear decoupled equations which can be solved iteratively for $r = 1, 2 \ldots$. We start from a an appropriate initial approximation $F_{i,0}$ which satisfy boundary conditions. The iterations are repeated until convergence is reached. The decoupling error can be used to assess the desired convergence. The decoupling error E_r at the $(r+1)$th iteration is defined by

$$E_r = \text{Max}\left(\left\|f_{1,r+1} - f_{1,r}\right\|_\infty, \left\|f_{2,r+1} - f_{2,r}\right\|_\infty, \ldots, \left\|f_{m,r+1} - f_{m,r}\right\|_\infty\right). \tag{2.28}$$

The idea incorporated in this method is the Gauss-Seidel relaxation method which is normally used for solving large systems of algebraic equations. To implement the spectral collocation method, we define the differentiation matrix

$$\frac{df_i(\eta_l)}{d\eta} = \sum_{k=0}^{N} \boldsymbol{D}_{l,k} f_i(\tau_k) = \boldsymbol{D}\boldsymbol{F}_i, l = 0, \ldots, N. \tag{2.29}$$

Where $N+1$ is the number collocation points, $\boldsymbol{D} = 2D/(b-a)$ and $\boldsymbol{F} = \left[f(\tau_0), f(\tau_1), \ldots, f(\tau_N)\right]^T$ is the vector function of the collocation points and higher order derivatives are obtained in powers of $\boldsymbol{D}$ given by

$$f_j^{(p)} = \boldsymbol{D}^p \boldsymbol{F}_j. \tag{2.30}$$

We then apply the Chebyshevpseudo spectral method to the iteration scheme shown in Eqs. (2.24)-(2.27). This then gives

$$\sum_{j=1}^{n}\sum_{p=0}^{m_j} \beta_{i,j}^{[p]} f_j^{(p)} + \mathcal{N}_i\left[\boldsymbol{F}_1, \boldsymbol{F}_2, \ldots, \boldsymbol{F}_n\right] = \mathcal{G}_i, \tag{2.31}$$

where $\beta_{i,j}^{(p)}$ are constants coefficients of $f_j^{(p)}$, the derivative of $f_j (j = 1, 2, \ldots, n)$ that is in the ith equation for $i = 1, 2, \ldots, n$. The iteration scheme used in Eqs.(2.24-2.27) can e expressed as

$$\begin{aligned}\sum_{j=1}^{i}\sum_{p=0}^{n_j} \beta_{i,j}^{[p]} f_{j,r+1}^{(p)} &= \mathcal{G}_i - \sum_{j=1+1}^{m}\sum_{p=0}^{n_j} \beta_{i,j}^{[p]} f_{j,r+1}^{(p)} \\ &-\mathcal{N}_i\left[F_{1,r+1}, \ldots, F_{i-1,r+1}, F_{i,r}, \ldots, F_{m,r}\right]\end{aligned} \tag{2.32}$$

for $i = 1, 2, \ldots, m$. Using the Eq. (2.30) on Eq. (2.32) and the boundary conditions we otain the spectral Gauss-Seidel relaxation method iteration scheme given by

$$\begin{aligned}\sum_{j=1}^{i}\sum_{p=0}^{n_j} \beta_{i,j}^{[p]} \mathbf{D}^{(\mathbf{p})} \mathbf{F}_{\mathbf{j,r+1}} &= \mathcal{G}_{\mathbf{i}} - \sum_{\mathbf{j=1+1}}^{\mathbf{m}}\sum_{\mathbf{p=0}}^{\mathbf{n_j}} \beta_{\mathbf{i,j}}^{[\mathbf{p}]} \mathbf{D}^{(\mathbf{p})} \mathbf{F}_{\mathbf{j,r}} \\ &-\mathcal{N}_i\left[\mathbf{F}_{\mathbf{1,r+1}}, \ldots, \mathbf{F}_{\mathbf{i-1,r+1}}, \mathbf{F}_{\mathbf{i,r}}, \ldots, \mathbf{F}_{\mathbf{m,r}}\right]\end{aligned} \tag{2.33}$$

subject to

$$\sum_{j=1}^{m}\sum_{p=0}^{n_j-1}\alpha_{\nu,j}^{(p)}\sum_{k=0}^{N}\mathbf{D}_{\mathbf{N},\mathbf{k}}^{\mathbf{p}}\mathbf{f}_{\mathbf{j},\mathbf{r+1}}(\tau_{\mathbf{k}})=\mathbf{K}_{\mathbf{a},\nu},\ \nu=\mathbf{1},\mathbf{2},\ldots,\mathbf{m_a}, \tag{2.34}$$

$$\sum_{j=1}^{m}\sum_{p=0}^{n_j-1}\gamma_{\sigma,j}^{[p]}\sum_{k=0}^{N}\mathbf{D}_{\mathbf{N},\mathbf{k}}^{\mathbf{p}}\mathbf{f}_{\mathbf{j},\mathbf{r+1}}(\tau_{\mathbf{k}})=\mathbf{K}_{\mathbf{b},\sigma},\ \sigma=\mathbf{1},\mathbf{2},\ldots,\mathbf{m_b}, \tag{2.35}$$

The substitution of previously known functions decouples the system of equations and an efficient iteration scheme is created giving accurate results. The spectral relaxation method (SRM) will be implemented in Chapter 7.

2.6. Review of the quasi-linearization method (QLM)

This quasi-linearization method was introduced by Bellman and Kalaba, (1965) as a generalization of the Newton Raphson method for solving a system of nonlinear equations (Saeed and Rehman, 2014). In the implementation of the quasi-linearization method the nonlinear terms are expanded using the Taylor series expansion. The spectral based quasi-linearization schemes have been successfully applied to a range of fluid based ODEs (Motsa et al., 2014). The quasi-linearization method is a powerful tool for finding approximate solutions of nonlinear systems and converges quadratically to the solution (Wang and Kong, 2013).

Consider the general nth order nonlinear differential equation of the form

$$\mathcal{L}\left[y(x),y^{(1)}(x),y^{(2)}(x),\ldots,y^{(n)}(x)\right] + \mathcal{F}\left[y(x),y^{(1)}(x),y^{(2)}(x),\ldots,y^{(n)}(x)\right]=\psi(x). \tag{2.36}$$

Where ψ is a known function of the independent variable x and $y(x)$ is an unknown function. The operators $\mathcal{L}$ and $\mathcal{F}$ represent linear and nonlinear components of the governing equation, respectively. We assume that Eq. (2.36) is to be solved for $x\in[a,b]$ subject to the boundary conditions

$$B_a(y(a), y^{(1)}(a), y^{(2)}(a), \ldots, y^{(n-1)}(a)) = 0, \tag{2.37}$$

$$B_b(y(b), y^{(1)}(b), y^{(2)}(b), \ldots, y^{(n-1)}(b)) = 0, \tag{2.38}$$

where B_a and B_b are linear operators. Following Motsa and Sibanda (2013) we assume that the true solution of Eq. (2.36) is $y_\alpha(x)$ and that $y_\gamma(x)$ is an initial approximation that is sufficiently close to $y_\alpha(x)$. After expanding $\mathcal{F}$ using Taylor series up to the first order about $y_\gamma, y'_\gamma, \ldots, y^{(n)}_\gamma$ we obtain the following system

$$\begin{aligned}\mathcal{L}\left[y_{r+1}, y^{(1)}_{r+1}, \ldots, y^{(n)}_{r+1}\right] + \sum_{s=0}^{n}(y^{(s)}_{r+1} - y^{(s)}_r)\frac{\partial \mathcal{F}}{\partial y^{(s)}}(y_r, y^{(1)}_r, \ldots, y^{(n)}_r) \\ +\mathcal{F}\left(y_r, y^{(1)}_r, \ldots, y^{(n)}_1\right) = 0.\end{aligned} \tag{2.39}$$

The iterative scheme Eq. (2.39) is the quasi-linearization method of Bellman and Kalaba (1965). At this stage the iterative scheme can be used with any method such as finite differences, finite elements and spline collocation method. In this thesis we demonstrate the power of spectral method and use the Chebyshev spectral collocation method (Makanda et al., 2013; Makanda et al., 2014b; Motsa and Sibanda, 2013). The quasi-linearization method (QLM) will be implemented in Chapter 6.

2.7. Strengths and weaknesses of the quasi-linearization method (QLM)

The QLM provides better and accurate results as compared to the variational iteration method and the decomposition method (Saeed and Rehman, 2014). The construction of iterative schemes is simple and straight forward. The method does not require any calculation of polynomials like in the case of the ADM (Alaidarous et al., 2013). The QLM can handle different types of nonlinearities (Saeed and Rehman, 2014). The QLM only requires one inversion of the Jacobian (Alaidarous et al., 2013). The limitation of the method is that when

solving problems in fluid flow one needs to have an idea of the boundary layer thickness. The number of collocation points needed for convergence is sometimes not easy to obtain.

2.8. Bivariate quasi-linearization method (BQLM)

The bivariate spectral quasi-linearization was proposed by Motsa et al. (2014). In this section we review the bivariate spectral quasi-linearization Method (BSQLM) for solutions of nonlinear PDEs of the form.

$$\frac{\partial v}{\partial \tau} = \mathcal{H}(v, \frac{\partial v}{\partial \eta}, \frac{\partial^2 v}{\partial \eta^2}, \ldots, \frac{\partial^n v}{\partial \eta^n}). \tag{2.40}$$

With the physical region $\tau \in [0, T]$, $\eta \in [a, b]$ (Motsa et al.,2014). n is the order of differentiation, $v(\eta, \tau)$ is the required solution and $\mathcal{H}$ is the nonlinear operator which contains all spatial derivatives of v. The implementation of this method can be carried out in four stages namely, transformation of domains, splitting of nonlinear operators, quasi-linearization and collocation.

The physical region, $\tau \in [0, T]$ is converted to the region $t \in [-1, 1]$ using the linear transformation $\tau = T(t + 1)/2$ and $\eta \in [a, b]$ is converted to the region $x \in [-1, 1]$ using the linear transformation for the bivariate spectral quasi-linearization method (BSQLM) for solutions of nonlinear PDEs of the form

$$\eta = \frac{1}{2}(b - a)x + \frac{1}{2}(b + a), \tag{2.41}$$

Equation (2.40) can be written as

$$\frac{\partial v}{\partial t} = \mathcal{H}(v, \frac{\partial v}{\partial x}, \frac{\partial^2 v}{\partial x^2}, \ldots, \frac{\partial^n v}{\partial x^n}), \quad t \in [-1, 1], x \in [-1, 1] \tag{2.42}$$

Further following Motsa et al. (2014) the solution procedure can be approximated by

the bivariate interpolation polynomial of the form

$$v(x,t) \approx \sum_{i=0}^{N_x} \sum_{j=0}^{N_t} v(x_i, t_j) L_i(x) L_j(t), \tag{2.43}$$

which interpolates $v(x,t)$ at selected points both the x and t directions defined by

$$\{x_i\} = \{\cos(\frac{\pi_i}{N_x})\}_{i=0}^{N_x}, \{t_j\} = \{\cos(\frac{\pi_j}{N_t})\}_{j=0}^{N_t}, \tag{2.44}$$

The Chebyshev-Gauss-Lobatto grid points ensure that there is simple conversion of continuous derivatives, in both space and time, to discrete derivatives at the grid points. The functions $L_i(x)$ are the characteristic Lagrange cardinal polynomials

$$L_i(x) = \prod_{i=0, i\neq k}^{N_x} \frac{x - x_k}{x_i - x_k}, \tag{2.45}$$

where

$$L_i(x_k) = \delta_{ik}, \tag{2.46}$$

The function $L_j(t)$ is defined in a similar manner. Before linearizing Eq. (2.42), it is convenient to split $\mathcal{H}$ into its linear and nonlinear components and rewrite the governing equations in the form

$$\mathcal{F}[v, v', \ldots, v^{(n)}] + \mathcal{G}[v, v', \ldots, v^{(n)}] - \dot{v} = 0, \tag{2.47}$$

where the dot and primes denote the time and space derivatives, respectively, $\mathcal{F}$ in the

linear operator, and $\mathcal{G}$ is the nonlinear operator. Assuming that the difference $v_{r+1} - v_r$ and all its derivatives are small, we first approximate the nonlinear operator $\mathcal{G}$ using linear terms of the Taylor series or linearizing by the QLM due to Bellman and Kalaba (1965),

$$\mathcal{G}[v, v', \ldots, v^{(n)}] \approx \mathcal{G}[v_r, v'_r, \ldots, v_r^{(n)}] + \sum_{k=0}^{n} \frac{\partial \mathcal{G}}{\partial v^{(k)}}(v_{r+1}^{(k)} - v_r^{(k)}), \tag{2.48}$$

where r and $r+1$ denote previous and current iterations, respectively.

Eq. (2.48) can be written as

$$\begin{aligned}&\mathcal{G}[v, v', \ldots, v^{(n)}] \approx \mathcal{G}[v_r, v'_r, \ldots, v_r^{(n)}] + \\ &\sum_{k=0}^{n} \psi_{k,r}[v_r, v'_r, \ldots, v_r^{(n)}] v_{r+1}^{(k)} - \sum_{k=0}^{n} \psi_{k,r}[v_r, v'_r, \ldots, v_r^{(n)}] v_r^{(k)},\end{aligned} \tag{2.49}$$

where

$$\psi_{k,r}[v_r, v'_r, \ldots, v_r^{(n)}] = \frac{\partial \mathcal{G}}{\partial v^{(k)}}[v_r, v'_r, \ldots, v_r^{(n)}], \tag{2.50}$$

Substituting Eq. (2.49) into Eq. (2.47) we have

$$\mathcal{F}[v_{r+1}, v'_{r+1}, \ldots, v_{r+1}^{(n)}] + \sum_{k=0}^{n} \psi_{k,r} v_{r+1}^{(k)} - \dot{v}_{r+1} = R_r[v_r, v'_r, \ldots, v_r^{(n)}], \tag{2.51}$$

where

$$R_r[v_r, v'_r, \ldots, v_r^{(n)}] = \sum_{k=0}^{n} \psi_{k,r} v_r^{(k)} - \dot{v}_{r+1} - \mathcal{G}[_r, v'_r, \ldots, v_r^{(n)}]. \tag{2.52}$$

An important step in the implementation of the solution as in Motsa et al. (2014), is the evaluation of the time derivatives at the grid points $t_j(j = 0, 1, \ldots, N_t)$ and spatial derivatives at the grid points $x_i(i = 0, 1, \ldots, N_x)$. The values of the time derivatives at the Chebyshev-Gauss-Lobatto points (x_i, t_j) are computed as

$$\begin{aligned}\left.\frac{\partial v}{\partial t}\right|_{x=x_i,t=t_j} &= \sum_{p=0}^{N_x}\sum_{k=0}^{N_t} v(x_p,t_k)L_p(x_i)\frac{dL_k(t_j)}{dt} \\ &= \sum_{k=0}^{N_t} v(x_i,t_k)d_{jk} = \sum_{k=0}^{N_t} d_{jk}v(x_i,t_k),\end{aligned} \tag{2.53}$$

where $d_{jk} = dL_k(t_j)/dt$ is the standard first derivative Chebyshev differentiation matrix of size $(N_t+1)\times(N_t+1)$. The values of the space derivatives at the Chebyshev-Gauss-Lobatto points $(x_i, t_j)(i = 0, 1, 2, \ldots, N_x)$ are computed as

$$\begin{aligned}\left.\frac{\partial v}{\partial x}\right|_{x=x_i,t=t_j} &= \sum_{p=0}^{N_x}\sum_{k=0}^{N_t} u(x_p,t_k)L_p(x_i)\frac{dL_p(x_i)}{dx}L_k(t_j) \\ &= \sum_{p=0}^{N_x} v(x_p,t_j)D_{jp} = \sum_{p=0}^{N_x} D_{jp}v(x_p,t_k),\end{aligned} \tag{2.54}$$

where $D_{ip} = dL_p(x_i)/dx$ is the standard first derivative Chebyshev differentiation matrix of size $(N_x + 1) \times (N_x + 1)$. Similarly, for the nth order derivative, we have

$$\left.\frac{\partial v}{\partial x}|\right|_{x=x_i,t=t_j} = \sum_{p=0}^{N_x} D_{ip}v(x_p,t_j) = \mathbf{D}^n\boldsymbol{V}_j, \tag{2.55}$$

$$i = 0, 1, 2, \ldots, N_x, \tag{2.56}$$

where the vector $\boldsymbol{V}_j$ is defined as

$$\boldsymbol{V}_j = [v_j(x_0), v_j(x_1), \ldots, v_j(x_{N_x})]^T, \tag{2.57}$$

the superscript T denotes the matrix transpose. Substituting Eq. (2.55) into Eq. (2.51) we have

$$\begin{aligned} F[\boldsymbol{V}_{r+1,j}, \boldsymbol{V}'_{r+1,j}, \ldots, \boldsymbol{V}^{(n)}_{r+1,j}] + \sum_{k=0}^{n} \Phi_{k,r} \boldsymbol{V}^{(k)}_{r+1,j} \\ - \sum_{k=0}^{N_t} d_{jk} \boldsymbol{V}_{r+1,k} = R_r[\boldsymbol{V}_{r,j}, \boldsymbol{V}'_{r,j}, \ldots, \boldsymbol{V}^{(n)}_{r,j}], \end{aligned} \tag{2.58}$$

for $j = 0, 1, 2, \ldots, N_t$, where $\boldsymbol{V}^{(n)}_{r+1,j} = \boldsymbol{D}^n \boldsymbol{V}_{r+1,j}$

$$\Phi_{k,r} = \begin{bmatrix} \phi_{k,r}(x_0, t_j) & & & \\ & \phi_{k,r}(x_1, t_j) & & \\ & & \ddots & \\ & & & \phi_{k,r}(x_{N_x}, t_j) \end{bmatrix} \tag{2.59}$$

The initial condition for Eq. (2.42) corresponds to $\tau_{N_t} = -1$ and we can express Eq. (2.58) as

$$\begin{aligned} F[\boldsymbol{V}_{r+1,j}, \boldsymbol{V}'_{r+1,j}, \ldots, \boldsymbol{V}^{(n)}_{r+1,j}] + \sum_{k=0}^{n} \Phi_{k,r} \boldsymbol{V}^{(k)}_{r+1,j} \\ - \sum_{k=0}^{N_t - 1} d_{jk} \boldsymbol{V}_{r+1,k} = \boldsymbol{R}_j \end{aligned} \tag{2.60}$$

where

$$\boldsymbol{R}_j = R_r[\boldsymbol{V}_{r,j}, \boldsymbol{V}'_{r,j}, \ldots, \boldsymbol{V}^{(n)}_{r,j}] + d_{jN_t}\boldsymbol{V}_{N_t}, \tag{2.61}$$

$$j = 0, 1, 2, \ldots, N_t - 1 \tag{2.62}$$

Motsa et al. (2014) expressed Eq. (2.60) as the $N_t(N_x+1) \times N_t(N_x+1)$ matrix system

$$\begin{bmatrix} A_{0,0} & A_{0,1} & \ldots & A_{0,N_t-1} \\ A_{1,0} & A_{1,1} & \ldots & A_{1,N_t-1} \\ \vdots & \vdots & \ddots & \vdots \\ A_{N_t-1,0} & A_{N_t-1,1} & \ldots & A_{N_t-1,N_t-1} \end{bmatrix} \begin{bmatrix} V_0 \\ V_1 \\ \vdots \\ V_{N_t-1} \end{bmatrix} = \begin{bmatrix} R_0 \\ R_1 \\ \vdots \\ R_{N_t-1} \end{bmatrix} \tag{2.63}$$

where

$$A_{i,i} = F[\boldsymbol{I}, \boldsymbol{D}, \ldots, \boldsymbol{D}^{(n)}] + \sum_{k=0}^{n} \Phi_{k,r}\boldsymbol{D}^{(k)} - d_{i,i}\boldsymbol{I}, \tag{2.64}$$

$$A_{i,j} = -d_{i,j}\boldsymbol{I}, \text{when} i \neq j, \tag{2.65}$$

and $\boldsymbol{I}$ is the identity matrix of size $(N_x+1)\times(N_x+1)$. We use Eq. (2.43) to approximate the solution $u(x,t)$. The bivariate quasi-linearization method (BQLM) will be implemented in Chapters 6 and 8

2.9. Strengths and weaknesses of the BSQLM

The accuracy of the BSQLM improves with the increase in the number of collocation points N_x (Motsa et al., 2014). In the examples given by Motsa et al. (2014) it was shown that the errors up to the order of 10^{-14} were obtained using few collocation points in both x and t directions variables $N_t \leq 10, N_x \leq 10$. The computational time for the BSQLM is small up to a fraction of a second. The iteration scheme takes about three to four iterations to converge fully.

3

Radiation effects on magnetohydrodynamic Newtonian flow due to an exponentially stretching sheet

3.1. Introduction

In this chapter we start by examining the literature concerning fluid flow on an exponentially stretching sheet. In particular we will focus on radiation effects on magnetohydrodynamic Newtonian flow due to an exponentially stretching sheet. We then investigate the effects of the magnetic, radiation and viscous dissipation parameters on fluid flow and heat transfer characteristics of an exponentially stretching sheet. In these cases, the momentum, energy and mass transfer equations thus obtained are coupled and nonlinear. By using suitable similarity variables these equations are then converted into coupled ordinary differential equations. These are then solved both analytically and numerically, by applying the Runge-Kutta-Fehlberg with shooting method (see sections 1.1.2 & 1.1.7) and Newton-Raphson scheme to the problem. In this chapter we present the analytical zero order approximate solution for the momentum equation and the energy equation solution is obtained in terms of the confluent hyper geometric functions. The accuracy of the solution so obtained is then estimated by comparing it with that obtained by the successive linearization method (Kameswaran et al., 2012).

3.2. Review of literature on fluid flow on exponentially stretching sheet

Laminar flow occurs when fluid flows in parallel layers without disruption. The study of this type of fluid flow is important as it leads to understanding of flows with disruption within its layers referred to as turbulent flow. A stretching surface is a region held at one end and moves as a result of a pull at one end. Laminar boundary layer fluid flow occurs in many industrial situations, such as glass fibre and paper production; polymer extrusion from dyes; drawing, tinning and annealing of copper wires, and bath cooling of metallic plates. Consequently, the study of laminar boundary layer flow over a stretching sheet was studied as far back as the 1970s, and this interest still continues. Many authors have investigated the flow of a linear stretching sheet for example Crane (1970), Gupta and Gupta (1977), Grubka and Bobba (1985), Dutta and Gupta (1987), Siddappa and Abel (1985), Chen and Char (1988), Laha et al. (1989), Chakrabarti and Gupta (1979), Andersson et al. (1992), Siddheshwar and Mahabaleswar (2005), Abel and Mahesha (2008), Abel et al. (2009a), and Abel et al. (2009b) In this chapter we focus on nonlinear systems, in particular exponential stretching sheet.

Chapter 3 – Radiation effects on magnetohydrodynamic Newtonian flow due to an exponentially stretching sheet

Many practical situations involve a nonlinear stretching sheet. With this in mind it is often necessary to consider the velocity of the sheet to vary exponentially with the distance from the extrusion slit. Early studies on exponentially stretching sheets by Magyari and Keller (1999) showed that fluid flow and heat transfer characteristics derived this way could be compared with those from well- known literature. The Elbashbeshy (2001) considered a perforated sheet, and examined the effect of wall mass suction on the fluid flow and heat transfer over an exponentially stretching surface. The influence of thermal radiation on the boundary layer flow due to an exponentially stretching sheet was studied by Sajid and Hayat (2008). Khan (2006) presented an elegant solution of the viscoelastic boundary layer flow over an exponentially stretching sheet, giving it in terms of Whittaker's function. The characteristic of an industrial extrusion product will depend on the rates of stretching and cooling the sheet. Consequently, to ensure the desired characteristic, external means of controlling the flow are necessary, as could be done with a magnetic field. Early work in external control by means of magnetic fields was directed at controlling plasmas (Tonks, 1939). Sanjayanand and Khan (2006) studied the heat and mass transfer in a viscoelastic boundary layer flow over an exponentially stretching sheet.

In fluid flow, we can consider two types of fluids, Newtonian fluids and Non-Newtonian fluids. In this chapter we investigate the flow of a Newtonian fluid. Newtonian fluids are whose viscous stresses are linearly proportional to the local strain rate. Newtonian fluids have the simplest mathematical models than non-Newtonian fluids. There are no real fluids that conform to these mathematical models but, however water and air are assumed to be Newtonian fluids (Bar-Meir, 2009). We describe non-Newtonian fluids in Chapter 4. Studies on Newtonian fluids include the work of Alim et al. (2006) who studied pressure work effect in Newtonian fluid, Awad et al. (2011) studied convection from a cone in Newtonian fluid, Boivin et al. (2000) investigated Navier-Stokes equations on incompressible flows, Chen (2004) investigated heat and mass transfer in a Newtonian fluid. Gebhart (1962) studied viscous dissipation on natural convection in a Newtonian fluid.

Magnetohydrodynamics (MHD) is the study of magnetic properties of electrically conducting fluids; these include electrolytes, liquid metals and plasmas. When conductive fluids flow across a magnetic field, a current is induced polarizing the fluid and in turn change the

magnetic field itself Radiation is the transmission of energy in the form of waves or particles through space or through a material medium. As already mentioned, the temperature and rate of cooling of extrusion product will affect its properties. Analysis has been directed at thermal radiation magnetohydrodynamics. Until recently, radiation effects on exponentially stretching sheets had received little attention. However, if polymer extrusion takes place in a thermally controlled environment, thermal radiation and magnetic field effects will affect fluid flow characteristics. Studies on thermal radiation and magnetohydrodynamics include the work of Reddy et al. (2012) who investigated radiation effects on MHD flow past an exponentially accelerated isothermal vertical plate with uniform mass diffusion in the presence of heat source. They observed that the velocity of fluid flow decreases with an increase in the magnetic parameter. This is due to a resistive drag force that tends to resist the fluid flow, thus reducing the fluid flow velocity. Ishak (2011) studied the MHD boundary layer flow due to an exponentially stretching sheet with radiation effect. Pavlov (1974) considered the magnetohydrodynamic flow of an incompressible viscous fluid over a linearly stretching surface. Sarpakaya (1961) extended Pavlov's work to non-Newtonian fluids. Most of the earlier work neglected radiation effects making it necessary to conduct this study. If the polymer extrusion process is placed in a thermally controlled environment, radiation becomes important. Many researchers have considered the effect of thermal radiation on flows over stretching sheets (see, for instance, Raptis, 1988; Raptis and Perdikis, 1998). Bidin and Nazar (2009) studied the boundary layer flow over an exponentially stretching sheet with thermal radiation. Reddy and Reddy (2011) studied the effect of thermal radiation on magnetohydrodynamic flow due to an exponentially stretching sheet. Elbashbeshy and Dimian (2002) analyzed boundary layer flow in the presence of radiation and heat transfer over the wedge with viscous dissipation. Raptis et al. (2004) studied the effect of thermal radiation on the magnetohydrodynamic flow of a viscous fluid past semi-infinite stationary plate and Hayat et al. (2007) extended the analysis to a second grade fluid.

Analysis has also been directed to viscous dissipation, which may affect the rate of cooling. Viscous dissipation is the energy produced by work done between fluid layers. This heat energy produced affect the fluid temperature and therefore important to consider. In most studies in fluid flow, viscous mechanical dissipation is neglected. A number of authors have considered viscous heating effects on Newtonian flows. Zueco (2007) studied

the dissipation effects on unsteady free convection over vertical porous plate. The influence of viscous dissipation on a grey absorbing-emitting fluid flowing past moving vertical plate has been studied by Suneetha et al. (2009). Kameswaran et al. (2012) studied the effect of the viscous dissipation on magnetohydrodynamic nanofluid flow due to a stretching or shrinking sheet. With regard to viscous dissipation, we note the work done by Partha et al. (2005) who studied the effect of viscous dissipation on the mixed convection heat transfer from an exponentially stretching surface. They observed a rapid growth in the non-dimensional skin friction coefficient with the mixed convection parameter. In addition to a magnetic field and thermal radiation, one has to consider the viscous dissipation effects due to frictional heating between fluid layers. Gebhart (1962) and Gebhart and Mollendorf (1969) investigated the effect of viscous dissipation in natural convection processes, they observed that the effect of viscous dissipation is predominant in both vigorous natural convection and mixed convection processes. Vajravelu and Hadjinicalaou (1993) studied the heat transfer characteristics over a stretching surface with viscous dissipation in the presence of internal heat generation or absorption. Abel et al. (2009a) investigated viscous dissipation in a Newtonian fluid; in this study it was revealed that viscous dissipation increase thermal energy in the fluid.

In brief, this section has shown that firstly, it is necessary to study radiation effects on magnetohydrodynamic fluid flow over an exponentially stretching sheet, secondly, considering viscous dissipation on Newtonian fluid requires is required and finally, the use of an appropriate numerical method to solve the governing differential equations. In this chapter we investigate the effects of magnetic, radiation, and viscous dissipation parameters on the fluid flow and heat transfer characteristics of an exponentially stretching sheet. These aspects will be considered in the formulation of the problem of fluid flow on an exponentially stretching sheet.

3.3. Mathematical formulation of fluid flow on an exponentially stretching sheet

Consider the two dimensional magnetohydrodynamic flow of a Newtonian fluid over a stretching sheet, as shown in Figure 3.1. The origin of the system is located at the extrusion slit, from which the sheet is drawn. The x-axis is taken along the continuous stretching surface

and points in the direction of motion. The y-axis is perpendicular to the sheet. A magnetic field of strength B is applied perpendicular to the sheet.

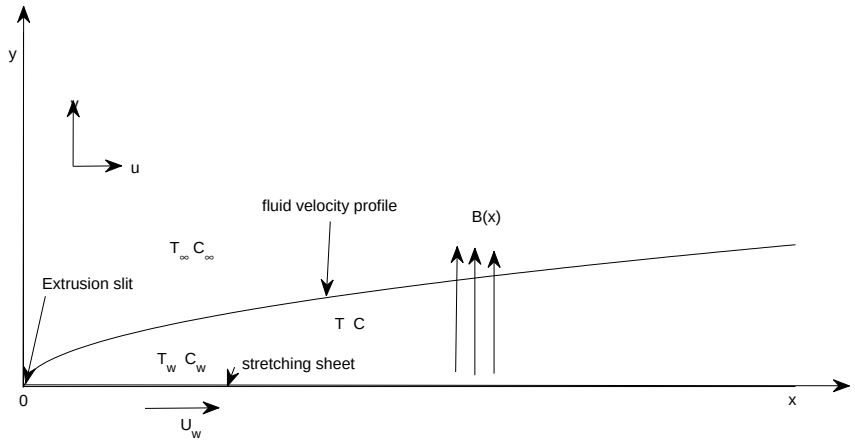

Figure 3.1: Schematic diagram showing the exponentially stretching sheet

The sheet velocity is assumed to vary as an exponential function of the distance from the slit. The temperature of the fluid (T) and concentration (C) of the solute are also assumed to be exponential functions of the distance x from the slit. Accordingly under the usual boundary layer approximation, and subject to radiation and viscous dissipation effects, the equations governing the momentum, heat and mass transport can be written as

$$\frac{\partial u}{\partial x}+\frac{\partial v}{\partial y}=0, \tag{3.1}$$

$$u\frac{\partial u}{\partial x}+v\frac{\partial u}{\partial y}=\nu\frac{\partial^2 u}{\partial y^2}-\frac{\sigma B(x)^2}{\rho}u, \tag{3.2}$$

$$u\frac{\partial T}{\partial x}+v\frac{\partial T}{\partial y}=\alpha\frac{\partial^2 T}{\partial y^2}-\frac{1}{\rho C_p}\frac{\partial q_r}{\partial y}+\frac{\sigma B(x)^2}{\rho C_p}u^2+\frac{\nu}{C_p}\left(\frac{\partial u}{\partial y}\right)^2, \tag{3.3}$$

$$u\frac{\partial C}{\partial x}+v\frac{\partial C}{\partial y}=D\frac{\partial^2 C}{\partial y^2}, \tag{3.4}$$

where u and v are the velocity components of the velocity of fluid flow in the x and y directions respectively, ν is the kinematic viscosity, ρ is the fluid density, σ is the electrical

conductivity of the fluid, T is the temperature of the fluid, C is the solute concentration, $\alpha = k/\rho C_p$ is the thermal diffusivity, k is the thermal conductivity, C_p is the specific heat at constant pressure, q_r is the radiative heat flux and D is the soulte diffusivity.

The boundary conditions for equations (3.1) - (3.4) take the form:

$$\begin{aligned} &\text{At} \quad y = 0 : u = U_w = U_0 e^{\frac{x}{L}}, \quad v = 0, \quad T = T_w = T_\infty + T_0 e^{\frac{2x}{L}}, \quad C = C_w = C_\infty + C_0 e^{\frac{2x}{L}} \\ &\text{As} \quad y \to \infty : u \to 0, \quad T \to T_\infty, \quad C \to C_\infty \end{aligned} \tag{3.5}$$

Here the subscripts w, ∞ refer to the stretching surface and free stream conditions respectively, T_0 and C_0 are positive constants, U_0 is the characteristic fluid velocity and L is the characteristic length of the stretching surface.

To facilitate a similarity solution, the magnetic field $B(x)$ is assumed to be of the form

$$B(x) = B_0 e^{\frac{x}{2L}}, \tag{3.6}$$

where B_0 is a constant. It is also assumed that the fluid is weakly electrically conducting so that the induced magnetic field is negligible. Following Rosseland's approximation the radiative heat flux q_r is modeled as

$$q_r = -\frac{4\sigma^*}{3k^*}\frac{\partial T^4}{\partial y}, \tag{3.7}$$

where σ^* is the Stefan-Boltzman constant and k^* is the mean absorption coefficient. Assuming that the temperature differences within the fluid flow are sufficiently small such that T^4 may be expressed as a linear function of temperature, $T^4 \equiv 4T_\infty^3 T - 3T_\infty^4$, then we have

$$\frac{\partial q_r}{\partial y} = -\frac{16\sigma^* T_\infty^3}{3k^*}\frac{\partial T}{\partial y}. \tag{3.8}$$

The continuity equation (3.1) is satisfied by introducing a stream function ψ such that

$$u = \frac{\partial \psi}{\partial y}, \quad v = -\frac{\partial \psi}{\partial x}. \tag{3.9}$$

In order for the governing equations to apply to all similar systems regardless of units, the following similarity variables are introduced:

$$\left.\begin{aligned} &u = U_0 e^{\frac{x}{L}} f_\eta(\eta), \quad v = -\left(\frac{\nu U_0}{2L}\right)^{\frac{1}{2}} e^{\frac{x}{2L}}[f(\eta) + \eta f_\eta(\eta)], \\ &T = T_\infty + T_0 e^{\frac{2x}{L}}\theta(\eta), \quad C = C_\infty + C_0 e^{\frac{2x}{L}}\phi(\eta), \\ &\eta = \left(\frac{U_0}{2\nu L}\right)^{\frac{1}{2}} y e^{\frac{x}{2L}}, \end{aligned}\right\} \tag{3.10}$$

where η is the similarity variable, $f(\eta)$ is the dimensionless stream function, $\theta(\eta)$ is the dimensionless temperature and $\phi(\eta)$ is the dimensionless concentration.

On using Eqs. (3.6), (3.8) and (3.10), Eqs. (3.2) - (3.5) transform into the following two-point boundary value problem:

$$f_{\eta\eta\eta} + f f_{\eta\eta} - 2f_\eta^2 - M f_\eta = 0, \tag{3.11}$$

$$\left(1 + \frac{4}{3}K\right)\theta_{\eta\eta} + Pr\left(f\theta_\eta - 4f_\eta\theta\right) + GbPr\left(M f_\eta^2 + f_{\eta\eta}^2\right) = 0, \tag{3.12}$$

$$\phi_{\eta\eta} + Sc\left(f\phi_\eta - 4f_\eta\phi\right) = 0, \tag{3.13}$$

$$f(0) = 0, \quad f_\eta(0) = 1, \quad f_\eta(\infty) \to 0, \tag{3.14}$$

$$\theta(0) = 1, \quad \theta(\infty) \to 0, \tag{3.15}$$

$$\phi(0) = 1, \quad \phi(\infty) \to 0. \tag{3.16}$$

The non-dimensional constants appearing in Eqs. (3.11) - (3.13) are the magnetic parameter M, radiation parameter K, Prandtl number Pr, Gebhart number Gb and Schmidt number Sc; respectively defined as

$$M = \frac{2\sigma B_0^2 L}{\rho U_0}, \quad K = \frac{4\sigma^* T_\infty^3}{k^* k}, \quad Pr = \frac{\rho\nu C_p}{k},$$
$$Gb = \frac{U_0^2}{C_p T_0}, \quad Sc = \frac{\nu}{D}.$$

We have formulated the governing equations for a fluid flow on an exponentially stretching sheet and the assumptions under which they apply. We now derive expressions for important parameters which are the skin friction, heat transfer and mass transfer coefficients.

3.4. Skin friction, heat and mass transfer coefficients

The parameters of engineering interest in heat and mass transport problems are the skin friction coefficient C_f, the heat transfer coefficient (local Nusselt number) Nu_x and the mass transfer coefficient (local Sherwood number) Sh_x. These parameters respectively characterize the stretching surface drag, wall heat and mass transfer rates.

The shear stress at the stretching surface (sometimes referred to as the wall shear stress) τ_w is then given by

$$\tau_w = -\mu \left[\frac{\partial u}{\partial y}\right]_{y=0} = -\frac{\mu U_0}{L}\sqrt{\frac{Re}{2}} e^{\frac{3x}{2L}} f''(0)\,, \tag{3.17}$$

where μ is the coefficient of viscosity and $Re = \dfrac{LU_0}{\nu}$ is the Reynolds number. The skin friction coefficient is defined as

$$C_f = \frac{2\tau_w}{\rho U_w^2} \tag{3.18}$$

and using Eq. (3.17) in Eq. (3.18) we obtain

$$\frac{C_f\sqrt{Re_x/2}}{\sqrt{x/L}} = -f''(0). \tag{3.19}$$

The heat flux at the stretching surface (sometimes referred to as the wall heat flux) is given by

$$q_w = -k\left[\frac{\partial T}{\partial y}\right]_{y=0} = \frac{-k\,(T_w - T_\infty)}{L}\sqrt{\frac{Re}{2}} e^{\frac{x}{2L}}\theta'(0)\,, \tag{3.20}$$

where k is the thermal conductivity of the fluid. The heat transfer coefficient (Nusselt number) is defined as

$$Nu_x = \frac{x}{k}\frac{q_w}{T_w - T_\infty}. \tag{3.21}$$

Using Eq. (3.20) in Eq. (3.21) the dimensionless wall heat transfer rate is obtained as

$$\frac{Nu_x}{\sqrt{x/L}\sqrt{Re_x/2}} = -\theta'(0)\,. \tag{3.22}$$

The mass flux at the stretching surface (sometimes referred to as the wall mass flux) is given

by

$$J_w = -D\left[\frac{\partial C}{\partial y}\right]_{y=0} = \frac{-D\left(C_w - C_\infty\right)}{L}\sqrt{\frac{Re}{2}}e^{\frac{x}{2L}}\phi'\left(0\right) \tag{3.23}$$

The Sherwood number is defined as

$$Sh_x = \frac{x}{D}\frac{J_w}{C_w - C_\infty}. \tag{3.24}$$

Using Eq. (3.23) in Eq. (3.24) the dimensionless wall mass transfer rate is obtained as

$$\frac{Sh_x}{\sqrt{x/L}\sqrt{Re_x/2}} = -\phi'\left(0\right). \tag{3.25}$$

In Eqs. (3.19), (3.22) and (3.25) Re_x represents the local Reynolds number which is defined as $Re_x = \dfrac{xU_w}{\nu}$.

We have calculated the important engineering parameters which are the skin friction, heat transfer, and mass transfer coefficients. Thus, we are now ready to solve equations analytically.

3.5. Analytical solutions for the momentum, heat and mass transfer equations

The momentum boundary layer equation, which was established in Eq. (3.11) is partially decoupled from the energy and species equations as follows. Integrating Eq. (3.11) once with respect to η over the interval $[0,\ \eta]$, we obtain

$$f_{\eta\eta} + ff_\eta = -s + \int_0^\eta \left[3f_\eta^2 + Mf_\eta\right]\ d\eta, \tag{3.26}$$

where $s = -f_{\eta\eta}(0)$. Letting $\eta \to \infty$ we obtain

$$s = \int_0^\infty \left[3f_\eta^2 + Mf_\eta\right]\ d\eta. \tag{3.27}$$

Again, integrating Eq. (3.26) once, we obtain

$$f_\eta + \frac{1}{2}f_\eta^2 = 1 - s\eta + \int_0^\eta \left[\int_0^{\eta_1} \left[3f_{\eta_2}^2 + Mf_{\eta_2}\right]\, d\eta_2\right]\, d\eta_1. \tag{3.28}$$

The solution procedure for Eq. (3.28) can be reduced to the sequential solutions of the Riccati-type equation, of the form

$$f_\eta^{(n)} + \frac{1}{2}f^{(n)^2} = RHS\left[f_\eta^{(n-1)}\right]. \tag{3.29}$$

This iteration procedure proceeds by substituting suitable zero-order approximations, of the form $f_\eta^{(0)}(\eta)$, in the right hand side of Eq. (3.28). We assume a zero-order approximation as

$$f_\eta^{(0)}(\eta) = e^{-s_0\eta}, \tag{3.30}$$

which satisfies the condition at infinity. Integrating Eq. (3.30) with respect to η and using the condition $f_\eta^{(0)}(0) = 0$ we get

$$f_\eta^{(0)}(\eta) = \frac{1 - e^{-s_0\eta}}{s_0}. \tag{3.31}$$

Using the above solution in Eq. (3.27), the approximate value of s can be obtained as

$$s_0 = \sqrt{\frac{3}{2} + M}, \quad f_{\eta\eta}^{(0)}(0) = -s_0. \tag{3.32}$$

Now substituting all the derivatives of the zero-order approximation $f_\eta^{(0)}(\eta)$ into the right hand side of Eq. (3.28), we obtain the first-order iteration $f_\eta^{(1)}$ as follows:

$$f_\eta^{(1)} + \frac{1}{2}f^{(1)^2} = 1 + \frac{3}{4s_0^2}\left[e^{-2s_0\eta} - 1\right] + \frac{M}{s_0^2}\left[e^{-s_0\eta} - 1\right]. \tag{3.33}$$

Further, we assume that the first-order iterate satisfies the boundary conditions on f as given in Eq. (3.14). The above nonlinear Riccati type equation can be solved in terms of a confluent hyper geometric Whittaker function, as discussed by Khan (2006). However we restrict ourselves here to the zero-order solution. A similar restriction will apply to the heat

and mass transport equations. We have obtained the analytical solution for the momentum equation, thus we now find the analytical solution for the heat transfer equation.

To find the analytical solution for the heat transfer Eq. (3.12) we use the zero-order approximations of f and f_η given by equation Eq. (3.34). We further need to introduce a new variable ξ, which represents temperature change across the boundary layer.

$$\xi = -\frac{Pr}{s_0^2} e^{-s_0 \eta}. \tag{3.34}$$

Accordingly, Eq. (3.12) and the thermal boundary conditions Eq. (3.15) take the form:

$$\left(1 + \tfrac{4}{3}K\right) \xi \theta_{\xi\xi} + \left(1 + \tfrac{4}{3}K - Pr^* - \xi\right) \theta_\xi + 4\theta = -\tfrac{Gb}{Pr} s_0^2 \left(M + s_0^2\right) \xi, \tag{3.35}$$

$$\theta(-Pr^*) = 1, \quad \theta(0^-) \to 0. \tag{3.36}$$

where $Pr^* = Pr/s_0^2$ is the modified Prandtl number. The solution of Eq. (3.35) is assumed to have the form of

$$\theta(\xi) = \theta_c(\xi) + \theta_p(\xi)$$

where $\theta_c(\xi)$ is the complementary solution and $\theta_p(\xi)$ is the particular solution. The complementary solution of Eq. (3.35) is obtained in terms of confluent hyper geometric function in the following form

$$\theta_c(\xi) = C_0 \, \xi^\alpha \, M\left[\alpha - 4, \; \alpha + 1, \; \frac{-\xi}{1 + \frac{4}{3}K}\right], \tag{3.37}$$

where

$$M[a, \; b, \; z] = \sum_{r=0}^{\infty} \frac{a(a+1)\ldots(a+r-1)}{b(b+1)\ldots(b+r-1)} \frac{z}{r!}$$

is Kummer's function (Abramowitz and Stegun, 1972) and

$$\alpha = \frac{Pr^*}{1 + \frac{4}{3}K}.$$

The particular solution is obtained as

$$\theta_p(\xi) = a_0 \xi^2 + a_1 \xi^3 + a_2 \xi^4, \tag{3.38}$$

where

$$\begin{aligned} a_0 &= -\left(\frac{Gb}{Pr^*}\right)\frac{M+s_0^2}{4\left(1+\frac{4}{3}K\right)-2Pr^*}, \\ a_1 &= \frac{-2a_0}{9\left(1+\frac{4}{3}K\right)-3Pr^*}, \\ a_2 &= \frac{-a_1}{16\left(1+\frac{4}{3}K\right)-4Pr^*}. \end{aligned}$$

Now, the complete solution can be written as

$$\theta(\xi) = \theta_c(\xi) + \theta_p(\xi). \tag{3.39}$$

Making use of the boundary conditions Eq. (3.36) and rewriting the solution in terms of the variable η, we get

$$\theta(\eta) = C_1\,\frac{e^{-s_0\eta\alpha}\;M\left[\alpha-4,\;\alpha+1,\;-\alpha e^{-s_0\eta}\right]}{M\left[\alpha-4,\;\alpha+1,\;-\alpha\right]} + a_0 Pr^{*2}e^{-2s_0\eta} - a_1 Pr^{*3}e^{-3s_0\eta} + a_2 Pr^{*4}e^{-4s_0\eta}, \tag{3.40}$$

where

$$C_1 = 1 - a_0 Pr^{*2} + a_1 Pr^{*3} - a_2 Pr^{*4}.$$

We have found the analytical solution for the heat transfer equation; we therefore proceed to find the analytical solution for the mass transfer equation.

We now find the analytical solution for the mass transfer Eq. (3.13) and again introducing a new variable ζ for convenience, which represents concentration change across the boundary layer, given by

$$\zeta = -\frac{Sc}{s_0^2}e^{-s_0\eta}, \tag{3.41}$$

Eq. (3.13) and the thermal boundary conditions in Eq. (3.16) take the form:

$$\zeta\phi_{\zeta\zeta} + \left(1 - Sc^* - \zeta\right)\phi_\zeta + 4\phi = 0, \tag{3.42}$$

$$\phi(-Sc^*) = 1, \quad \phi(0^-) \to 0. \tag{3.43}$$

where $Sc^* = Sc/s_0^2$ is the modified Schmidt number. Following the solution procedure discussed in the case of energy equation, the solution of Eq. (3.42) is obtained in terms of confluent hyper geometric function as

$$\phi(\eta) = \frac{e^{-s_0 Sc^* \eta}\, M\left[Sc^* - 4,\ Sc^* + 1,\ -Sc^* e^{-s_0\eta}\right]}{M\left[Sc^* - 4,\ Sc^* + 1,\ -Sc^*\right]} \tag{3.44}$$

3.6. Numerical solution procedure

The set of non-linear differential Eqs. (3.11) - (3.13) subject to the boundary conditions Eqs. (3.14) - (3.16) were solved numerically using the efficient Runge-Kutta-Fehlberg method with a shooting technique as described in Pal and Shivakumara (2006). The critical step in this method is choosing an appropriate finite value of $\eta \to \infty$. Consequently, in order to determine $\eta \to \infty$ for the boundary value problem described by Eqs. (3.11) - (3.13), we start with initial estimated values for a particular set of physical parameters, so as to obtain $f''(0)$, $\theta'(0)$ and $\phi'(0)$. The solution procedure is repeated with another large value of $\eta \to \infty$ until for each $f''(0)$, $\theta'(0)$ and $\phi'(0)$, pairs of successive values of skin friction, heat transfer and mass transfer coefficients differ by a specified significant digit. The value of η may change for a different set of physical parameters. Once the appropriate value of η is determined, the coupled boundary value problem given by Eqs. (3.11) - (3.13) is solved numerically, using the method of superposition. By this method the third-order nonlinear equation Eq. (3.11), second order equations Eqs. (3.12) and (3.13) have been reduced to seven ordinary differential equations as follows:

$$\begin{aligned}
f_1' &= f_2, \quad f_2' = f_3 \\
f_3' &= 2f_2^2 + Mf_2 - f_1 f_3 \\
f_4' &= f_5 \\
f_5' &= -\frac{Pr}{\left(1 + \frac{4}{3}K\right)}\left[f_1 f_5 - 4f_2 f_4 + Gb(Mf_2^2 + f_3^2)\right] \\
f_6' &= f_7 \\
f_7' &= Sc\,(4f_2 f_6 - f_1 f_7)
\end{aligned} \tag{3.45}$$

where

$$f_1 = f, \quad f_2 = f', \quad f_3 = f'', \quad f_4 = \theta, \quad f_5 = \theta', \quad f_6 = \phi, \quad f_7 = \phi', \tag{3.46}$$

and a prime denote differentiation with respect to η. The boundary conditions now become

$$f_1 = 0, \quad f_2 = 1, \quad f_3 = s_1, \quad f_4 = 1, \quad f_5 = s_2, \quad f_6 = 1,$$
$$f_7 = s_3, \quad \text{at} \quad \eta \to 0 \tag{3.47}$$
$$f_2 = 0, \quad f_4 = 0, \quad f_6 = 0, \quad \text{as} \quad \eta \to \infty, \tag{3.48}$$

where s_1, s_2 and s_3 are determined such that $f_2(\infty) = 0$, $f_4(\infty) = 0$ and $f_6(\infty) = 0$. Thus, to solve this system of equations we require six initial conditions. However, we have only three initial conditions for f and two initial conditions for θ and ϕ. Consequently the conditions $f''(0), \theta'(0), \phi'(0)$ are to be determined by the shooting method, using the initial guess values s_1, s_2 and s_3 until the conditions $f_2(\infty) = 0, f_3(\infty) = 0$ and $f_5(\infty) = 0$ are satisfied. In this chapter, we employed the shooting technique with Runge-Kutta-Fehlberg scheme to determine two more unknowns in order to convert the boundary value problem to an initial value problem. Once all the six initial conditions were determined the resulting differential equations were integrated, using an initial value solver. For this purpose, the fifth-order Runge-Kutta-Fehlberg integration scheme was used.

3.7. Results and discussion

In the previous sections MHD fluid flow over an exponentially stretching sheet has been modelled and analytical and numerical solutions were thus obtained for the effects of radiation and viscous dissipation. Similarity transformations were applied to the governing partial differential equations of fluid flow, heat and mass transfer thereby a system of nonlinear ordinary differential equations. From this system, the zero-order approximate analytical solution for the dimensionless stream function f has been obtained. Solutions of the heat transfer and mass transfer equations were obtained in terms of confluent hyper geometric functions. The numerical solution was then obtained by the Runge-Kutta-Fehlberg integration scheme with the shooting method and the Newton-Raphson schemes. Finally, the accuracy of the numerical method could be established by comparing the analytical solution with the numer-

ical solution. To this end, this chapter shows the results for the two methods. In comparing these methods we adopt well known fluid flow parameters for Newtonian fluids. In particular we use the values of the Prandtl number, $Pr = 1 - 7$ for a variety of Newtonian fluids at 20^oC, similarly we use a range of acceptable values of the magnetic parameter, $M = 1$, the radiation parameter, $K = 0.5$ and the Gebhart number, $GB = 0.2$ as in Shateyi and Marewo (2014).

The results are presented in two categories. Firstly, Tables 3.1 - 3.3 show the skin friction, and the heat and mass transfer coefficients obtained both analytically and numerically, or compared with previously published results. The tables and their discussions are followed by Figures 3.2 - 3.6 which show the effects of magnetic, radiation and viscous dissipation parameters on the velocity $f'(\eta)$, temperature, $\theta(\eta)$ and concentration, $\phi(\eta)$ profiles. η is the similarity space variable.

Table 3.1: A comparison of skin friction coefficient obtained by analytical method with the one by Runge-Kutta method for different values of M

M	$-f''(0)$	
	Analytical	Numerical
0	1.22474	1.281809
1	1.58114	1.629178
2	1.87083	1.912620
3	2.12132	2.158736
5	2.54951	2.581130
10	3.39116	3.41529

Table 3.1 provides values of the skin friction coefficient $-f''(0)$ for different values of the magnetic parameter M. From the data in Table 3.1 it can be seen that Increasing values of M results in the increase in the values of the skin friction coefficient. This means that increasing the strength of the magnetic field will result in considerable opposition to, or drag on, the fluid flow. This occurs because the increased magnetic field results in a Lorenz drag, which in turn increases the value of the skin friction coefficient. In practical terms this means that one could reduce the fluid flow rate by increasing the strength of the magnetic field, which could be useful solution to controlling the final properties of the extrusion properties.

Table 3.2: Comparison of the heat transfer coefficient obtained by Runge-Kutta method with one obtained by analytical method for different values of M, Gb and K for a fixed values of $Pr = 7$

M	K	Gb	$-\theta'(0)$	
			Analytical	Numerical
0	0.5	0.2	3.82684	3.822508
1			3.48576	3.483155
2			3.19181	3.191131
3			2.92781	2.928577
1	0	0.2	4.56379	4.556219
	0.5		3.48576	3.483155
	1		2.90556	2.905805
	2		2.25649	2.260503
	3		1.88314	1.889815
1	0.5	0	3.94905	3.946604
		0.1	3.71740	3.714879
		0.2	3.48576	3.483155
		0.5	2.79082	2.787982
		1	1.63260	1.629360

Table 3.2 shows the effect of the magnetic field M, radiation K, and viscous dissipation Gb, on the dimensionless heat transfer coefficient $-\theta'(0)$. It is evident from the data in the table that increasing the values of all three parameters will reduce value of the heat transfer coefficient. This means that increasing the strength of the magnetic field, exposing the fluid flow regime to thermal radiation and considering the thermal energy produced by frictional heating due to fluid flow, will result in the reduction of the heat transfer coefficient. This occurs because the magnetic field reduce fluid flow rate causing a slow heat transfer from the wall to the fluid. Increasing both thermal radiation and viscous dissipation increase the temperature of the fluid, this also reduces heat transfer from the wall to the fluid. Practically controlling the heat transfer on the stretching sheet on its fluid interface can be achieved by increasing the magnetic field strength and increasing the temperature of the fluid.

In Table 3.3 data shows the effect of different values of the magnetic parameter M and the Schmidt number Sc on the mass transfer coefficient $-\phi'(0)$. It can be seen that increasing the magnetic parameter M, results in the decrease of the mass transfer coefficient whereas

Table 3.3: Comparison of the mass transfer coefficient obtained by Runge-Kutta method with one obtained by analytical method for different values of M, Sc

M	Sc	$-\phi'(0)$	
		Analytical	Numerical
0	1	1.79791	1.805684
1		1.69115	1.699309
2		1.60312	1.611410
3		1.52781	1.535984
1	1	1.69115	1.699309
	2	2.58672	2.589044
	5	4.34813	4.344825
	10	6.32456	6.318568

the opposite trend is observed for the Schmidt number. This occurs because increasing the magnetic field reduces the fluid flow rate; this in turn does not facilitate species transfer, thereby reducing the mass transfer coefficient. The significance of this result is that if controlling of species transfer is required a magnetic field can be used. This result also reveals that species transfer can be controlled by the change in the kinematic viscosity of the fluid. The Schmidt number is the ratio of the kinematic viscosity and the solute diffusivity.

In all three tables (3.1 to 3.3), we note that the results confirm a good agreement between the analytical and the numerical results. This validates using the Runge-Kutta-Fehlberg integration scheme with shooting method.

Table 3.4: Comparison of the skin friction coefficient for different values of M for fixed values of $Pr = Sc = K = Gb = 0$

M	$-f''(0)$	
	Reddy and Reddy (2011)	Runge-Kutta
0	1.28213	1.28181
1	1.62918	1.62918
2	-	1.91262
3	-	2.15874
4	-	2.37937

The skin friction coefficients $-f''(0)$ are shown in Table 3.4 for different values of mag-

netic parameter (M) in the absence of the other physical parameters (i.e., $Pr = Sc = K = Gb = 0$). We observe that the skin friction coefficient increases with an increase in magnetic parameter. In particular, it is noteworthy that the value of the skin-friction coefficient, in the non-magnetic ($M = 0$) and magnetic ($M = 1$) cases, are in good agreement with the results by Reddy and Reddy (2011).

The five analyses of the effect of the magnetic parameter M on velocity and temperature profiles, and the effect of the radiation parameter K and Gebhart number Gb on temperature profiles is shown next in Figures 3.2-3.6.

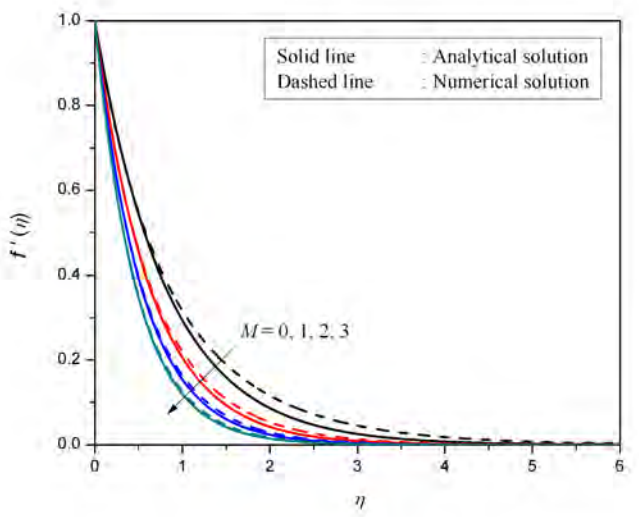

Figure 3.2: Effect of magnetic parameter (M) on velocity profiles $f'(\eta)$ for $Pr = 7, Gb = 0.2, K = 0.5, Sc = 1$

The variation of the magnetic parameter M on velocity profiles is shown in Figure 3.2. We notice that increasing the value of the magnetic parameter will reduce the velocity of the fluid in the boundary layer region. This is due to an increase in the Lorentz force which acts on the flow regime. The Lorenz force is against motion, so it is responsible for slowing down the motion of the fluid in the boundary layer region. Once again, we note that these results are similar to those obtained by Reddy and Reddy (2011).

The variation of the temperature distribution with the magnetic parameter is shown in Figure 3.3. It can be seen that the thermal boundary layer thickness increases with increasing values of the magnetic parameter M. This effect can be explained by the opposing force

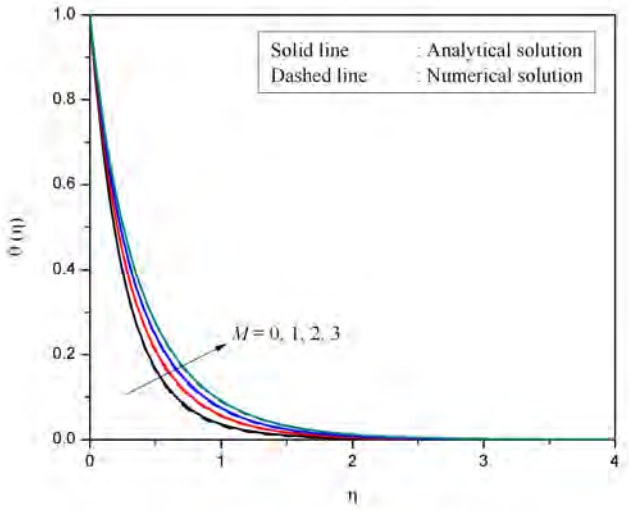

Figure 3.3: Effect of M on temperature profiles $\theta(\eta)$ for $Pr = 7, Gb = 0.2, K = 0.5, Sc = 1$

introduced in Eq. (3.12) in the form of the Lorentz drag, which contributes to increased frictional heating between the fluid layers, and hence energy is released in the form of heat. This results in thickening of the thermal boundary layer.

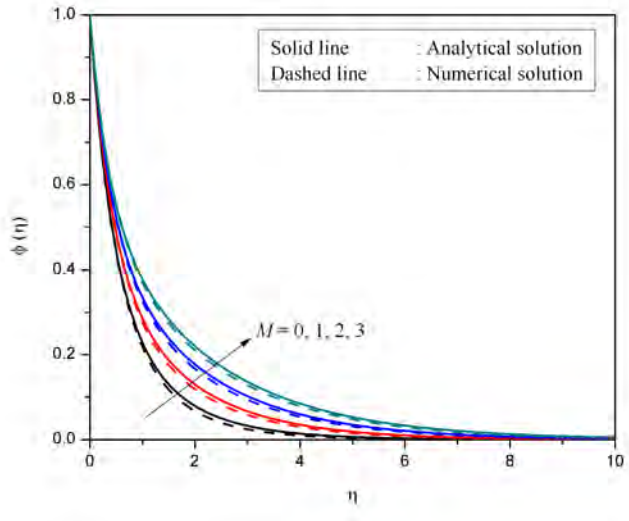

Figure 3.4: Effect of M on concentration profiles $\phi(\eta)$ for $Pr = 7, Gb = 0.2, K = 0.5, Sc = 1$

The effect of magnetic parameter M on the concentration profile $\phi(\eta)$ is shown in Figure 3.4. It is observed that increasing the values of M results in the thickening of the species boundary layer. It has been observed that in Figure 3.3 that increasing the magnetic param-

eter results in the increase in the temperature profiles, this causes increased temperature in the boundary layer. In turn, the effect causes motion across the boundary layer causing the movement of species.

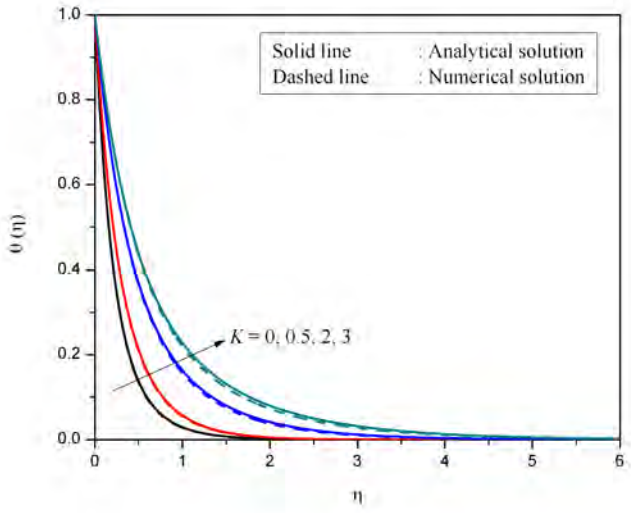

Figure 3.5: Effect of radiation parameter on temperature profiles $\theta(\eta)$ for $Gb = 0.2, M = 1, Pr = 7, Sc = 1$

The influence of the thermal radiation parameter K on the temperature profile $\theta(\eta)$ is shown in Fig. 3.5. It is clear that increased thermal radiation enhances the temperature in the boundary layer region. Thus radiation parameter K defines the relative contribution of conduction heat transfer to thermal radiation transfer. Thus radiation should be kept at its minimum in order to facilitate better cooling environment.

The effect of the Gebhart number Gb on the temperature profile $\theta(\eta)$ is shown in Figure 3.6. It is clear that the temperature in the boundary layer region (in other words) increases with an increase in the viscous dissipation parameter.

For all figures 3.2 - 3.6, we note that because the energy equation Eq. (3.12) is partially decoupled from the momentum and species conservation equations, the parameters affecting the energy equation, namely, the Prandtl number, radiation parameter and the Gebhart number, do not alter the velocity and concentration profiles. In all five figures, we also observe good agreement between the analytical and numerical solutions, particularly in Figures 3.2 - 3.6. Thus we can be confident that analytical and numerical results showed good agreement.

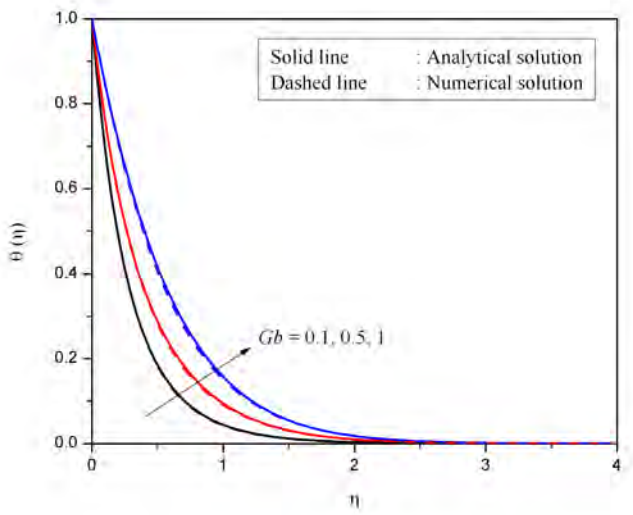

Figure 3.6: Effect of viscous dissipation on temperature profile $\theta(\eta)$ for $Pr = 7, M = 1, K = 0.5, Sc = 1$

This means that the Runge-Kutta-Fehlberg integration scheme is accurate.

We also found that the effect of increasing the magnetic parameter is to reduce the velocity of the fluid in the boundary layer, while the magnetic parameter increasing it results in reducing heat transfer rates. These findings show a trend similar to that of Shateyi (2014) but the results appear to be new findings, unreported until now. Under some limiting conditions $Pr, Sc, K; Gb$ are zero, the current results agree well with those available in the literature.

3.8. Summary

In this chapter the problem of radiation effects on magnetohydrodynamic Newtonian fluid flow due to an exponentially stretching sheet was considered. The results on the effect of various physical parameters were as follows; increasing the magnetic parameter supressed velocity profiles while it increased both temperature and concentration profiles. Increasing the radiation parameter increased temperature profiles. Increasing the Gebhart number increased temperature profiles.

The consideration of magnetohydrodynamic fluid flow due to an exponentially stretching sheet was fairly new in this area. The calculation of the analytical solutions in this problem

is a new contribution to the study of fluid flow under these conditions. These analytical solutions can be used as basic solutions in the extensions of this problem.

In this chapter the Runge-Kutta-Fehlberg method together with the shooting technique was used to find numerical solutions of the fluid flow equations arising in an exponentially stretching sheet problem. The exact solutions were found in terms of hyper geometric functions and a comparison of the analytical solution and numerical results show the accuracy of the Runge-Kutta-Fehlberg method. More accurate numerical solutions were observed in the energy equation of the problem than in the momentum equation. The numerical solution of the problem was compared to those available in the literature and was found to be in excellent agreement.

4

Natural convection from a cone embedded in viscoelastic fluid in porous medium with viscous dissipation

4.1. Introduction

In this chapter we examine fluid flow from a heated cone embedded in viscoelastic fluid. We focus on the effects of natural convection, viscoelasticity, and fluid flow and heat transfer characteristics in porous medium. In this study the momentum and energy equations are coupled and nonlinear. The equations are solved numerically using the successive linearization method. The accuracy of the solution is determined by comparing it to previously published results in the literature.

4.2. Review of literature on fluid flow from a cone in viscoelastic fluid

In this chapter we study the flow of a viscoelastic fluid, other studies include those of Cortell (2006a) who investigated flow and heat transfer of a viscoelastic fluid over a stretching sheet and Abbas et al. (2008) who considered unsteady viscoelastic fluid flow. In addition, fluid flow has been studied for other geometrical shapes, such as cylinders, wedges, vertical walls, and parallel plates. Among these we note the study on a horizontal cylinder Anwar et al. (2008); wedge by Hsiao (2011); Hsiao (2012) studied vertical stretching walls; Damseh et al. (2008) and Hayat et al. (2008) studied vertical surface; Jha and Ajibade (2012) studied fluid flow between parallel plates.

Chapter 4 – Natural convection from a cone embedded in viscoelastic fluid in porous medium with viscous dissipation

In this chapter we consider fluid flow around a heated cone embedded in a viscoelastic fluid. Under these conditions a buoyant driven fluid flow is induced in the vicinity of the cone. This situation arises in the design of automatic cooking machinery and in automotive designs in which silicone is sometimes applied to different parts that are normally exposed to heat. Other studies on cone geometry include those of Alim et al. (2006), who studied pressure work effect from a cone in a Newtonian fluid, Awad et al. (2011) investigated effects of cross diffusion from a downward pointing cone in a Newtonian fluid, Cheng (2011a) studied Soret and Dufour effects of flow past a cone in a Newtonian fluid, Cheng (2011b) studied a permeable cone in a micropolar fluid, Ece (2005) investigated natural convection in a Newtonian fluid, and Kairi and Murthy (2011) considered flow past a cone in a non-Newtonian fluid in porous medium.

Chapter 4 – Natural convection from a cone embedded in viscoelastic fluid in porous medium with viscous dissipation

The study of Newtonian fluids has been discussed in Chapter 3. In this chapter we discuss the study of non-Newtonian fluids. Non-Newtonian fluids differ from Newtonian fluids in viscosity, which is defined in terms of shear or tensile stresses; it is the fluid's ability to resist gradual deformation. The relationship between shear rate and shear stress can be time dependent (Bar-Meir, 2009). Some non-Newtonian fluids are exhibit plastic or elastic behavior, examples include paint, ketchup, soup, blood and toothpaste. The studies on non-Newtonian fluid were carried out by among others Abel et al. (2001) who studied viscoelastic fluids, Chamkha and Rashad (2012) investigated flow of nanofluid, Ramachandra et al. (2013) studied Casson fluid flow, Datta (1964) investigated flow of Reiner-Rivlin fluid and Dinarvand et al. (2014) studied micropolar fluid flow.

Natural or free convection fluid flow occurs when there are density differences in different regions created by temperature differences. Fluid molecules close to the heated surface expand and become less dense and rise, colder molecules then move to the heated surface thereby inducing motion. Natural convection fluid flow has practical application such as thermal insulation, extraction of petroleum resources and the so called "fracking", metal processing, performance of lubricants, application of paints and extrusion of plastic sheets. The study of natural convection in non-Newtonian fluids has been studied by, among others Hsiao (2011) who studied mixed convection (fluid flow driven by both natural and forced convection) for viscoelastic fluid past a porous wedge, Kasim et al. (2011) investigated free convection boundary layer fluid flow of a viscoelastic fluid in the presence of heat generation, Massoudi et al. (2008) studied natural convection fluid flow of generalized non-Newtonian fluid between two vertical walls. Olajuwon (2011) studied the free convection heat and mass transfer in a magnetohydrodynamic fluid flow of a non-Newtonian fluid in the presence of thermal radiation and thermal diffusion, wherein it was shown that increasing the non-Newtonian parameter causes reduction in the rate of the fluid flow and mass transfer, although heat transfer increased. Sajid et al. (2010) investigated fully developed mixed convection flow of a viscoelastic fluid between permeable parallel vertical plates.

Viscoelastic fluids may be classified as non-Newtonian fluids. These fluids have both viscous and elastic properties. Properties of Newtonian and non-Newtonian fluids have been described in the previous chapter (see section 3.1). Examples of viscoelastic fluids include

toothpaste, custard, earth's mantle and jelly. In some studies, the authors have assumed that fluids are more viscous than elastic, so they neglect the fluid's elastic properties in the energy equation or in the viscous dissipation term (for example, Abel., 2008). In other studies which considered the same assumption include the works of Cortell (2011) power-law fluid; Kameswaran et al. (2012) micropolar fluid; Andersson (1992) viscoelastic fluid; Lawrence and Rao (1995) viscoelastic fluid; Abel et al. (2001) viscoelastic fluid; Siddheshwar and Mahabaleswar (2005) viscoelastic fluid. In this work we consider the elastic properties of the viscoelastic fluid. This will be shown in the momentum and energy equations of the governing equations.

Viscous dissipation effects are also considered in this chapter. As discussed earlier in the previous chapter, viscous dissipation is the energy produced by work done between fluid layers. Further to the studies mentioned in the previous chapter on viscous dissipation, other studies include those of Jha and Ajibade (2012) who investigated the effects of viscous dissipation on natural convection flow between parallel plates with time periodic boundary conditions. Chen (2010) studied fluid flow in viscoelastic fluid with energy dissipation; Hsiao (2012) investigated viscoelastic fluid flow with viscous dissipation.

A porous medium is a material containing pores; these pores are often filled with a fluid or gas. A porous medium is characterized by its permeability. The ability of a fluid to flow in a porous medium is enhanced by the medium's permeability. The flow through a porous medium is described by Darcy's law, which states that the fluid flow rate is directly proportional to the pressure gradient. If the flow is laminar with Reynolds number less than unity or ten, then Darcy's law applies. If the Reynolds number exceeds ten, Darcy's law still apply. When inertial effects start to be in effect when Reynolds number ($Re > 100$), then the fluid flow in porous medium becomes non-Darcy. Studies have been done in porous media by among others Awad et al. (2011), Butt (2012), Cheng (2011a), Kairi and Murthy (2011) and Singh and Agarwal (2012) who studied heat transfer in a non-Newtonian fluid over an exponentially stretching sheet through porous medium with thermal radiation and elastic deformation under the effect of magnetic field.

As can be seen from the literature cited above, it appears that no analysis has yet been published concerning natural convection from a cone embedded in viscoelastic fluid

in porous medium with viscous dissipation, under the given boundary conditions. These boundary conditions consider the linear surface temperature and no-slip conditions on the surface of the cone. The free stream conditions are considered to be at a lower temperature than at the surface of the cone. The model used in this chapter was based on the work put forward by Ece (2005) in the study of heat and mass transfer in a Newtonian fluid. We extend the model to take into account the fluid flow from a cone in a viscoelastic fluid in a porous medium, and furthermore viscous dissipation.

In brief this section has shown that firstly, it is necessary to study natural convection from a cone, secondly, considering viscous dissipation in non-Newtonian fluid is required and finally the use of the successive linearization method to obtain a numerical solution of the problem. In this chapter we investigate the effects of varying the Prandtl number, Eckert number, permeability and viscoelastic parameters on velocity and temperature profiles. These aspects will be considered in the formulation of the problem of fluid flow on natural convection from a cone in viscoelastic fluid.

4.3. Mathematical formulation of fluid flow from a cone in viscoelastic fluid

We consider the two dimensional downward pointing solid cone embedded in a viscoelastic fluid filled in a porous medium as shown in Figure 4.1. The origin of the system is located at the cone vertex. The vertex angle of the cone is $2\theta^*$. The x axis is taken along the surface of the cone and y axis is perpendicular to the x axis from the origin.

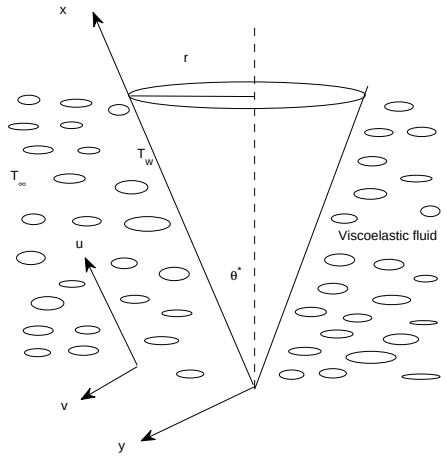

Figure 4.1: Schematic diagram of a cone in viscoelastic fluid

The temperature at the surface of the cone is $T_w(> T_\infty)$ is assumed to vary linearly as a function of the distance from the origin. The free stream conditions are maintained at T_∞, the fluid has a constant viscosity ν. . The velocity components u and v are in the directions of x and y respectively. Accordingly under the usual boundary layer approximation, and subject to viscous dissipation effects, the governing equations of the momentum and energy equations are given by (see Ece, 2005)

$$\frac{\partial}{\partial x}(ru) + \frac{\partial}{\partial y}(rv) = 0, \tag{4.1}$$

$$u\frac{\partial u}{\partial x} + v\frac{\partial u}{\partial y} = \nu\frac{\partial^2 u}{\partial y^2} - \frac{\nu}{K}u - k_o\left(u\frac{\partial^3 u}{\partial x \partial y^2} + v\frac{\partial^3 u}{\partial y^3} + \frac{\partial u}{\partial x}\frac{\partial^2 u}{\partial y^2} - \frac{\partial^2 u}{\partial x \partial y}\frac{\partial u}{\partial y}\right) + g\beta_T(T - T_\infty)\cos\theta^*, \tag{4.2}$$

$$u\frac{\partial T}{\partial x} + v\frac{\partial T}{\partial y} = \alpha\frac{\partial^2 T}{\partial y^2} + \frac{\nu}{C_p}\left(\frac{\partial u}{\partial y}\right)^2 + \frac{k_0}{\rho C_p}\left(u\frac{\partial^2 u}{\partial x \partial y}\frac{\partial u}{\partial y} + v\frac{\partial^2 u}{\partial y^2}\frac{\partial u}{\partial y}\right), \tag{4.3}$$

where $r = x\sin\theta^*$, g is the acceleration due to gravity, ν is the kinematic viscosity for the fluid, k_o is the non-Newtonian parameter of the viscoelastic fluid, β_T is the coefficient of thermal expansion, α is the thermal diffusivity, C_p is the specific heat capacity for the fluid, ρ is the density of the fluid and K is the permeability coefficient of the porous medium. The

boundary conditions are given as

$$\text{at } y = 0,\ u = v = 0,\ T = T_w(x) = T_\infty + A_0\left(\frac{x}{L}\right) \tag{4.4}$$

$$\text{as } y \to \infty, \frac{\partial u}{\partial y},\ u \to 0,\ T \to T_\infty. \tag{4.5}$$

where $A_0 > 0$ is a constant and $L > 0$ is the characteristic length of the cone surface and the subscripts w and ∞ refers to the cone surface and free stream conditions respectively.

We introduce the non-dimensional variables

$$X = \frac{x}{L}, \qquad Y = \frac{Gr^{\frac{1}{4}}y}{L}, \qquad R^* = \frac{r}{L}, \tag{4.6}$$

$$U = \frac{u}{U_0}, \quad V = \frac{Gr^{\frac{1}{4}}v}{U_0} \tag{4.7}$$

$$\overline{T} = \frac{T - T_\infty}{T_w - T_\infty}, \quad Gr = \left(\frac{U_0 L}{\nu}\right)^2. \tag{4.8}$$

where $U_0 = [g\beta\cos\phi L(T_w - T_\infty)]^{\frac{1}{2}}$. Using Eqs. (5.7) - (4.8) in Eqs. (4.1)-(4.3) gives the following equations

$$\frac{\partial}{\partial X}(R^*U) + \frac{\partial}{\partial Y}(R^*V) = 0, \tag{4.9}$$

$$U\frac{\partial U}{\partial X} + V\frac{\partial U}{\partial Y} = \frac{\partial^2 U}{\partial Y^2} - \Lambda\left(U\frac{\partial^3 U}{\partial X \partial Y^2} + V\frac{\partial^3 U}{\partial Y^3} + \frac{\partial U}{\partial X}\frac{\partial^2 U}{\partial Y^2} - \frac{\partial^2 U}{\partial X \partial Y}\frac{\partial U}{\partial Y}\right) + \overline{T} - \frac{\nu U}{K}, \tag{4.10}$$

$$U\frac{\partial \overline{T}}{\partial X} + V\frac{\partial \overline{T}}{\partial Y} = \frac{1}{Pr}\frac{\partial^2 \overline{T}}{\partial Y^2} + Ec(\frac{\partial U}{\partial Y})^2 + \Lambda Ec\left(U\frac{\partial^2 U}{\partial X \partial Y}\frac{\partial U}{\partial Y} + V\frac{\partial^2 U}{\partial Y^2}\frac{\partial U}{\partial Y}\right). \tag{4.11}$$

where, $R^* = X\sin\theta^*$, $\Lambda = (k_0 U_0/\nu L)$ is the viscoelastic parameter known as the Deborah number, Gr is the Grashof number and $Pr = \nu/\alpha$ is the Prandtl number, $Ec = (U_0^2/C_p A)$ is the Eckert number. The corresponding boundary conditions are given as

$$U = V = 0, \quad \overline{T} = X \quad \text{at} \quad Y = 0, \tag{4.12}$$

$$\frac{\partial U}{\partial Y}, U \to 0, \quad \overline{T} \to 0 \quad \text{as} \quad Y \to \infty. \tag{4.13}$$

We now introduce the stream function $\psi = XR^* f(Y)$ and $\overline{T} = X\theta(Y)$ defined by

$$U = \frac{1}{R^*}\frac{\partial \psi}{\partial Y}, \qquad V = -\frac{1}{R^*}\frac{\partial \psi}{\partial X}. \tag{4.14}$$

Substituting Eqs. (4.14) and the similarity variables in Eqs. (4.9)-(4.11) gives the following ordinary differential equations

$$f''' + 2ff'' - (f')^2 + \theta - \gamma f' - \Lambda(2f'f''' - 2ff^{iv} - (f'')^2) = 0, \tag{4.15}$$

$$\theta'' + Pr(2f\theta' - f'\theta) + PrEcf''^2 + \Lambda PrEc(f'f''^2 - ff''f''') = 0. \tag{4.16}$$

With boundary conditions,

$$f(0) = f'(0) = 0, \quad \theta(0) = 1, \tag{4.17}$$

$$f'(\infty) \to 0, \quad f''(\infty) \to 0, \quad \theta(\infty) \to 0. \tag{4.18}$$

We have formulated the momentum and energy equations for the problem of natural convection from a cone in viscoelastic fluid. We therefore now derive the important fluid parameters which are the skin friction and the heat transfer coefficients.

4.4. Skin friction and heat transfer coefficients

It is of interest to discuss the skin friction and heat transfer coefficients in this context. The shear stress at the surface of the cone is defined as (see Olajuwon, 2011)

$$\tau_w = \mu \left[\frac{\partial u}{\partial y}\right]_{y=0} + k_0 \left[u\frac{\partial^2 u}{\partial x \partial y} - 2\frac{\partial u}{\partial x}\frac{\partial u}{\partial y}\right]_{y=0}. \tag{4.19}$$

where μ is the coefficient of viscosity. The skin friction defined as

$$C_f = \frac{\tau_w}{\frac{1}{2}\rho U_0^2}, \tag{4.20}$$

$$C_f = \frac{2X}{Gr^{\frac{1}{4}}} f''(0)(1 + 3\Lambda f'(0)). \tag{4.21}$$

The skin friction coefficient can be expressed as

$$\frac{C_f Gr^{\frac{1}{4}}}{2X} = f''(0). \tag{4.22}$$

The heat transfer rate at the surface of the cone is given by

$$q_w = -\frac{k}{X}\left[\frac{\partial T}{\partial y}\right]_{y=0}. \tag{4.23}$$

The Nusselt number can be expressed as

$$Nu = \frac{Lq_w}{k(T_w - T_\infty)}. \tag{4.24}$$

Using the non-dimensional variables Eqs. (4.17) - (4.18), the dimensionless wall heat transfer rate is given by

$$NuGr^{-\frac{1}{4}} = -\theta'(0). \tag{4.25}$$

We have derived the important parameters, the skin friction and the heat transfer coefficients, thus we now solve the governing equations numerically.

4.5. Numerical solution procedure

In this study, Eqs. (4.15) - (4.18) were solved using the successive linearization method. The inclusion of the non-Newtonian term brings about the fourth order ordinary differential equation for the momentum equation. The given boundary conditions are thus insufficient to

obtain a unique solution. To overcome this problem the system is decomposed into the zeroth, first and second order systems of the viscoelastic parameter. This type of decomposition only applied in the perturbation method in which its theory leads to an expression for the required solution in terms of a formal power series in some "small" parameter Abel et al. (2008). In this context the "small" parameter is the viscoelastic parameter. The method restricts this parameter to be small when in fact the actual values of the viscoelastic parameter do not necessarily need to be small. Anwar et al. (2008) also confirmed the same observation in which the system of differential equations was simultaneously solved and only required small values of the viscoelastic parameter.

To this effect we apply the successive linearization method to the systems of the differential equations formed, which does not require small parameters as discussed in section 1.1.5. The successive linearization method (SLM) has been found to be suitable for systems of differential equations. To elaborate, to solve the equations we seek the series solution as in Abel et al. (2008) in the form;

$$f(y) = f_0(y) + \Lambda f_1(y) + \Lambda^2 f_2(y) + \dots \tag{4.26}$$

$$\theta(y) = \theta_0(y) + \Lambda \theta_1(y) + \Lambda^2 \theta_2(y) + \dots \tag{4.27}$$

The skin friction coefficient can be computed using

$$f''(0) = f_0''(0) + \Lambda f_1''(0) + \Lambda^2 f_2''(0) + \dots \tag{4.28}$$

Then substituting Eqs. (4.26)-(4.27) into the system Eqs. (4.15)-(4.18). We then take the zeroth, first and second order of the viscoelastic parameter Λ. We obtain the following systems of differential equations. The zeroth order system is obtained by comparing coefficients of Λ^0;

$$f_0''' + 2f_0 f_0'' - f_0'^2 + \theta_0 - \gamma f_0' = 0, \tag{4.29}$$

$$\theta'' + 2Pr f_0 \theta_0' - Pr f_0' \theta_0 + PrEc f_0''^2 = 0, \tag{4.30}$$

$$f_0(0) = 0, f_0'(0) = 0, \theta_0(0) = 1, \tag{4.31}$$

$$f_0'(\infty) = 0, \theta_0(\infty) = 0. \tag{4.32}$$

The first order system is obtained by comparing coefficients of Λ

$$f_1''' + (2f_0)f_1'' - (2f_0' + \gamma)f_1' + (2f_0'')f_1 + \theta_1 = 2f_0' f_0''' - 2f_0 f_0^{iv} - f_0''^2, \tag{4.33}$$

$$\theta_1'' + (2Pr f_0)\theta_1' - (Pr f_0')\theta_1 + (2PrEc f_0'')f_0'' - (Pr\theta_0)f_1' + (2Pr\theta_0')f_1 = 0 \tag{4.34}$$

$$f_1(0) = 0, f_1'(0) = 0, f_1'(\infty) = 0, \tag{4.35}$$

$$\theta_1(0) = 0, \theta_1(\infty) = 0. \tag{4.36}$$

The second order system is obtained by comparing the coefficients of Λ^2

$$f_2''' + (2f_0)f_2'' - (2f_0)f_2' + (2f_0'')f_2 + \theta_2 = \gamma f_2' - 2f_1 f_1'' + f_1'^2, \tag{4.37}$$

$$\theta_2'' + (2Pr f_0)\theta_2' - (2Pr f_0')\theta_2 - (Pr\theta_0)f_2 - (2Pr\theta_0')f_2 = Pr f_1'\theta_1 - 2Pr f_1\theta_1' \tag{4.38}$$

$$f_2(0) = 0, f_2'(0) = 0, f_2'(\infty) = 0 \tag{4.39}$$

$$\theta_2(0) = 0, \theta_2(\infty) = 0. \tag{4.40}$$

The functions in the system Eqs. (4.29) - (**??**) may be expanded in series form as

$$f_0(y) = f_{0i}(y) + \sum_{m=0}^{i-1} f_{0m}(y), \tag{4.41}$$

$$\theta_0(y) = \theta_{0i}(y) + \sum_{m=0}^{i-1} \theta_{0m}(y). \tag{4.42}$$

where f_{0i} and θ_{0i} $(i = 1, 2, 3...)$ are unknown functions and f_{0m} and θ_{0m} are approxima-

tions that are found by successively solving the linear part of equations that are obtained after substituting Eqs. (4.41) - (4.42) into system Eqs. (4.29) - (4.40). These linear equations have the form

$$f'''_{0i} + a_{01,i-1}f''_{0i} + a_{02,i-1}f'_{0i} + a_{03,i-1}f_{0i} + a_{04,i-1}\theta_{0i} = r_{01,i-1}, \tag{4.43}$$

$$\theta''_{0i} + b_{01,i-1}\theta'_{0i} + b_{02,i-1}\theta_{0i} + b_{03,i-1}f''_{0i} + b_{04,i-1}f'_{0i} + b_{05,i-1}f_{0i} = r_{02,i-1}. \tag{4.44}$$

$$f_{0i}(0) = 0, f'_{0i}(0) = 0, \theta_{0i}(0) = 0, \tag{4.45}$$

$$f'_{0i}(\infty) = 0, \theta_{0i}(\infty) = 0, f''_{0i}(\infty) = 0. \tag{4.46}$$

The zeroth system was solved using the successive linearization method to obtain the solutions for f_0 and θ_0. The first and second order systems (4.33)-(4.36) and (4.37)-(4.40) respectively become linear. The solutions for f_1, θ_1 and f_2, θ_2 are easily obtained as follows;

$$f'''_1 + a_1 f''_1 + a_2 f'_{1i} + a_3 f_1 + a_4\theta_1 = r_1, \tag{4.47}$$

$$\theta''_1 + b_1\theta'_1 + b_2\theta_1 + b_3 f''_1 + b_4 f'_1 + b_5 f_1 = r_2. \tag{4.48}$$

$$f_1(0) = 0, f'_1(0) = 0, \theta_1(0) = 0, \tag{4.49}$$

$$f'_1(\infty) = 0, \theta_1(\infty) = 0, f''_1(\infty) = 0. \tag{4.50}$$

$$f'''_2 + a_1 f''_2 + a_2 f'_2 + a_3 f_2 + a_4\theta_2 = r_{21}, \tag{4.51}$$

$$\theta''_2 + b_{21}\theta'_2 + b_{22}\theta_2 + b_{23}f''_2 + b_{24}f'_2 + b_{25}f_2 = r_{22}. \tag{4.52}$$

$$f_{2i}(0) = 0, f'_{2i}(0) = 0, \theta_{2i}(0) = 0, \tag{4.53}$$

$$f'_{2i}(\infty) = 0, \theta_{2i}(\infty) = 0, f''_{2i}(\infty) = 0. \tag{4.54}$$

The coefficients $a_{k,i-1}, b_{k,i-1}, (k = 1, 2), r_{1,i-1}\text{and}r_{2,i-1}$ are defined as

$$a_{01,i-1} = a_{11,i-1} = a_{21,i-1} = 2\sum_{m=0}^{i-1} f_{0m}, \quad a_{02,i-1} = a_{12,i-1} = a_{22,i-1} = -(2\sum_{m=0}^{i-1} f'_{0m} + \gamma),$$

$$a_{03,i-1} = a_{13,i-1} = a_{23,i-1} = 2\sum_{m=0}^{i-1} f''_{0m}, \quad a_{04,i-1} = a_{14,i-1} = a_{24,i-1} = \mathbf{I},$$

$$b_{01,i-1} = b_{11,i-1} = b_{21,i-1} = 2Pr\sum_{m=0}^{i-1} f_{0m}, \quad b_{02,i-1} = b_{12,i-1} = b_{22,i-1} = -Pr\sum_{m=0}^{i-1} f'_{0m},$$

$$b_{03,i-1} = b_{13,i-1} = b_{23,i-1} = PrEc\sum_{m=0}^{i-1} f''_{0m}, \quad b_{04,i-1} = b_{14,i-1} = b_{24,i-1} = -Pr\sum_{m=0}^{i-1} \theta_{0m},$$

$$b_{05,i-1} = b_{15,i-1} = b_{25,i-1} = 2Pr\sum_{m=0}^{i-1} \theta'_{0m}$$

$$r_{01,i-1} = -[\sum_{m=0}^{i-1} f'''_{0m} + 2\sum_{m=0}^{i-1} f_{0m}\sum_{m=0}^{i-1} f''_{0m} - (\sum_{m=0}^{i-1} f'_{0m})^2 - \sum_{m=0}^{i-1} \theta_{0m} - \gamma\sum_{m=0}^{i-1} f'_{0m}],$$

$$r_{02,i-1} = -[\sum_{m=0}^{i-1} \theta''_{0m} + 2Pr\sum_{m=0}^{i-1} f_{0m}\sum_{m=0}^{i-1} \theta'_{0m} - Pr\sum_{m=0}^{i-1} f'_{0m}\sum_{m=0}^{i-1} \theta_{0m} + PrEc(\sum_{m=0}^{i-1} f''_{0m})^2].$$

Eqs. (4.33) - (4.36) were solved subject to certain initial approximations f_0 and θ_0. We choose these initial approximations so that they satisfy the given boundary conditions. In this case suitable initial approximations are

$$f_0(Y) = 1 - e^{-Y} - Ye^{-Y} \quad \text{and} \quad \theta_0(Y) = e^{-Y}.$$

We note that when f_i and $\theta_i (i > 1)$ have been found, the approximate solutions $f(Y)$ and $\theta(Y)$ are obtained as

$$f(Y) \approx \sum_{n=0}^{M} f_n(Y) \quad \text{and} \quad \theta(Y) \approx \sum_{n=0}^{M} \theta_n(Y), \tag{4.55}$$

where M is the order of the SLM approximation. Eqs. (4.43) and (4.54) can be solved by any numerical method. In this work the equations have been solved by the Chebyshev spectral collocation method as in Awad et al. (2011).

4.6. Results and discussion

The problem investigated in this chapter is the steady laminar fluid flow and natural convection from a cone in a viscoelastic fluid in the presence of viscous dissipation in a porous medium. The coupled nonlinear differential equations Eqs. (4.15) - (4.18) were solved numerically using the successive linearization method (SLM). In this section we discuss the effects of the viscoelastic parameter (Λ), permeability parameter (γ), Prandtl number (Pr) and Eckert number (Ec) on both the velocity and temperature profiles.

In this chapter we used the Prandtl number $Pr = 2-10$ for most non-Newtonian fluids. The viscoelastic parameter $\Lambda = -0.01\text{to} - 0.1$. The values of the other parameters were arbitrarily chosen being careful to avoid unrealistic values.

In Table 4.1 the comparison between our results for the local skin friction coefficient $f''(0)$ and heat transfer coefficient $-\theta'(0)$ are given together with those of Ece (2005) who used the Thomas algorithm. The agreement between our values and those of Ece (2005) shows that our method gives satisfactory results, thus confirming that our method is sufficiently accurate.

Table 4.1: Comparison of the values of skin friction coefficient $f''(0)$ and heat transfer coefficient $-\theta'(0)$ obtained by Ece (2005) with those of SLM when Λ=0

Pr	Ece (2005)		SLM	
	$f''(0)$	$-\theta'(0)$	$f''(0)$	$-\theta'(0)$
1	0.681483	0.638855	0.68148334	0.63885473
10	0.433268	1.275499	0.43327820	1.27552877

In order to further our understanding of the physical effects of natural convection of

fluid flow from a cone in a viscoelastic fluid with viscous dissipation, we sought to investigate the effect, according to our model, of varying the viscoelastic parameter (Λ), permeability parameter (γ), the Eckert number (Ec) and the Prandtl number (Pr) on the coefficients of skin friction $f''(0)$ and heat transfer $\theta'(0)$.

Table 4.2: Effects of the viscoelastic Λ, permeability parameters γ and Eckert number Ec for $Pr = 1$ on the local skin friction $f''(0)$ and heat transfer $-\theta(0)$ coefficients.

Λ	γ	Ec	Pr	$f''(0)$	$-\theta'(0)$
-0.1	1	0.1	1	0.51437649	0.64214087
-0.05	1	0.1	1	0.53489736	0.59964040
-0.01	1	0.1	1	0.55491411	0.56204002
0	1	0.1	1	0.56041829	0.55213993
0.01	1	0.1	1	0.56612247	0.54203983
0.05	1	0.1	1	0.59093920	0.49963495
0.1	1	0.1	1	0.62646010	0.44213898
0.01	0	0.1	1	0.68990728	0.61800108
0.01	1	0.1	1	0.56612247	0.54203983
0.01	2	0.1	1	0.49213165	0.48868800
0.01	3	0.1	1	0.44155007	0.44852699
0.01	1	0.1	1	0.56612247	0.54203983
0.01	1	0.2	1	0.56678919	0.53544933
0.01	1	0.3	1	0.56745956	0.52882111
0.01	1	0.4	1	0.56813364	0.52215479
0.01	1	0.1	0.7	0.59466242	0.47714847
0.01	1	0.1	1	0.56612247	0.54203983
0.01	1	0.1	2	0.50981746	0.68640396
0.01	1	0.1	10	0.38403617	1.13367723

The results in Table 4.2 show that increasing the viscoelastic parameter increases the skin friction coefficient, while the opposite effect is noted on the heat transfer coefficient.

Cortell (2006) noted the same results. Furthermore, this increase is more rapid for zero values of the permeability parameter and the Eckert number. We can interpret this trend as increases in permeability of the medium reducing local skin friction and heat transfer coefficients. Skin friction increases with increasing Eckert number, and the opposite trend is noted on the heat transfer coefficient. The skin friction decreases with increasing Prandtl number, and the opposite trend is noted on the Nusselt number. We also note that the successive linearization method admitted a larger value of the viscoelastic parameter $\Lambda = 0.1$.

We then sought greater insight into the effect of some fluid properties on thermal behavior and velocity of the fluids. Figures 4.2 - 4.5 respectively show the influence on the fluid velocity profile of different values for viscoelastic parameter Λ, Prandtl number Pr, permeability parameter γ and Eckert number Ec. Similarly, Figures 4.6 - 4.9 show the effect of the same parameters on temperature profiles. Finally, Figures 4.10 - 4.15 represent some relationships among, viscoelastic and permeability parameter, the heat transfer coefficient, Eckert and Prandtl numbers.

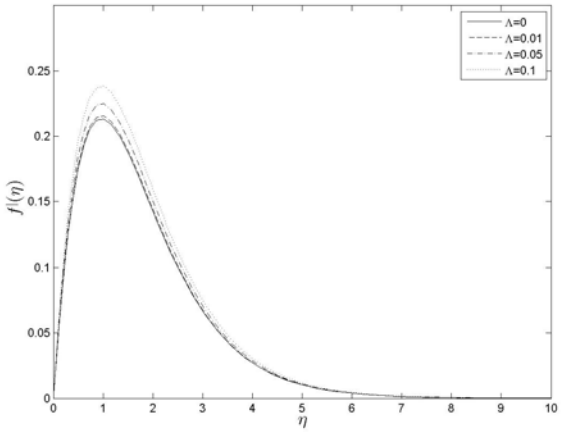

Figure 4.2: Velocity profiles for different values of the viscoelastic parameter Λ at $Pr = 1, Ec = 0.1, \gamma = 1$

The variation of the viscoelastic parameter Λ on velocity profiles $f'(\eta)$ is shown in Figure 4.2. It can be seen from the graph that increasing the viscoelastic parameter results in the increase the velocity across the boundary layer. Butt et al. (2012) noted the same results. This means that if the non-Newtonian parameter is increased the fluid flow velocity

is increased. Practically, this means that fluid flow properties in viscoelastic fluids can be controlled by influencing the change in the non-Newtonian parameter. For example it is not desirable for toothpaste to flow when placed on a toothbrush, but under certain temperatures in the mouth, flow properties are expected to change.

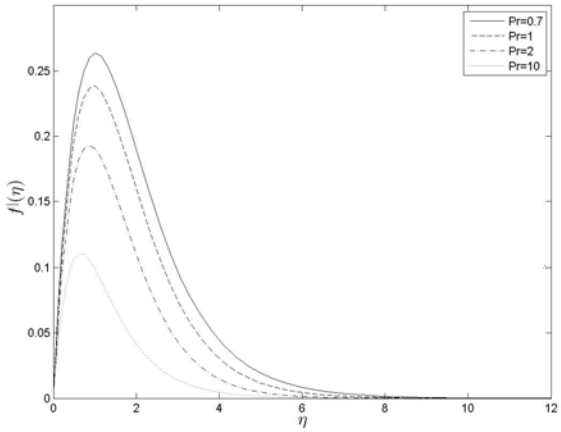

Figure 4.3: Velocity profiles $f'(\eta)$ for different values of the Prandtl number Pr at $Ec = 0.1, \gamma = 1, \Lambda = 0.1$

The variation of the Prandtl number Pr with the velocity profiles $f'(\eta)$ is shown in Figure 4.3. It is clear that increasing the Prandtl number Pr, decreases the velocity profile in the boundary layer. We can interpret increases in the Prandtl number as increasing conduction more than it does convection, suggesting a thicker fluid, which results in decrease in fluid velocity.

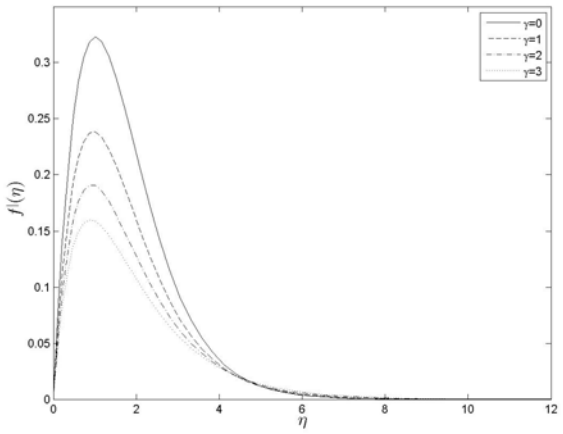

Figure 4.4: Velocity profiles $f'(\eta)$ for different values of the permeability parameter γ at $Pr = 1, Ec = 0.1, \Lambda = 0.1$

Figure 4.4 shows the variation of the permeability parameter with velocity profile. Increasing permeability parameter reduces the velocity profile across the boundary layer. Similarly we interpret that fluid particles move slower as the medium becomes less porous (see Singh and Agarwal, 2012).

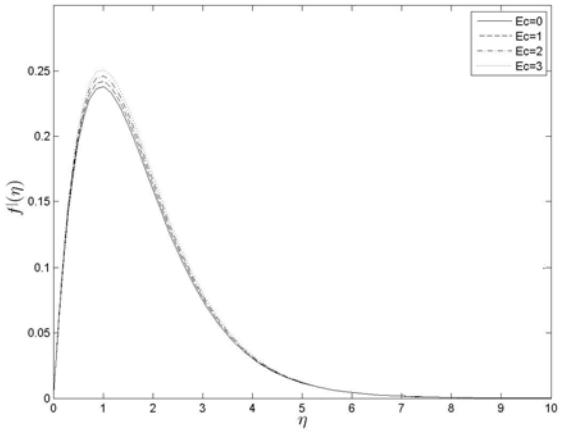

Figure 4.5: Velocity profiles $f'(\eta)$ for different values of the Eckert number Ec at $Pr = 1, \gamma = 1, \Lambda = 0.1$

Figure 4.5 shows that increasing the Eckert number increases the velocity profile. This can be explained by the increase in the kinetic energy caused by viscous dissipation in the boundary layer leading to a lower temperature gradient.

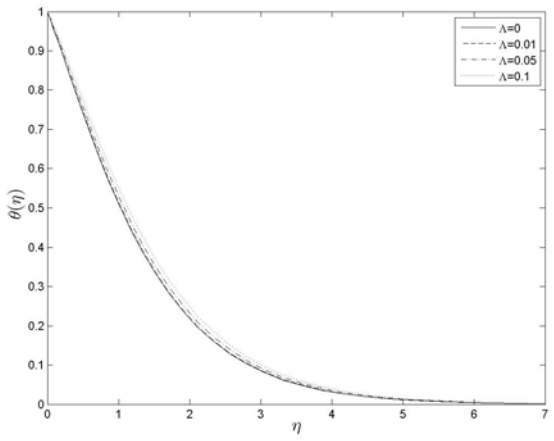

Figure 4.6: Temperature profiles $\theta(\eta)$ for different values of the viscoelastic parameter Λ at $Pr = 1, \gamma = 1, Ec = 0.1$.

Figure 4.6 shows the effect of increasing the viscoelastic parameter on the temperature profiles. Increasing the viscoelastic parameter increases the temperature profile. We can thus interpret an increase in the viscoelastic parameter as having the effect of thickening the fluid thereby making increasing the conduction effect.

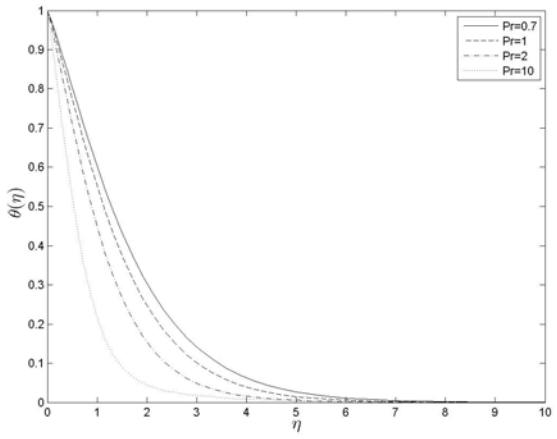

Figure 4.7: Temperature profiles $\theta(\eta)$ for different values of the Prandtl number Pr at $Ec = 0.1, \gamma = 0.1, \Lambda = 0.1$

Figure 4.7 depicts the variation of the Prandtl number with temperature profiles. Increasing the Prandtl number decreases the temperature profile, conduction is more enhanced and fluid is much thicker heat transfer is much slower across the boundary layer.

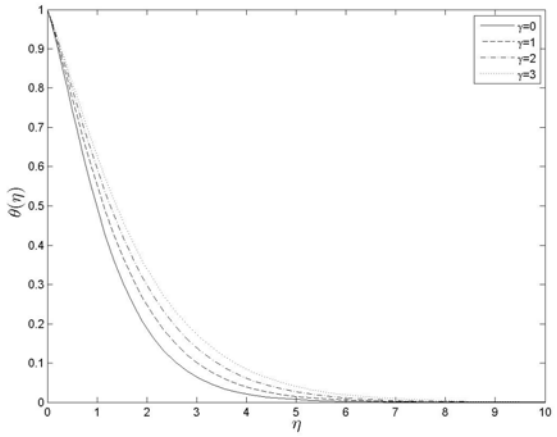

Figure 4.8: Temperature profiles $\theta(\eta)$ for different values of the permeability parameter γ at $Pr = 1, \Lambda = 0.1, Ec = 0.1$.

Figure 4.8 shows the variation of the permeability parameter with the temperature profile. Increasing the permeability parameter increases the temperature profile, when the fluid moves much slower due to the reduction in permeability heat transfer becomes more rapid.

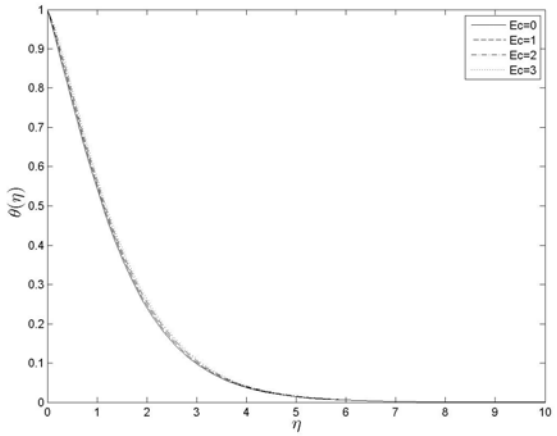

Figure 4.9: Temperature profiles $\theta(\eta)$ for different values of the Eckert number Ec at $Pr = 1, \gamma = 1, \Lambda = 0.1$

In Figure 4.9 increasing the Eckert number increases the temperature profile, the heat produced due to viscous dissipation increases the temperature across the boundary layer.

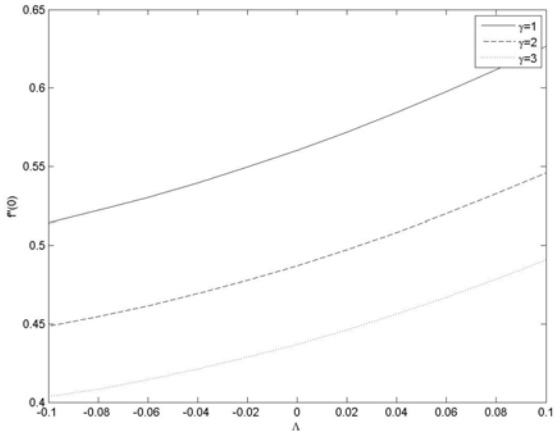

Figure 4.10: Skin friction coefficient $f''(0)$ against viscoelastic parameter Λ for different values of permeability parameter

Figure 4.10 shows the variation of the skin friction with the viscoelastic parameter at different values of the permeability parameter. Skin friction increases with increasing viscoelastic parameter and increasing the permeability parameter reduces skin friction.

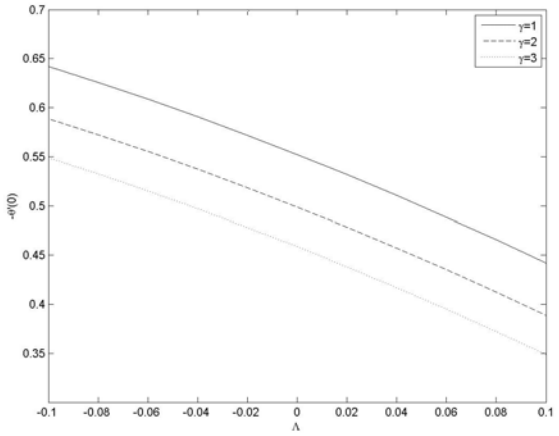

Figure 4.11: Heat transfer coefficient $-\theta'(0)$ against viscoelastic parameter Λ for different values of permeability parameter

Figure 4.11 shows the variation of the heat transfer coefficient with the viscoelastic parameter; increasing the viscoelastic parameter reduces heat transfer coefficient and increasing the permeability parameter reduce the Nusselt number.

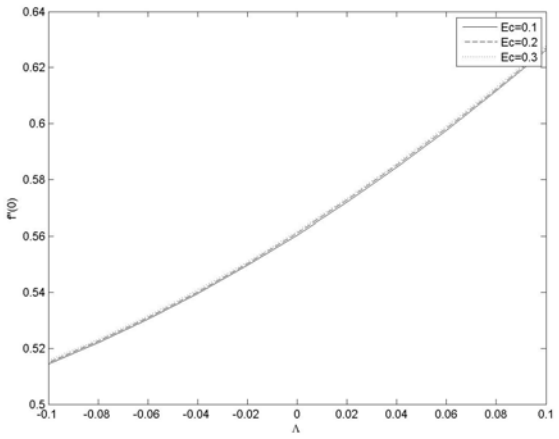

Figure 4.12: Skin friction coefficient $f''(0)$ against viscoelastic parameter Λ for different values of Eckert numbers

Figure 4.12 shows the effect of increasing the Eckert number on the skin friction and viscoelastic parameter. Increasing viscoelastic parameter increases skin friction and increasing the Eckert number increase the skin friction.

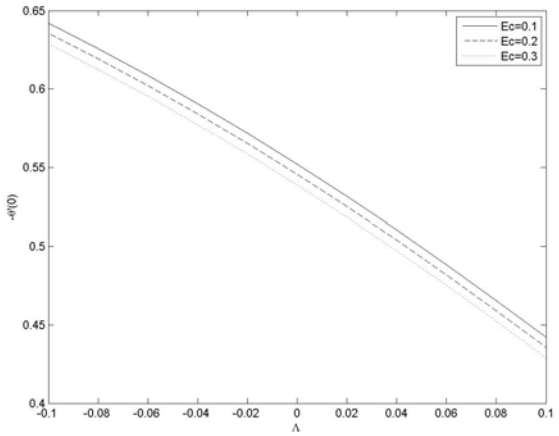

Figure 4.13: Heat transfer coefficient $-\theta'(0)$ against viscoelastic parameter Λ for different values of Eckert numbers Ec

In Figure 4.13 the increase of viscoelastic parameter reduces the heat transfer coefficient and increasing the Eckert number reduces the heat transfer coefficient.

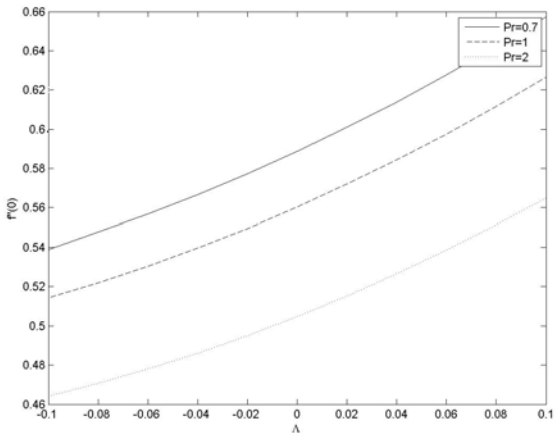

Figure 4.14: Skin friction coefficient $f''(0)$ against viscoelastic parameter Λ for different values of Prandtl numbers Pr

Figure 4.14 shows that generally increasing the viscoelastic parameter increase the skin friction and increasing the Prandtl number reduces skin friction.

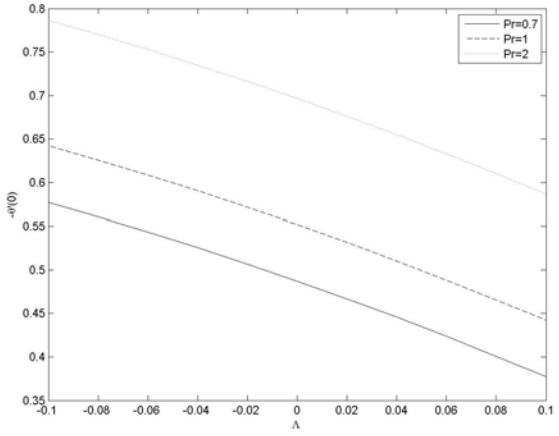

Figure 4.15: Heat transfer coefficient $-\theta'(0)$ against viscoelastic parameter Λ for different values of Prandtl numbers Pr

In Figure 4.15 increasing the viscoelastic parameter reduce the heat transfer coefficient and increasing the Prandtl number increase the heat transfer coefficient.

From Figures 4.10, 4.12 and 4.14 we note that the skin friction increases with increasing viscoelastic parameter. The skin friction is however reduced with increasing values of the

permeability parameter (Figure 4.10) and Prandtl number (Figure 4.14), whereas the Eckert number (Figure 4.12) has little effect on it. The graphs in Figures 4.11, 4.13 and 4.15 all show that increasing the viscoelastic parameter reduces the heat transfer coefficient. We further note that the heat transfer coefficient is decreased with increased values of the permeability parameter (Figure 4.11) and the Eckert number (Figure 4.13), but that increasing the Prandtl number increases the heat transfer coefficient (Figure 4.15).

4.7. Summary

This study presented an analysis of fluid flow and heat transfer in natural convection of a viscoelastic fluid from a cone embedded in a porous medium with viscous dissipation. The velocity and temperature profiles, together with local skin friction and heat transfer coefficient were presented and investigated. It was found that increasing the viscoelastic parameter increased the skin friction and reduced the heat transfer coefficient and increased the velocity and temperature profiles, while it reduced the heat transfer coefficient. Increasing the permeability parameter decreased the skin friction, heat transfer coefficient, decreased the velocity profile but the opposite effect was noted for the temperature profile. Finally, increasing the Eckert number increased both velocity and temperature profiles, but decreased the heat transfer coefficient, while it had little effect on the skin friction coefficient.

The study presented in this chapter on natural convection from a cone embedded in a viscoelastic fluid with viscous dissipation under linear surface temperature introduced new source terms; the viscous dissipation and linear surface temperature terms. These terms had not been considered in previous similar studies under the same conditions. The consideration of three systems of equations and solving them numerically together is fairly new in the implementation of the successive linearization method.

The nonlinear coupled governing equations were solved using the successive linearization method (SLM). In most cases such problems require the use of small parameters and are solved by the perturbation method. However, the perturbation method has limitations, such as requiring the parameter to be small, and in our model, the viscoelastic parameter does not necessarily need to be small, although small values can be considered. Consequently we used

the successive linearization method to solve this problem. The system of equations were first written as the zeroth, first and second order equations, as in the case of the perturbation method, before solving them together using the successive linearization method. The SLM was shown to be a very accurate method; the results obtained for the fluid parameters were found to be in excellent agreement when compared to those in the literature. The successive linearization method converged after four to five iterations. The method showed great accuracy when compared to other methods used in the literature.

5

Diffusion of chemically reactive species in Casson fluid flow over an unsteady stretching surface in porous medium in the presence of a magnetic field

5.1. Introduction

In this chapter we study the problem of diffusion of chemically reactive species in in Casson fluid flow over an unsteady stretching surface in the presence of a magnetic field. In this study the momentum, energy and mass transfer equations are coupled and nonlinear. The equations are solved by the successive linearization method and the Matlab `bvp4c` algorithm (see sections 1.1.5 and 1.1.3). The choice of using the successive linearization method that was used in the previous chapter is to test this method on time dependent variables included in this problem. The accuracy of the solution is determined by comparing it to the `bvp4c` results and previously published results in the literature.

5.2. Review of literature on Casson fluid flow over a stretching sheet

In this chapter we start by reviewing literature on flow of Casson fluid, its application in blood flow and diffusion of chemically reactive species in fluid flow. We then briefly discuss the literature on the stretching surface, magnetohydrodynamic effects, and porous medium effects already discussed in Chapters 3 and 4. We then end by discussing the numerical

method used in this chapter.

"Casson fluid can be defined as a shear thinning liquid which is assumed to have an infinite viscosity at zero rate of shear, a yield stress below which no flow occurs, and a zero viscosity at an infinite rate of shear" (Dash et al., 1992). Casson fluid is classified as a non-Newtonian fluid due to its unique rheological characteristics. These characteristics show shear stress- strain relationships that are significantly different from Newtonian fluids and other non-Newtonian fluids. The study of non-Newtonian fluids has not been thoroughly covered due to the complex representation of their constitutive equations (Makinde, 2009). The nonlinear Casson's constitutive equation was derived by Casson (1959), It describes the properties of many polymers over a wide range of shear rates (Vinogradov and Malkin, 1979). At low shear rates when blood flows through small vessels, the blood flow is described by the Casson fluid model (McDonald, 1974); Shaw et al.,2009). These constitutive equations will be fully described by mathematical equations in section 5.3.

Chapter 5 – Diffusion of chemically reactive species in Casson fluid flow over an unsteady stretching surface in porous medium in the presence of a magnetic field

Casson fluid is a non-Newtonian fluid as discussed in Chapter 4. The study of Casson fluid has attracted attention to many researchers due to its application in the field of metallurgy, food processing, drilling operations and bio-engineering operations. Its application extends to the manufacturing of pharmaceutical products, coal in water, china clay, paints, synthetic lubricants, biological fluids such as synovial fluids, sewage sludge, jelly, tomato sauce, honey, soup and blood due to its contents such as plasma, fibrinogen and protein, making the study of Casson fluid important in fluid dynamics (Pramanik, 2013). Some studies in Casson fluid flow include the work of Mukhopadhyay and Vajravelu (2013) who studied chemical reaction in Casson fluid but did not study heat transfer, Mukhopadhyay et al. (2013) investigated heat transfer on Casson fluid flow over a stretching sheet, Pramanik (2013) also studied heat transfer on Casson fluid flow, but none of these studies investigated momentum, heat and mass transfer of Casson fluid flow.

One of the most important applications of Casson fluid flow is the study of blood flow. The flow of blood in humans needs to be thoroughly understood as it can be used to save human lives. Recent studies include the work of Sibanda and Shaw (2014) in which a magnetic field is used to direct nanoparticles to cancerous cells. Studies that involved blood as Casson fluid include among others the work of Rohlf and Tenti (2001) who investigated the role of Womerseley number in pulsatile blood flow a theoretical study of the Casson model. Sankar and Lee (2008) and Sankar and Lee (2010) investigated two-fluid nonlinear model for flow in catheterized blood vessels and two-fluid Casson model for pulsatile blood flow through stenosed arteries respectively. Shaw et al. (2009) studied Pulsatile Casson fluid flow through stenosed bifurcated artery. In relation to blood flow there are other research works that were done in different geometries such as flows in micro-slit channels, slightly curved channels and peristaltic transport (Mernone et al.,2002; Das and Batra, 1993; Ng,2013). The theoretical representations in this chapter also apply to blood flow.

When some chemicals interact with certain fluids, a chemical reaction takes place and affects the flow characteristics. These reactions can result in a constructive reaction in which more solute species are added to the fluid or a destructive reaction in which the species are removed from the fluid. The study of fluid flows with chemical reactions was investigated by Mukhopadhyay and Vajravelu (2013) who studied diffusion of chemically reactive species in

Casson fluid. Other studies that investigated fluid flow with chemical reactions include the work of Kameswaran et al. (2013) who investigated homogeneous-heterogeneous reactions in a nanofluid flow due to a porous stretching sheet. Shaw et al. (2013) studied homogeneous-heterogeneous reactions in a nanofluid flow due to a porous stretching sheet. Chamkha and Mansour (2010) investigated similarity solutions for unsteady heat and mass transfer from a stretching surface embedded in a porous medium with suction/injection and chemical reaction effects.

The study of fluid flow on a stretching surface has been studied in Chapter 3 in which we considered an exponentially stretching sheet. In this chapter we consider an unsteady stretching sheet; the velocity of the stretching sheet depends on time and position from the extrusion slit. This model is considered to be a more practical representation of how an actual flow takes place making it necessary to conduct this study. Studies on unsteady stretching surfaces have been done by among others Mukhopadhyay et al. (2013) who investigated Casson fluid flow over an unsteady stretching surface in which the mass transfer equations was not considered. El-Aziz (2013) studied mixed convection flow of a micropolar fluid from an unsteady stretching surface with viscous dissipation, in which a similar stretching velocity was considered. In this chapter we extended the work of Grubka and Bobba (1985) who investigated heat transfer characteristics of a continuous stretching surface with variable temperature in which we introduced magnetohydrodynamics (MHD), porous medium and chemical reaction effects. Further to the studies mentioned in section 3.1 we consider the work of Sharidan et al. (2006) who studied similarity solutions for the unsteady boundary layer flow and heat transfer due to a stretching sheet; Nadeem et al. (2012) exponentially stretching sheet, Nadeem et al. (2014) Maxwell fluid flow past a stretching sheet, Ahmed and Nazar (2011) also studied Casson fluid over a stretching sheet and in their work they assumed that the velocity of the stretching surface is linearly proportional to the distance from fixed origin.

Magnetohydrodynamics (MHD) affect the flow of a fluid as discussed in Chapter 4. A porous medium also affects the momentum, heat and mass transfer as discussed in section 4.1. Consequently, to make sure that this is indeed true, we control the permeability of the porous medium. Earlier work in the effect of varying permeability of a porous medium

in Casson fluid include the work of Dash et al. (1996) who studied Casson fluid flow in a pipe filled with homogeneous porous medium. Nadeem et al. (2013) who considered MHD three dimensional Casson fluid flow past a porous linearly stretching sheet. Ramachandra et al. (2013a) investigated flow and heat transfer of Casson fluid from a horizontal circular cylinder with partial slip in a non-Darcy porous medium, In their work they considered slip conditions at the wall. Tripathi (2013) investigated the transient peristaltic heat flow through a finite porous channel. More recently a study by Pramanik (2014) studied Casson fluid flow and heat transfer past an exponentially porous stretching surface in the presence of thermal radiation.

As can be seen from the literature cited above, it appears that no analysis has yet been published on diffusion of chemically reactive species in Casson fluid flow for the momentum, heat and mass transfer, under the given boundary conditions. The velocity and temperature on the stretching sheet depends on time. The free stream velocity is considered to be zero. The model considered in this chapter is based on the work put forward by Mukhopadhyay and Vajravelu (2013) and Pramanik (2013) in the study of heat and mass transfer in Casson fluid flow. We extend the models to include heat and mass transfer, magnetohydrodynamic effects and porous medium.

In conclusion, this section has shown that it is necessary to study the effects of magnetic field, porous medium and chemical reaction on Casson fluid flow. In this chapter we investigate the effect of varying unsteadiness parameter, Casson, Schmidt and Prandtl numbers and the reaction rate parameter on the velocity, temperature and concentration profiles with the use of graphical illustrations. The numerical method used to solve the equations is the successive linearization method (SLM) and the results are validated by comparing them to those obtained by the Matlab `bvp4c` and to other previously published results in the literature. These aspects will be considered in the formulation of the problem of diffusion of chemically reactive species in Casson fluid flow.

5.3. Mathematical formulation of Casson fluid flow over a stretching sheet

Consider two dimensional laminar boundary-layer flow, temperature and mass transfer of an incompressible Casson fluid flow over an unsteady stretching sheet, as shown in Figure 5.1. The origin of the system is located at the extrusion slit, from which the sheet is drawn. The x-axis is taken along the unsteady stretching surface and points in the direction of motion. The y-axis is perpendicular to the sheet. A magnetic strength B is applied perpendicular to the sheet.

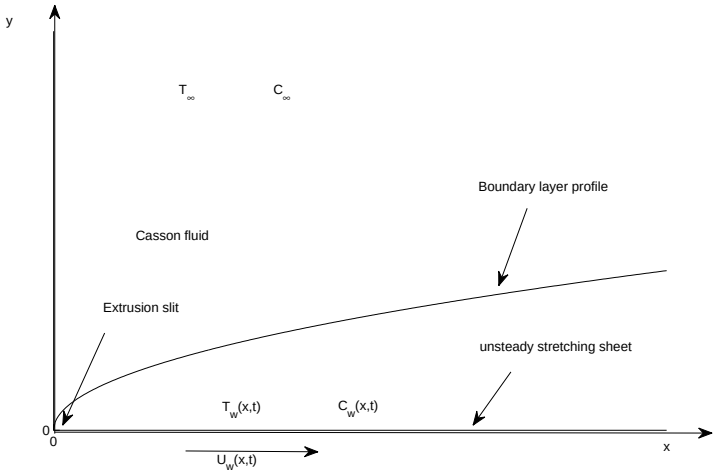

Figure 5.1: Physical model and coordinate system

The sheet velocity is assumed to vary as a linear function of the distance from the slit, $U_w(x,t) = ax/(1-\alpha_0 t)$, $a > 0$, $\alpha_0 \geq 0$ are constants and a. The temperature of the fluid (T) and concentration of the solute (C) are also assumed to be a linear function of the distance x from the slit as, $T_w(x,t) = T_\infty + bx/(1-\alpha_0 t)^2$, $C_w(x,t) = C_\infty + cx/(1-\alpha_0 t)^2$. where b and c are constants. It is assumed that radiation effects and viscous dissipation are negligible. The expressions $U_w(x,t)$, $T_w(x,t)$ and $C_w(x,t)$ are only valid for $t < \alpha_0^{-1}$ but not when $\alpha_0 = 0$.

The rheological equation of state for an isotropic and incompressible flow of a Casson fluid is given as in (Mukhopadhyay and Vajravelu, 2013; Mukhopadhyay et al. 2013; Ramachandra et al. 2013a) by:

$$\tau_{ij} = \begin{cases} 2(\mu_B + \frac{P_y}{\sqrt{2\pi}})e_{ij}, & \pi > \pi_c \\ 2(\mu_B + \frac{P_y}{\sqrt{2\pi_c}})e_{ij}, & \pi < \pi_c \end{cases} \tag{5.1}$$

where $\pi = e_{ij}e_{ij}$ and e_{ij} is the $(i,j)^{th}$ component of the deformation rate, π is the product of the deformation rate with itself, π_c is a critical value of this product based on the non-Newtonian model, μ_B is the plastic dynamic viscosity of the non-Newtonian fluid, P_y is the yield stress of the fluid. Given that T_w and C_w are respectively the temperature and concentration at the sheet and T_∞ and C_∞ are respectively the ambient conditions. Under these assumptions the governing equations in this flow are given as

$$\frac{\partial}{\partial x}(u) + \frac{\partial}{\partial y}(v) = 0, \tag{5.2}$$

$$\frac{\partial u}{\partial t} + u\frac{\partial u}{\partial x} + v\frac{\partial u}{\partial y} = \nu(1 + \frac{1}{\beta})\frac{\partial^2 u}{\partial y^2} - \frac{\nu}{K}u - \frac{\sigma B^2}{\rho}u \tag{5.3}$$

$$\frac{\partial T}{\partial t} + u\frac{\partial T}{\partial x} + v\frac{\partial T}{\partial y} = \alpha\frac{\partial^2 T}{\partial y^2} \tag{5.4}$$

$$\frac{\partial C}{\partial t} + u\frac{\partial C}{\partial x} + v\frac{\partial C}{\partial y} = D\frac{\partial^2 C}{\partial y^2} - k_1(C - C_\infty) \tag{5.5}$$

where ν is kinematic viscosity of Casson fluid, β is the non-Newtonian Casson parameter. σ is the electrical conductivity, B is the strength of the magnetic field, ρ, is the density of the Casson fluid. D is the diffusion coefficient of species in the fluid and α is the thermal diffusivity. k_1 is the time dependent reaction rate. $k_1 > 0$ represents destructive reaction and $k_1 < 0$ represents constructive reaction. The boundary conditions are given as

$$\begin{aligned} &u = U(x,t), v = 0, \quad T = T_w(x,t) \quad y = 0, \\ &u \to 0, \quad T \to T_\infty, \quad C \to C_\infty, \text{as} \quad y \to \infty. \end{aligned} \tag{5.6}$$

where the subscript ∞ refer to the free stream condition.

We introduce the non-dimensional variables

$$\left.\begin{aligned} u = \frac{\partial \psi}{\partial y}, \quad v = -\frac{\partial \psi}{\partial x}, \\ \eta = \sqrt{\frac{a}{\nu(1-\alpha_0 t)}}y, \quad \psi = \sqrt{\frac{\nu a}{1-\alpha_0 t}}x f(\eta), \\ T_w(x,t) = T_\infty + \frac{bx}{(1-\alpha_0 t)^2}\theta(\eta), \quad C_w(x,t) = C_\infty + \frac{cx}{(1-\alpha_0 t)^2}\phi(\eta). \end{aligned}\right\} \tag{5.7}$$

where $\psi(x, y, t)$ is the stream function which satisfies the continuity Eqs. (4.2). a, b, c and α_0 are positive constants. The velocity components are defined as:

$$u = \frac{\partial \psi}{\partial y} = U_w f'(\eta), \quad v = -\frac{\partial \psi}{\partial x} = -\sqrt{\frac{\nu a}{1-\alpha_0 t}} f(\eta) \tag{5.8}$$

The governing equations reduce to

$$A(\frac{\eta}{2}f'' + f') - ff'' + (f')^2 = \left(1 + \frac{1}{\beta}\right) f''' - (\gamma + M^2), \tag{5.9}$$

$$\frac{A}{2}(\eta\theta' + 3\theta) + 2f'\theta - f\theta' = \frac{1}{Pr}\theta'', \tag{5.10}$$

$$\frac{A}{2}(\eta\phi' + 3\phi) + 2f'\phi - f\phi' = \frac{1}{Sc}\phi'' - R\phi. \tag{5.11}$$

with boundary conditions;

$$\begin{aligned} &f(0) = 0, f'(0) = 1, \quad \theta(0) = 1, \quad \phi(0) = 1 \\ &f'(\infty) \to 0, \quad \theta(\infty) \to 0, \quad \phi(\infty) \to 0. \end{aligned} \tag{5.12}$$

where $A = \alpha_0/a$ is the unsteadiness parameter, $Pr = \nu/\alpha$ is the Prandtl number, $Sc = \nu/D$ is the Schmidt number and $R = k_1/a$ is the reaction parameter. $\gamma = \nu(1 - \alpha_0 t)/a\bar{K}$ is the permeability parameter coefficient, $M^2 = \sigma B^2(1 - \alpha_0 t)/\rho a$ is the magnetic parameter. The non-dimensional temperature and concentration are respectively given by $\theta = (T - T_\infty)/(T_w - T_\infty)$ and $\phi = (C - C_\infty)/(C_w - C_\infty)$.

5.4. Skin friction, heat transfer and mass transfer coefficients

The parameters of engineering interests are the local skin friction, heat transfer and mass transfer coefficients are defined as (see Mukhopadhyay and Vajravelu, 2013)

$$C_{fx} = 2(1 + \frac{1}{\beta})Re_x^{-\frac{1}{2}} f''(0), \tag{5.13}$$

The heat and mass fluxes can be written as

$$Nu_x = \frac{x}{\alpha_0}\frac{q_w}{(T_w - T_\infty)},\ q_w = -\alpha_0 \left[\frac{\partial T}{\partial y}\right]_{y=0}, \tag{5.14}$$

$$Sh_x = \frac{x}{D}\frac{J_w}{(C_w - C_\infty)},\ J_w = -D \left[\frac{\partial C}{\partial y}\right]_{y=0} \tag{5.15}$$

Using Eqs. (5.14) and (5.7), the heat transfer coefficient (Nusselt number) and mass transfer coefficient (Sherwood number) are defined as

$$Nu_x = -Re_x^{\frac{1}{2}}\theta'(0), \quad Sh_x = -Re_x^{\frac{1}{2}}\phi'(0) \tag{5.16}$$

where Re_x is the Reynolds number defined as $Re_x = U_w x/\nu$. It is important at this stage to mention that for the Newtonian fluid $(1/\beta \to 0)$ and that $\Lambda = M = A = Sc = 0$. The present problem reduce to that of Grubka and Bobba (1985), $A = 0$ denote steady flow and in their work they obtained an exact solution in terms of Kummer's functions written in terms of the confluent hyper geometric functions.

The boundary value problems in Eqs. (5.9) - (5.12) are solved using the successive linearization method. In the method we choose finite values of $\eta \to \infty$. This value is the boundary layer thickness given by η_∞. We begin by choosing an initial guess of η_∞ to obtain the values $f''(0)$, $-\theta'(0)$ and $-\phi'(0)$. The solution is repeated with new values until two consecutive values differ by 10^{-6}.

5.5. Results and discussion

The problem considered in this chapter is diffusion of chemically reactive species in Casson fluid flow in porous medium in the presence of magnetic field. The nonlinear differential equations were solved by the successive linearization method (SLM). In this section we discuss the physics of the problem by studying the effects of the unsteadiness (A), permeability (γ), magnetic (M), Prandtl (Pr), Schmidt (Sc) and reaction rate (R) numbers on velocity, temperature and concentration profiles. We also study the variation of skin friction $f''(0)$, heat transfer $-\theta'(0)$ and mass transfer $-\phi'(0)$ coefficients with unsteadiness parameter.

The Casson fluid discussed in this section covers a wide range of this type of fluid which normally has a Prandtl number between $Pr = 5$ at 20^oC and $Pr = 20$ for blood. The Grashof number is fixed at $Gr = 10$ and Darcy number $Da = 0.1$ giving a fixed value $k_p = 1/DaGr^{\frac{1}{2}} = 3$. All other parameters are chosen arbitrarily being careful to stay within the acceptable range of the Casson fluid.

For validation of the numerical method used in this study, results for the heat transfer coefficient $-\theta'(0)$ for the Newtonian fluid were compared to those of El-Aziz (2013) and Grubka and Bobba (1985) for the unsteadiness parameter $A = \gamma = M = Sc = 0$. The comparison is shown in Table 6.1 and it is found to be in agreement to at least four decimal places. To further verify the accuracy of the successive linearization method (SLM), the Matlab `bvp4c` was used.

Table 5.1: Comparison of the values of $-\theta(0)$ for $\gamma = M = Sc = 0$ and various values of A and Pr with those of Grubka and Bobba (1985), El-Aziz (2013), SLM and bvp4c.

A	Pr	Grubka and Bobba (1985)	El-Aziz (2013)	SLM	bvp4c
0	0.72	0.8086	0.80873135	0.80873007	0.80863761
-	1	1.0000	1.00000000	1.00000000	1.00000006
-	3	1.9237	1.92368255	1.92367361	1.92367736
-	10	3.7207	3.72067395	3.72066225	3.72066701

We then sought to get a clear understanding of the behavior of velocity, temperature and concentration profiles of Casson fluid flow, a detailed numerical calculation was done for different parameter values that describe the fluid flow and the results are depicted as graphs in Figures 5.2 - 5.25. The variation of the Casson parameter β, unsteadiness parameter A, permeability parameter γ, magnetic parameter M and the Prandtl number Pr on velocity profiles $f'(\eta)$ is shown in Figures 5.2 - 5.5. The variation of the same parameters on temperature profiles $\theta(\eta)$ is shown in Figures 5.6 - 5.11. The variation of the Casson parameter β, unsteadiness parameter A, permeability parameter γ, magnetic parameter M, reaction rate parameter R and the Schmidt number Sc on concentration profiles are shown in Figures 5.12 - 5.19 . The plots of the skin friction, heat transfer, and mass transfer coefficients against the unsteadiness parameter A are shown in Figures 5.20 - 5.21, Figures 5.22 - 5.23 and Figures 5.24 - 5.25 respectively.

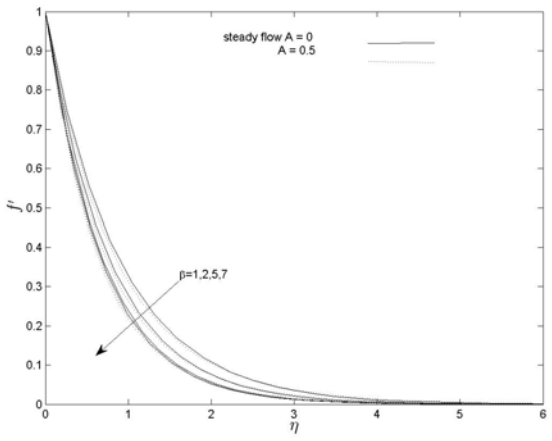

Figure 5.2: Velocity profiles $f'(\eta)$ for different values of the Casson parameter β and unsteadiness parameter A at $\gamma = 0.5, M = 1, Pr = 5, Sc = 1, R = 0.5$.

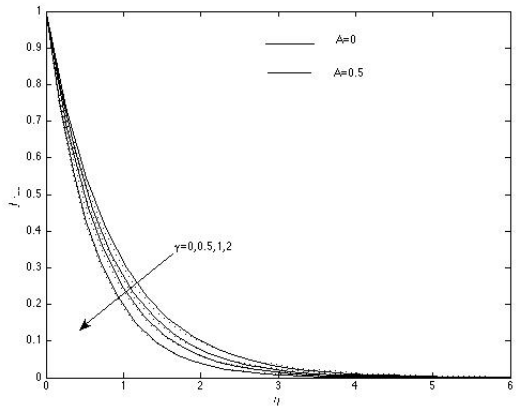

Figure 5.3: Velocity profiles $f'(\eta)$ for different values of the permeability parameter γ and unsteadiness parameter Aat $\beta = 2, M = 1, Pr = 5, Sc = 1, R = 0.5$.

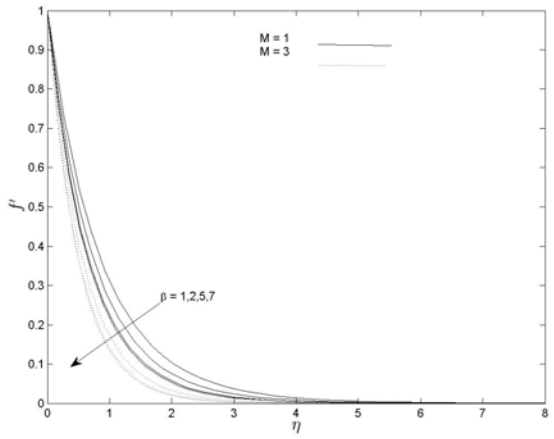

Figure 5.4: Velocity profiles $f'(\eta)$ for different values of the Casson parameter β and magnetic parameter M at $A = 0.5, \gamma = 0.5, Pr = 5, Sc = 1, R = 0.5$.

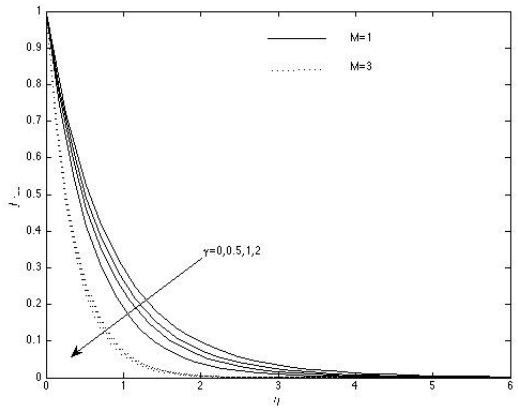

Figure 5.5: Velocity profiles $f'(\eta)$ for different values of the permeability parameter γ and magnetic parameter Mat $\beta = 2, A = 0.5, Pr = 5, Sc = 1, R = 0.5$

The variation of the Casson parameter β and permeability parameter γ on velocity profiles $f'(\eta)$ for steady ($A = 0$) and unsteady conditions ($A = 0.5$) are shown in Figures 5.2 and 5.3 respectively. It can be seen from Figure 5.2 that increasing the Casson parameter (fluid behaves as Newtonian as Casson parameter becomes large) results in the decrease in the velocity profiles. This would be expected because increasing the Casson parameter would have an effect of reducing yield stress thereby suppressing its motion. Increasing the unsteadiness parameter A results in the decrease of velocity profiles. Increasing the unsteadiness parameter A would naturally mean that the fluid motion is retarded by the slight interaction of fluid layer. The same result was recorded by Mukhophadhyay et al. (2013). It can be seen from Figure 5.3 that increasing the permeability parameter results in the decrease in the velocity profiles in both steady $A = 0$ and unsteady conditions $A = 0.5$. This would be expected because increasing the permeability parameter would have an effect of reducing the size of media pores thereby reducing fluid motion as explained in the results of the previous chapter.

The variation of the Casson parameter β and permeability parameter γ on velocity profiles $f'(\eta)$ for different values of the magnetic parameter M are shown in Figures 5.4 and 5.5 respectively. It can be seen from the graph that increasing the magnetic parameter reduces velocity profiles as explained in the results in Chapter 4.

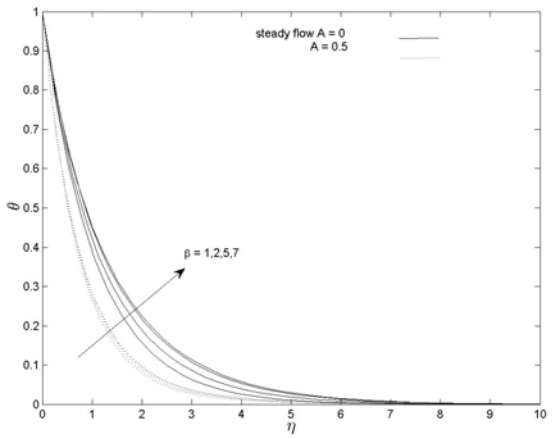

Figure 5.6: Temperature profiles $\theta(\eta)$ for different values of the Casson parameter β and unsteadiness parameter A at $\gamma = 0.5, M = 1, Pr = 5, Sc = 1, R = 0.5$

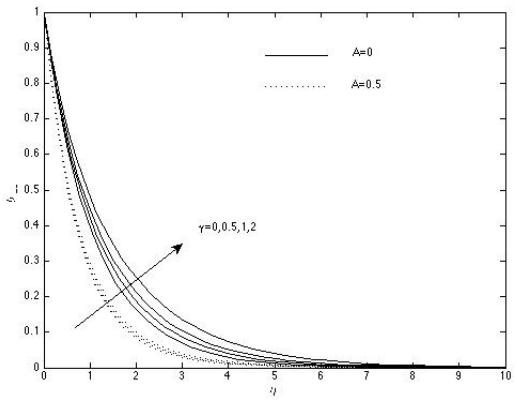

Figure 5.7: Temperature profiles $\theta(\eta)$ for different values of the permeability parameter γ and unsteadiness parameter A at $\beta = 2, M = 1, Pr = 5, Sc = 1, R = 0.5$

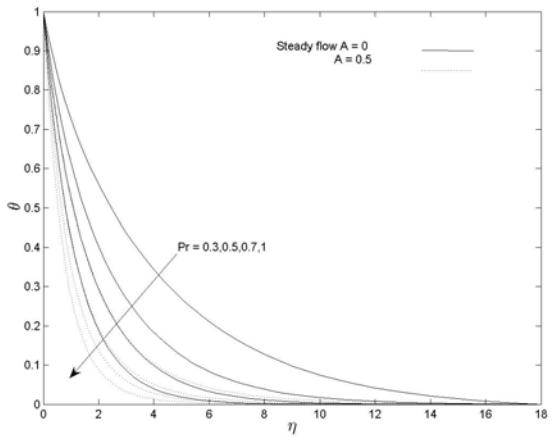

Figure 5.8: Temperature profiles $\theta(\eta)$ for different values of the Prandtl numbers Pr and unsteadiness parameter A at $\beta = 2, \gamma = 0.5, M = 1, Sc = 1, R = 0.5$

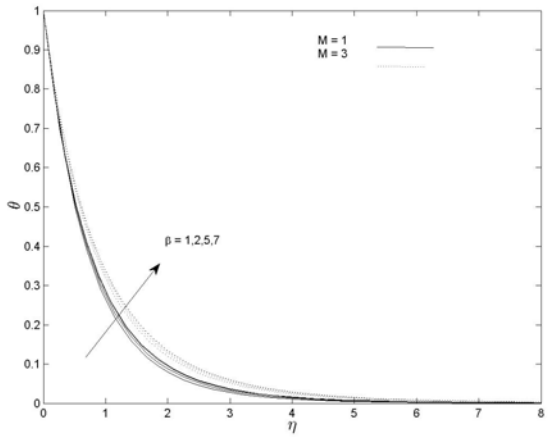

Figure 5.9: Temperature profiles $\theta(\eta)$ for different values of the Casson parameter β and magnetic parameter M at $A = 0.5, \gamma = 0.5, Pr = 5, Sc = 1, R = 0.5$

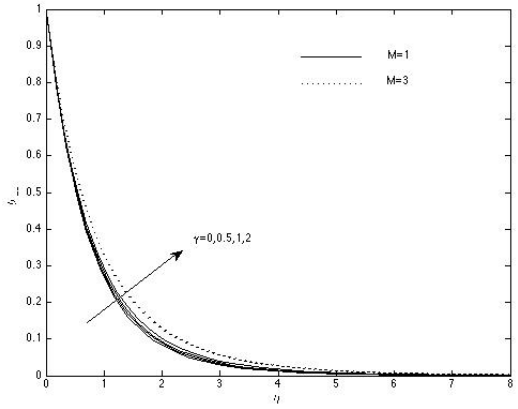

Figure 5.10: Temperature profiles $\theta(\eta)$ for different values of the permeability parameter γ and Magnetic parameter Mat $\beta = 2, A = 0.5, Pr = 5, Sc = 1, R = 0.5$

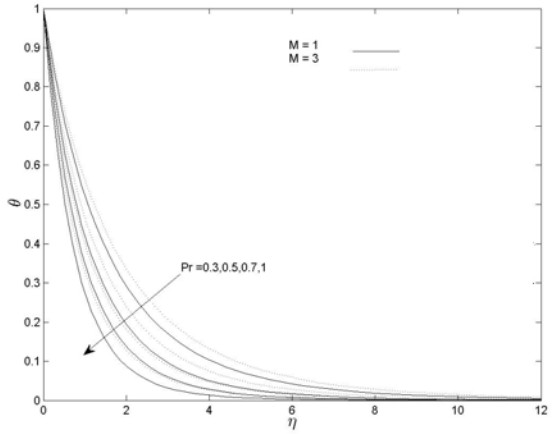

Figure 5.11: Temperature profiles $\theta(\eta)$ for different values of the Prandtl number Pr and magnetic parameter Mat $\beta = 2, A = 0.5, \gamma = 0.5, Sc = 1, R = 0.5$

The variation of Casson parameter β, permeability parameter γ, and Prandtl number Pr on temperature profiles for steady ($A = 0$) and unsteady conditions ($A = 0.5$) are shown in Figures 5.6 - 5.8. It can be seen from these figures that increasing both the Casson parameter β and the permeability parameter γ results in the increase in temperature profiles. This is to be expected because increasing the Casson parameter would be interpreted as the fluid being Newtonian, therefore temperature profiles are increased. Increasing the permeability parameter γ, would be interpreted as reducing media pores reducing fluid motion and increasing temperature profiles. The variation is more enhanced in steady motion than in

unsteady motion. It can be seen from Figure 5.8 that increasing the Prandtl number Pr results in the decrease in the temperature profiles. This effect is due to the definition of the Prandtl number which is the ratio of the thermal diffusivity to the momentum diffusivity. This relationship suggest that low Prandtl number numbers mean high thermal conductivity, high Prandtl numbers mean low thermal conductivity.

The variation of Casson parameter β, permeability parameter γ, and Prandtl number Pr on temperature profiles for different values of the magnetic parameter M are shown in Figures 5.9 - 5.11. It can be seen from all these figures that increasing the magnetic parameter increase temperature profiles and the same observation was noted in Pramanik (2014). Increasing the permeability Casson parameter β result in the increase in temperature profiles as shown in Figure 5.9. This is to be expected the fluid departs from plastic flow this facilitates increase of temperature in the boundary layer. Heat transfer is more pronounced in lower magnetic numbers $M = 1$ than in higher magnetic numbers $M = 2$. We can thus interpret an increase in the magnetic parameter as having an effect of slowing down the fluid flow as discussed in chapter 1. The same observation is noted in Figure 5.10. Increasing the permeability parameter γ results in the increase in the temperature profiles. It can be seen from Figure 5.11 that increasing the Prandtl number Pr, result in the decrease in the temperature profiles. The wall temperature gradient or the heat transfer coefficient is negative for all values of the Prandtl number which can be interpreted to mean that heat is transferred from the surface to the fluid.

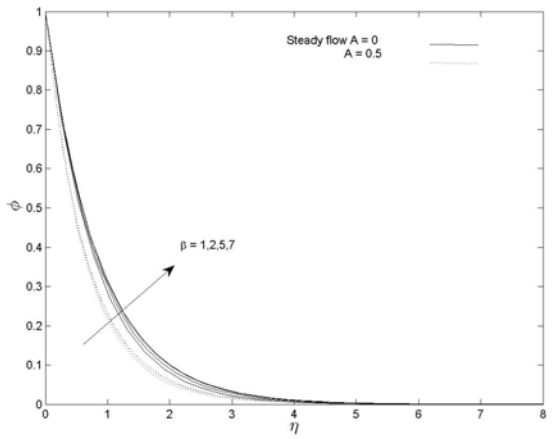

Figure 5.12: Concentration profiles $\phi(\eta)$ for different values of the Casson parameter β and unsteadiness parameter A at $\gamma = 0.5, M = 1, Pr = 5, Sc = 1, R = 0.5$

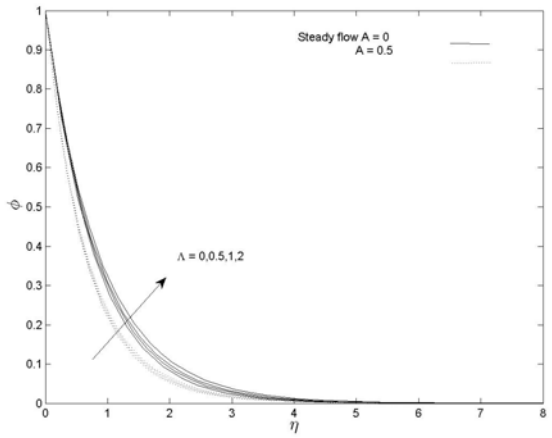

Figure 5.13: Concentration profiles $\phi(\eta)$ for different values of the permeability parameter γ and unsteadiness parameter A at $\beta = 2, M = 1, Pr = 5, Sc = 1, R = 0.5$

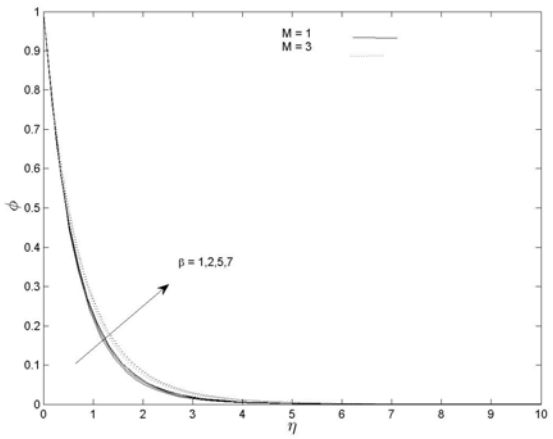

Figure 5.14: Concentration profiles $\phi(\eta)$ for different values of the Casson parameter β and magnetic parameter M at $A = 0.5, \gamma = 0.5, Pr = 5, Sc = 1, R = 0.5$

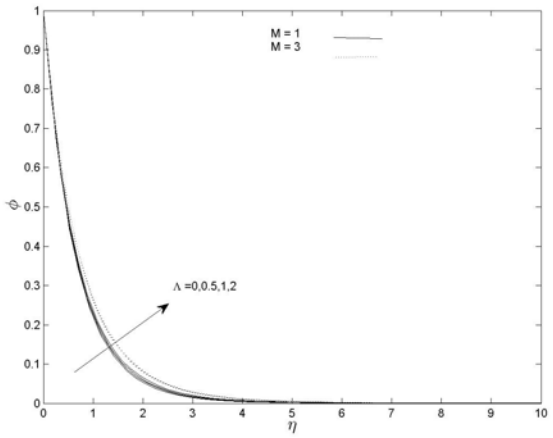

Figure 5.15: Concentration profiles $\phi(\eta)$ for different values of the permeability parameter γ and magnetic parameter M at $A = 0.5, \beta = 2, Pr = 5, Sc = 1, R = 0.5$

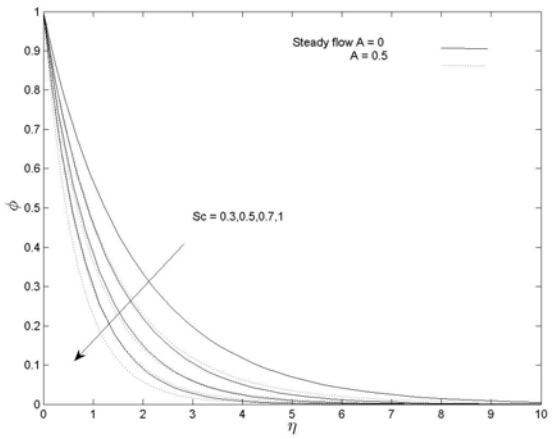

Figure 5.16: Concentration profiles $\phi(\eta)$ for different values of the Schmidt number Sc and unsteadiness parameter A at $\beta = 2, \gamma = 0.5, Pr = 5, M = 1, R = 0.5$

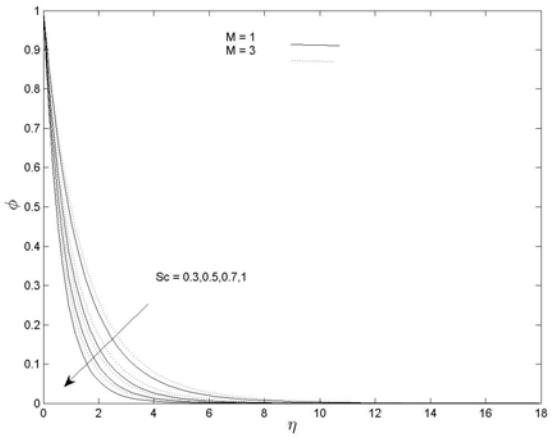

Figure 5.17: Concentration profiles $\phi(\eta)$ for different values of the Schmidt number Sc and magnetic parameter M at $A = 0.5, \beta = 2, \gamma = 0.5, Pr = 5, R = 0.5$

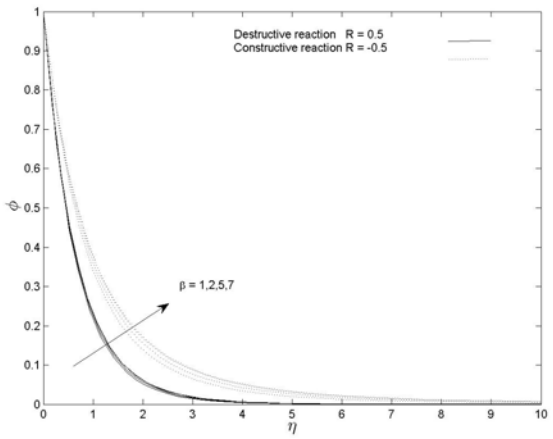

Figure 5.18: Concentration profiles $\phi(\eta)$ for different values of the Casson parameter β and reaction rate R at $A = 0.5, M = 1, \gamma = 0.5, Pr = 5, Sc = 1$.

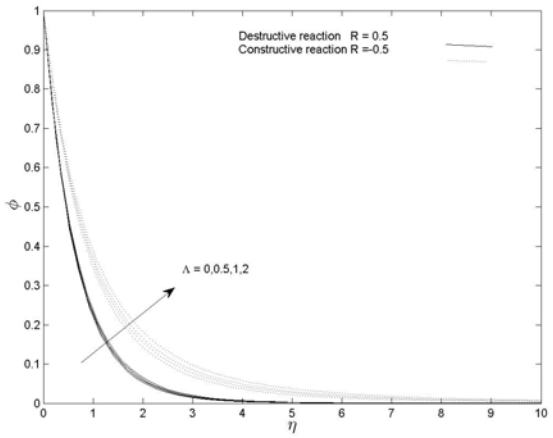

Figure 5.19: Concentration profiles $\phi(\eta)$ for different values of the permeability parameter γ and reaction rate R at $A = 0.5, \beta = 2, M = 1, Pr = 5, Sc = 1$.

The variation of Casson parameter β, permeability parameter γ and Schmidt number Sc on concentration profiles $-\phi'(\eta)$ for different values of the magnetic M, unsteadiness A and reaction rate R parameters are shown in Figures 5.12 - 5.19.

The influence of Casson parameter β, permeability parameter γ and the Schmidt number Sc on concentration profiles for both steady ($A = 0$) and unsteady conditions ($A = 0.5$) is shown in Figures 5.12, 5.13 and 5.16. It can be seen from Figures 5.12 and 5.13 that increasing both the Casson parameter β and permeability parameter γ result in increasing

the concentration profiles. This is to be expected because increasing the Casson parameter β would have an effect of increasing fluid velocity thereby increasing the species transfer in the boundary layer. Increasing the permeability parameter would have an effect decreasing the fluid velocity and this increases the convection current and thereby facilitates solutal movement. Figure 5.16 shows that increasing Schmidt number Sc result in the decrease in the concentration profiles. The effect is due to the definition of the Schmidt number Sc, that it is inversely proportional to the diffusion coefficient. The wall concentration gradient is negative for all values of the Schmidt number which means that the mass is always transferred from the surface of the sheet to the fluid. The same result was noted in Mukhopadhyay et al. (2013).

The influence of Casson parameter β, permeability parameter γ and the Schmidt number Sc on concentration profiles for both for different values of the magnetic parameter M is shown in Figures 5.14, 5.15 and 5.17. Figures 5.14 and 5.15 show that increasing both the Casson parameter β and permeability parameter γ result in increasing the concentration profiles. Solutal transfer is more pronounced for lower values of the magnetic field.

The variation of Casson parameter β and permeability parameter γ on concentration profiles for both for different values of the reaction rate parameter R is shown in Figures 5.18 and 5.19. It can be seen from Figure 5.18 that increasing the Casson parameter β increase the concentration profile, this is more pronounced in the case of $(R < 0)$ normally referred to as constructive reaction. The opposite trend is noted in the case of destructive reaction $(R > 0)$. This is normally expected because, in constructive reaction more solute is introduced in the fluid flow regime, and the opposite process removes some solute from the fluid flow regime. The same results were noted by Mukhophadhyay and Vajravelu (2013).

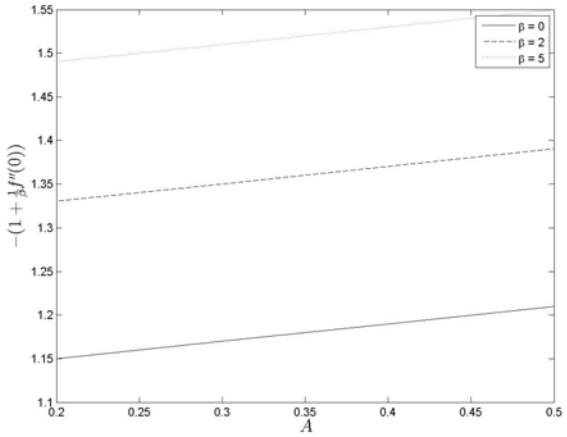

Figure 5.20: Skin friction $-(1+1/\beta)f''(0)$ against unsteadiness parameter A at different values of the Casson parameter β at $M = 1, \gamma = 0.5, Pr = 5, Sc = 1, R = 0.5$.

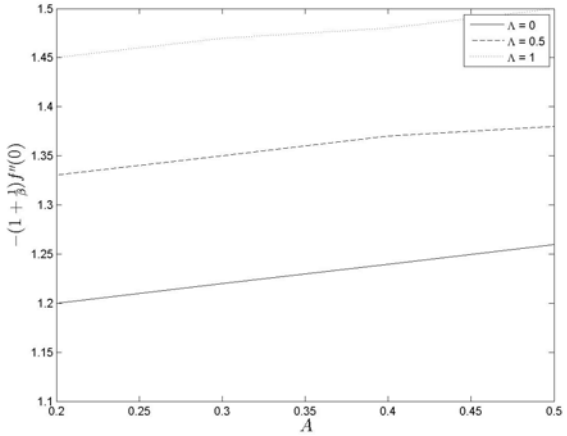

Figure 5.21: Skin friction $-(1+1/\beta)f''(0)$ against unsteadiness parameter A at different values of the permeability parameter γ at $M = 1, \beta = 2, Pr = 5, Sc = 1, R = 0.5$.

The variation of skin friction coefficient related to $-(1+1/\beta)f''(0)$ against the unsteadiness parameter A for different values of the Casson parameter β and permeability parameter γ is shown in Figures 5.20 and 5.21. It can be seen from Figure 5.20 that increasing the Casson parameter decrease the skin friction coefficient. Increasing the Casson parameter would naturally mean the decrease in yield stress and exerting less force on the surface. Practically, this means that less force may be needed to pull a moving sheet at a given withdrawal

velocity. The skin friction coefficient increase with increasing unsteadiness parameter.

Figure 5.21 shows that increasing the permeability parameter γ result in the increase in the skin friction coefficient. This is to be expected because fluid motion is decreased exerting more force on the surface. This means that the force exerted on the surface may be controlled by varying the permeability parameter; this may be done to achieve a desired force.

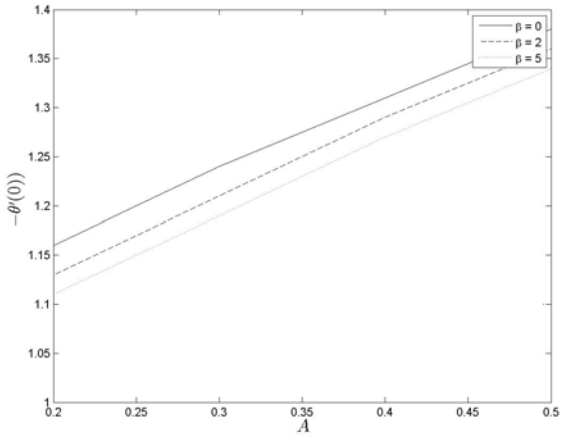

Figure 5.22: Heat transfer coefficient $-\theta(0)$ against unsteadiness parameter A at different values of the Casson parameter β at $M = 1, \gamma = 0.5, Pr = 5, Sc = 1, R = 0.5$.

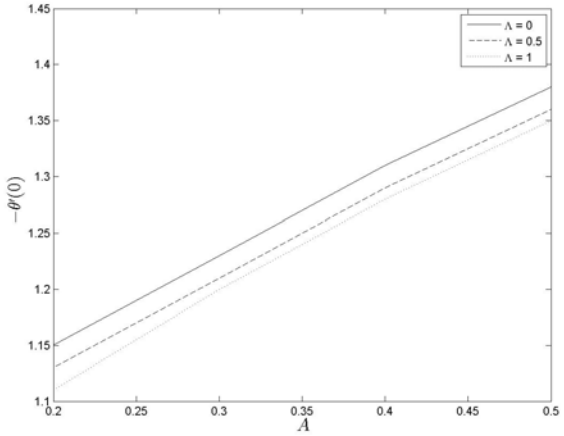

Figure 5.23: Heat transfer coefficient $-\theta'(0)$ against unsteadiness parameter A at different values of the permeability parameter γ at $M = 1, \beta = 0.5, Pr = 5, Sc = 1, R = 0.5$.

The variation of heat transfer coefficient related to $-\theta'(0)$ against the unsteadiness parameter A for different values of the Casson parameter β and permeability parameter γ is shown in Figures 5.22 and 5.23. It can be seen from Figure 5.22 that increasing the Casson parameter decrease the heat transfer coefficient. Increasing the Casson parameter would naturally mean the decrease in yield stress and exerting less force on the surface. Heat transfer is reduced

Figure 5.23 shows that increasing the permeability parameter γ result in the decrease in the heat transfer coefficient. This is to be expected because fluid motion is decreased exerting more force on the surface.

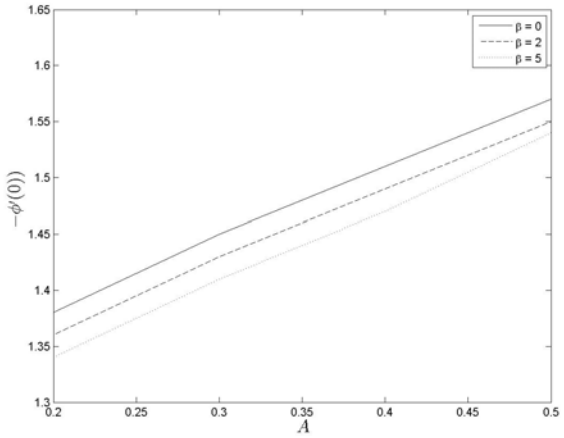

Figure 5.24: Mass transfer coefficient $-\phi'(0)$ against unsteadiness parameter A at different values of the Casson parameter β at $M = 1, \gamma = 0.5, Pr = 5, Sc = 1, R = 0.5$.

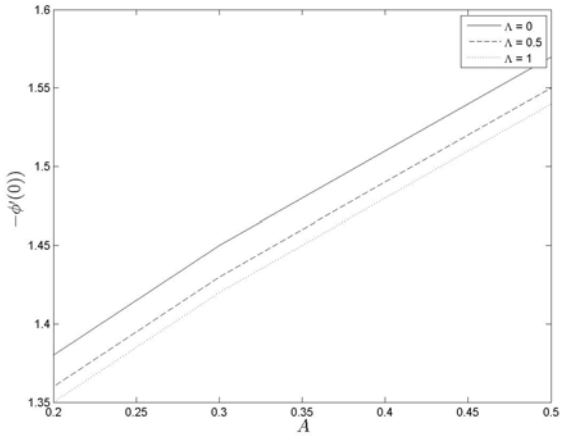

Figure 5.25: Heat transfer coefficient $-\phi'(0)$ against unsteadiness parameter A at different values of the permeability parameter γ at $M = 1, \beta = 2, Pr = 5, Sc = 1, R = 0.5$.

The variation of mass transfer coefficient related to $-\phi'(0)$ against the unsteadiness parameter A for different values of the Casson parameter β and permeability parameter γ is shown in Figures 5.24 and 5.25. It can be seen from Figure 5.24 that increasing the Casson parameter decrease the mass transfer coefficient. Increasing the Casson parameter would naturally mean the decrease in yield stress and exerting less force on the surface.

Figure 5.25 shows that increasing the permeability parameter γ result in the decrease in the mass transfer coefficient. This is to be expected because fluid motion is decreased exerting more force on the surface.

5.6. Summary

The study of diffusion of chemically reactive species in Casson fluid flow over an unsteady stretching surface in a porous medium in the presence of a magnetic field was considered. The results in this study were as follows; increasing the unsteadiness parameter decreases velocity profiles. Increasing the Casson parameter decreases the velocity profiles. Increasing the permeability parameter result in the reduction in velocity profiles. Increasing the Prandtl number result in the decrease in the temperature profiles. Increasing the positive values of reaction rate increase the concentration profiles (constructive) and increasing the negative

values of the reaction rate reduce concentration profiles (destructive)

The presentation of the momentum, energy and mass transfer equations had not been considered in the study of heat and mass transfer in Casson fluid. In this chapter we presented this unique problem which reported some new results.

In this chapter the successive linearization method (SLM) was used to find solutions of the governing equations. The problem consisted of three coupled ordinary differential equations. The accuracy of the method was tested on system of equations that contained the unsteadiness parameter. The numerical solution was further was compared to those available in the literature and was found to be in excellent agreement. The numerical method was further compared to the results obtained by the Matlab `bvp4c` and there was excellent agreement.

6

Effects of radiation on MHD free convection of Casson fluid from a horizontal circular cylinder with partial slip in non-Darcy porous medium with viscous dissipation

6.1. Introduction

In this chapter we investigate the problem of free convection of Casson fluid flow from a horizontal circular cylinder with partial slip in non-Darcy porous medium with radiation and viscous dissipation effects. The momentum and energy equations are transformed into non-similar coupled partial differential equations. Non-similarity arises when a fluid flow is unsteady or sometimes caused by a flow in a different direction to the main flow. Effects such as suction, injection and partial slip sometimes give rise to unsteadiness. The equations are solved by the bivariate quasi-linearization method (BQLM). The accuracy of the method is determined by comparison with other results in the literature.

6.2. Review of literature on Casson fluid flow from a horizontal cylinder

In this section we review literature on the problem of free convection of Casson fluid flow from a horizontal circular cylinder with partial slip, porous medium and viscous dissipation.

Chapter 6 – Effects of radiation on MHD free convection of Casson fluid from a horizontal circular cylinder with partial slip in non-Darcy porous medium with viscous dissipation

We start by discussing flow around cylinders and the effect of partial slip in fluid flow. Further to the discussions of radiation effects, Casson fluid flow, porous medium and viscous dissipation in previous chapters, we present a brief review of these fluid flow phenomena in this context.

The study of Casson fluid around cylinders is important in the understanding of fluid flow around veins and arteries in humans, in the circulation of oil in automotive engines and design of automatic cooking machines, in which cooking oil and soup are used. With this in mind it is necessary to conduct a study of Casson fluid flow with partial slip, porous medium, magnetic field and viscous dissipation effects. The flow of Casson fluid is applied in many situations in industry such as petroleum production, multiphase mixtures, pharmaceutical formulations, coal in water, paints, lubricants, jams, sewage, soup, blood, contaminated lubricants, molten metal and synovial fluid. These fluids show different characteristics from the Newtonian fluids which cannot be fully represented by the Navier-Stokes equations. To represent these non-Newtonian fluids some modifications to the Navier-Stokes equations are necessary (Ramachandra et al., 2013a; Mukhophadhyay and Vajravelu, 2013).

Chapter 6 – Effects of radiation on MHD free convection of Casson fluid from a horizontal circular cylinder with partial slip in non-Darcy porous medium with viscous dissipation

The study of fluid flow over different geometries is important as it refers to many practical situations, some of which have been mentioned earlier in this section. The study of fluid flow past a cylindrical geometry was studied by among others Anwar et al. (2008) who investigated mixed convection boundary layer flow of a viscoelastic fluid over a horizontal cylinder; Deka et al. (2014) investigated transient free convection flow past an accelerated vertical cylinder in a rotating cylinder; Ribeiro et al. (2014) studied viscoelastic flow past a confined cylinder with three dimensional effects and stability and Patel and Chhabra (2013) studied steady flow of Bingham plastic fluids past an elliptical cylinder. In this chapter we consider a cylinder embedded in Casson fluid with transpiration at its walls. We also consider partial slip at the surface of the cylinder.

In 1823, Navier deduced that there is a partial slipping at a solid boundary, and that this slip force is directly proportional to the slip velocity (Prabhakara and Deshpande, 2004). Partial slip is a condition of a surface with little or no friction, it is characteristic of a lubricated surface. In many practical situations it is often important to consider partial slip conditions depending on the problem concerned. It is therefore important to study the fluid flow in Casson fluid with partial slip conditions. Studies which included partial slip include the work of Ramachandra et al. (2013a) which considered velocity and thermal slip factors.

In this chapter, the flow of fluid is affected by the presence of radiation and magnetic field. Further to the studies referred to in Chapter 3, we highlight the studies that focused on effects of radiation and magnetic field in a non-Newtonian fluid. Shateyi and Marewo (2013) investigated numerical analysis of MHD stagnation point flow of Casson fluid; they considered thermal radiation in their work. Chamkha et al. (2003) studied thermal radiation effects on MHD forced convection flow adjacent to a non-isothermal wedge in the presence of heat source or sink. Pramanik (2013) studied Casson fluid flow and heat transfer past an exponentially porous stretching surface in the presence of thermal radiation. Narayana et al. (2013) studied free magnetohydrodynamic fluid flow and convection from a vertical spinning cone with cross diffusion effects. Nadeem et al. (2014) studied numerical study of MHD boundary layer flow of a Maxwell fluid past a stretching sheet in the presence of nano-particles. Chen (2004) investigated combined heat and mass transfer in MHD free convection from a vertical surface with Ohmic heating and viscous dissipation.

Chapter 6 – Effects of radiation on MHD free convection of Casson fluid from a horizontal circular cylinder with partial slip in non-Darcy porous medium with viscous dissipation

The flow of fluid in porous medium was discussed in Chapter 4 and in this section we investigate the effect of non-Newtonian fluid flow in porous medium. Studies in porous media and viscous dissipation have been carried out by among others, Makanda et al. (2013) who studied natural convection of viscoelastic fluid from a cone embedded in a porous medium with viscous dissipation. Awad et al. (2011) investigated convection from an inverted cone in a porous medium with cross diffusion effects. Hayat et al. (2010) studied heat and mass transfer for Soret and Dufour effects on mixed convection boundary layer flow over a stretching vertical surface in a porous medium filled with viscoelastic fluid. Cheng (2010) studied Soret and Dufour effects on free convection boundary layer over a vertical cylinder in a saturated porous medium. Chamkha and Rashad (2012) investigated natural convection from a vertical permeable cone in nanofluid saturated porous media for uniform heat and nanoparticles volume fraction fluxes.

From the literature cited above, it appears that no analysis has yet been published concerning effects of radiation on MHD free convection of Casson fluid from a horizontal circular cylinder with partial slip in non-Darcy porous medium with viscous dissipation, under the given boundary conditions. The velocity and thermal slip conditions and transpiration effect are considered at the surface of the cylinder. The free stream conditions are considered to be at a lower temperature than the surface of the cylinder. The work considered in this chapter was based on the work put forward by Ramachandra et al. (2013a) in the study of momentum and heat transfer in Casson fluid. We extend the model to consider the radiation, magnetohydrodynamics and viscous dissipation effects.

In summary, this section has shown that investigating fluid flow over circular geometry, free convection, partial slip, radiation and magnetic effects is necessary to study. The system of partial differential equations will be solved by the bivariate quasi-linearisation method (BQLM). These aspects will be considered in the mathematical formulation of the problem of free convection of fluid flow from a horizontal circular cylinder. Studies in Casson fluid include among others Mukhopadhyay et al. (2013) and Nadeem et al. (2012).

6.3. Mathematical formulation of Casson fluid from a horizontal cylinder

The two dimensional cross-section of a horizontal circular cylinder in Casson fluid as shown in Figure 6.1. x is the tangential coordinate of the circle and y is the radial coordinate of the circle. A magnetic field is applied perpendicular to the y- axis.

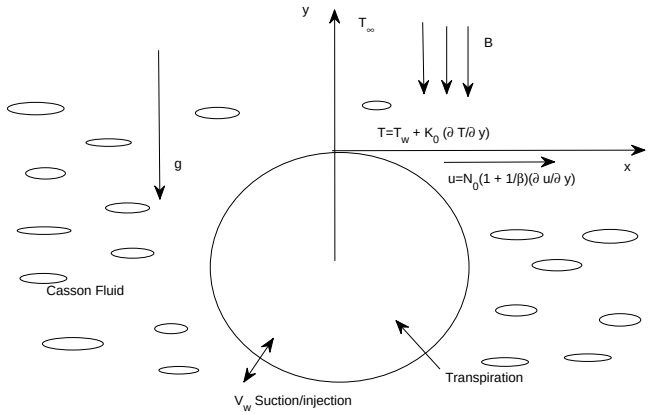

Figure 6.1: Schematic diagram of cross-section of cylinder in Casson fluid

The circle wall is maintained at a uniform temperature T_w ($> T_\infty$), the transpiration velocity V_w, in the direction y, u and v are the velocity components in the x and y directions respectively

The rheological equation of state for an isotropic and incompressible flow of a Casson fluid is given as in Mukhophadhyay and Vajravelu (2013) by:

$$\tau_{ij} = \begin{cases} 2(\mu_B + \dfrac{P_y}{\sqrt{2\pi}})e_{ij}, & \pi > \pi_c \\ 2(\mu_B + \dfrac{P_y}{\sqrt{2\pi_c}})e_{ij}, & \pi < \pi_c \end{cases} \tag{6.1}$$

$\pi = e_{ij}e_{ij}$ and e_{ij} is the $(i,j)^{th}$ component of the deformation rate, π is the product of the deformation rate with itself, π_c is a critical value of this product based on the non-

Newtonian model, μ_B is the plastic dynamic viscosity of the non-Newtonian fluid, P_y is the yield stress of the fluid.

The governing equations in this fluid flow are given as (see Ramachandra et al., 2013a);

$$\frac{\partial}{\partial x}(ru) + \frac{\partial}{\partial y}(rv) = 0, \tag{6.2}$$

$$u\frac{\partial u}{\partial x} + v\frac{\partial u}{\partial y} = \nu(1+\frac{1}{\beta})\frac{\partial^2 u}{\partial y^2} + g\beta_T(T-T_\infty)\sin(\frac{x}{r}) - \Gamma u^2 - \frac{\nu}{\bar{K}}u - \frac{\sigma B^2}{\rho}u \tag{6.3}$$

$$u\frac{\partial T}{\partial x} + v\frac{\partial T}{\partial y} = \alpha\frac{\partial^2 T}{\partial y^2} - \frac{1}{\rho C_p}\frac{\partial q_r}{\partial y} + \frac{\nu}{\rho C_p}(1+\frac{1}{\beta})\left(\frac{\partial u}{\partial y}\right)^2 + \frac{\sigma B^2 u^2}{\rho C_p} \tag{6.4}$$

where u and v are the velocity components in the x and y directions respectively, a is the radius of the cylinder, ν is kinematic viscosity of Casson fluid, $\beta = \mu_B\sqrt{2\pi_c}/P_y$ is the non-Newtonian Casson parameter, $\alpha = k/\rho C_p$ is the thermal diffusivity, k is thermal conductivity of the fluid, q_r is the radiative heat flux, C_p is the specific heat, $\bar{g}$ is the acceleration due to gravity, β_T is the coefficient of thermal expansions, and T is the temperature of the fluid, T_{infty} is the free stream temperature, ρ is the density of the fluid, $\bar{K}$ is the permeability of the porous medium, Γ is the inertia coefficient, σ is the electrical conductivity, and B is the magnetic flux density. The Rosseland approximation for radiation may be written as follows;

$$q_r = -\frac{4\sigma^*}{3k^*}\frac{\partial T^4}{\partial y} \tag{6.5}$$

where σ^* is the Stefan-Boltzman constant and k^* is the absorption coefficient. If the temperature difference within the flow is such that T^4 may be expanded in Taylor series about T_∞ and neglecting higher powers we obtain $T^4 - 4T_\infty^3 - 3T_\infty^4$ and therefore the Eq. (6.4) can be written as

$$u\frac{\partial T}{\partial x} + v\frac{\partial T}{\partial y} = \alpha\frac{\partial^2 T}{\partial y^2} + \frac{16\sigma^* T_\infty^3}{3\rho C_p k^*}\frac{\partial^2 T}{\partial y^2} + \frac{\nu}{\rho C_p}(1+\frac{1}{\beta})\left(\frac{\partial u}{\partial y}\right)^2 + \frac{\sigma B^2 u^2}{\rho C_p} \tag{6.6}$$

The boundary conditions are given as

$$\left.\begin{aligned} u = N_0(1+\frac{1}{\beta})\frac{\partial u}{\partial y}, \quad v = -V_w, \quad T = T_w + K_0\frac{\partial T}{\partial y}. \end{aligned}\right\} \quad y = 0, \tag{6.7}$$

$$u \to 0, \quad T \to T_\infty, \quad \text{as} \quad y \to \infty. \tag{6.8}$$

where N_0 is the velocity slip factor, K_0 is the thermal slip factor. $N_0 = K_0 = 0$ corresponds to no-slip conditions. The subscripts w and ∞ refer to surface and free stream conditions respectively.

We introduce the non-dimensional variables

$$\left.\begin{aligned} \xi = \frac{x}{r}, \quad \eta = \frac{y}{r}Gr^{\frac{1}{4}}, \quad Pr = \frac{\nu}{\alpha} \\ Gr = \frac{g\beta_T(T_w - T_\infty)a^3}{\nu^2}, \quad \beta_{cr} = \mu_B\frac{\sqrt{2\pi_{cr}}}{P_y} \\ \Lambda^* = \Gamma r, \quad k_p = \frac{1}{DaGr^{\frac{1}{2}}}, \quad Da = \frac{\bar{K}}{r^2}, \quad f_w = -\frac{V_w a}{\nu Gr^{\frac{1}{4}}}, \quad U_0 = \frac{\nu Gr^{\frac{1}{2}}}{r} \end{aligned}\right\} \tag{6.9}$$

Introducing the stream function ψ and similarity variables

$$u = \frac{\partial \psi}{\partial y} \quad \text{and} \quad v = -\frac{\partial \psi}{\partial x} \tag{6.10}$$

$$f(\xi,\eta) = \frac{\psi}{\nu\xi Gr^{\frac{1}{4}}}, \quad \theta(\xi,\eta) = \frac{T - T_\infty}{T_w - T_\infty}. \tag{6.11}$$

Using the stream function defined in Eqs. (6.10) and similarity variables in Eqs. (6.11), Eqs. (6.2)- (6.6) together with boundary conditions Eqs. (6.7) and (6.8) reduces to the following system of partial differential equations.

$$\left(1+\frac{1}{\beta}\right)f''' + ff'' - (1+\Lambda^*\xi)f'^2 - (k_p + M^2)f' + \frac{\sin(\xi)}{\xi}\theta = \xi\left(f'\frac{\partial f'}{\partial \xi} - f''\frac{\partial f}{\partial \xi}\right) \tag{6.12}$$

$$\frac{1}{Pr}(1+\frac{4}{3}K)\theta'' + f\theta' + \xi^2 Ec\left[\left(1+\frac{1}{\beta}\right)f''^2 + M^2(f')^2\right] = \xi\left(f'\frac{\partial \theta}{\partial \xi} - \theta'\frac{\partial f}{\partial \xi}\right) \tag{6.13}$$

with boundary conditions;

$$\eta = 0, \quad f = f_w, \quad f' = \left(1 + \frac{1}{\beta}\right) S_f f'', \quad \theta = 1 + S_T \theta' \tag{6.14}$$

$$\eta \to \infty, f' \to 0, \quad \theta \to 0. \tag{6.15}$$

where β is the Casson parameter, Λ^* is the Forchheimer parameter, k_p is the Darcian drag coefficient, M is the magnetic field parameter, K is the radiation parameter, Pr is the Prandtl number, Ec is the Eckert number, $f_w > 0$ corresponds to suction and $f_w < 0$ corresponds to blowing, $S_f = N_0 Gr^{\frac{1}{4}}/L$ is the velocity slip factor and $S_T = kGr^{\frac{1}{4}}/L$ is the thermal slip factor. In the above equations the primes refer to the derivative with respect to η.

We have formulated the partial differential equations in terms of the non-dimensional radial distance ξ. We then derive expressions for important engineering parameters which are the skin friction and heat transfer coefficients.

6.4. Skin friction and heat transfer coefficients

In this section we derive the skin friction and the heat transfer coefficients as follows; The shear stress at the surface of the cylinder is given can be expressed as (see Ramachandra et al., 2013a)

$$\tau_w = \mu \left[\left(1 + \frac{1}{\beta}\right) \frac{\partial u}{\partial y}\right]_{y=0} = \frac{\mu \left(1 + \frac{1}{\beta}\right) \nu \xi G r^{\frac{3}{4}}}{r^2} f''(0), \tag{6.16}$$

where μ is the coefficient of viscosity, the skin friction coefficient is given by

$$C_f = \frac{\tau_w}{\frac{1}{2}\rho U_\infty^2}. \tag{6.17}$$

Using Eqs. (6.16) and (6.17) together with Eqs. (6.10) and (6.11) give

$$C_f Gr^{-\frac{3}{4}} = (1 + \frac{1}{\beta})\xi f''(0). \tag{6.18}$$

The heat transfer from the surface of the circle into the fluid is given by

$$q_w = -k\left[\frac{\partial T}{\partial y}\right]_{y=0} = \frac{-k(T_w - T_\infty)}{aGr^{-\frac{1}{4}}} X\theta'(0), \tag{6.19}$$

where k is the thermal conductivity of the fluid. The heat transfer coefficient (Nusselt number) is given by

$$Nu = \frac{r}{k}\frac{q_w}{T_w - T_\infty}, \tag{6.20}$$

Using Eqs. (8.16) and (8.17) together with Eqs.(7.19) and (7.20) give

$$NuGr^{-\frac{1}{4}} = -\theta'(0). \tag{6.21}$$

We have formulated the mathematical model describing the flow of Casson fluid from a cylinder with partial slip, radiation, magnetic and viscous dissipation effects. The expressions for the skin friction and heat transfer coefficients have been derived. We now solve the system of partial differential equations obtained in this section using the bivariate quasi-linearization method (BQLM).

6.5. Numerical solution procedure

The differential Eqs. (4.15)-(5.10) of this type are normally solved by the Keller-box method described in section 1.1.6. This method involves rigorous procedures and result in a large

system of block matrices which require a considerable amount of computer memory and computation time. As already been discussed in Chapter 2 that spectral methods are accurate and robust. In this section we describe the implementation of the local linearization variant of the quasi-linearization. We apply the quasi-linearization method (QLM) first proposed by Bellman and Kalaba (1965) to Eqs. (4.15)-(5.10) with the assumption that the differences $(f_{r+1} - f_r)$,$(\theta_{r+1} - \theta_r)$ and all its derivatives are small. We obtain the following equations

$$\left(1 + \frac{1}{\beta}\right) f'''_{r+1} + a_{1,r}(\eta,\xi) f''_{r+1} + a_{2,r}(\eta,\xi) f'_{r+1} + a_{3,r}(\eta,\xi) f_{r+1} + a_{4,r}(\eta,\xi)\frac{\partial f'_{r+1}}{\partial \xi} + a_{5,r}(\eta,\xi)\frac{\partial f_{r+1}}{\partial \xi} = a_{6,r}(\eta,\xi). \tag{6.22}$$

$$\frac{1}{Pr}\left(1 + \frac{4}{3}K\right)\theta''_{r+1} + b_{1,r}(\eta,\xi)\theta'_{r+1} + b_{2,r}(\eta,\xi)\frac{\partial \theta_{r+1}}{\partial \xi} = b_{3,r}(\eta,\xi). \tag{6.23}$$

where

$$a_{1,r} = f_r + \xi\frac{\partial f_r}{\partial \xi} \tag{6.24}$$

$$a_{2,r} = -\left[2(1 + \Lambda^*\xi) f'_r + k_p + M^2 + \xi\frac{\partial f'_r}{\partial \xi}\right] \tag{6.25}$$

$$a_{3,r} = f''_r \tag{6.26}$$

$$a_{4,r} = -\xi f'_r \tag{6.27}$$

$$a_{5,r} = \xi f''_r \tag{6.28}$$

$$a_{6,r} = f_r f''_r - (1 + \Lambda^*\xi)(f'_r)^2 - \frac{\sin\xi}{\xi}\theta_r - \xi\left(\frac{\partial f'_r}{\partial \xi} - f''_r\frac{\partial f_r}{\partial \xi}\right) \tag{6.29}$$

$$b_{1,r} = f_r + \xi\frac{\partial f_r}{\partial \xi} \tag{6.30}$$

$$b_{2,r} = -\xi f' \tag{6.31}$$

$$b_{3,r} = -Ec\xi^2\left[(1 + \frac{1}{\beta})(f''_r)^2 + M^2(f'_r)^2\right] \tag{6.32}$$

The solution for the now linear partial differential Eq. (6.22)-(6.23) is obtained by approximating the exact solutions of $f(\eta,\xi)$ and $\theta(\eta,\xi)$ by the Lagrange form of polynomial $F(\eta,\xi)$ and $\Theta(\eta,\xi)$ at the selected collocation points

$$0 = \xi_0 < \xi_1 < \xi_2 < \cdots < \xi_{N_\xi} = 1$$

The approximation for $f(\eta, \xi)$ and $\theta(\eta, \xi)$ has the form

$$f(\eta, \xi) \approx \sum_{j=0}^{N_\xi} F(\eta, \xi_j) L_j(\xi) = \sum_{j=0}^{N_\xi} F_j(\eta) L_j(\xi), \tag{6.33}$$

$$\theta(\eta, \xi) \approx \sum_{j=0}^{N_\xi} \Theta(\eta, \xi_j) L_j(\xi) = \sum_{j=0}^{N_\xi} \Theta_j(\eta) L_j(\xi). \tag{6.34}$$

where $F_j(\eta) = F(\eta, \xi_j)$ and $\Theta_j(\eta) = \Theta(\eta, \xi_j)$, L_j is the characteristic Lagrange cardinal polynomial defined as

$$L_j(\xi) = \prod_{k=0, k\neq j}^{M} \frac{\xi - \xi_k}{\xi_j - \xi_k}, \tag{6.35}$$

that obey the Kronecker delta equation

$$L_j(\xi_k) = \delta_{jk} = \begin{cases} 0 & \text{if} \quad j \neq k \\ 1 & \text{if} \quad j = k \end{cases} \tag{6.36}$$

The equations for the solution of $F_j(\eta)$ and $\Theta_j(\eta)$ are obtained by substituting Eqs. (6.33)-(6.34) into Eqs. (6.22)-(6.23) and letting the equations be satisfied at the points $\xi_i, i = 0, 1, 2, \ldots, N_\xi$. To compute the derivatives of the Lagrange polynomial analytically we transform $\xi \in [0, L_\xi]$ to $\zeta \in [-1, 1]$ then choose Chebyshev-Gauss-Lobatto points $\zeta_i = \cos \frac{i\pi}{N_\xi}$. After using linear transformation $\xi = L_\xi(\zeta + 1)/2$, the derivatives of f' with respect to the collocation points ζ_j is computed as

$$\frac{\partial f'}{\partial \xi}|_{\xi=\xi_i} = 2 \sum_{j=0}^{N_\xi} F'_j(\eta) \frac{dL_j}{d\zeta}(\zeta_i) = \sum_{j=0}^{N_\xi} \mathbf{d}_{i,j} F'_j(\eta), i = 0, 1, 2, \ldots, N_\xi, \tag{6.37}$$

where $\mathbf{d}_{i,j} = \frac{dL_j}{d\zeta}(\zeta_i)(i = 0, 1, \ldots, N_\xi)$ are entries of the standard Chebyshev differentiation matrix, $\mathbf{d} = \frac{2}{L_\xi} d$. We now apply the collocation (η, ξ_i) in Eqs. (6.22)-(6.23) we obtain

$$\left(1+\frac{1}{\beta}\right)F'''_{r+1,i}(\eta)+a^{(i)}_{1,r}F''_{r+1,i}(\eta)+a^{(i)}_{2,r}F'_{r+1,i}(\eta)+a^{(i)}_{3,r}F_{r+1,i}(\eta)$$
$$+a^{(i)}_{4,r}\sum_{j=0}^{N_\xi}\mathbf{d}_{i,j}F'_{r+1,i}(\eta)+a^{(i)}_{5,r}\sum_{j=0}^{N_\xi}\mathbf{d}_{i,j}F_{r+1,i}(\eta)=a^{(i)}_{6,r}. \quad (6.38)$$

$$\frac{1}{Pr}\left(1+\frac{4}{3}K\right)\Theta''_{r+1,i}(\eta)+b^{(i)}_{1,r}\Theta'_{r+1,i}(\eta)+b^{(i)}_{2,r}\sum_{j=0}^{N_\xi}\mathbf{d}_{i,j}\Theta_{r+1,i}(\eta)=b^{(i)}_{3,r}. \quad (6.39)$$

where $a^{(i)}_{k,r}=a_{k,r}(\eta,\xi_i)\quad(k=1,2,3,4,5,6)$ and $b^{(i)}_{k,r}=b_{k,r}(\eta,\xi_i)\quad(k=1,2,3)$. The equations (6.12)-6.14 are solved for $\xi=0(\zeta=\zeta_{N_\xi})$ using the spectral quasi-linearization method, this is then solved like a PDE with initial conditions. We evaluate Eqs. (6.38)-(6.39) for $i=0,1,\ldots,N_\xi-1$ the system becomes

$$\left(1+\frac{1}{\beta}\right)F'''_{r+1,i}+a^{(i)}_{1,r}F''_{r+1,i}+a^{(i)}_{2,r}F'_{r+1,i}+a^{(i)}_{3,r}F_{r+1,i}+a^{(i)}_{4,r}\sum_{j=0}^{N_\xi-1}\mathbf{d}_{i,j}F'_{r+1,i}$$
$$+a^{(i)}_{5,r}\sum_{j=0}^{N_\xi-1}\mathbf{d}_{i,j}F_{r+1,i}=a^{(i)}_{6,r}-a^{(i)}_{4,r}\mathbf{d}_{i,N_\xi}F'_{r+1,N_\xi}-a^{(i)}_{5,r}\mathbf{d}_{i,N_\xi}F_{r+1,N_\xi}. \quad (6.40)$$

$$\frac{1}{Pr}\left(1+\frac{4}{3}K\right)\Theta''_{r+1,i}+b^{(i)}_{1,r}\Theta'_{r+1,i}+b^{(i)}_{2,r}\sum_{j=0}^{N_\xi-1}\mathbf{d}_{i,j}\Theta_{r+1,i}=b^{(i)}_{3,r}-b^{(i)}_{2,r}\mathbf{d}_{i,N_\xi}\Theta_{r+1,N_\xi}. \quad (6.41)$$

For each ξ_i, the Eqs. (6.40)-(6.41) forms a system of linear ordinary differential equations with variable coefficients. In this system we apply the Chebyshev spectral collocation independently in the η direction by choosing $N_\eta+1$ Chebyshev-Gauss-Lobatto points $0=\eta_0<\eta_1<\eta_2<\cdots<\eta_{N_\eta}=\eta_e$, where η_e is a finite value that is chosen to be adequately large to approximate the conditions at ∞. We now implement the collocation in the interval $[0,\eta_e]$ on the $\eta-$ axis which is then transformed into the interval $[-1,1]$ using a linear transformation $\eta=\eta_e(\tau+1)/2$. The collocation points are chosen as $\tau_j=\cos\frac{j\pi}{N_\eta}$. The derivatives with respect to η are defined in terms of the Chebyshev differentiation matrix as

$$\left.\frac{d^p F'_{r+1,i}}{d\eta^p}\right|_{\eta=\eta_j} = \left(\frac{2}{\eta_e}\right)^p \sum_{k=0}^{N_\eta} D^p_{j,k} F_{r+1,i}(\tau_k) = \left[\mathbf{D}^p \mathbf{F}_{r+1,i}\right]. \tag{6.42}$$

where p is the order of the derivative, $\mathbf{D} = \frac{2}{\eta_e} D, (j,k = 0,1,2,\ldots,N_\eta)$ with D being an $(N_\eta+1)\times(N_\eta+1)$ Chebyshev derivative matrix, and the vector $\mathbf{F}_{r+1,i}$ is defined as

$$\mathbf{F}_{r+1,i} = [F_{r+1,i}(\tau_0), F_{r+1,i}(\tau_1), \ldots, F_{r+1,i}(\tau_{N_\eta})]^T, \tag{6.43}$$

$$\Theta_{r+1,i} = [\Theta_{r+1,i}(\tau_0), \Theta_{r+1,i}(\tau_1), \ldots, \Theta_{r+1,i}(\tau_{N_\eta})]^T \tag{6.44}$$

substituting Eq. (6.42) into Eq. (6.40) we get

$$\mathbf{A}^{(i)}\mathbf{F}_{r+1,i} + \mathbf{a}^{(i)}_{4,r} \sum_{j=0}^{N_\xi-1} d_{i,j}\mathbf{D}\mathbf{F}_{r+1,j} + \mathbf{a}^{(i)}_{5,r} \sum_{j=0}^{N_\xi-1} d_{i,j}\mathbf{F}_{r+1,j} = R^{(i)}_1. \tag{6.45}$$

$$\mathbf{A}^{(i)} = (1+\frac{1}{\beta})\mathbf{D}^3 + \mathbf{a}^{(i)}_{1,r}\mathbf{D}^2 + a^{(i)}_{2,r}\mathbf{D} + \mathbf{a}^{(i)}_{2,r}, \tag{6.46}$$

$$\mathbf{R}^{(i)}_1 = \mathbf{a}^{(i)}_{6,r} - \mathbf{a}^{(i)}_{4,r} d_{i,N_\xi}\mathbf{D}\mathbf{F}_{r+1,N_\xi} - \mathbf{a}^{(i)}_{5,r} d_{i,N_\xi}\mathbf{F}_{r+1,N_\xi} \tag{6.47}$$

$$\mathbf{B}^{(i)}\Theta_{r+1,i} + \mathbf{b}^{(i)}_{2,r} \sum_{j=0}^{N_\xi-1} d_{i,j}\Theta_{r+1,j} = R^{(i)}_2, \tag{6.48}$$

$$\mathbf{B}^{(i)} = \frac{1}{Pr}(1+\frac{4}{3}K)\mathbf{D}^2 + \mathbf{b}^{(i)}_{1,r}\mathbf{D}, \tag{6.49}$$

$$\mathbf{R}^{(i)}_2 = \mathbf{b}^{(i)}_{3,r} - \mathbf{b}^{(i)}_{2,r} d_{i,N_\xi}\Theta_{r+1,N_\xi}. \tag{6.50}$$

$\mathbf{a}_{k,r}(k=1,2,3,4,5,6), \mathbf{b}_{k,r}(k=1,2,3)$ is the diagonal matrix with vector $[a_{k,r}(\tau_0), a_{k,r}(\tau_1), \ldots, a_{k,r}(\tau_{N_x})]^T$ and $[b_{k,r}(\tau_0), b_{k,r}(\tau_1), \ldots, b_{k,r}(\tau_{N_x})]^T$. We then obtain a matrix system formed as follows.

$$\begin{pmatrix} A_{0,0} & A_{0,1} & \ldots & A_{0,N_\xi-1} \\ A_{1,0} & A_{1,1} & \ldots & A_{1,N_\xi-1} \\ \vdots & \vdots & \ddots & \vdots \\ A_{N_{\xi-1},0} & A_{N_{\xi-1},1} & \ldots & A_{N_{\xi-1},N_\xi-1} \end{pmatrix} \begin{pmatrix} \mathbf{F}_{r+1,0} \\ \mathbf{F}_{r+1,1} \\ \vdots \\ \mathbf{F}_{r+1,N_\xi-1} \end{pmatrix} = \begin{pmatrix} R^{(0)}_1 \\ R^{(1)}_1 \\ \vdots \\ R^{(N_\xi-1)}_1 \end{pmatrix}$$

$$\begin{pmatrix} B_{0,0} & B_{0,1} & \dots & B_{0,N_\xi-1} \\ B_{1,0} & B_{1,1} & \dots & B_{1,N_\xi-1} \\ \vdots & \vdots & \ddots & \vdots \\ B_{N_{\xi-1},0} & B_{N_{\xi-1},1} & \dots & B_{N_{\xi-1},N_\xi-1} \end{pmatrix} \begin{pmatrix} \Theta_{r+1,0} \\ \Theta_{r+1,1} \\ \vdots \\ \Theta_{r+1,N_\xi-1} \end{pmatrix} = \begin{pmatrix} R_2^{(0)} \\ R_2^{(1)} \\ \vdots \\ R_2^{(N_\xi-1)} \end{pmatrix}$$

The above matrix systems can be solved independently to reduce large matrix inversions. Where

$$\begin{aligned} A_{i,i} &= \mathbf{A}^{(i)} + \mathbf{a}^{(\mathbf{i})}_{\mathbf{4,r}}\mathbf{d_{i,i}D} + \mathbf{a}^{(\mathbf{i})}_{\mathbf{5,r}}\mathbf{d_{i,i}}, \\ B_{i,i} &= \mathbf{B}^{(i)} + \mathbf{b}^{(\mathbf{i})}_{\mathbf{2,r}}\mathbf{d_{i,i}} \quad \mathbf{i = 0, 1, \dots, N_\xi - 1}, \end{aligned} \tag{6.51}$$

The off-diagonal entries of $\mathbf{AA}$ are expressed as

$$\begin{aligned} A_{i,j} &= \mathbf{a}^{(\mathbf{i})}_{\mathbf{4,r}}\mathbf{d_{i,j}D} + \mathbf{a}^{(\mathbf{i})}_{\mathbf{5,r}}\mathbf{d_{i,j}}, \quad \mathbf{i \neq j} \\ B_{i,j} &= \mathbf{b}^{(\mathbf{i})}_{\mathbf{2,r}}\mathbf{d_{i,j}} \quad \mathbf{i \neq j} \end{aligned} \tag{6.52}$$

The solution procedure described in this section was used to solve the mathematical model for free convection of Casson fluid flow from a circular cylinder in porous medium with radiation, magnetic and viscous dissipation effects. We are therefore ready to report the results in the next section.

6.6. Results and discussion

The problem that was investigated in this chapter as described in the previous section is solved using the local linearization method (LLM). In this section we discuss the effects of Casson parameter β, Forchheimer parameter Λ^*, Darcian drag force coefficient k_p, magnetic parameter M, Prandtl number Pr, radiation parameter K, the Eckert number Ec, suction/injection parameter f_w, velocity slip S_f and thermal slip S_T factors, and the transverse coordinate ξ on the velocity $f'(\eta)$ and temperature $\theta(\eta)$ profiles. η is the distance describing

the boundary layer thickness.

In this section we assume that the Casson fluid discussed covers a wide range of this type of fluid which normally has a Prandtl number between $Pr = 10$ at 20^oC and $Pr = 20$ for blood. The Grashof number is fixed at $Gr = 10$ and Darcy number $Da = 0.1$ giving a fixed value $k_p = 1/DaGr^{\frac{1}{2}} = 3$. All other parameters are chosen arbitrarily being careful to stay within the acceptable range of the Casson fluid.

The validation of the numerical method is performed by comparing the results obtained by the local linearization method (LLM) by those obtained by the successive linearization method (SLM) as shown in Table 6.1. These results could not be compared to any results in the literature as Ramachandra et al. (2013a) did not report any numerical results.

Table 6.1: Comparison of the values of skin friction coefficient and heat transfer coefficients obtained by LLM with SLM for $1/\beta = \Lambda^* = k_p = M = \xi = K = f_w = S_f = S_T = 0$

	SLM		LLM	
Pr	$f''(0)$	$-\theta'(0)$	$f''(0)$	$-\theta'(0)$
1	0.87100777	0.42143140	0.81700776	0.42143144
10	0.54471433	0.88046306	0.54471422	0.88046307

To understand the behavior of the velocity and temperature profiles the illustrations for the numerical solution obtained are depicted as graphs in Figures 6.2 - 6.8.

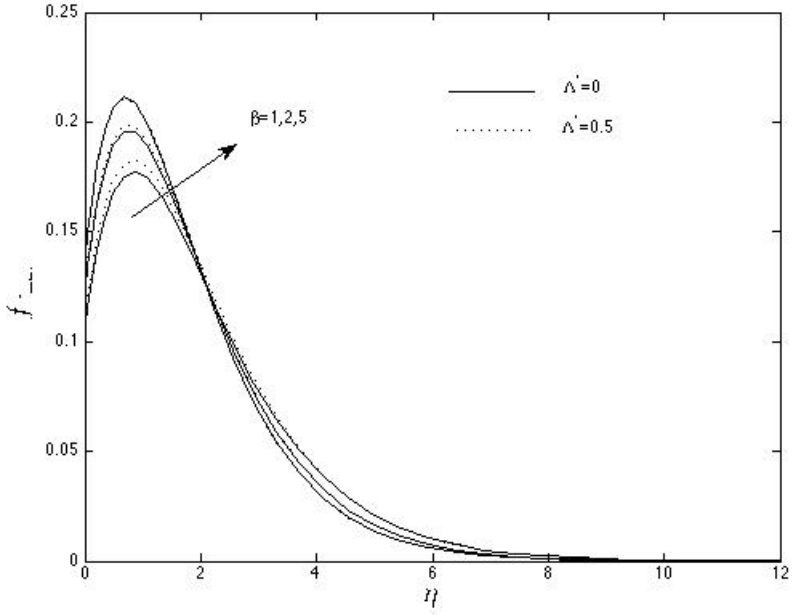

Figure 6.2: Effects of Casson parameter on velocity profiles $f'(\eta, \xi)$ for different values of the Forchheimer parameter Λ^* and S_f, at $k_p = 3, K = 0.5, Pr = 5, Ec = 1, M = 1, f_w = 0.5, S_T = 0.5$

Figure 6.2 shows the influence of Casson parameter β on velocity and temperature profiles $f'(\eta)$ at different values of the Forhheimer parameter Λ. The case $\Lambda = 0$ corresponds to no inertia or no transpiration. It can be seen from the graph that increasing the Casson parameter increase velocity profiles close to the surface as would be expected (see section 5.5). We note the reverse effect resulting in the thinning of the momentum boundary layer. This reverse effect noticed is caused by the presence of the magnetic effect. Ramachandra et al. (2013a) did not obtain at reverse effect because of the absence of the magnetic field.

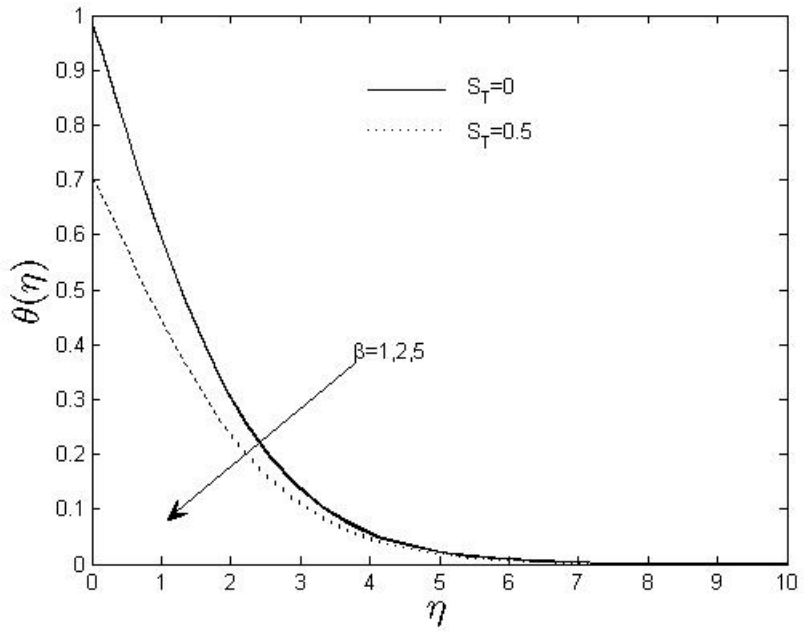

Figure 6.3: Effects of Casson parameter on temperature profiles $\theta(\eta, \xi)$ for different values of the thermal slip parameter S_T and S_f, at $k_p = 3, K = 0.5, Pr = 5, Ec = 1, M = 1, f_w = 0.5$.

The variation of Casson parameter β on temperature profiles at different values of the thermal slip factor S_T is shown in Figure 6.3. It can be seen from the graph that increasing the Casson parameter decrease temperature profiles as discussed in section 5.5. It is noted that increasing the thermal slip factor result in the decrease of temperature profile. The highest temperature associated with no-slip ($S_T = 0$) and minimum temperature associated with the strongest thermal slip ($S_T = 0.5$). The temperature profiles are strongly depressed with increasing thermal slip with the highest effect noticed at the wall of the circle. We can thus interpret an increase in the thermal slip factor S_T as having the effect of reducing the heat transfer from the surface of the circle to the fluid.

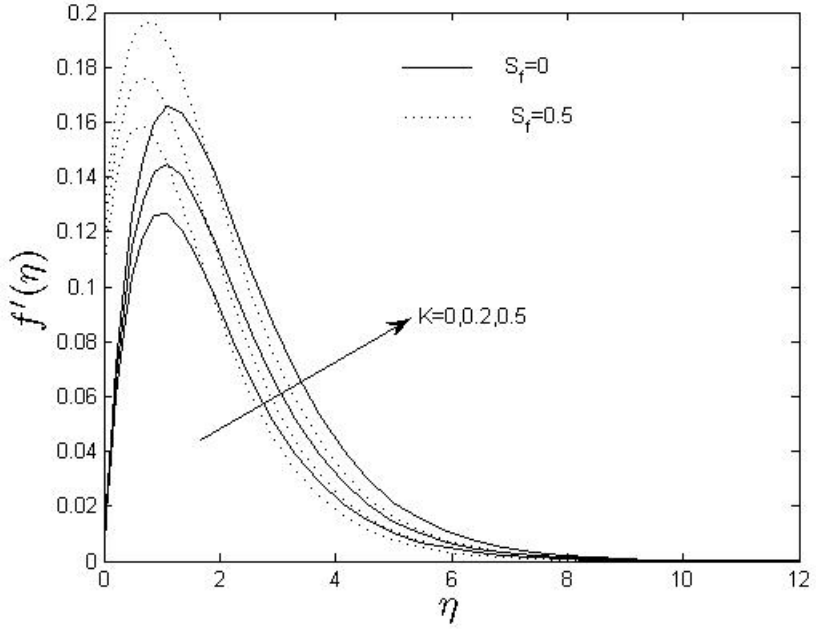

Figure 6.4: Effects of radiation parameter on velocity profiles $f'(\eta, \xi)$ for different values of the velocity slip factor S_f, at $k_p = 3, K = 0.5, Pr = 5, Ec = 1, f_w = 0.5, S_T = 0.5, \beta = 2$

The variation of the radiation parameter K on velocity profiles for different values of the velocity slip factor S_f as shown in Figure 6.4. The effect of the radiation parameter K on velocity profiles is experienced indirectly via coupling of the momentum equation and the energy equation. It can be seen from the Figure that increasing the radiation parameter result in the increase in temperature profiles. This is interpreted as the motion caused by higher temperatures induced in the fluid. It is also noted that this does not affect the boundary layer thickness. It can be seen that increasing the velocity slip factor S_f result in increasing the velocity profiles. This is to be expected because increasing the velocity slip factor would have an effect of assisting the flow, in particular it decreases the shear stress at the wall and a slip is facilitated. The case $S_f = 0$ corresponds to the no-slip condition.

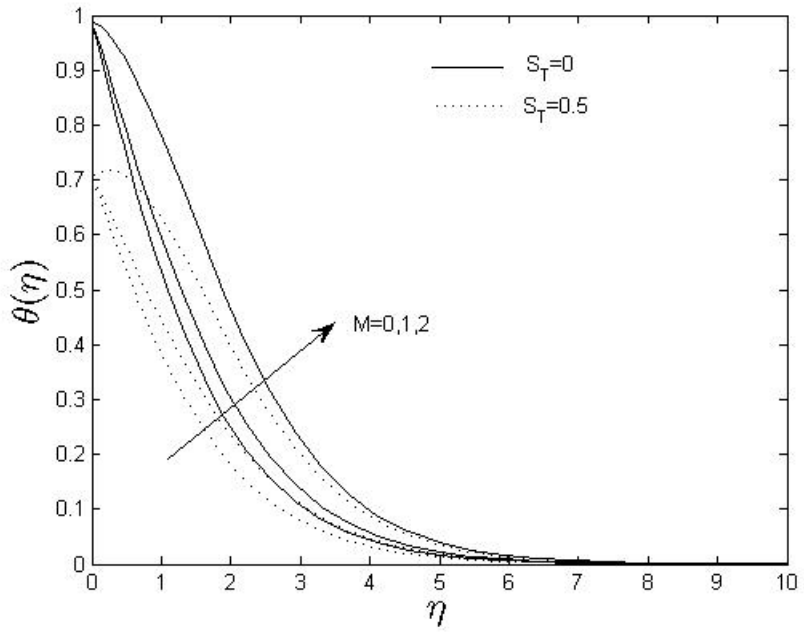

Figure 6.5: Effects of magnetic parameter on temperature profiles $\theta(\eta, \xi)$ for different values of the thermal slip parameter S_T and S_f, at $k_p = 3, K = 0.5, Pr = 5, Ec = 1, f_w = 0.5, \beta = 2$

The variation of the magnetic parameter M on temperature profiles for different values of the thermal slip factor is shown in Figure 6.5. Increasing the magnetic parameter increase the temperature profiles. In this figure we note the smooth decays of the temperature profiles; this shows an excellent convergence of the numerical solution. We also note that the effect of the magnetic parameter is more pronounced in the case of the thermal slip condition ($S_T = 0.5$) than in no-slip condition ($S_T = 0$).

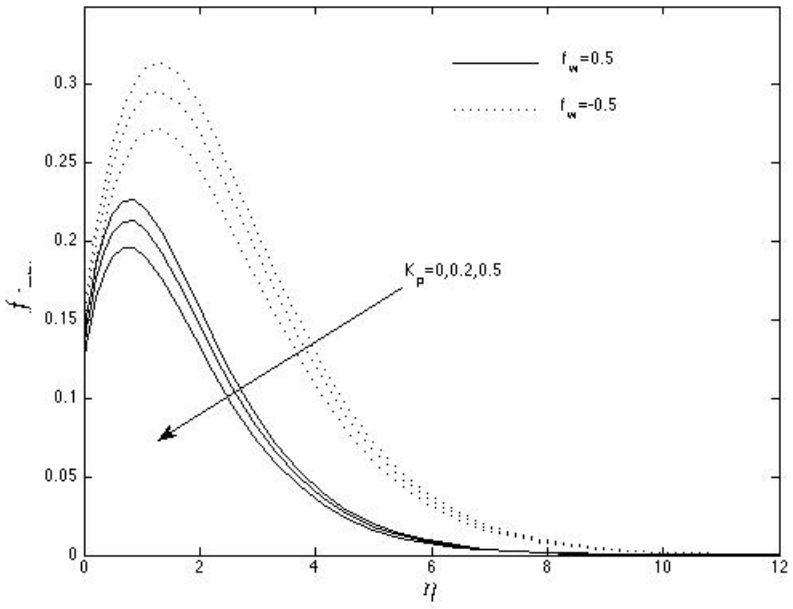

Figure 6.6: Effects of Darcian drag force coefficient k_p on velocity and profiles $f'(\eta, \xi)$ for different S_f, at $\beta = 2, k_p = 3, K = 0.5, Pr = 5, Ec = 1, M = 1, f_w = 0.5, S_T = 0.5$

The variation of the Darcian drag force coefficient k_p on velocity profiles $f'(\eta)$ for different values of the suction/injection parameter f_w is shown in Figure 6.6. It can be seen that increasing the Darcian drag force coefficient result in the decrease of velocity profiles. In this case the Darcian drag force coefficient k_p is inversely proportional to the Darcy number Da. This relationship suggests that increasing the Darcian drag force coefficient would have an effect of reducing the Darcy number associated with the permeability of the porous medium. This in turn affects the velocity of the fluid. We also note that velocity profiles are more pronounced for the case of injection $f_w = -0.5$ than in the case of suction $f_w = 0.5$. The same observation was noted by Chamkha (2003).

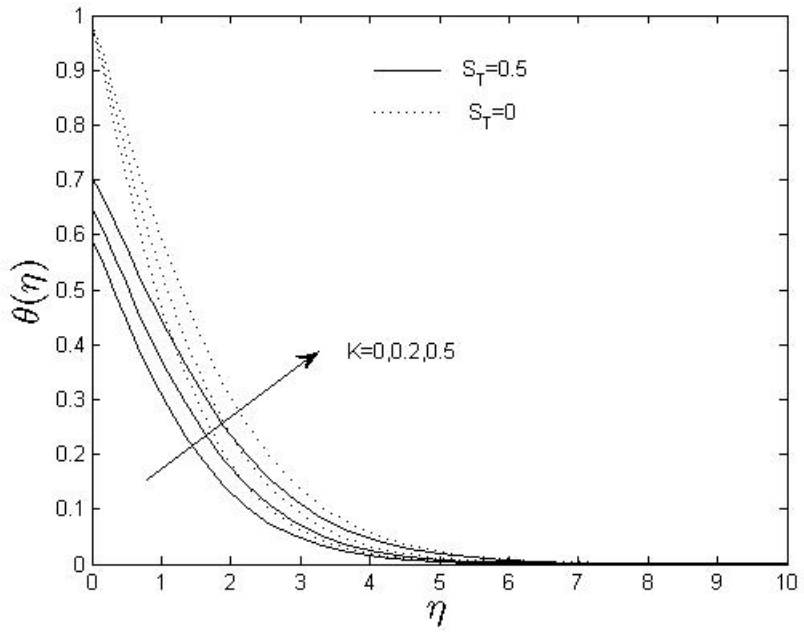

Figure 6.7: Effects of radiation parameter K on temperature profiles $\theta(\eta, \xi)$ for different S_T, at $\beta = 2, k_p = 3, K = 0.5, Pr = 5, Ec = 1, M = 1, f_w = 0.5, S_T = 0.5$

The variation of the radiation parameter K on temperature profiles for different values of the thermal slip factor as shown in Figure 6.7. It can be seen from this figure that increasing the radiation parameter K result in the increase temperature profiles. We can thus interpret an increase in the radiation parameter as having an effect of increasing the conduction effect, this in turn cause the temperature to increase at every point away from the circular surface. It is also noted that there is a variation of the initial temperature at the surface of the circle under slip conditions ($S_T = 0.5$) and no variation under the no-slip condition ($S_T = 0$).

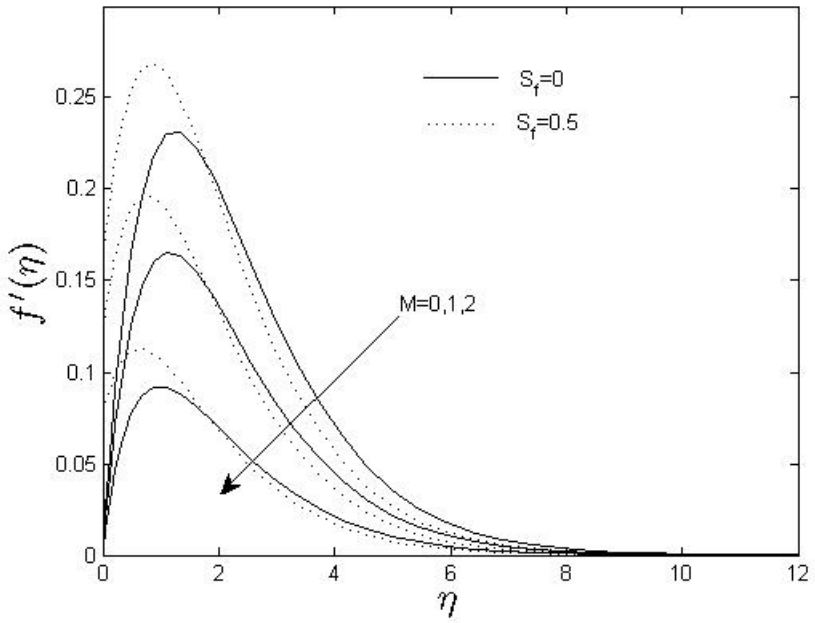

Figure 6.8: Effects of magnetic parameter M on velocity profiles $f'(\eta, \xi)$ for different values of S_f at $\beta = 2, k_p = 3, \Lambda^* = 0.5, K = 0.5, M = 1, K = 0.5, Pr = 5, S_T = 0.5$

The variation of the magnetic parameter M on velocity profiles for different values of the velocity slip factor S_f as shown in Figure 6.8. It can be seen from the graph that increasing the magnetic parameter result in suppressing velocity profiles as discussed in section 5.5. It is noted that in this figure the maximum velocity is moved close to the boundary due to the effect caused by the slip.

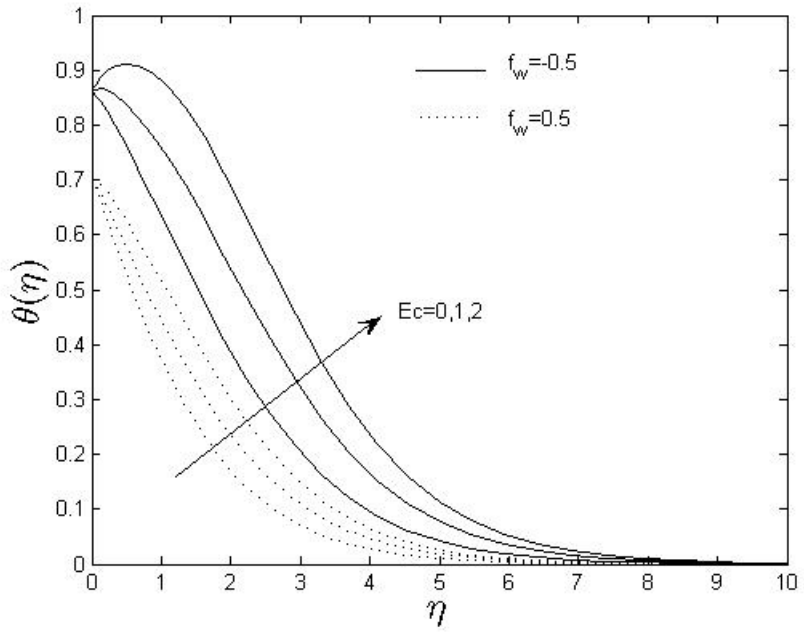

Figure 6.9: Effects of Eckert number Ec on temperature profiles $\theta(\eta, \xi)$ for different values of the suction/injection parameter f_w at $\beta = 2, k_p = 3, \Lambda^* = 0.5, K = 0.5, M = 1, K = 0.5, Pr = 5, S_T = 0.5$

The variation of the Eckert number Ec on temperature profiles for different values of suction/injection parameter f_w as shown in Figure 6.9. It can be seen from the figure that increasing the Eckert number result in the increase in temperature profiles. We can thus interpret that increasing the Eckert number which represents viscous dissipation as having an effect of increasing the temperature of the fluid. We note the transition from heat transfer from the surface to the fluid to the heat transfer from the fluid to the surface. This can be deduced from the change on the wall temperature gradient from negative ($Ec = 1$) to positive $Ec = 2$. It is also noted that under suction ($f_w > 0$) there is no transition in heat flow. The wall temperature gradient is negative for all values of the Eckert number Ec meaning that the heat is transferred from the surface to the fluid.

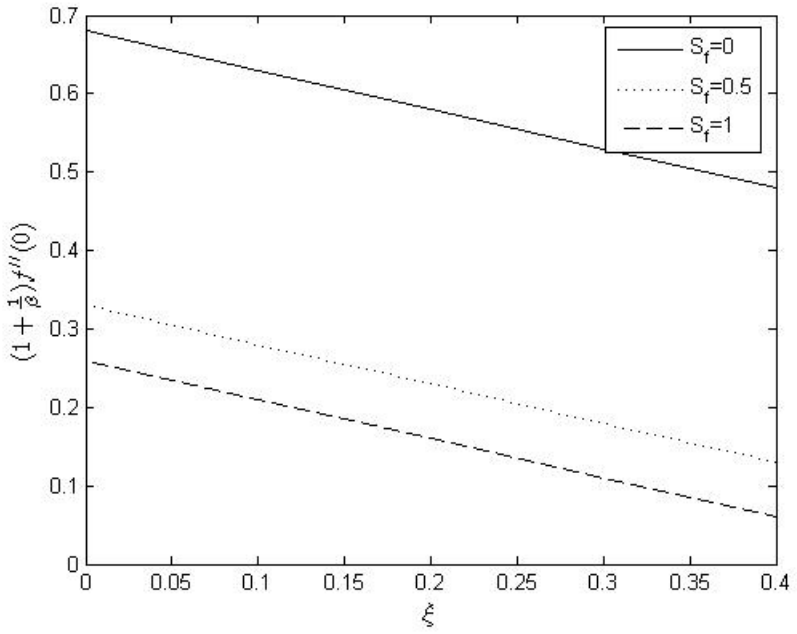

Figure 6.10: Skin friction coefficient against transverse coordinate ξ for different S_f at $\beta = 2, k_p = 3, K = 0.5, M = 1, Pr = 5, Ec = 1, f_w = 0.5, \Lambda^* = 0.5$

Figure 6.10 shows the plot of the skin friction coefficient related to $-(1 + 1/\beta)f''(0)$ against the non-dimensional transverse distance ξ for different values of the velocity slip factor S_f. It can be seen that increasing the velocity slip factor result in the decrease in skin friction coefficient. This is to be expected because increasing the velocity slip factor would have an effect of lubricating the surface as also reported by Ramachandra et al. (2013), thereby reducing the skin friction coefficient. Increasing ξ results in decreasing the skin friction coefficient, this is because the contact of the fluid and the circle is maximum at the origin and this contact reduces with the increase in the transverse coordinate.

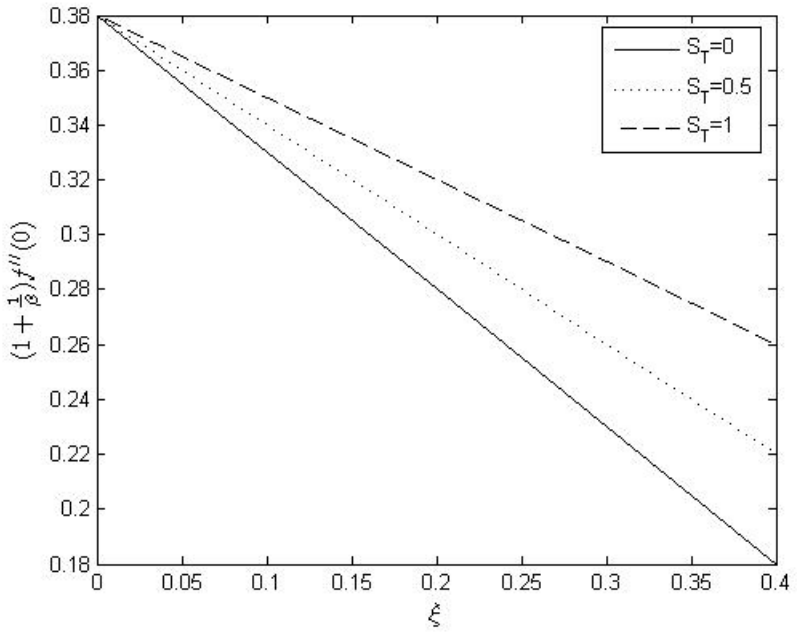

Figure 6.11: Skin friction coefficient against transverse coordinate ξ for different S_T at $\beta = 2, k_p = 3, K = 0.5, M = 1, Pr = 5, Ec = 1, f_w = 0.5, \Lambda^* = 0.5$

Figure 6.11 shows the plot of skin friction coefficient related to $-(1+1/\beta)f''(0)$ against the non-dimensional transverse distance ξ for different values of the thermal slip factor S_T. It can be seen from the figure that increasing the thermal slip factor S_T results in the increase in the skin friction coefficient. This is to be expected because increasing the thermal slip factor S_T would have an effect of reducing heat transfer to the fluid, this effect does not affect the skin friction coefficient at the surface.

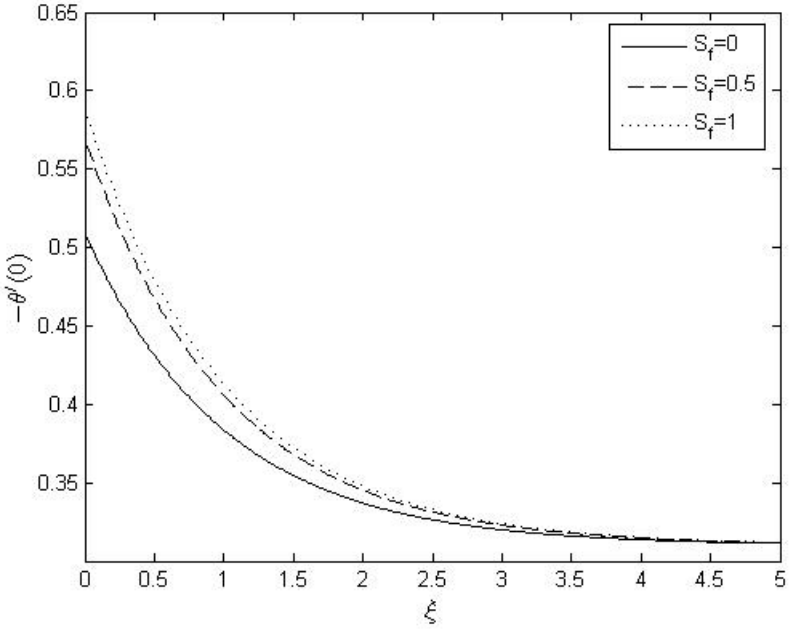

Figure 6.12: Heat transfer coefficient against transverse coordinate ξ for different S_f at $\beta = 2, k_p = 3, K = 0.5, M = 1, Pr = 5, Ec = 1, f_w = 0.5, \Lambda^* = 0.5$

The plot of heat transfer coefficient $-\theta'(0)$ against ξ for different values of the velocity slip factor S_f is shown in Figure 6.11 It can be seen from the figure that increasing the velocity slip factor S_f result in the increase in the heat transfer coefficient. This is to be expected because increasing the velocity slip factor S_f would have an effect of reducing the shear stress, this effect permits effective heat transfer of heat from the wall to the fluid. Heat transfer coefficient decreases with increasing transverse distance ξ. This is caused by the fact that as the fluid loses contact with the cylinder with increasing ξ, heat transfer is not facilitated.

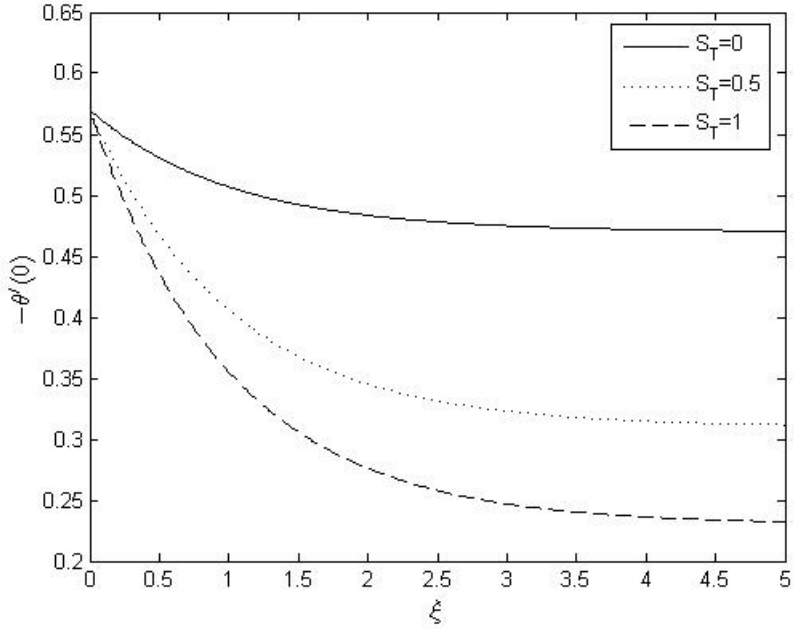

Figure 6.13: Heat transfer coefficient against transverse coordinate ξ for different S_T at $\beta = 2, k_p = 3, K = 0.5, M = 1, Pr = 5, Ec = 1, f_w = 0.5, \Lambda^* = 0.5$

Figure 6.13 shows the plot of heat transfer coefficient related to $-\theta'(0)$ against the non-dimensional transverse coordinate ξ for different values of the thermal slip factor S_T. It can be seen from the figure that increasing the thermal slip factor S_T result in the decrease in the heat transfer coefficient. This is to be expected because increasing the thermal slip factor S_T would have an effect of reducing heat transfer to the fluid, this effect does not affect the heat transfer coefficient at the surface. Heat transfer is reduced as the distance ξ increases.

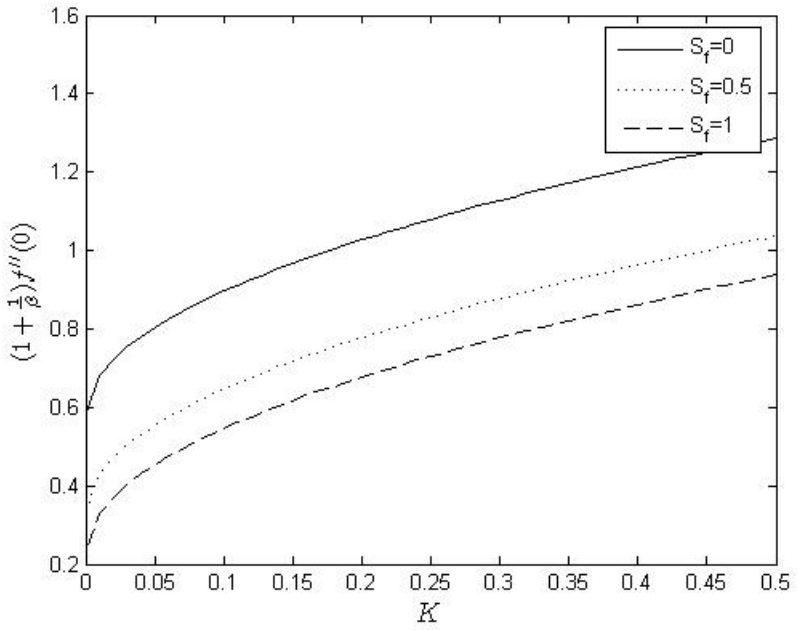

Figure 6.14: Skin friction coefficient $f''(0)$ against radiation parameter K for different S_f at $\beta = 2, k_p = 3, M = 1, Pr = 5, Ec = 1, f_w = 0.5, \Lambda^* = 0.5$

The plot of skin friction coefficient $-(1 + 1/\beta)f''(0)$ against radiation parameter K for different values of the velocity slip factor S_f is shown in Figure 6.14 It can be seen from the figure that increasing the velocity slip factor S_f result in the decrease in skin friction coefficient. This is to be expected because increasing the velocity slip factor S_f would have an effect of reducing the shear stress, this effect lubricates the surface thereby reducing the skin friction coefficient. Skin friction coefficient increases with increasing radiation parameter K.

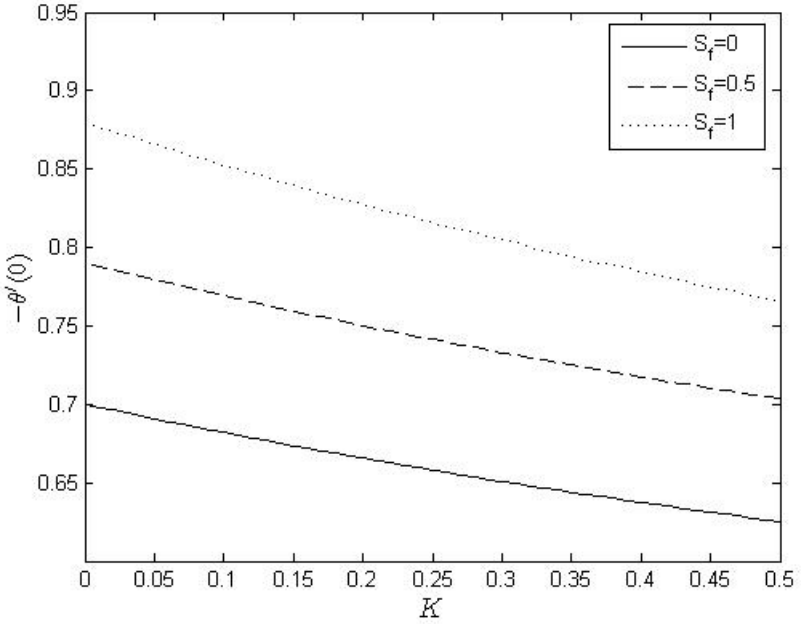

Figure 6.15: Heat transfer coefficient $-\theta'(0)$ against radiation parameter K for different S_f at $\beta = 2, k_p = 3, M = 1, Pr = 5, Ec = 1, f_w = 0.5, \Lambda^* = 0.5$

Figure 6.15 shows the plot of heat transfer coefficient related to $-\theta'(0)$ against the radiation parameter K for different values of the velocity slip factor S_f. It can be seen from the figure that increasing the thermal slip factor S_T result in the increase in the heat transfer coefficient. Increasing the radiation parameter K decrease the heat transfer coefficient; this is to be expected because increasing the radiation parameter would have an effect of increasing the temperature of the fluid. This would reduce heat transfer from the surface to the fluid.

6.7. Summary

The problem of the effects of radiation on magnetohydrodynamic free convection of Casson fluid from a horizontal circular cylinder with partial slip in non-Darcy porous medium was studied. Some physical aspects were considered; increasing the Casson parameter result in the increase in the velocity profiles but reduce temperature profiles. Increasing the radiation parameter result in the increase in the both velocity and temperature profiles. Increasing the magnetic parameter increase temperature profiles but reduces velocity profiles. Increasing the Eckert number increases the temperature profiles. Increasing the Forchheimer parameter

increase the velocity profiles. Increasing the thermal slip factor reduce the temperature profiles while increasing the velocity slip factor increase velocity profiles. Blowing tend to assist the fluid flow while suction reduce velocity profiles.

The problem that was considered in this chapter is a unique non-similar differential equation. Problems of this type pose a challenge in solving them. The method which is normally used is the Keller-box method which is rigorous and less accurate than the spectral methods. We solve this problem using the local linearization method (LLM). The use of this method in such problems is fairly new.

In this chapter the local linearization method (LLM) is used to find solutions of the governing equations. The problem consists of two coupled partial differential equations differential equations, which are normally solved by the Keller-box method. The Keller-box method involves rigorous finite differences and large block matrices which require both considerable computation time and memory. Consequently, we applied the LLM. It was deduced that the LLM converged faster than both the SLM. The LLM solution rapidly converged to the solution. The numerical solutions obtained by LLM were compared to those obtained by the successive linearization method; they were found to be in excellent agreement.

7

Effects of radiation on free convection from a spinning cone with partial slip in Casson fluid in non-Darcy porous medium with cross diffusion and viscous dissipation

7.1. Introduction

In this chapter we investigate the problem of free convection from a spinning cone in Casson fluid with partial slip, radiation, porous medium, cross diffusion and viscous dissipation effects. In this study the governing equations are transformed to a system of coupled and nonlinear differential equations. These equations are solved by spectral relaxation method (SRM) (see section 1.1.8). In this chapter we demonstrate the implementation of this method and show the use of the successive over-relaxation (SOR) to accelerate convergence. The accuracy of the method is determined by comparison with the Matlab `bvp4c` and related results in the literature.

7.2. Review of literature on Casson fluid from a spinning cone

In this chapter we review literature concerning the problem of free convection from a spinning cone in Casson fluid with partial slip, radiation, porous medium cross diffusion and viscous

dissipation. We begin by discussing flow past spinning cones and cross diffusion effects. Further to the studies on radiation and viscous dissipation effects (Chapter 3), free convection and porous medium (Chapter 4), flow of Casson fluid (Chapter 5) and partial slip (Chapter 6) previously discussed, we briefly review each of these again.

The problem of heat and mass transfer in spinning objects is important. In particular, in the design of cooking machinery and movement of automotive parts in engines. These designs incorporate different solid shapes including spinning cones immersed in lubricants. It is important how heat is generated at these surfaces, the partial slip due to these lubricants and the presence of solid particles in the ambient fluid. Other examples arise in the formation of microstructures, cooling of molten metals and fluid flowing close to shrouded fins (Narayana et al. 2013).

Chapter 7 – Effects of radiation on free convection from a spinning cone with partial slip in Casson fluid in non-Darcy porous medium with cross diffusion and viscous dissipation

In free convection, a heated surface of a cone embedded in a fluid cause a fluid flow around it. The movement of the cone in the form of a rotation or spin will affect the flow of the fluid around it. In the study of fluid flow around spinning objects, it is often necessary to consider the effect of spinning on fluid flow. Earlier work include the work of Agarwal and Rakich (1982) who investigated hypersonic laminar viscous flow past spinning cones at angle of attack, the study revealed that, the spinning effect affects fluid flow. Other studies which corroborate these findings include the works of Datta (1964) Reiner-Rivlin fluid flow over a spinning cone, Dinarvand et al. (2014) micropolar fluid flow over a spinning cone, Kumar and Sivaraj (2012) viscoelastic fluid flow along a moving cone. In this chapter we consider natural convection from a spinning cone with cross diffusion effects.

The mass flux caused by the temperature gradient result in the Soret effect sometimes called thermal-diffusion or thermophoresis effect. The thermophoretic force due to temperature gradients causes the movement of solute in the fluid flow regime. The energy flux caused by concentration gradient result in the Dufour effect sometimes called diffusion-thermo effect (Narayana et al. 2013). The combination of these phenomena is called cross-diffusion. These effects are generally neglected in many studies; in light of this it is necessary to consider these aspects in this study. Cross diffusion effects have been studied by among others Awad et al. (2011) who studied convection from an inverted cone in a porous medium with cross diffusion effects, Hayat et al. (2010) investigated heat and mass transfer for Soret and Dufour effects on mixed convection boundary layer flow over a stretching vertical surface in a porous medium filled with viscoelastic fluid. Cheng (2010) studied Soret and Dufour effects on free convection boundary layer over a vertical cylinder in a saturated porous medium. The cross diffusion effects considered in this chapter are studied together with natural or free convection.

Natural or free convection in fluid flow is a flow caused by density differences between the flow surface and a distance away from it caused by a temperature gradient. This process creates a buoyant force causing fluid flow. Casson fluid flow can be buoyant driven and this situation is found in many practical applications such as soup simmering in a pot, effect of application of heat on blood and synovial fluid in humans, flow of sewage sludge on heated surfaces. Further to the studies discussed in Chapter 4, natural or free convection

has been studied by many authors among others Alim et al. (2006) natural convection from a vertical cone, Anilkumar and Roy (2004) mixed convection flow on a rotating cone, Cheng (2011a) natural convection over a vertical cone, Cheng (2011b) natural convection from a permeable cone, Takhar et al.(1988), free convection from a slender cone, Saleh (2005) natural convection from a cone and wedge and Chamkha and Rashad (2012) natural convection from a vertical permeable cone. In this chapter we consider the effects of radiation, viscous dissipation, porous medium and Casson fluid flow which have been discussed in Chapters 4, 5 and 6.

As can be seen from the literature cited above, it appears no analysis has been published in the problem of free convection from a spinning cone in Casson fluid with cross diffusion, partial slip, radiation, porous medium and viscous dissipation effects, under the given boundary conditions. Velocity slip, rotational slip, thermal slip and solutal slip factors are considered. Suction and injection is considered at the surface of the cone. The free stream conditions are assumed to be at lower states that those at the surface. The work in this chapter is extended from the work of Narayana et al. (2013) which considered a spinning cone in a Newtonian fluid.

In brief, this section has shown that firstly considering a spinning cone is necessary, secondly, cross diffusion effects is also required and finally the use of the spectral relaxation method to solve the system of ordinary differential equations. In this chapter we also demonstrate the use of the successive over-relaxation technique to accelerate convergence. In this chapter we consider a spinning cone in Casson fluid and the effects of partial slip, porous medium, cross diffusion and viscous dissipation on flow characteristics. These aspects will be considered in the mathematical formulation of free convection flow of Casson fluid from a spinning cone.

7.3. Mathematical formulation of Casson fluid flow from a spinning cone

We consider a two dimensional downward pointing spinning cone in Casson fluid in porous medium as shown in Figure 7.1. The origin of the system is located at the cone vertex. The

angular velocity of rotation is given by Ω. The cone vertex angle is $2\theta^*$. The x axis is taken along the surface of the cone and the y axis perpendicular to the x axis from the origin.

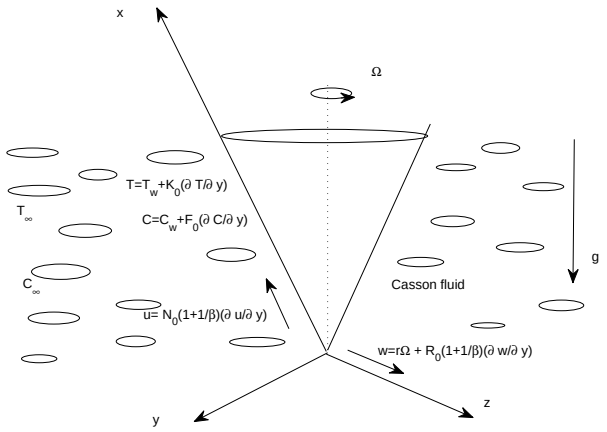

Figure 7.1: Schematic diagram of the spinning cone

The temperature at the surface of the cone is T_w ($> T_\infty$). The solute concentration is considered to be C_w ($> C_\infty$) at the surface of the cone and C_∞ the concentration in the ambient fluid. Velocity, rotational, thermal and solutal slip factors are considered at the surface of the cone.

The rheological equation of state for an isotropic and incompressible flow of a Casson fluid is given as in Mukhopadhyay et al. (2013) and Mukhopadhyay and Vejrravelu (2013) by:

$$\tau_{ij} = \begin{cases} 2(\mu_B + \dfrac{P_y}{\sqrt{2\pi}})e_{ij}, & \pi > \pi_c \\ 2(\mu_B + \dfrac{P_y}{\sqrt{2\pi_c}})e_{ij}, & \pi < \pi_c \end{cases} \tag{7.1}$$

$\pi = e_{ij}e_{ij}$ and e_{ij} is the $(i,j)^{th}$ component of the deformation rate, π is the product of the deformation rate with itself, π_c is a critical value of this product based on the non-Newtonian model, μ_B is the plastic dynamic viscosity of the non-Newtonian fluid, P_y is the yield stress of the fluid. Accordingly, under the usual boundary layer approximations, and subject to radiation, cross diffusion, viscous dissipation effects, the governing equations of

the momentum, energy and mass transfer equations are given as (see Narayana et al., 2013);

$$\frac{\partial}{\partial x}(ru) + \frac{\partial}{\partial y}(rv) = 0, \tag{7.2}$$

$$u\frac{\partial u}{\partial x} + v\frac{\partial u}{\partial y} - \frac{w^2}{x} = \nu(1+\frac{1}{\beta})\frac{\partial^2 u}{\partial y^2} + g\beta_T(T-T_\infty)\cos\theta^* + g\beta_C(C-C_\infty)\cos\theta^* - \frac{\nu}{\bar{K}}u \tag{7.3}$$

$$u\frac{\partial w}{\partial x} + v\frac{\partial w}{\partial y} + \frac{uw}{x} = \nu(1+\frac{1}{\beta})\frac{\partial^2 w}{\partial y^2} - \frac{\nu}{\bar{K}}w \tag{7.4}$$

$$u\frac{\partial T}{\partial x} + v\frac{\partial T}{\partial y} = \alpha\frac{\partial^2 T}{\partial y^2} + \bar{D}\frac{\partial^2 C}{\partial y^2} - \frac{1}{\rho C_p}\frac{\partial q_r}{\partial y} + \frac{\nu}{\rho C_p}(1+\frac{1}{\beta})\left(\frac{\partial u}{\partial y}\right)^2 \tag{7.5}$$

$$u\frac{\partial C}{\partial x} + v\frac{\partial C}{\partial y} = D\frac{\partial^2 C}{\partial y^2} + \bar{S}\frac{\partial^2 T}{\partial y^2} \tag{7.6}$$

where u, v and w are the velocity components in the x, y and z directions respectively, the radius of the cone $r = x\sin\theta^*$, ν is kinematic viscosity of Casson fluid, $\beta = \mu_B\sqrt{2\pi_c}/P_y$ is the non-Newtonian Casson parameter, $\alpha = k/\rho C_p$ is the thermal diffusivity, k is thermal conductivity of the fluid, q_r is the radiative heat flux. C_p is the specific heat. g is the acceleration due to gravity, β_T and β_C are respectively the coefficients of thermal and concentration expansions, T is the temperature of the fluid, C is the solute concentration in the boundary layer, D is the mass diffusivity, $\bar{S}$ and $\bar{D}$ are Soret and Dufour coefficients respectively. The Rosseland approximation for radiation may be written as follows;

$$q_r = -\frac{4\sigma^*}{3k^*}\frac{\partial T^4}{\partial y} \tag{7.7}$$

where σ^* is the Stefan-Boltzman constant and k^* is the absorption coefficient. If the temperature difference within the flow is such that T^4 may be expanded in Taylor series about T_∞ and neglecting higher powers we obtain $T^4 - 4T_\infty^3 - 3T_\infty^4$ and therefore the equation (4.9) can be written as

$$u\frac{\partial T}{\partial x} + v\frac{\partial T}{\partial y} = \alpha\frac{\partial^2 T}{\partial y^2} + \bar{D}\frac{\partial^2 C}{\partial y^2} + \frac{16\sigma^* T_\infty^3}{3\rho C_p k^*}\frac{\partial^2 T}{\partial y^2} \tag{7.8}$$

The boundary conditions are given as

$$\left.\begin{aligned} u = N_0(1+\frac{1}{\beta})\frac{\partial u}{\partial y}, \quad v = -v_w, \quad w = r\Omega + M_0(1+\frac{1}{\beta})\frac{\partial w}{\partial y}, \\ T = T_w + K_0\frac{\partial T}{\partial Y}, \quad C = C_w + F_0\frac{\partial C}{\partial Y} \end{aligned}\right\} \quad y = 0, \tag{7.9}$$

$$u \to 0, w \to 0, \quad T \to T_\infty, \quad C \to C_\infty \quad \text{as} \quad y \to \infty. \tag{7.10}$$

where the subscripts w and ∞ refer to surface the free stream conditions respectively, N_0, M_0, K_0 and F_0 are the velocity, rotational, thermal and solutal slip coefficients respectively.

we introduce the non-dimensional variables

$$\left.\begin{aligned} (X,Y,R) = \left(\frac{x, yGr^{\frac{1}{4}}, r}{L}\right), \quad (U,V) = \left(\frac{u, vGr^{\frac{1}{4}}}{U_0}\right), \\ W = \frac{w}{\Omega L} \quad \bar{T} = \frac{T-T_\infty}{T_w - T_\infty}, \bar{C} = \frac{C-C_\infty}{C_w - C_\infty} U_0 = [g\beta_T(T_w - T_\infty)\cos\psi L]^{\frac{1}{2}}, \\ Da = \frac{K}{L^2}, \quad Gr = (\frac{U_0 L}{\nu})^2 \end{aligned}\right\} \tag{7.11}$$

The governing Eqs. (7.12) -(7.16) reduce to

$$\frac{\partial}{\partial X}(RU) + \frac{\partial}{\partial Y}(RV) = 0, \tag{7.12}$$

$$U\frac{\partial U}{\partial X} + V\frac{\partial U}{\partial Y} - \frac{Re^2}{Gr}\frac{W^2}{X} = (1+\frac{1}{\beta})\frac{\partial^2 U}{\partial Y^2} + \bar{T} + N\bar{C} - k_p U \tag{7.13}$$

$$U\frac{\partial W}{\partial X} + V\frac{\partial W}{\partial Y} + \frac{UW}{X} = (1+\frac{1}{\beta})\frac{\partial^2 W}{\partial Y^2} - k_p W \tag{7.14}$$

$$U\frac{\partial \bar{T}}{\partial X} + V\frac{\partial \bar{T}}{\partial Y} = \frac{1}{Pr}\{\frac{\partial^2 \bar{T}}{\partial Y^2} + D_f\frac{\partial^2 \bar{C}}{\partial Y^2}\} + \frac{4K}{3Pr}\frac{\partial^2 T}{\partial Y^2} + Ec\left(1+\frac{1}{\beta}\right)\left(\frac{\partial U}{\partial Y}\right)^2 \tag{7.15}$$

$$U\frac{\partial \bar{C}}{\partial X} + V\frac{\partial \bar{C}}{\partial Y} = \frac{1}{Sc}\{\frac{\partial^2 \bar{C}}{\partial Y^2} + S_r\frac{\partial^2 \bar{T}}{\partial Y^2}\} \tag{7.16}$$

The non-dimensional parameters in Eqs. (7.12)- (7.16) are the rotational Reynolds number Re, Grashof number Gr, the Prandtl number Pr, Dufour parameter D_f, the Eckert

number Ec, the Schmidt number Sc and Soret parameter S_r. These parameters are defined as

$$Re = \frac{\Omega L^2}{\nu}, \quad N = \frac{\beta_C}{\beta_T}\left(\frac{C_r - C_\infty}{T_r - T_\infty}\right), K = \frac{4\sigma^* T_\infty^3}{k^* Gr^{\frac{1}{4}}}$$
$$Pr = \frac{\nu}{\alpha}, \quad Sc = \frac{\nu}{D},$$
$$Ec = \frac{U_0^2}{C_p(T_w - T_\infty)}, D_f = \frac{\bar{D}}{\alpha}\left(\frac{C_r - C_\infty}{T_r - T_\infty}\right), \quad S_r = \frac{\bar{S}}{D}\left(\frac{T_r - T_\infty}{C_r - C_\infty}\right).$$

The boundary conditions of Eqs. (7.12)- (7.16) are given by

$$U = S_f\left(1 + \frac{1}{\beta}\right)\frac{\partial U}{\partial Y}, \quad V = V_w, \quad W = R + S_g\left(1 + \frac{1}{\beta}\right)\frac{\partial W}{\partial Y}, \quad \bar{T} = 1 + S_T\frac{\partial \bar{T}}{\partial Y},$$
$$\bar{C} = 1 + S_{co}\frac{\partial \bar{C}}{\partial Y}\text{at} \quad Y = 0 \tag{7.17}$$
$$U \to 0, \quad W \to 0, \quad \bar{T} \to 0, \quad \bar{C} \to 0 \quad \text{as} \quad Y \to \infty. \tag{7.18}$$

Introducing the stream function $\psi(X, Y)$ and similarity variables

$$U = \frac{1}{R}\frac{\partial \psi}{\partial Y} \quad \text{and} \quad V = -\frac{1}{R}\frac{\partial \psi}{\partial X} \tag{7.19}$$
$$\psi(X, Y) = XRf(Y), \quad W(X, Y) = Rg(Y),$$
$$\bar{T}(X, Y) = X\theta(Y), \quad \bar{C}(X, Y) = X\phi(Y). \tag{7.20}$$

Using the stream function defined in Eq. (7.19) and similarity variables in Eq. (7.20), Eqs. (7.12)- (7.16) together with boundary conditions Eqs. (7.17) and (7.18) reduces to the following system of ordinary differential equations.

$$\left(1 + \frac{1}{\beta}\right)f''' + 2ff'' - f'^2 + \epsilon g^2 + \theta + N\phi - k_p f' = 0, \tag{7.21}$$
$$\left(1 + \frac{1}{\beta}\right)g'' + 2fg' - 2f'g - k_p g = 0, \tag{7.22}$$
$$(1 + \frac{4}{3}K)\theta'' + Pr(2f\theta' - f'\theta) + D_f\phi'' + EcPr\left(1 + \frac{1}{\beta}\right)f''^2 = 0, \tag{7.23}$$
$$\phi'' + Sc(2f\phi' - f'\phi) + S_r\theta'' = 0 \tag{7.24}$$

with boundary conditions;

$$Y = 0, \quad f = f_w, \quad f' = \left(1 + \frac{1}{\beta}\right) S_f f'', \quad g = 1 + \left(1 + \frac{1}{\beta}\right) S_g g'$$
$$\theta = 1 + S_T \theta', \quad \phi = 1 + S_{co} \phi', \tag{7.25}$$
$$Y \to \infty, f' \to 0, \quad g \to 0, \quad \theta \to 0. \quad \phi \to 0. \tag{7.26}$$

where β is the Casson parameter, ϵ is the spin parameter, $k_p = 1/DaGr^{\frac{1}{2}}$ is the Darcian drag force coefficient, Da is the Darcy number, Pr is the Prandtl number, D_f is the Dufour number, Ec is the Eckert number, Sc is the Schmidt number and Sr is the Soret number. In the above equations the primes refer to the derivative with respect to Y, $S_f = N_0 Gr^{\frac{1}{4}}/L$, $S_g = M_0 Gr^{\frac{1}{4}}/L$, $S_T = kGr^{\frac{1}{4}}/L$ and $S_{co} = F_0 Gr^{\frac{1}{4}}/L$ are the non-dimensional velocity, rotational, thermal and solutal slip parameters respectively. The parameter f_w is the blowing/suction parameter. The case $f_w < 0$ represents blowing and $f_w > 0$ represents suction.

7.4. Skin friction, heat transfer and mass transfer coefficients

The engineering parameters of interest are the local skin friction, heat transfer and mass transfer coefficients which are defined as follows. The shear stress at the surface of the cone is given by (see Narayana et al., 2013)

$$\tau_w = \mu \left[\left(1 + \frac{1}{\beta}\right) \frac{\partial u}{\partial y}\right]_{y=0} = \frac{\mu \left(1 + \frac{1}{\beta}\right) U_0}{LGr^{-\frac{1}{4}}} X f''(0), \tag{7.27}$$

where μ is the coefficient of viscosity, The skin friction coefficient is given by,

$$C_f = \frac{\tau_w}{\frac{1}{2}\rho U_0^2}. \tag{7.28}$$

Using Eqs. (7.27) and (7.28) gives

$$C_f Gr^{\frac{1}{4}} = 2(1 + \frac{1}{\beta})Xf''(0). \tag{7.29}$$

The heat transfer from the cone surface into the fluid is given by

$$q_w = -k\left[\frac{\partial T}{\partial y}\right]_{y=0} = \frac{-k(T_w - T_\infty)}{LGr^{-\frac{1}{4}}}X\theta'(0), \tag{7.30}$$

where k is the thermal conductivity of the fluid. The heat transfer coefficient (Nusselt number) under linear surface temperature (LST) is given by

$$Nu = \frac{L}{k}\frac{q_w}{T_w - T_\infty}. \tag{7.31}$$

Using Eqs. (7.30) and (7.31) gives

$$NuGr^{-\frac{1}{4}} = -X\theta'(0). \tag{7.32}$$

The mass flux at the cone surface into the fluid is given by

$$J_w = -D\left[\frac{\partial C}{\partial y}\right]_{y=0} = \frac{-D(C_w - C_\infty)}{LGr^{-\frac{1}{4}}}X\phi'(0), \tag{7.33}$$

The mass transfer coefficient (Sherwood number) is given by

$$Sh = \frac{L}{D}\frac{J_w}{C_w - C_\infty}. \tag{7.34}$$

Using Eqs. (7.33) and (7.34) gives

$$ShGr^{-\frac{1}{4}} = -X\phi'(0). \tag{7.35}$$

We have derived the skin friction, heat transfer and mass transfer coefficients. We are now ready to describe the numerical solution procedure for the problem of numerical analysis of free convection Casson fluid flow from a spinning cone in non-Darcy porous medium with radiation, partial slip and cross diffusion and viscous dissipation effects.

7.5. Numerical solution procedure

In this section we present the implementation of the spectral relaxation method for the problem of free convection from a spinning cone with partial slip in Casson fluid in non-Darcy porous medium with cross diffusion and viscous dissipation. The method is described in Motsa (2014) and implemented in the works of Shateyi (2013), Kameswaran et al. (2013b) and Motsa and Makukula (2013). The method is based on the Gauss-Seidel method normally used to solve a system of linear equations. The system of Eqs. (7.21)-(7.25) can be written as a numerical scheme.

$$f'_{r+1} = p_r, \tag{7.36}$$

$$\left(1+\frac{1}{\beta}\right)p''_{r+1} + 2f_{r+1}p'_{r+1} - k_p p_{r+1} = p_r^2 - \epsilon g_r^2 - \theta - N\phi_r, \tag{7.37}$$

$$\left(1+\frac{1}{\beta}\right)g''_{r+1} + 2f_{r+1}g'_{r+1} - 2p_{r+1}g_{r+1} - k_p g_{r+1} = 0, \tag{7.38}$$

$$(1+\frac{4}{3}K)\theta''_{r+1} + Pr(2f_{r+1}\theta' - p_{r+1}\theta_{r+1}) = -D_f\phi''_r - EcPr\left(1+\frac{1}{\beta}\right)(p'_{r+1}),^2 \tag{7.39}$$

$$\phi''_{r+1} + 2Scf_{r+1}\phi'_{r+1} - ScP_{r+1}\phi_{r+1} = -S_r\theta''_r, \tag{7.40}$$

with boundary conditions

$$
\begin{aligned}
&f(0)_{r+1} = f_w,\ p(0)_{r+1} = \left(1+\frac{1}{\beta}\right) S_f p(0)'_{r+1},\\
&g(0)_{r+1} = 1 + \left(1+\frac{1}{\beta}\right) S_g g(0)'_{r+1},\\
&\theta(0)_{r+1} = 1 + S_T \theta(0)'_{r+1},\\
&\phi(0)_{r+1} = 1 + S_{co}\phi(0)'_{r+1}, \qquad (7.41)\\
&p_{r+1}(\infty) \to 0,\ g(\infty)_{r+1} \to 0,\\
&\theta(\infty)_{r+1} \to 0,\ \phi(\infty)_{r+1} \to 0. \qquad (7.42)
\end{aligned}
$$

Applying the Chebyshev pseudo spectral method on Eqs. (7.36) - (4.18) we obtain

$$A_1\mathbf{f}_{r+1} = B_1,\ f(0)_{r+1} = f_w \qquad (7.43)$$

$$A_2\mathbf{p}_{r+1} = B_2,\ p(0)_{r+1} = \left(1+\frac{1}{\beta}\right) S_f p(0)'_{r+1} \qquad (7.44)$$

$$A_3\mathbf{g}_{r+1} = B_3,\ g(0)_{r+1} = 1 + \left(1+\frac{1}{\beta}\right) S_g g(0)'_{r+1} \qquad (7.45)$$

$$A_4\theta_{r+1} = B_4,\ \theta(0)_{r+1} = 1 + S_T\theta(0)'_{r+1} \qquad (7.46)$$

$$A_5\phi_{r+1} = B_5,\ \phi(0)_{r+1} = 1 + S_{co}\phi(0)'_{r+1} \qquad (7.47)$$

where

$$A_1 = \mathbf{D},\ B_1 = \mathbf{p}_r, \tag{7.48}$$

$$A_2 = \left(1 + \frac{1}{\beta}\right)\mathbf{D}^2 + 2\ \mathrm{diag}[\mathbf{f}_{r+1}]\mathbf{D} - k_p\mathbf{I}$$

$$B_2 = \mathbf{p}_r^2 - \epsilon\mathbf{g}_r^2 - \theta_r - N\phi_r, \tag{7.49}$$

$$A_3 = \left(1 + \frac{1}{\beta}\right)\mathbf{D}^2 + 2\ \mathrm{diag}[\mathbf{f}_{r+1}]\mathbf{D} - \left(2\ \mathrm{diag}[\mathbf{p}_{r+1}]\mathbf{g}_{r+1} - k_p\right)\mathbf{I},\ B_3 = \mathbf{0}, \tag{7.50}$$

$$A_4 = (1 + \frac{4}{3}K)\mathbf{D}^2 + 2Pr\ \mathrm{diag}[\mathbf{f}_{r+1}]\mathbf{D} - Pr\ \mathrm{diag}[\mathbf{p}_{r+1}]\mathbf{I}$$

$$B_4 = -D_f\phi_r'' - EcPr\left(1 + \frac{1}{\beta}\right)(\mathbf{p}_{r+1}')^2, \tag{7.51}$$

$$A_5 = \mathbf{D}^2 + 2Sc\ \mathrm{diag}[\mathbf{f}_{r+1}]\mathbf{D} - Sc\ \mathrm{diag}[\mathbf{p}_{r+1}]$$

$$B_5 = -S_r\theta_r'' \tag{7.52}$$

7.6. Improving the convergence of the spectral relaxation method (SRM)

In this section we use the concept of successive over-relaxation (SOR) to accelerate the convergence rate of the spectral relaxation method (SRM). If the general SRM scheme is given by Eqs. (7.43)-(7.47), then the modified SRM scheme is defined as

$$A_1\mathbf{f}_{r+1} = (1-\omega)A_1\mathbf{f}_r + \omega B_1 \tag{7.53}$$

$$A_2\mathbf{p}_{r+1} = (1-\omega)A_2\mathbf{p}_r + \omega B_2 \tag{7.54}$$

$$A_3\mathbf{g}_{r+1} = (1-\omega)A_3\mathbf{g}_r + \omega B_3 \tag{7.55}$$

$$A_4\boldsymbol{\theta}_{r+1} = (1-\omega)A_4\boldsymbol{\theta}_r + \omega B_4 \tag{7.56}$$

$$A_5\boldsymbol{\phi}_{r+1} = (1-\omega)A_5\boldsymbol{\phi}_r + \omega B_5 \tag{7.57}$$

where A_i and B_i are matrices and ω is the convergence controlling parameter. By applying this modified SRM in solving the Eqs. (7.36)-(7.42). Using the values of the controlling parameter $\omega = 0.9$ (accelerates convergence), $\omega = 1$(usual SRM scheme) and $\omega = 1.1$(slows down convergence). Figure 7.2 shows the decoupling error E_d against iterations.

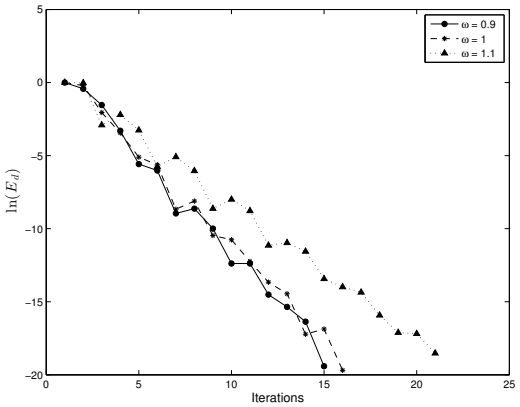

Figure 7.2: Effects of the controlling parameter on decoupling error

In Figure 7.2, the spectral relaxation method (SRM) error reduces with the increasing number of iterations, showing the accuracy of the spectral relaxation method (SRM). The decrease in the error shows that the method is convergent and gives stable solutions. It is also shown that convergence can be controlled obtaining the results in a fewer number of iterations.

7.7. Results and discussion

The problem that was investigated in this chapter was solved by the spectral relaxation method (SRM). In this section we will not study the effect of Casson parameter β, Darcian drag force coefficient k_p, radiation parameter K, Prandtl number Pr and suction/injection parameter f_w whose significance has been widely studied in the previous chapters. We focus on the variation of the , spin parameter ϵ, buoyancy parameter N, Dufour number D_f, Eckert number Ec, Schmidt number Sc, Soret number Sr, velocity slip S_f, rotational slip S_g, thermal slip S_T and solutal slip S_{co} factors on velocity, temperature and concentration profiles. We also study the variation of skin friction, heat transfer and mass transfer coefficients with other physical parameters.

In this chapter we assume that the Prandtl number is between $Pr = 5$ at 20^oC and $Pr = 20$ for blood. The appropriate Grashof number is fixed at $Gr = 10$ and Darcy number $Da = 0.1$ giving a fixed value $k_p = 1/DaGr^{\frac{1}{2}} = 3$. All other parameters are chosen arbitrarily

being careful to stay within the acceptable range of the Casson fluid.

For validation of the numerical method used in this study, results for the skin friction coefficient $f''(0)$ and heat transfer coefficient $-\theta'(0)$ for the Newtonian fluid were compared to those of Narayana et al. (2013) and the SRM, for $1/\beta \to 0, \epsilon = N = K = D_f = S_r = Sc = Ec = 0$ and the Darcian drag force terms $k_p f' = k_p g = 0$. The comparison is shown in Tables 7.1 -7.2 and it is found to be in excellent agreement to five decimal places.

Table 7.1: Comparison of the values of skin friction $f''(0)$ and heat transfer $-\theta'(0)$ coefficients of Narayana et al. (2013) with the SRM

Pr	Narayana et al. (2013) Runge-Kutta $f''(0) - \theta'(0)$	SRM $f''(0) - \theta'(0)$
1	0.68150212 0.63886614	0.68148625 0.63885897
10	0.43327726 1.27552680	0.43327848 1.27552816

The results obtained by this method are discussed in Tables 7.2 and 7.3 and are compared with the results obtained using the spectral relaxation method (SRM) and were found to be in excellent agreement.

The problem of free convection Casson fluid from a spinning cone in non-Darcy porous medium with radiation, partial slip, cross diffusion and viscous dissipation effects was solved numerically using the spectral relaxation method (SRM). The results depicted in Table 7.3 are the results generated by the SRM and the Matlab `bvp4c`. A tolerance of 10^{-8} for both methods was used. Comparison of the basic SRM ($\omega = 1$) of the skin friction coefficient against those of SRM with (SOR) ($\omega = 0.9$). The advantage of accelerating convergence is noted in all cases in which the results are obtained accurately in less iterations (see also Shateyi and Marewo, 2013). The values are generated at selected values of the Darcian drag force term k_p, the Prandtl number Pr and the Casson parameter β. Increasing the k_p and Pr decreases the skin friction coefficient while increasing the Casson parameter increase skin friction coefficient.

Table 7.2: Comparison of SRM solutions for the skin friction coefficient $f''(0)$ against those of bvp4c.

k_p	Pr	β	SRM(basic) ($\omega = 1$) it	it	SRM(SOR) ($\omega = 0.9$)f"(0)	bvp4c f"(0)
0	5	2	100	47	0.68148334	0.68148334
1	5	2	66	40	0.55974072	0.55974072
2	5	2	46	35	0.48675875	0.48675875
3	5	2	40	33	0.43677770	0.43677770
1	7	2	50	35	0.40562674	0.40562673
1	8	2	48	33	0.39565072	0.39565073
1	9	2	48	33	0.38695722	0.38695722
1	1	2	61	38	0.35629327	0.35629327
1	1	5	62	37	0.43037422	0.43037422
1	1	9	63	39	0.49760348	0.49760348

In Table 7.3, the heat transfer coefficient decreases with decreasing Darcian drag force term k_p, but increases with increasing both Prandtl Pr and Casson parameter β.

Table 7.3: Comparison of SRM solutions for the heat transfer coefficient$-\theta'(0)$ against those of bvp4c.

k_p	Pr	β	SRM(basic) $(\omega = 1)$ it	it	SRM(SOR) $(\omega = 0.9) - \theta'(0)$	bvp4c f"(0)
0	5	2	91	36	0.59446782	0.59446782
1	5	2	62	37	0.52386360	0.52386360
2	5	2	48	36	0.47594764	0.47594764
3	5	2	42	33	0.44000560	0.44000560
1	7	2	50	33	0.96287011	0.96287011
1	8	2	50	33	1.00136750	1.00136750
1	9	2	49	32	1.03638459	1.03638459
1	1	2	61	37	0.52386360	0.52386360
1	1	5	62	39	0.54308263	0.54308263
1	1	9	63	40	0.54968947	0.54968947

We then sought greater insight into the effect of some fluid properties on velocity, heat and mass transfer. Figures 7.3 - 7.5 show the variation of spin parameter ϵ, buoyancy parameter N and rotational slip factor S_g on velocity profiles. Figure 7.6 shows the variation of the Dufour number D_f on the temperature profiles. Figures 7.7-7.9 shows the variation of the Soret number S_r, concentration slip factor S_{co} and Casson parameter β on concentration profiles. Figures 7.10 - 7.12 shows the variation velocity slip factor S_f of velocity profiles and the variation of thermal slip factor S_T and Eckert number Ec on temperature profiles. These results have been discussed in the previous chapters; they are displayed in this section to show the accuracy of the spectral relaxation method (SRM). Figures 7.13 - 7.14 shows the plot of skin friction coefficient $f''(0)$ against the Casson parameter β and the radiation parameter K. Figures 7.15 - 7.16 shows the plot of heat transfer coefficient $\theta'(0)$ against the Casson parameter β and the radiation parameter K. Figures 7.17 - 7.18 shows the plot of mass transfer coefficient $-\phi'(0)$ against the Dufour parameter D_f and the radiation parameter K.

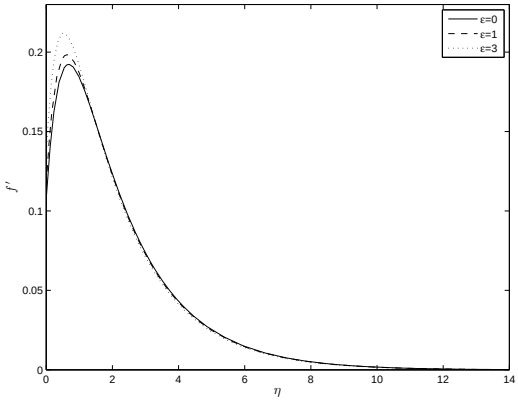

Figure 7.3: Effect of spin parameter on velocity profiles $f'(\eta)$ for $\beta = 2, N = 1, k_p = 3, K = 0.5, D_f = 0.5, Ec = 1, S_r = 0.5, f_w = 0.5, S_f = 0.5, S_g = 0.5, S_T = 1, S_{co} = 1, Pr = 5, Sc = 0.7$.

The variation of spin parameter ϵ on velocity profiles is shown in Figure 7.3. It can be seen from the graph that increasing the spin parameter result in the increase in velocity profiles. This is to be expected because increasing the spin parameter would have an effect of increasing motion in the fluid regime thereby increasing the velocity of the fluid. The same result was noted in Narayana et al. (2013).

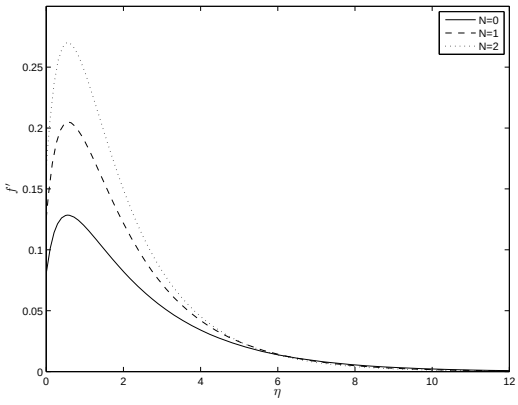

Figure 7.4: Effect of buoyancy parameter on velocity profiles $f'(\eta)$ for $\beta = 2, \epsilon = 2, k_p = 3, K = 0.5, D_f = 0.5, Ec = 1, S_r = 0.5, f_w = 0.5, S_f = 0.5, S_g = 0.5, S_T = 1, S_{co} = 1, Pr = 5, Sc = 0.7$.

The effect of the buoyancy parameter N on velocity profiles is shown in Figure 7.4. It

can be seen from the figure that increasing the buoyancy parameter N result in the increase in velocity profiles. We thus interpret an increase in the buoyancy parameter N as having an effect of increasing the concentration gradient, thereby creating an energy flux which in turn increase fluid motion in the fluid.

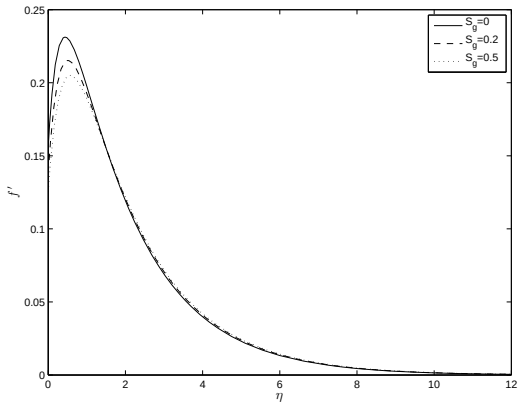

Figure 7.5: Effect of rotational slip factor on velocity profiles $f'(\eta)$ for $\beta = 2, \epsilon = 2, N = 1, k_p = 3, K = 0.5, D_f = 0.5, Ec = 1, S_r = 0.5, f_w = 0.5, S_f = 0.5, S_T = 1, S_{co} = 1, Pr = 5, Sc = 0.7$.

The effect of the rotational slip factor S_g on velocity profiles is shown in Figure 7.5. It can be seen from the figure that increasing the rotational slip factor result in the decrease in the velocity profiles. We can thus interpret an increase in the rotational slip factor as having an effect of dragging fluid molecules perpendicular to the direction of motion thereby reducing fluid motion. This result not been reported in the literature.

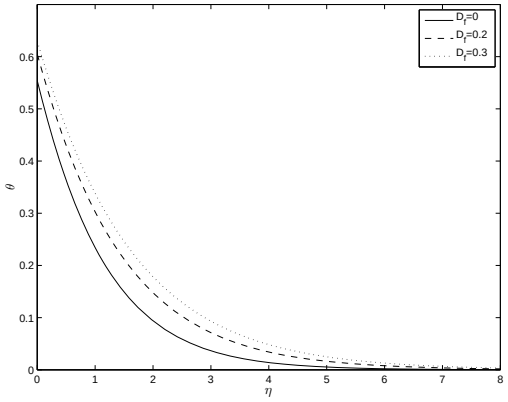

Figure 7.6: Effect of Dufour parameter on temperature profiles $\theta(\eta)$ for $\beta = 2, \epsilon = 2, N = 1, k_p = 3, K = 0.5, Ec = 1, S_r = 0.5, f_w = 0.5, S_f = 0.5, S_g = 0.5, S_T = 1, S_{co} = 1, Pr = 5, Sc = 0.7$.

The variation of the Dufour number D_f on temperature profiles is shown in Figure 7.6. Increasing the Dufour number results in the increase in temperature profiles. Narayana et al. (2013) has interpreted a similar finding to show that increasing the Dufour number has an effect of creating an energy flux caused by concentration gradient thereby causing an increase in the fluid temperature.

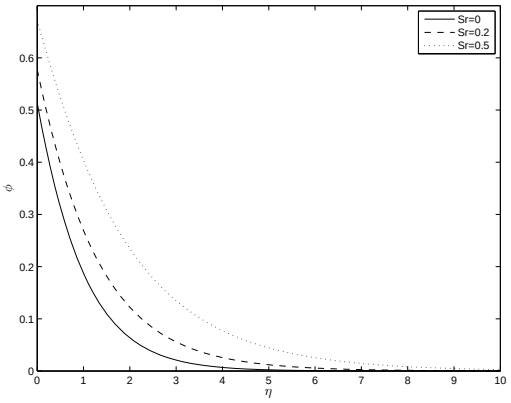

Figure 7.7: Effect of Soret parameter on concentration profiles $\phi(\eta)$ for $\beta = 2, \epsilon = 2, N = 1, k_p = 3, K = 0.5, D_f = 0.5, Ec = 1, f_w = 0.5, S_f = 0.5, S_g = 0.5, S_T = 1, S_{co} = 1, Pr = 5, Sc = 0.7$.

The variation of the Soret number S_r on concentration profiles is shown in Figure 7.7.

Increasing the Soret number results in the increase in concentration profiles. We can thus interpret that increasing the Soret number has an effect of creating a mass flux caused by temperature gradient thereby causing an increase in the solute movement in the fluid regime.

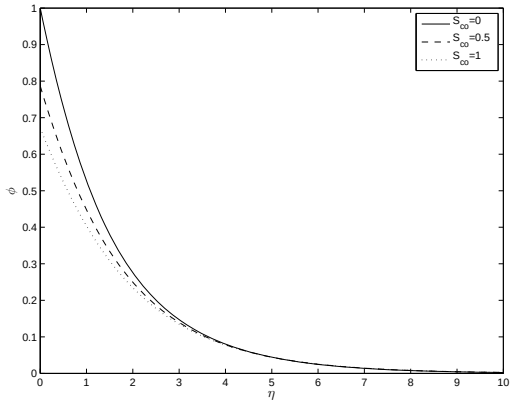

Figure 7.8: Effect of solutal slip factor on concentration profiles $\phi(\eta)$ for $\beta = 2, \epsilon = 2, N = 1, k_p = 3, K = 0.5, D_f = 0.5, Ec = 1, S_r = 0.5, f_w = 0.5, S_f = 0.5, S_g = 0.5, S_T = 1, Pr = 5, Sc = 0.7$.

The variation of the solutal slip factor S_{co} on concentration profiles is shown in Figure 7.8. Increasing the solutal slip factor S_{co} result in the decrease in concentration profiles. We can thus interpret that increasing the solutal slip factor has an effect of reducing the mass transfer coefficient at the surface thereby causing a decrease in the solute movement in the fluid regime.

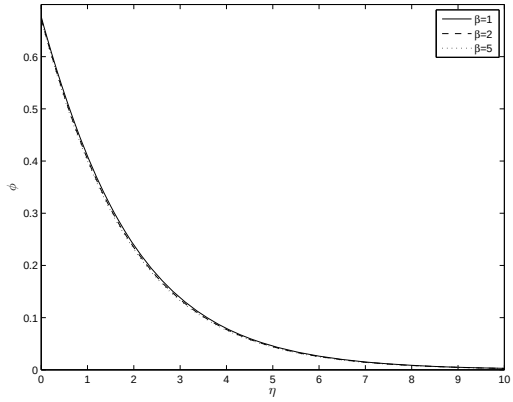

Figure 7.9: Effect of Casson parameter on concentration profiles $\phi(\eta)$ for $\epsilon = 2, N = 1, k_p = 3, K = 0.5, D_f = 0.5, Ec = 1, S_r = 0.5, f_w = 0.5, S_f = 0.5, S_g = 0.5, S_T = 1, S_{co} = 1, Pr = 5, Sc = 0.7$.

The variation of the Casson paramter β on concentration profiles is shown in Figure 7.9. It can be seen from the figure that increasing the Casson parameter β result in the decrease in concentration profiles. The effect of Casson parameter indirectly affects the concentration profiles via coupling. We can thus interpret an increase in the Casson parameter as having an effect of reducing fluid motion as discussed in the previous chapters, this in turn reduce mass transfer in the fluid regime.

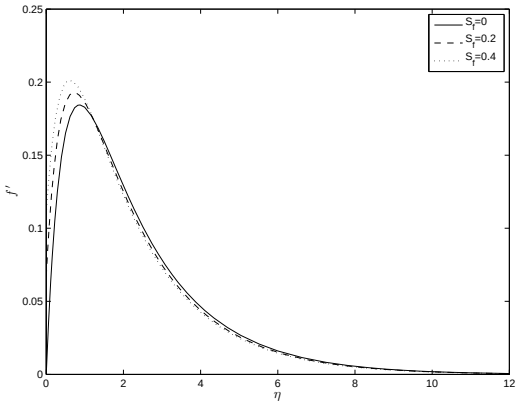

Figure 7.10: Effect of velocity slip factor on velocity profiles $f'(\eta)$ for $\beta = 2, \epsilon = 2, N = 1, k_p = 3, K = 0.5, D_f = 0.5, Ec = 1, S_r = 0.5, f_w = 0.5, S_g = 0.5, S_T = 1, S_{co} = 1, Pr = 5, Sc = 0.7$.

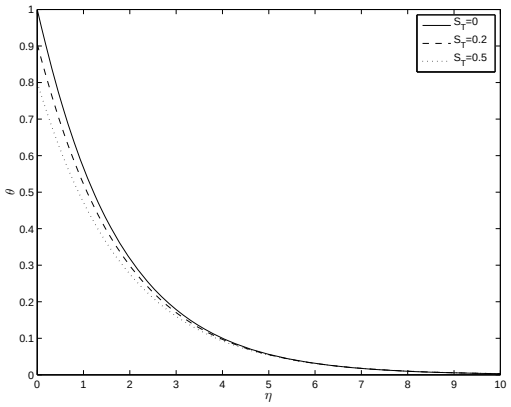

Figure 7.11: Effect of thermal slip factor on temperature profiles $\theta(\eta)$ for $\beta = 2, \epsilon = 2, N = 1, k_p = 3, K = 0.5, D_f = 0.5, Ec = 1, S_r = 0.5, f_w = 0.5, S_f = 0.5, S_g = 0.5, S_{co} = 1, Pr = 5, Sc = 0.7$.

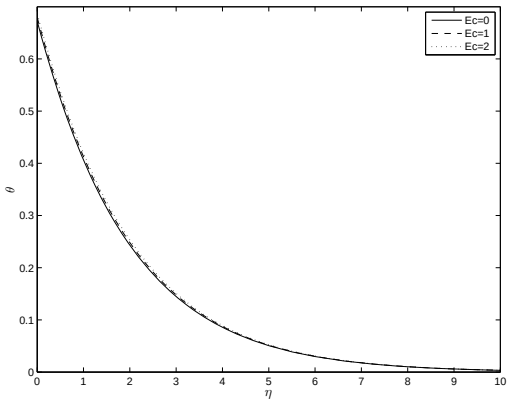

Figure 7.12: Effect of Eckert number on temperature profiles $\theta(\eta)$ for $\beta = 2, \epsilon = 2, N = 1, k_p = 3, K = 0.5, D_f = 0.5, S_r = 0.5, f_w = 0.5, S_f = 0.5, S_g = 0.5, S_T = 1, S_{co} = 1, Pr = 5, Sc = 0.7$.

The variation of velocity slip factor S_f of velocity profiles, thermal slip factor S_T on temperature profiles and Eckert number Ec on temperature profiles are respectively shown in Figures 7.10 - 7.12. These results have been reported in the previous chapter and show an excellent agreement. This verifies that the spectral relaxation method is robust and accurate. In particular Figures 7.10 and 7.11 have been reported in Ramachandra et al. (2013), showing the same observation. Figure 7.12 has been widely reported in for instance

the works of Makanda et al. (2013), Chen (2010) and Hsiao (2012).

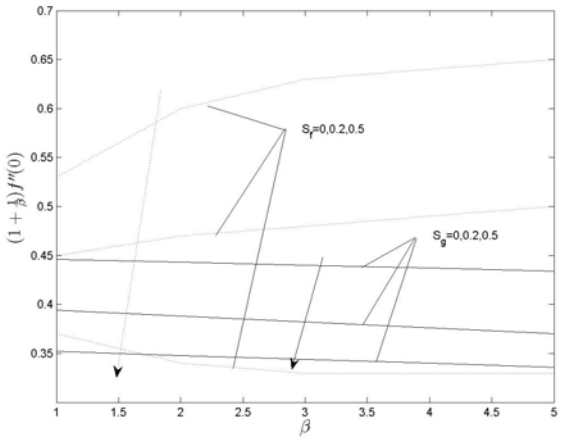

Figure 7.13: Plot of skin friction coefficient $-(1 + 1/\beta)f''(0)$ against Casson parameter β for different values of the velocity S_f and rotational S_g slip factors for $\epsilon = 2, N = 1, k_p = 3, K = 0.5, D_f = 0.5, Ec = 1, S_r = 0.5, f_w = 0.5, S_T = 1, S_{co} = 1, Pr = 5, Sc = 0.7$.

Figure 7.13 shows the plot of $(1 + 1/\beta)f''(0)$ related to skin friction coefficient against the Casson parameter β at different values of the velocity slip factor S_f and the rotational slip factor S_g. In the case of no-slip condition $S_f = S_g = 0$, it can be seen from the figure that skin friction coefficient increases with increasing Casson parameter β. Skin friction coefficient reduces with increasing velocity slip factor as expected on a lubricated surface. At higher values of the velocity slip factor the skin friction coefficient decreases with increasing Casson parameter β. Increasing the Casson parameter β would naturally mean that the fluid becomes Newtonian exerting less force on the surface. The same effect is noted on the rotational slip factor S_g. We also note that for no-slip condition $S_f = S_g = 0$, we observe a decrease in the skin friction coefficient due to the fact that rotational slip factor acts perpendicular to the flow.

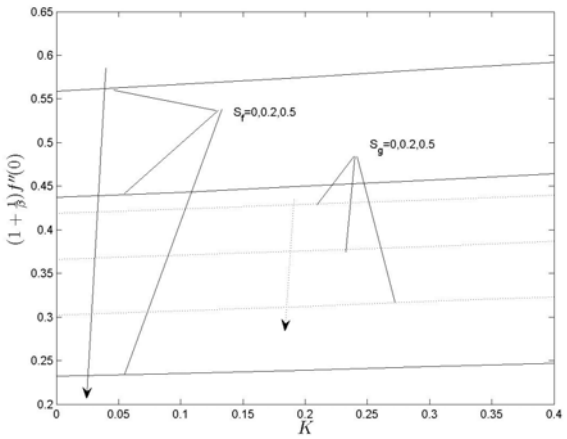

Figure 7.14: Plot of skin friction coefficient $-(1+1/\beta)f''(0)$ against radiation parameter K for different values of the velocity S_f and rotational S_g slip factors for $\beta = 2, \epsilon = 2, N = 1, k_p = 3, D_f = 0.5, Ec = 1, S_r = 0.5, f_w = 0.5, S_T = 1, S_{co} = 1, Pr = 5, Sc = 0.7$.

The plot of skin friction coefficient $-(1+1/\beta)f''(0)$ against the radiation parameter K is shown in Figure 7.14. It can be seen from the figure that increasing the radiation parameter K result in the increase in the skin friction coefficient. We can thus interpret an increase in the radiation parameter as having an effect of having an energy transfer is increase in the boundary layer, which in turn facilitates motion exerting more stress on the wall. Increasing the velocity S_f and rotational S_g slip factors results in decreasing the skin friction coefficient.

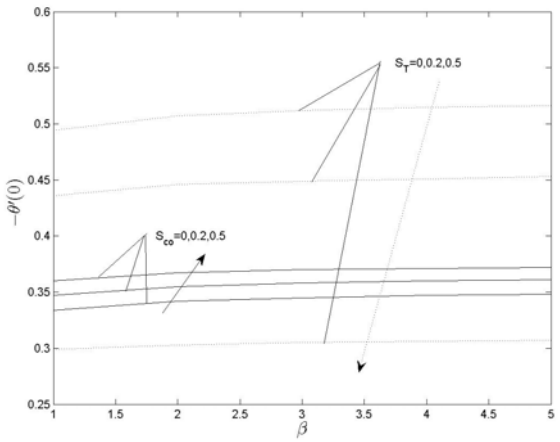

Figure 7.15: Plot of heat transfer coefficient $-\theta'(0)$ against Casson parameter β for different values of the thermal S_T and solutal S_{co} slip factors for $\epsilon = 2, N = 1, k_p = 3, K = 0.5, D_f = 0.5, Ec = 1, S_r = 0.5, f_w = 0.5, S_f = 0.5, S_g = 0.5, Pr = 5, Sc = 0.7$.

Figure 7.15 shows a plot of the heat transfer coefficient $-\theta'(0)$ against the Casson parameter β. It can be seen from the figure that increasing the Casson parameter does not affect the heat transfer coefficient significantly. It is noted that increasing the thermal slip factor S_T significantly reduce the heat transfer coefficient and increasing the concentration slip factor S_{co} increase the heat transfer coefficient.

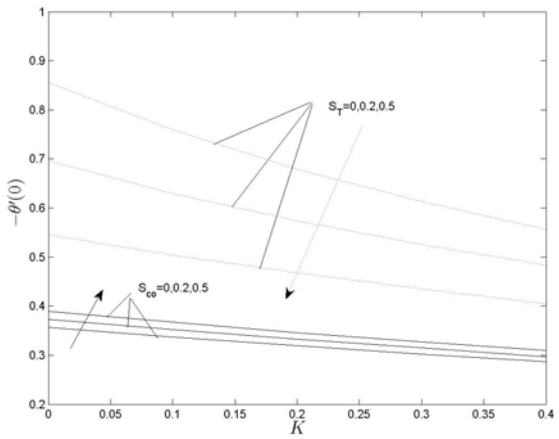

Figure 7.16: Plot of heat transfer coefficient $-\theta'(0)$ against radiation parameter K for different values of the thermal S_T and solutal S_{co} slip factors for $\beta = 2, \epsilon = 2, N = 1, k_p = 3, D_f = 0.5, Ec = 1, S_r = 0.5, f_w = 0.5, S_f = 0.5, S_g = 0.5, Pr = 5, Sc = 0.7$.

Figure 7.16 show the plot of heat transfer coefficient $-\theta'(0)$ against radiation parameter K. It is seen in the graph that increasing the thermal slip factor results in the decreases of the heat transfer coefficient. Increasing the concentration slip factor S_{co} results in the increase of the heat transfer coefficient. Increasing the thermal radiation K result in the reduction of the heat transfer coefficient. We can thus interpret an increase in the thermal radiation as increasing the fluid temperature thereby resulting in the heat being transferred from the fluid to the solid surface.

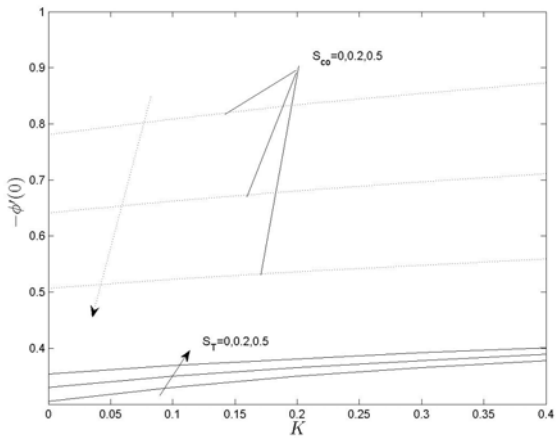

Figure 7.17: Plot of mass transfer coefficient $-\phi'(0)$ against radiation parameter K for different values of the thermal S_T and solutal S_{co} slip factors for $\beta = 2, \epsilon = 2, N = 1, k_p = 3, D_f = 0.5, Ec = 1, S_r = 0.5, f_w = 0.5, S_f = 0.5, S_g = 0.5, Pr = 5, Sc = 0.7$.

Figure 7.17 shows a plot of the mass transfer coefficient $-\phi'(0)$ against the radiation parameter K. It can be seen from the graph that increasing the concentration slip factor S_{co} result in the reduction of the mass transfer coefficient, while increasing the thermal slip factor S_T result in the increase of the mass transfer coefficient. Increasing the thermal radiation parameter K increase the mass transfer coefficient.

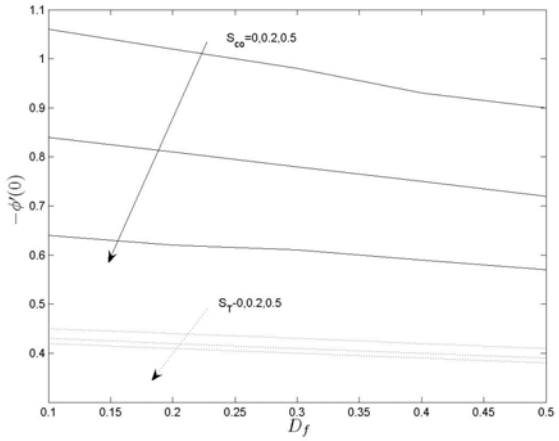

Figure 7.18: Plot of mass transfer coefficient $-\phi'(0)$ against Dufour parameter D_f for different values of the thermal S_T and solutal S_{co} slip factors for $\beta = 2, \epsilon = 2, N = 1, k_p = 3, K = 0.5, Ec = 1, S_r = 0.5, f_w = 0.5, S_f = 0.5, S_g = 0.5, Pr = 5, Sc = 0.7$.

Figure 7.18 shows the plot of the mass transfer coefficient $-\phi'(0)$ against the Dufour number D_f. It can be seen from the figure that increasing the Dufour number results in the decrease of the mass transfer coefficient. We thus interpret an increase in the Dufour number as having the effect of increasing the energy flux which increases the solute concentration in the fluid regime, thereby reducing mass transfer into the fluid. Increasing both thermal S_T and concentration S_{co} slip factors decrease the mass transfer coefficient.

7.8. Summary

The problem of free convection from a spinning cone in Casson fluid with partial slip, radiation effects, cross diffusion and viscous dissipation in non-Darcy porous medium was considered. Increasing the Casson parameter reduces the concentration profiles. Increasing the spin parameter increases velocity profiles. Increasing the buoyancy parameter tend to assist the fluid flow. Increasing the Dufour number increases the temperature profiles. Increasing the Soret number results in the increase in the concentration profiles. Increasing the velocity slip factor result in the increase in velocity profiles. Increasing the thermal slip factor results in the decrease in the temperature profiles.

Chapter 7 – Effects of radiation on free convection from a spinning cone with partial slip in Casson fluid in non-Darcy porous medium with cross diffusion and viscous dissipation

In this chapter we point out the new results on the effects of increasing rotational and solutal slip factors which have not been previously reported in the literature. Increasing the solutal slip factor result in the decrease of concentration profiles. Increasing the rotational slip factor reduce velocity profiles.

In this chapter the spectral relaxation method (SRM) was used to find solutions of the governing differential equations. The problem consisted of four coupled ordinary differential equations. The boundary conditions contain the velocity slip and thermal slip factors and the newly introduced rotational and solutal slip factors. The numerical solution for the skin friction coefficient $f''(0)$ and the heat transfer coefficient $-\theta'(0)$ was compared to the spectral relaxation method (SRM) and to previously published results in the literature and was found to be in agreement to five decimal places. Furthermore, we demonstrated how to improve the convergence of the spectral relaxation method. This was done by considering the concept of the successive over-relaxation. This technique is used to obtain solutions in less iterations than the ordinary SRM. This shows the robustness of this method which is a powerful advantage over methods such as finite differences.

8

Effects of double dispersion on Casson fluid flow with viscous dissipation and convective boundary conditions

8.1. Introduction

In this chapter we study the effects of double dispersion in Casson fluid flow with viscous dissipation and convective boundary conditions. The system of governing equations is transformed to a system of partial differential equations. The equations are solved by the bivariate quasi-linearization method (BQLM) (see section 1.1.8). The implementation of this method is also shown in this chapter. The accuracy of the method is determined by comparison with the Matlab `bvp4c` and previously published results in the literature.

8.2. Review of literature on double dispersion on Casson fluid flow

In this chapter we review literature about the problem of effects of double dispersion in Casson fluid flow with viscous dissipation and convective boundary conditions. We start by discussing the concept of double dispersion, convective boundary conditions and flow from a vertical plate. Further to the studies encountered in the previous chapters, we briefly discuss Casson fluid flow and viscous dissipation.

The study of the double dispersion has become popular due to its interesting and important engineering and environmental applications. Engineering applications such as under-

ground spreading of chemical waste and other pollutants, grain storage, evaporation, cooling and solidification, thermal energy storage system such as solar ponds; heat transfer from thermal sources such as condensers of power plants and environmental related application such as heat rejection into lakes, rivers and seas (El-Amin et al., 2008). The fluid flow in this study is driven by the action of buoyancy forces as a result of combined effect of both heat and concentration on the density of the fluid.

Dispersion in fluid flow is the mechanical movement of heat and solute in the flow regime. 'Dispersion' is often confused with 'diffusion', diffusion is the movement caused by the Brownian motion which is the random movement of fluid molecules. The study of double dispersion has been studied by among others, Narayana and Murthy (2006) who studied the heat and mass transfer in a double stratified non-Darcy porous medium. Kairi and Murthy (2009) investigated free convection in a thermally stratified non-Darcy porous medium. The effect of the double dispersion in a micropolar fluid has been studied by Srinivasacharya and RamReddy (2011). Murthy et al. (2013) investigated the effect of thermal stratification on nanofluid saturated non-Darcy porous medium. Kameswaran and Sibanda (2013) studied the thermal dispersion effects on convective heat and mass transfer of Ostwald de Waele nanofluid flow in a porous media. The study in this chapter takes into consideration convective boundary conditions.

Chapter 8 – Effects of double dispersion on Casson fluid flow with viscous dissipation and convective boundary conditions

Convective boundary conditions define heat transfer at the solid-fluid interface. It describes how fluid is transferred from the vertical plate to the fluid and vice-versa. The mathematical description links heat transfer in a vertical plate in terms of plate's thermal conductivity to the heat transfer in the fluid in terms of the fluid's thermal conductivity. The mathematical representation is consistent with Newton's law of cooling. The study of fluid flow which considered convective boundary conditions include the work of Narayana et al. (2013) who studied natural convection from a spinning, Murthy et al. (2013) who studied magnetic effect in nanofluid under convective boundary conditions and Narayana and Murthy (2006) who investigated convective heat and mass transfer in non-Darcy porous medium.

A heated impermeable vertical plate with both temperature and concentration kept constant is immersed in Casson fluid. Heat and species disperse across the fluid, causing the density to change in space. This then result in the fluid flowing upwards close to the wall surface (El-Amin et al. 2008). The study of fluid flow on vertical plates or vertical geometries have been studied by among others Abel et al. (2008) who studied MHD heat transfer past a vertical stretching sheet; Chen (2004) investigated combined heat and mass transfer from a vertical surface, Hayat et al. (2998) studied mixed convection in a stagnation point flow adjacent to a vertical surface in a viscoelastic fluid and the work of Massoudi et al. (2008) who studied natural convection between two vertical walls. In this chapter we consider the effects of viscous dissipation which have been discussed in Chapter 3.

It can be seen from the literature cited above that no analysis has been published in the problem of double dispersion on Casson fluid with viscous dissipation and convective boundary conditions. Fluid flow from a vertical wall induced by convection is considered. This work is extended from the work of El-Amin et al. (2008) in which double dispersion is considered in a Newtonian fluid in non-Darcy medium.

In summary, this section has firstly considered literature on double dispersion and convective boundary conditions, secondly, fluid flow from a vertical surface, thirdly, flow of Casson fluid and finally, viscous dissipation effects. In this chapter we make use of the bivariate quasi-linearization method (BQLM) to solve the system of partial differential equations. These aspects will be considered in the mathematical formulation of the effects of double

dispersion in Casson fluid flow with viscous dissipation and convective boundary conditions.

8.3. Mathematical formulation of double dispersion in Casson fluid flow

Consider steady, incompressible two dimensional flow of a Casson fluid adjacent to a vertical surface as shown in Figure 8.1. The Cartesian coordinates x and y are along the vertical surface and normal to it respectively, u and v are the respective velocity components in the x and y directions.

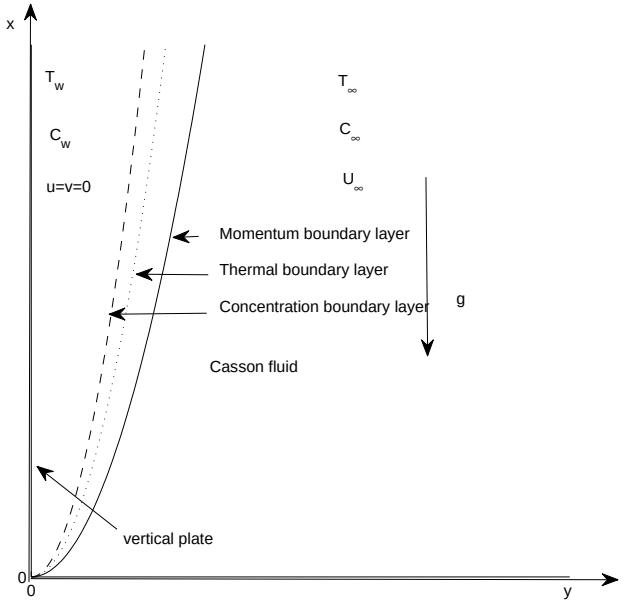

Figure 8.1: Physical model and coordinate system

The vertical wall is maintained at constant temperature $T_w(> T_\infty)$ and solute concentration $C_w(> C_\infty)$. The free stream velocity is maintained at U. At the wall-fluid interface we consider no-slip conditions and there is heat transfer from the solid wall to the fluid.

An equation of an isotropic and incompressible flow of Casson fluid is written as (Nakamura and Sawada (1988));

$$\tau_{ij} = \begin{cases} \left(\mu + \tau_y/\sqrt{2\pi}\right) 2e_{ij} & \pi > \pi_c, \\ \left(\mu + \tau_y/\sqrt{2\pi_c}\right) 2e_{ij} & \pi < \pi_c, \end{cases} \tag{8.1}$$

where μ is plastic dynamics viscosity of the Casson fluid, τ_y is the yield stress of fluid, π is the product of the component of deformation rate with itself, namely, $\pi = e_{ij}e_{ij}$, e_{ij} is the (i, j)-th component of the deformation rate, and π_c is the critical value π.

Taking into account the effect of the thermal and solute dispersion, the double diffusion convection equation of the Casson fluid is written as

$$\frac{\partial u}{\partial x} + \frac{\partial v}{\partial y} = 0, \tag{8.2}$$

$$u\frac{\partial u}{\partial x} + v\frac{\partial u}{\partial y} = \nu\left(1 + \frac{1}{\beta}\right)\frac{\partial^2 u}{\partial y^2} + g\beta_T(T - T_\infty) + g\beta_c(C - C_\infty), \tag{8.3}$$

$$u\frac{\partial T}{\partial x} + v\frac{\partial T}{\partial y} = \frac{\partial}{\partial y}\left(\alpha_y\frac{\partial T}{\partial y}\right) + \frac{\nu}{Cp}\left(1 + \frac{1}{\beta}\right)\left(\frac{\partial u}{\partial y}\right)^2, \tag{8.4}$$

$$u\frac{\partial C}{\partial x} + v\frac{\partial C}{\partial y} = \frac{\partial}{\partial y}\left(D_y\frac{\partial C}{\partial y}\right) + \frac{\alpha}{T_m}\frac{\partial^2 T}{\partial y^2}. \tag{8.5}$$

and the corresponding boundary conditions are written as

$$\begin{aligned} &u = 0,\ v = 0,\ k\frac{\partial T}{\partial y} = h(T_w - T),\ \ C = C_w, \quad \text{at } y = 0,\\ &u \to U,\ T \to T_\infty,\ C \to C_\infty, \ \ \text{as } y \to \infty, \end{aligned} \tag{8.6}$$

where ν is the viscosity of the fluid, $\beta = \mu\sqrt{2\pi_c}/\tau_y$ is the Casson parameter, g is the acceleration due to gravity, β_T and β_C are the coefficients of thermal and solutal expansions, T is the solute temperature, T_∞ is uniform ambient temperature, C is the solute concentration, C_∞ is uniform free stream concentration, α_y and D_y are variables defined by $\alpha_y = \alpha + \gamma_0 d(\partial\psi/\partial y)$ and $D_y = D_{sm} + \zeta_0 d(\partial\psi/\partial y)$. α and D represent the molecular thermal and solutal diffusivities respectively. $\gamma_0 d(\partial\psi/\partial y)$ and $\zeta_0 d(\partial\psi/\partial y)$ the dispersion thermal and solutal diffusivities, γ_0 is the mechanical thermal-dispersion coefficient, ζ_0 is the mechanical solutal-dispersion coefficient, C_p is the specific heat capacity, T_m is the mean fluid temperature. Introducing the convective boundary condition at the bottom of the surface which is heated by the convection from a hot fluid of temperature T and provide a heat transfer coefficient h and thermal conductivity k where $T > T_w > T_\infty$.

Using the following similarity transformations

$$\xi = \frac{x}{l},\ \eta = \sqrt{\frac{U}{\nu x}}y,\ \psi = \sqrt{\nu U x} f(\xi,\ \eta),\ \theta = \frac{T - T_\infty}{T_w - T_\infty},\ \phi = \frac{C - C_\infty}{C_w - C_\infty}, \tag{8.7}$$

Using the similarity transformation, the governing equations are written as

$$\left(1 + \frac{1}{\beta}\right) f''' + \frac{1}{2} f f'' \pm \lambda\xi(\theta + N\phi) = \xi\left(f'\frac{\partial f'}{\partial \xi} - f''\frac{\partial f}{\partial \xi}\right), \tag{8.8}$$

$$\left(\frac{1}{Pr} + K\right)\theta'' + \frac{1}{2} f\theta' + \left(1 + \frac{1}{\beta}\right) Ec f''^2 + \gamma_0 Ra_d\left(f''\theta' + f'\theta''\right) = \xi\left(f'\frac{\partial \theta}{\partial \xi} - \theta'\frac{\partial f}{\partial \xi}\right), \tag{8.9}$$

$$\frac{1}{Sc}\phi'' + \frac{1}{2} f\phi' + Sr\theta'' + \zeta_0 Ra_d\left(f''\phi' + f'\phi''\right) = \xi\left(f'\frac{\partial \phi}{\partial \xi} - \phi'\frac{\partial f}{\partial \xi}\right), \tag{8.10}$$

and the boundary conditions are written as

$$\begin{aligned} &f' = 0,\ f + 2\xi\frac{\partial f}{\partial \xi} = 0,\ \theta' = -Bi\left(1 - \theta(0)\right),\ \phi = 1, \quad \text{at } \eta = 0, \\ &f' \to 1,\ \theta \to 0,\ \phi \to 0, \quad \text{as } \eta \to \infty \end{aligned} \tag{8.11}$$

where 'prime' denoted the differentiation with respect to η. Thermal Grashof number Gr, Reynolds number Re, Solute Grashof number Gr^*, thermal convection parameter λ, solutal convection parameter λ^*, double diffusion parameter N, stratification parameter Ra_d, radiation parameter R, Eckert number Ec, Schmidt number Sc, Soret number Sr and Biot number Bi defined as

$$\begin{aligned} &Gr = \frac{g\beta_T \Delta T L^3}{\nu^2},\ Re = \frac{UL}{\nu},\ Gr^* = \frac{g\beta_c \Delta C L}{U^2},\ \lambda = \frac{Gr}{Re^2}, \lambda^* = \frac{Gr^*}{Re^2},\ N = \frac{\lambda^*}{\lambda}, Ra_d = \frac{dU}{\nu} \\ &K = \frac{16T_\infty^2\sigma^*}{3\nu k^*},\ Ec = \frac{\nu U^2}{Cp\Delta T},\ Sc = \frac{\nu}{D},\ Sr = \frac{DK_T\Delta T}{\nu T_m \Delta C},\ Bi = \frac{a}{k_f}\sqrt{\frac{\nu}{U}}, \end{aligned} \tag{8.12}$$

We have formulated a system of partial differential equations describing the effects of

double dispersion on Casson fluid flow with viscous dissipation and convective boundary conditions. We now derive the expressions for the skin friction, heat and mass transfer coefficients.

8.4. skin friction, heat and mass transfer coefficients

In this section we derive the important engineering parameters for the problem for this chapter which are the skin friction, heat and mass transfer coefficients. The skin friction coefficient is derived as follows;

$$\tau_w = \mu \left[\left(1 + \frac{1}{\beta} \right) \frac{\partial u}{\partial y} \right]_{y=0} = \frac{\mu \left(1 + \frac{1}{\beta} \right) U_0}{l Ra_x^{-\frac{1}{2}}} x f''(0), \tag{8.13}$$

where μ is the coefficient of viscosity, The skin friction coefficient is given by,

$$C_f = \frac{\tau_w}{\frac{1}{2}\rho U_0^2}. \tag{8.14}$$

Using Eqs. (8.13) and (8.14) together with Eqs. (8.7) and (8.11) gives

$$Ra_x^{1/2}\, C_f = \left(1 + \frac{1}{\beta} \right) f''(0). \tag{8.15}$$

The heat transfer from the cone surface into the fluid is given by

$$q_w = k \left[\frac{\partial T}{\partial y} \right]_{y=0} = \frac{h(T_w - T_\infty)}{l Ra_x^{-\frac{1}{2}}} x \theta'(0), \tag{8.16}$$

where h is the thermal conductivity of the fluid. The heat transfer coefficient (Nusselt number) under convective boundary conditions is given by

$$Nu_x = \frac{l}{k}\frac{q_w}{T_w - T_\infty}. \tag{8.17}$$

Using Eqs. (8.16) and (8.17) together with Eqs. (8.7) and (8.11) gives

$$Ra_x^{-1/2}\ Nu_x = -[1 + \gamma Ra_d f'(0)]\theta'(0). \tag{8.18}$$

The mass flux at the cone surface into the fluid is given by

$$J_w = -D\left[\frac{\partial C}{\partial y}\right]_{y=0} = \frac{-D(C_w - C_\infty)}{lRa_x^{-\frac{1}{2}}} x\phi'(0), \tag{8.19}$$

The mass transfer coefficient (Sherwood number) is given by

$$Sh_x = \frac{l}{D}\frac{J_w}{C_w - C_\infty}. \tag{8.20}$$

Using Eqs. (8.19) and (8.20) together with Eqs. (8.7) and (8.11) gives

$$Ra_x^{-1/2}\ Sh_x = -[1 + \zeta Ra_d f'(0)]\phi'(0). \tag{8.21}$$

We have derived the skin friction, heat transfer and mass transfer coefficients. We are now ready to discuss the results for the system derived in the previous section.

8.5. Results and discussion

The problem of the effect of double dispersion in Casson fluid flow with viscous dissipation and convective boundary conditions was solved by the local linearization (LLM). The system of equations were validated by the Matlab `bvp4c` for the case $\xi = 0$ which gives a well known Blassius equation and compared to the results of Yih (1999). These comparisons of results were in excellent agreement. In this section we focus on the variation of the Casson parameter

β, thermal convection parameter λ, double diffusion parameter N, radiation parameter K, Eckert number Ec, stratification parameter Ra_d, Soret number Sr, the mechanical thermal-dispersion γ_0, the mechanical solutal-dispersion ζ_0 and the Biot number Bi on velocity, temperature and concentration profiles. We also study variation of some selected physical parameters with the skin friction, heat transfer and mass transfer coefficients.

In this section we assume that the Prandtl number is between $Pr = 10$ at 20^oC and $Pr = 20$ for blood. The appropriate Grashof number is fixed at $Gr = 10$ and Darcy number $Da = 0.1$ giving a fixed value $k_p = 1/DaGr^{\frac{1}{2}} = 3$. All other parameters are chosen arbitrarily being careful to stay within the acceptable range of the Casson fluid.

The numerical results were validated for the skin friction $f''(0)$ and heat transfer $-\theta'(0)$ coefficients for the Newtonian fluid. The results obtained by the LLM and the Matlab `bvp4c` were compared to the results obtained by Yih (1999) and were found to be in excellent agreement as shown in Table 8.1.

Table 8.1: Comparison of the values of $f''(0)$ and $-\theta'(0)$ obtained by LLM with those of bvp4c for $Pr = 5, 1/\beta \to 0, N = \xi = K = Ec = Ra_d = \gamma_0 = \zeta_0 = 0$

	Yih (1999)		bvp4c		BQLM	
Pr	$f''(0)$	$-\theta'(0)$	$f''(0)$	$-\theta'(0)$	$f''(0)$	$-\theta'(0)$
1	0.332057	0.332057	0.33205935	0.33205935	0.33205935	0.33205935
10	-	-	0.3305935	0.72814593	0.3305935	0.72814593

The problem of the effects of double dispersion in Casson fluid flow with viscous dissipation and convective boundary conditions was solved numerically using the local linearization method (LLM). The results are shown in Figures 8.2 - 8.13. Figures 8.2 and 8.3 respectively shows the variation of the Casson parameter β and buoyancy parameter N on velocity profiles. Figures 8.4 - 8.8 show the variation of the Casson parameter β, mechanical thermal-dispersion parameter γ_0, Biot number Bi and the stratification parameter Ra_d on temperature profiles. Figures 8.9 and 8.10 respectively show the variation of Casson parameter β and the stratification parameter Ra_d on concentration profiles. The plots of skin

friction and mass transfer coefficients against some selected physical parameters are shown in Figures 8.11 - 8.13

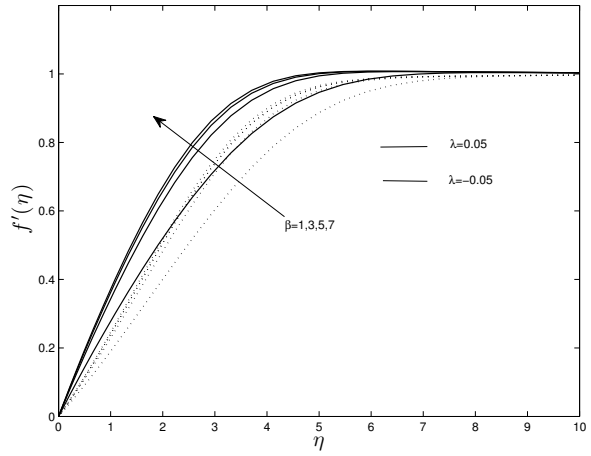

Figure 8.2: Effect of Casson parameter β on velocity profiles $f'(\eta)$ for both aiding ($\lambda = 0.05$) and opposing ($\lambda = -0.05$) solutal convection for $Pr = 5, N = 0.5, K = 0.5, Ec = 1, \gamma_0 = 1, Ra_d = 0.1, Sc = 0.7, Sr = 0.3, \zeta_0 = 1, Bi = 0.1$

The variation of Casson parameter β on velocity profiles for different values of the solutal convection parameter λ is shown in Figure 8.2. It can be seen from the graph that increasing the Casson parameter result in the increase in velocity profiles. This result has been discussed in the previous chapters. The interesting result is that, the increase in the solutal convection parameter λ result in the increase in velocity profiles. We thus interpret the increase in the solutal convection parameter as having an effect of increasing solutal motion thereby causing an increase in fluid motion.

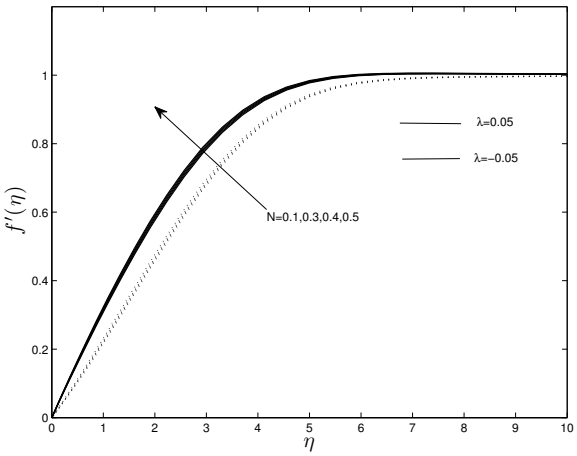

Figure 8.3: Effect of buoyancy parameter N on velocity profiles $f'(\eta)$ for both aiding ($\lambda = 0.05$) and opposing ($\lambda = -0.05$) solutal convection for $Pr = 5, \beta = 2, K = 0.5, Ec = 1, \gamma_0 = 1, Ra_d = 0.1, Sc = 0.7, Sr = 0.3, \zeta_0 = 1, Bi = 0.1$

In Figure 8.3, it can be seen that increasing the buoyancy parameter N result in the increase in velocity profiles as discussed in the previous chapters. It is noted that the increase in the buoyancy parameter is more pronounced in the case of opposing flow $\lambda = -0.05$ than in the aiding flow case $\lambda = 0.05$. We thus interpret the increase in the buoyancy as having an effect of assisting the fluid flow, this means that if the fluid is flowing slowly in the case of $\lambda = -0.05$, then increasing the buoyancy parameter would cause a larger variation. A smaller variation is noted in the case of $\lambda = 0.05$, the velocity profiles are already close to the maximum velocity and aiding fluid flow would have not have much effect.

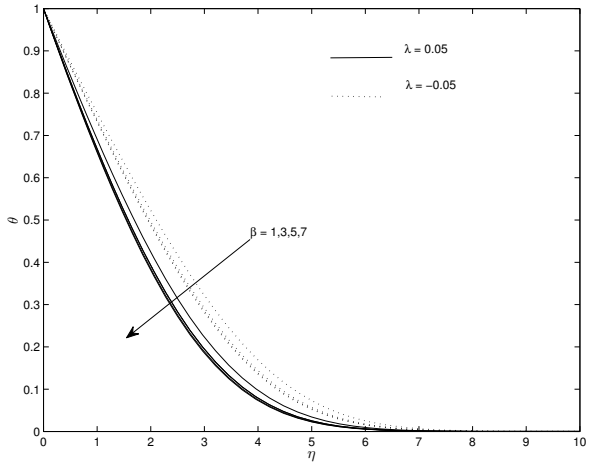

Figure 8.4: Effect of Casson parameter β on temperature profiles $\theta(\eta)$ for both aiding ($\lambda = 0.05$) and opposing ($\lambda = -0.05$) solutal convection for $Pr = 5, N = 0.5, K = 0.5, Ec = 1, \gamma_0 = 1, Ra_d = 0.1, Sc = 0.7, Sr = 0.3, \zeta_0 = 1, Bi = 0.1$

The variation of Casson parameter β at different values of the solutal convection parameter λ is shown in Figure 8.4. It can be seen from the graph that increasing the Casson parameter β result in the decrease in temperature profiles has been reported in the previous chapters. It is noted that in the case of $\lambda = 0.05$ lower temperature profiles are noted than the case of $\lambda = -0.05$.

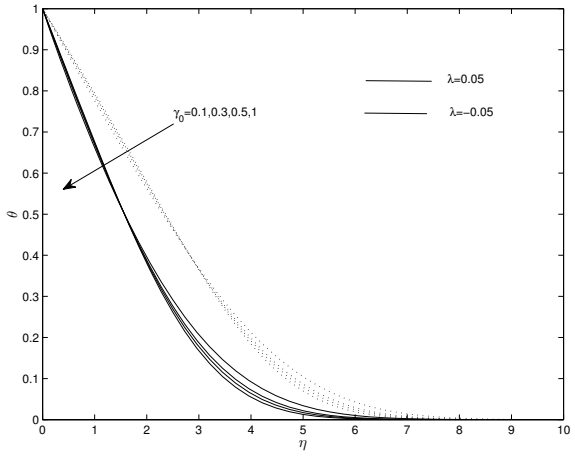

Figure 8.5: Effect of mechanical thermal-dispersion parameter γ_0 on temperature profiles $\theta(\eta)$ for both aiding ($\lambda = 0.05$) and opposing ($\lambda = -0.05$) solutal convection for $Pr = 5, \beta = 2, N = 0.5, K = 0.5, Ec = 1, Ra_d = 0.1, Sc = 0.7, Sr = 0.3, \zeta_0 = 1, Bi = 0.1$.

The variation of the mechanical thermal-dispersion γ_0 for different values of the solutal convection parameter λ on temperature profiles is shown in Figure 8.5. It can be seen from the graph that increasing the mechanical thermal-dispersion parameter γ_0 result in the increase in temperature profiles in both aiding and opposing situations. Increasing the mechanical thermal-dispersion parameter would naturally mean that the temperature in the fluid regime is increased. Increased temperature profiles are noted in the case of opposing situation, the same result was reported in Narayana et al. (2013).

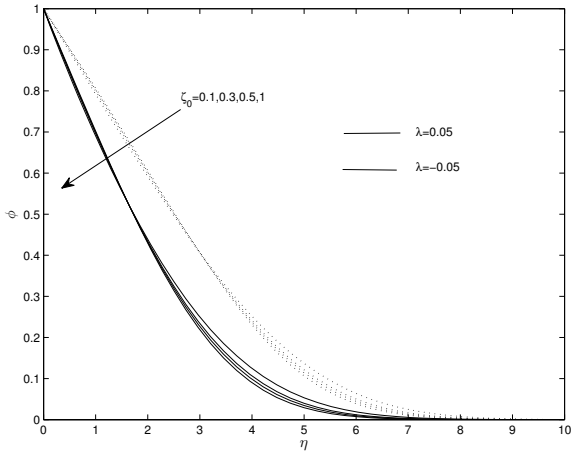

Figure 8.6: Effect of mechanical solutal-dispersion parameter ζ_0 on concentration profiles $\theta(\eta)$ for both aiding ($\lambda = 0.05$) and opposing ($\lambda = -0.05$) solutal convection for $Pr = 5, \beta = 2, N = 0.5, K = 0.5, Ec = 1, Ra_d = 0.1, Sc = 0.7, Sr = 0.3, \gamma_0 = 1, Bi = 0.1$.

The variation of the mechanical solutal-dispersion ζ_0 for different values of the solutal convection parameter λ on temperature profiles is shown in Figure 8.6. It can be seen from the graph that increasing the mechanical solutal-dispersion parameter ζ_0 result in the increase in concentration profiles in both aiding and opposing situations. Increasing the mechanical solutal-dispersion parameter would naturally mean that the concentration in the fluid regime is increased.

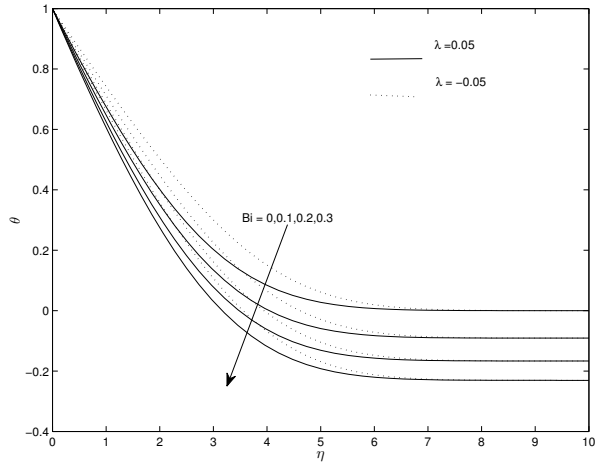

Figure 8.7: Effect of Biot number Bi on temperature profiles $\theta(\eta)$ for both aiding ($\lambda = 0.05$) and opposing ($\lambda = -0.05$) solutal convection for $Pr = 5, \beta = 2, N = 0.5, K = 0.5, Ec = 1, \gamma_0 = 1, Ra_d = 0.1, Sc = 0.7, Sr = 0.3, \zeta_0 = 1$.

The variation of the Biot number Bi on temperature profiles in both aiding and opposing situations is reflected in Figure 8.7. It can be seen from the graph that increasing the Biot number result in the decrease in the temperature profiles. We thus interpret the increase in the Biot number as having an effect of increasing the convective heat transfer thereby reducing temperature in the boundary layer.

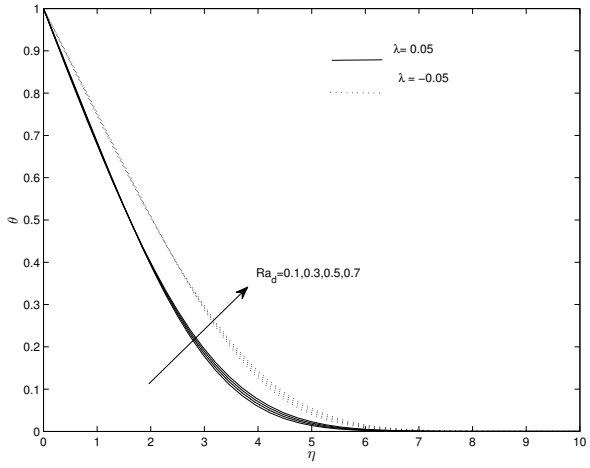

Figure 8.8: Effect of stratification parameter Ra_d on temperature profiles $\theta(\eta)$ for both aiding ($\lambda = 0.05$) and opposing ($\lambda = -0.05$) solutal convection for $Pr = 5, \beta = 2, N = 0.5, K = 0.5, Ec = 1, \gamma_0 = 1, Sc = 0.7, Sr = 0.3, \zeta_0 = 1, Bi = 0.1$.

The variation of the stratification parameter Ra_d on temperature profiles in both aiding and opposing situations is shown in Figure 8.8. It can be seen from the figure that increasing the stratification parameter result in the increase in the temperature profiles. We thus interpret the increase in the stratification parameter as having an effect of reducing the temperature difference between the vertical wall and the fluid in the boundary layer. The same result was noted by El-Amin et al. (2008).

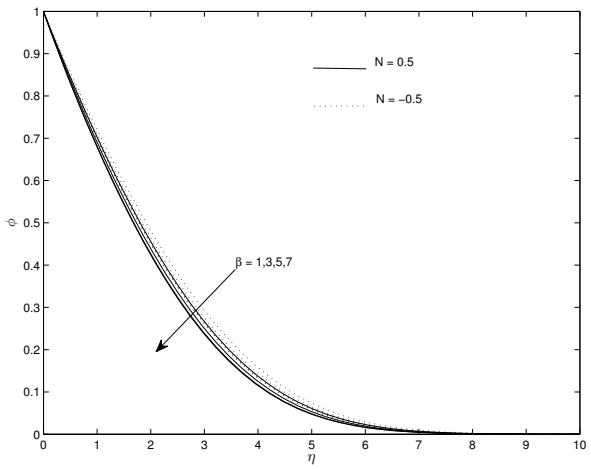

Figure 8.9: Effects of Casson parameter β on concentration profiles for both aiding $N = 0.5$ and opposing $N = -0.5$ buoyancy cases for $Pr = 5, \lambda = 0.05, K = 0.5, Ec = 1, \gamma_0 = 1, Ra_d = 0.1, Sc = 0.7, Sr = 0.3, \zeta_0 = 1, Bi = 0.1$

The variation of Casson parameter β on concentration profiles for both aiding and opposing buoyancy cases is shown in Figure 8.9. It can be seen from the figure that increasing the Casson parameter result in reducing the concentration profiles in both aiding and opposing buoyant cases. The Casson parameter causes for the retardation in the fluid motion which decrease the concentration boundary layer thickness. Lower temperatures are noted for the case of aiding buoyancy.

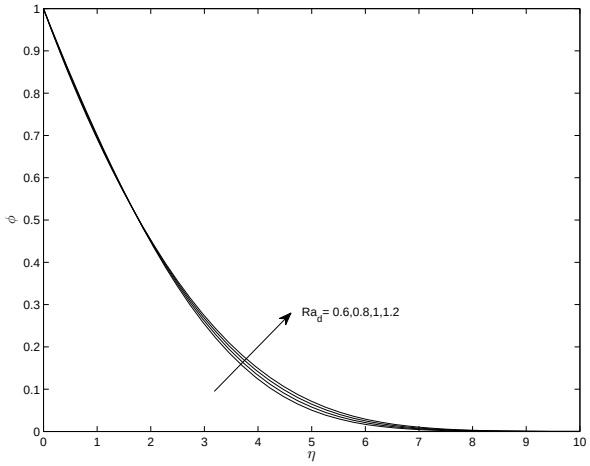

Figure 8.10: Effects of stratification parameter Ra_d on concentration profiles $\phi(\eta)$ for $Pr = 5, \beta = 2, \lambda = 0.05, N = 0.5, K = 0.5, Ec = 1, \gamma_0 = 1, Sc = 0.7, Sr = 0.3, \zeta_0 = 1, Bi = 0.1$.

The effect of stratification parameter on the concentration profiles is shown in Figure 8.10. It can be seen from the graph that increasing the Stratification parameter Ra_d result in the decrease the solute concentration near the surface and increase further away from the surface.

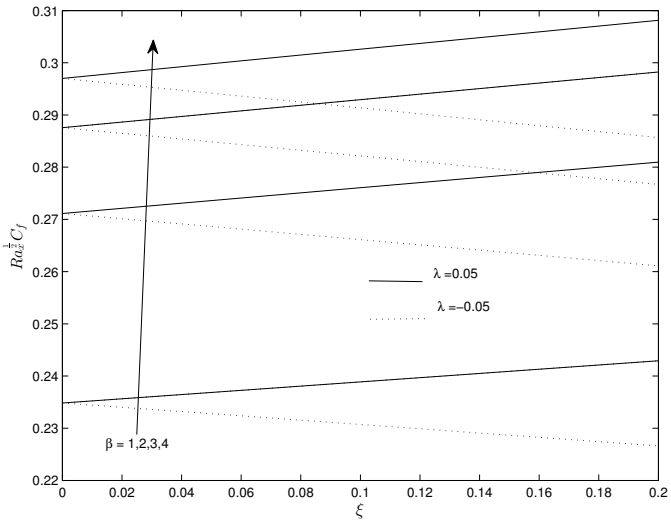

Figure 8.11: Plot of the skin friction coefficient $f''(0)$ against transverse coordinate ξ for different values of the Casson parameter β for $Pr = 5, \lambda = 0.05, N = 0.5, K = 0.5, Ec = 1, \gamma_0 = 1, Ra_d = 0.1, Sc = 0.7, Sr = 0.3, \zeta_0 = 1, Bi = 0.1$

The plot of the skin friction coefficient $f''(0)$ against the transverse coordinate ξ for different values of the Casson parameter β is shown in Figure 8.11. It can be seen from the graph that increasing the Casson parameter results in the decrease in skin friction coefficient. We can thus interpret the increase in the Casson parameter as having an effect of reducing the shear stress on the vertical surface thereby reducing the skin friction coefficient. It is also noted that the skin friction increases with increasing ξ for the aiding case ($\lambda = 0.05$) and decrease with increasing ξ for the opposing case ($\lambda = -0.05$).

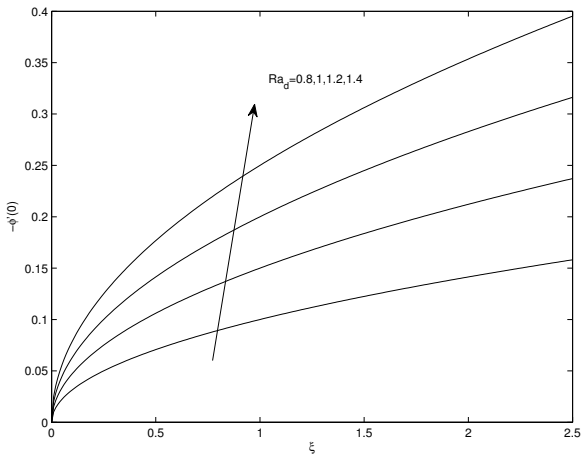

Figure 8.12: Plot of the mass transfer coefficient $-\phi'(0)$ against transverse coordinate ξ for different values of the stratification parameter Ra_d for $Pr = 5, \beta = 2, \lambda = 0.05, N = 0.5, K = 0.5, Ec = 1, \gamma_0 = 1, Sc = 0.7, Sr = 0.3, \zeta_0 = 1, Bi = 0.1$.

The plot of the mass transfer coefficient $-\phi'(0)$ against the transverse coordinate ξ for different values of the stratification parameter Ra_d is shown in Figure 8.12. It can be seen from the graph that increasing the stratification parameter results in the decrease in the mass transfer coefficient. We thus interpret the increase in the stratification parameter as having an effect of reducing the temperature gradient thereby reducing the solute transport from the surface of the vertical wall. It is noted that the mass transfer coefficient decreases with increasing ξ.

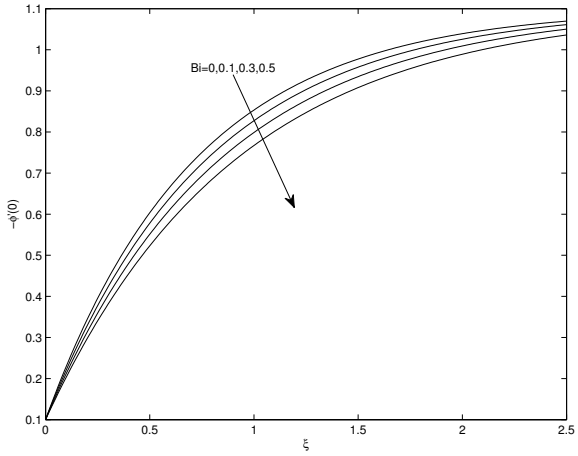

Figure 8.13: Plot of the mass transfer coefficient $-\phi'(0)$ against transverse coordinate ξ for different values of the Biot number Bi for $Pr = 5, \beta = 2, \lambda = 0.05, N = 0.5, K = 0.5, Ec = 1, \gamma_0 = 1, Ra_d = 0.1, Sc = 0.7, Sr = 0.3, \zeta_0 = 1$.

The plot of the mass transfer coefficient $-\phi'(0)$ against the transverse coordinate ξ for different values of the Biot number Bi is shown in Figure 8.13. It can be seen from the graph that increasing the Biot number results in the decrease in the mass transfer coefficient. Increasing the Biot number would e interpreted as increasing the heat transfer resistance in the solid boundary; this in turn slows down the solute movement. It is observed in general that the mass transfer coefficient increase with increasing transverse coordinate ξ.

8.6. Summary

The influence of double dispersion convection Casson fluid flow over a vertical plate has been studied. Double dispersion plays a vital role on the system. The increase in Casson parameter increases the skin friction coefficient and velocity profiles, but decreases both temperature and concentration profiles. Thermal stratification decreases the heat transfer coefficient at the surface, increase thermal and solute boundary layer thicknesses. Increasing the mechanical thermal-dispersion rate γ_0 and mechanical solutal-dispersion rate ζ_0 result in the decrease in both temperature and concentration profiles respectively. This decrease is noticed closer to the boundary due to the no-slip condition, the reverse effect is noted further away from the boundary, this is due to the high velocity close to the free stream region.

Chapter 8 – Effects of double dispersion on Casson fluid flow with viscous dissipation and convective boundary conditions

In this chapter we point out that new results have been obtained from this problem with new physical aspects in fluid flow considered. The application of the local linearization method (LLM) in similar studies is fairly new.

In this chapter the local linearization method (LLM) was used to find solutions of the effects of double dispersion on Casson fluid with convective boundary condition problem. The problem consists of three coupled partial differential equations. The numerical solution was compared to the Matlab `bvp4c` for the case $\xi = 0$ and to previously published results in the literature and was found to be in excellent agreement. The drawback of this method is that a good initial approximation is still required and that the one has to have an idea of the size of the boundary layer thickness. This thickness is sometimes referred to as the value at infinity or η_∞. Improvements of this method need to address these issues.

9

Conclusion

In this thesis we have used various recent numerical methods to solve nonlinear differential equations in fluid flow. The methods have been used to solve different fluid flow problems. The problems considered the effects of various physical aspects such as radiation, magnetohydrodynamics, viscous dissipation, cross diffusion effects and fluid flow in porous media. The findings for each problem are summarized below.

In Chapter 2, we gave a detailed description of all the numerical methods that were used in the thesis namely; the Matlab `bvp4c`, the successive linearization method (SLM), the spectral quasi-linearization method (QLM), the spectral relaxation method (SRM) and the local linearization method (LLM). These methods were generalized so that they can be adopted in other contexts. In Chapter 2 we adopted shorter versions of how to implement these methods. It was clearly shown in Chapter 2 that these methods are much easier to implement than traditionally used finite differences and other methods discussed in the introduction (Chapter 1).

Chapter 9 – Conclusion

In Chapter 3, we solved the problem of flow of a Newtonian fluid on an exponentially stretching surface. In Sections 3.1.4 to 3.1.6 we obtained analytical solutions of the momentum, energy and mass transfer equations respectively. The momentum equation was reduced to the Riccati-type equation which, together with the energy and mass transfer equations can be solved in terms of the confluent hyper geometric Whittaker function. The Runge-Kutta-Fehlberg method with the shooting technique was used to solve the system of equations. A comparison with the exact solutions showed an excellent agreement. The study showed the accuracy of the Runge-Kutta-Fehlberg method for the flow of the Newtonian fluid over an exponentially stretching sheet.

In Chapter 4, we investigated the problem of free convection flow of viscoelastic fluid from a cone in porous medium with viscous dissipation. The problem contained a parameter which sometimes would be considered small. In most cases such problems are solved by the perturbation method. Due to the limitations of the perturbation method such as requiring the parameter to be small, we proposed the successive linearization method to solve this problem. The system of equations was written as the zeroth, first and second order equations as in the case of the perturbation method. The system of equations was solved together using the successive linearization method. The successive linearization (SLM) was shown to be a very accurate method; the obtained results of the problem were compared to those available in the literature and were found to be in excellent agreement.

In Chapter 4, we gave a detailed description of the successive linearization method. The method is preferred because of its robustness; does not involve rigorous mathematical manipulations as in the case of the finite difference, finite element and finite volume methods. This method does not involve large block matrices as in the case with the Keller box method which take considerable computation time and memory space. In the solution of this problem the linearized system is solved by the Chebyshev spectral collocation method. The successive linearization method converges rapidly to the solution. This method converges after three to four iterations making it one of the most efficient methods in solving nonlinear differential equations. The disadvantage of the method is that an initial guess that satisfies the boundary condition needs to be provided. A poor initial guess results in divergence of the result. The number of collocation points is also difficult to determine, usually trial and error is used in

this process. So far there is no theory of the uniqueness and existence of solutions using this method. The method's accuracy was only tested experimentally in the works of (Motsa and Sibanda, 2013; Motsa and Shateyi, 2012; Motsa et al., 2014, Motsa and Sibanda, 2012, Motsa et al. 2012).However, this method has shown great accuracy when compared to other traditional methods such as; the Matlab `bvp4c`, finite difference, finite element etc. Another drawback of this method is that there is no check of the residual errors at each time step. The collocation points do not change in size. In solving fluid flow problems the user has to have an idea of the size of the boundary layer thickness.

In Chapter 5, we solve the problem of the flow of Casson fluid over an unsteady stretching surface with chemical reactions. The problem consists of three coupled ordinary differential equations. The problem was solved using the Matlab `bvp4c` algorithm and the successive linearization method (SLM). The numerical solutions were compared and were shown to be in excellent agreement. The numerical solution was further was compared to those available in the literature and was found to be in excellent agreement. The Matlab `bvp4c` algorithm has recently become the basic method for which researchers use for validation of other methods. The advantage of this algorithm is that it is an adaptive solver; it changes the step size at each time step. The main disadvantage of the method is that the governing equations need to be changed to a system of first order differential equations. This is sometimes not easy for highly nonlinear coupled differential equations. However, special boundary conditions are easy to implement in this method than any other method.

In Chapter 6, we solve the problem of the flow of Casson fluid from a horizontal circular cylinder with partial slip problem and transpiration. The problem consists of two coupled partial differential equations differential equations. The local linearization method (LLM) was used to solve this problem. This type of equations is normally solved using the Keller-box method which requires rigorous mathematical computations and results in large block matrices which requires considerable computer memory and computation time. The numerical solution of the LLM was compared to the solutions of the successive linearization method (SLM). The SLM is known to be better that the Keller-box method in terms of accuracy, computation time and memory space. The numerical solution was further was compared to the successive linearization method and `bvp4c` and was found to be in excellent agreement.

The local linearization method has become one of the most efficient pseudo spectral methods due to its fast convergence. The disadvantage of the method is that the number of collocation points need to be determined by trial and error. It is a challenge to handle special boundary conditions such as convective boundary conditions in fluid flow. An initial guess that satisfies boundary conditions has to be determined and this is usually not easy. A good initial guess results in good and rapid convergence.

In Chapter 7, we solved the problem of the flow of Casson fluid from a spinning cone with partial slip in non-Darcy porous medium with viscous dissipation. The problem consisted of four coupled ordinary differential equations which were solved by the spectral relaxation method (SRM), the numerical solution was compared to the previously published results and there was excellent agreement. The numerical solution was further compared to the available results in the literature and was found to be in excellent agreement. The spectral relaxation method (SRM) is an iterative scheme that is based on the Gauss-Seidel method for solving linear equations. The method is very accurate. This method is also equipped with the successive over-relaxation technique (SOR) which accelerates convergence.

In Chapter 8, we solve the problem of the effects of double dispersion on Casson fluid with convective boundary condition problem. The problem consisted of three coupled partial differential equations, which were solved using the local linearization method (LLM) and the spectral quasi-linearization method (SQLM). The numerical solution was compared to the successive linearization method (SLM) and there was a good agreement. The numerical solution was further compared to the available results in the literature and was found to be in excellent agreement. The only shortcoming encountered was the difficulty in handling convective boundary conditions. A small change in the parameter contained in the boundary conditions such affects convergence.

From this study we conclude that in comparison to some existing methods, spectral quasi-linearization method (QLM), the successive linearization method (SLM), spectral relaxation method (SRM), the Matlab `bvp4c` algorithm, and the local linearization method (LLM) are efficient, robust and accurate. The methods were used to solve a wide range of highly nonlinear differential equations. The methods gave accurate results with the Matlab `bvp4c` able to almost solve all numerical solutions in this study.

These methods can be extended to other types of differential equations such as difference equations and discrete time equations. These methods are highly accurate, converge faster and computationally efficient when compared to finite differences. In Chapter 6, the local linearization method was shown to converge faster showing the accuracy of the method. However, the thesis was only limited to fluid flow problems which were solved by spectral methods. The thesis discussed the implementation of numerical methods in general so they can be applied to other contexts.

Appendices

The original copies of published and sumitted papers are listed in the following Appendices;

Appendix A: On radiation effects on hydromagnetic Newtonian liquid flow due to an exponential stretching sheet.

Appendix B: Natural convection of viscoelastic fluid from a cone embedded in porous medium with viscous dissipation.

Appendix C: Diffusion of chemically reactive species in Casson fluid flow over an unsteady stretching surface in a porous medium in the presence of a magnetic field.

Appendix D: Effects of radiation on MHD free convection of a Casson fluid from a horizontal circular cylinder with partial slip in non-Darcy porous medium with viscous dissipation.

Appendix E: Numerical analysis of free convection Casson fluid flow from a spinning cone in non-Darcy porous medium with radiation, partial slip, cross diffusion and viscous dissipation.

Appendix F: Effects of doule dispersion on Casson fluid flow with viscous dissipation and convective boundary conditions.

The next page was intentionally left blank

Appendix A

Kameswaran et al. *Boundary Value Problems* 2012, **2012**:105
http://www.boundaryvalueproblems.com/content/2012/1/105

Boundary Value Problems
a SpringerOpen Journal

RESEARCH Open Access

On radiation effects on hydromagnetic Newtonian liquid flow due to an exponential stretching sheet

PK Kameswaran, M Narayana, P Sibanda* and G Makanda

*Correspondence:
sibandap@ukzn.ac.za
School of Mathematics, Statistics and Computer Sciences, University of KwaZulu-Natal, Private Bag X01, Pietermaritzburg, Scottsville 3209, South Africa

Abstract

The paper investigates the radiation effect on the magnetohydrodynamic Newtonian fluid flow over an exponentially stretching sheet. The effects of frictional heating and viscous dissipation on the heat transport are taken into account. The governing partial differential equations are transformed into ordinary differential equations using a suitable similarity transformation. Zero-order analytical solutions of the momentum equation and confluent hypergeometric solutions of heat and mass transport equations are obtained. The accuracy of analytical solutions is verified by numerical solutions obtained using a shooting technique that uses a Runge-Kutta-Felhberg integration scheme and a Newton-Raphson correction scheme. The effects of the radiation parameter, the magnetic parameter, Gebhart and Schmidt numbers on the momentum, heat and mass transports are discussed. The skin friction and heat and mass transfer coefficients for various physical parameters are discussed.

1 Introduction

The study of laminar boundary layer flow over a stretching sheet has received considerable attention in the recent past due to its immense application in industry, for example, in extrusion processes such as the polymer extrusion from a dye and wire drawing. Other engineering applications of the stretching sheet problem include polymer sheet extrusion from a dye, drawing, tinning and annealing of copper wires, glass fiber and paper production, the cooling of a metallic plate in a cooling bath and so on. There has been tremendous amount of work on the stretching sheet problem in the past several decades (see Crane [1], Gupta and Gupta [2], Grubka and Bobba [3], Dutta and Gupta [4], Siddappa and Abel [5], Chen and Char [6], Laha *et al.* [7], Chakrabarti and Gupta [8], Anderson *et al.* [9], Siddheshwar and Mahabaleswar [10], Abel and Mahesha [11], Abel *et al.* [12] and the references therein).

The above studies concern the linear stretching sheet problem but most of the practical situations involve a non-linear stretching sheet such as an exponential one. With this in mind, several authors have considered the velocity of the sheet to vary exponentially with the distance from the slit. Elbashbeshy [13] was among the first to study the exponentially stretching sheet problem. He considered a perforated sheet and examined the effect of wall mass suction on the flow and heat transfer over an exponentially stretching surface. Using a suitable similarity transformation, he transformed the momentum equation into a non-linear Riccati type equation and solved it iteratively. Ishak [14] studied the MHD boundary

layer flow due to an exponentially stretching sheet with radiation effect. He found that the local heat transfer rate at the surface decreased with increasing values of the magnetic and radiation parameters. The flow and heat transfer from an exponentially stretching surface was considered by Magyari and Keller [15]. They examined the heat and mass transfer characteristics and compared with the well-known results of the power-law models. Sanjayanand and Khan [16] studied the heat and mass transfer in a viscoelastic boundary layer flow over an exponentially stretching sheet. They found that the viscoelastic parameter enhances the thermal boundary layer thickness. The effect of viscous dissipation on the mixed convection heat transfer from an exponentially stretching surface was studied by Partha *et al.* [17]. They observed a rapid growth in the non-dimensional skin friction coefficient with the mixed convection parameter. The influence of thermal radiation on the boundary layer flow due to an exponentially stretching sheet is studied by Sajid and Hayat [18]. Khan [19] presented an elegant solution of the viscoelastic boundary layer flow over an exponentially stretching sheet in terms of Whittaker's function.

The characteristics desired of the final product in an extrusion process depend on the rate of stretching and cooling. Hence, it is very important to have a controlled cooling environment where the flow over the stretching sheet can be regulated by external agencies like a magnetic field. An exponential variation of a magnetic field is used, among other applications, to determine the diamagnetic susceptibility of plasma. Steenbeck [20] determined the diamagnetic susceptibility of a cylindrical plasma for axial magnetic fields with various gas pressure and magnetic field strengths. Tonks [21] studied the effects of a magnetic field in the plasma of an arc. Pavlov [22] considered the magnetohydrodynamic flow of an incompressible viscous fluid over a linearly stretching surface. Sarpakaya [23] extended Pavlov's work to non-Newtonian fluids. Subsequent studies by Andersson [24], Lawrence and Rao [25], Abel *et al.* [26], Cortell [27] concerned the magnetohydrodynamic flow of viscoelastic liquids over a stretching sheet. Radiation effects on MHD flow past an exponentially accelerated isothermal vertical plate with uniform mass diffusion in the presence of a heat source was studied by Reddy *et al.* [28]. They observed that the velocity decreases with an increase in the magnetic parameter due to a resistive drag force which tends to resist the fluid flow and thus reduces the velocity. The boundary layer thickness was also found to decrease with an increase in the magnetic parameter.

Most of the earlier work neglected radiation effects. If the polymer extrusion process is placed in a thermally controlled environment, radiation could become important. As with magnetohydrodynamics, careful control of thermal radiative heat transfer has an effect on the characteristics of the final product: Many researchers have considered the effect of thermal radiation on flows over stretching sheets. Studies by Raptis [29], Raptis and Perdikis [30] address the effect of radiation in various situations. Siddheshwar and Mahabaleswar [10] studied the effects of radiation and heat source on MHD flow of a viscoelastic liquid and heat transfer over a stretching sheet. Bidin and Nazar [31] studied the effects of numerical solution of the boundary layer flow over an exponentially stretching sheet with thermal radiation. They observed that the temperature profiles and the thermal boundary layer thickness increase slightly with an increase in the Eckert number. They also showed that an increase in Pr causes a decrease in temperature profiles and the thermal boundary layer thickness. Physically, if Pr increases, the thermal diffusivity decreases, and these phenomena lead to the decreasing of energy ability that reduces the thermal boundary layer. Elbashbeshy and Dimian [32] analyzed boundary layer flow in the presence of radi-

ation effect and heat transfer over the wedge with a viscous coefficient. Thermal radiation effects on hydro-magnetic flow due to an exponentially stretching sheet were studied by Reddy and Reddy [33]. They found that as radiation increases, the temperature profiles and thermal boundary layer thickness also increase. They also observed that the temperature profiles and thermal boundary layer thickness increase slightly with an increase in the Eckert number. Raptis *et al.* [34] studied the effect of thermal radiation on the magnetohydrodynamic flow of a viscous fluid past semi-infinite stationary plate and Hayat *et al.* [35] extended the analysis for the second grade fluid.

In addition to a magnetic field and thermal radiation, one has to consider the viscous dissipation effects due to frictional heating between fluid layers. The effect of viscous dissipation in natural convection processes has been studied by Gebhart [36] and Gebhart and Mollendorf [37]. They observed that the effect of viscous dissipation is predominant in vigorous natural convection and mixed convection processes. They also showed the existence of a similarity solution for the external flow over an infinite vertical surface with an exponential variation of surface temperature. Vajravelu and Hadjinicalaou [38] studied the heat transfer characteristics over a stretching surface with viscous dissipation in the presence of internal heat generation or absorption.

In this paper, we investigate the effects of various physical and fluid parameters such as the magnetic parameter, radiation parameter and viscous dissipation parameter on the flow and heat transfer characteristics of an exponentially stretching sheet. The momentum, energy and concentration equations are coupled and nonlinear. By using suitable similarity variables, these equations are converted into coupled ordinary differential equations and are solved analytically and numerically by using the Runge-Kutta-Fehlberg and Newton-Raphson schemes.

2 Mathematical formulation

Consider the two-dimensional magnetohydrodynamic flow of a Newtonian fluid over a stretching sheet. The origin of the system is located at the slit from which the sheet is drawn. The x-axis is taken along the continuous stretching surface and points in the direction of motion. The y-axis is perpendicular to the plate. The sheet velocity is assumed to vary as an exponential function of the distance x from the slit. The temperature and concentration far away from the fluid are assumed to be T_∞ and C_∞ respectively as shown in Figure 1. The sheet-ambient temperature and concentration differences are also assumed to be exponential functions of the distance x from the slit. A variable magnetic field of strength $B(x)$ is applied normally to the sheet. Under the usual boundary layer approximation, subject to radiation and viscous dissipation effects, the equations governing the momentum, heat and mass transports can be written as

$$\frac{\partial u}{\partial x} + \frac{\partial v}{\partial y} = 0, \tag{1}$$

$$u\frac{\partial u}{\partial x} + v\frac{\partial u}{\partial y} = \nu\frac{\partial^2 u}{\partial y^2} - \frac{\sigma B^2}{\rho}u, \tag{2}$$

$$u\frac{\partial T}{\partial x} + v\frac{\partial T}{\partial y} = \alpha\frac{\partial^2 T}{\partial y^2} - \frac{1}{\rho C_p}\frac{\partial q_r}{\partial y} + \frac{\sigma B^2}{\rho C_p}u^2 + \frac{\nu}{C_p}\left(\frac{\partial u}{\partial y}\right)^2, \tag{3}$$

$$u\frac{\partial C}{\partial x} + v\frac{\partial C}{\partial y} = D\frac{\partial^2 C}{\partial y^2}, \tag{4}$$

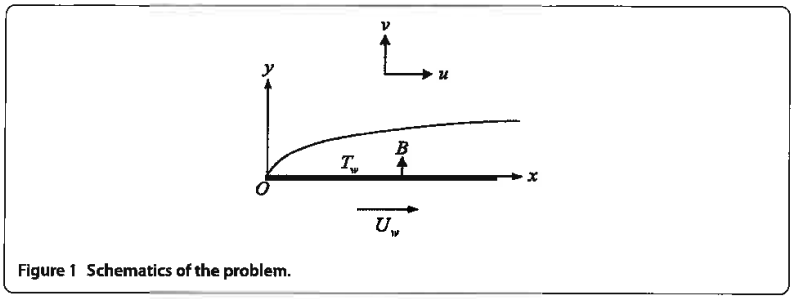

Figure 1 Schematics of the problem.

where u, v are the velocity components in the x, y directions respectively, ν is the kinematic viscosity, ρ is the density, σ is the electrical conductivity of the fluid, T is the temperature, C is the concentration, $\alpha = k/\rho C_p$ is the thermal diffusivity, k is the thermal conductivity, C_p is the specific heat at constant pressure, q_r is the radiative heat flux, and D is the species diffusivity.

The boundary conditions for Equations (1)-(4) have the form

$$\begin{aligned} &u = U_w = U_0 e^{\frac{x}{L}}, \qquad v = 0, \qquad T = T_w = T_\infty + T_0 e^{\frac{2x}{L}}, \\ &C = C_w = C_\infty + C_0 e^{\frac{2x}{L}} \quad \text{at } y = 0, \\ &u \to 0, \qquad T \to T_\infty, \qquad C \to C_\infty \quad \text{as } y \to \infty. \end{aligned} \tag{5}$$

Here the subscripts w, ∞ refer to the surface and ambient conditions respectively, T_0, C_0 are positive constants, U_0 is the characteristic velocity, and L is the characteristic length.

To facilitate a similarity solution, the magnetic field $B(x)$ is assumed to be of the form

$$B(x) = B_0 e^{\frac{x}{2L}}, \tag{6}$$

where B_0 is a constant. It is also assumed that the fluid is weakly electrically conducting so that the induced magnetic field is negligible. Following Rosseland's approximation, the radiative heat flux q_r is modeled as

$$q_r = -\frac{4\sigma^*}{3k^*}\frac{\partial T^4}{\partial y}, \tag{7}$$

where σ^* is the Stefan-Boltzman constant, k^* is the mean absorption coefficient. Assuming that the temperature differences within the flow are sufficiently small such that T^4 may be expressed as a linear function of temperature $T^4 \equiv 4T_\infty^3 T - 3T_\infty^4$, we have

$$\frac{\partial q_r}{\partial y} = -\frac{16\sigma^* T_\infty^3}{3k^*}\frac{\partial^2 T}{\partial y^2}. \tag{8}$$

Continuity Equation (1) is satisfied by introducing a stream function ψ such that

$$u = \frac{\partial \psi}{\partial y}, \qquad v = -\frac{\partial \psi}{\partial x}. \tag{9}$$

The following similarity variables are used:

$$\left.\begin{aligned} &u = U_0 e^{\frac{x}{L}} f_\eta(\eta), \qquad v = -\left(\frac{\nu U_0}{2L}\right)^{\frac{1}{2}} e^{\frac{x}{2L}}\left[f(\eta) + \eta f_\eta(\eta)\right], \\ &T = T_\infty + T_0 e^{\frac{2x}{L}}\theta(\eta), \qquad C = C_\infty + C_0 e^{\frac{2x}{L}}\phi(\eta), \\ &\eta = \left(\frac{U_0}{2\nu L}\right)^{\frac{1}{2}} y e^{\frac{x}{2L}}, \end{aligned}\right\} \tag{10}$$

where η is the similarity variable, $f(\eta)$ is the dimensionless stream function, $\theta(\eta)$ is the dimensionless temperature, and $\phi(\eta)$ is the dimensionless concentration.

On using Equations (6), (8) and (10), Equations (2)-(5) transform into the following two-point boundary value problem:

$$f_{\eta\eta\eta} + f f_{\eta\eta} - 2f_\eta^2 - M f_\eta = 0, \tag{11}$$

$$\left(1 + \frac{4}{3}K\right)\theta_{\eta\eta} + Pr(f\theta_\eta - 4f_\eta\theta) + GbPr\left(Mf_\eta^2 + f_{\eta\eta}^2\right) = 0, \tag{12}$$

$$\phi_{\eta\eta} + Sc(f\phi_\eta - 4f_\eta\phi) = 0, \tag{13}$$

$$f(0) = 0, \qquad f_\eta(0) = 1, \qquad f_\eta(\infty) \to 0, \tag{14}$$

$$\theta(0) = 1, \qquad \theta(\infty) \to 0, \tag{15}$$

$$\phi(0) = 1, \qquad \phi(\infty) \to 0. \tag{16}$$

The non-dimensional constants appearing in Equations (11)-(13) are the magnetic parameter M, the radiation parameter K, the Prandtl number Pr, the Gebhart number Gb, and the Schmidt number Sc respectively defined as

$$M = \frac{2\sigma B_0^2 L}{\rho U_0}, \qquad K = \frac{4\sigma^* T_\infty^3}{k^* k}, \qquad Pr = \frac{\rho\nu C_p}{k},$$

$$Gb = \frac{U_0^2}{C_p T_0}, \qquad Sc = \frac{\nu}{D}.$$

3 Skin friction, heat and mass transfer coefficients

The parameters of engineering interest in heat and mass transport problems are the skin friction coefficient C_f, the local Nusselt number Nu_x, and the local Sherwood number Sh_x. These parameters respectively characterize the surface drag, wall heat and mass transfer rates.

The shearing stress at the surface of the wall τ_w is given by

$$\tau_w = -\mu\left[\frac{\partial u}{\partial y}\right]_{y=0} = -\frac{\mu U_0}{L}\sqrt{\frac{Re}{2}} e^{\frac{3x}{2L}} f''(0), \tag{17}$$

where μ is the coefficient of viscosity and $Re = \frac{LU_0}{\nu}$ is the Reynolds number. The skin friction coefficient is defined as

$$C_f = \frac{2\tau_w}{\rho u_w^2}, \tag{18}$$

and using Equation (17) in Equation (18), we obtain

$$\frac{C_f\sqrt{Re_x/2}}{\sqrt{x/L}} = -f''(0). \tag{19}$$

The heat transfer rate at the surface flux at the wall is given by

$$q_w = -k\left[\frac{\partial T}{\partial y}\right]_{y=0} = \frac{-k(T_w - T_\infty)}{L}\sqrt{\frac{Re}{2}}e^{\frac{x}{2L}}\theta'(0), \tag{20}$$

where k is thermal conductivity of the fluid. The Nusselt number is defined as

$$Nu_x = \frac{x}{k}\frac{q_w}{T_w - T_\infty}. \tag{21}$$

Using Equation (20) in Equation (21), the dimensionless wall heat transfer rate is obtained as follows:

$$\frac{Nu_x}{\sqrt{x/L}\sqrt{Re_x/2}} = -\theta'(0). \tag{22}$$

The mass flux at the surface of the wall is given by

$$J_w = -D\left[\frac{\partial C}{\partial y}\right]_{y=0} = \frac{-D(C_w - C_\infty)}{L}\sqrt{\frac{Re}{2}}e^{\frac{x}{2L}}\phi'(0), \tag{23}$$

and the Sherwood is defined as

$$Sh_x = \frac{x}{D}\frac{J_w}{C_w - C_\infty}. \tag{24}$$

Using (23) in (24), the dimensionless wall mass transfer rate is obtained as

$$\frac{Sh_x}{\sqrt{x/L}\sqrt{Re_x/2}} = -\phi'(0). \tag{25}$$

In Equations (19), (22) and (25), Re_x represents the local Reynolds number and it is defined as $Re_x = \frac{xU_w}{\nu}$.

4 Analytical solution

4.1 Solution of momentum equation

The momentum boundary layer equation is partially decoupled from the energy and species equations. Integrating Equation (11) with η once over to the interval $[0, \eta]$, we obtain

$$f_{\eta\eta} + f f_\eta = -s + \int_0^\eta \left[3f_\eta^2 + Mf_\eta\right] d\eta, \tag{26}$$

where $s = -f_{\eta\eta}(0)$. Letting $\eta \to \infty$, we obtain

$$s = \int_0^\infty \left[3f_\eta^2 + Mf_\eta\right] d\eta. \tag{27}$$

Integrating Equation (26) once again, we obtain

$$f_\eta + \frac{1}{2}f_\eta^2 = 1 - s\eta + \int_0^\eta \left[\int_0^{\eta_1} \left[3f_{\eta_2}^2 + Mf_{\eta_2}\right] d\eta_2\right] d\eta_1. \tag{28}$$

The solution procedure of Equation (28) can be reduced to the sequential solutions of the Riccati type equation of the form

$$f_\eta^{(n)} + \frac{1}{2}f^{(n)^2} = RHS\left[f_\eta^{(n-1)}\right]. \tag{29}$$

This iteration algorithm has to be solved by substituting suitable zero-order approximations $f_\eta^{(0)}(\eta)$ for $f_\eta(\eta)$ into the right-hand side of Equation (28). We assume a zero-order approximation as

$$f_\eta^{(0)}(\eta) = e^{-s_0\eta}, \tag{30}$$

which satisfies the condition at infinity. Integrating Equation (30) with respect to η and using the condition $f_\eta^{(0)}(0) = 0$, we get

$$f_\eta^{(0)}(\eta) = \frac{1 - e^{-s_0\eta}}{s_0}. \tag{31}$$

Using the above solution in Equation (27), the approximate value of s can be obtained as

$$s_0 = \sqrt{\frac{3}{2} + M}, \qquad f_{\eta\eta}^{(0)}(0) = -s_0. \tag{32}$$

Now substituting all the derivatives of zero-order approximation $f_\eta^{(0)}(\eta)$ into the right-hand side of Equation (28), we obtain the equation for first-order iteration $f_\eta^{(1)}$ as follows:

$$f_\eta^{(1)} + \frac{1}{2}f^{(1)^2} = 1 + \frac{3}{4s_0^2}\left[e^{-2s_0\eta} - 1\right] + \frac{M}{s_0^2}\left[e^{-s_0\eta} - 1\right]. \tag{33}$$

Further, we assume that the first-order iterate of f satisfies the boundary conditions on f as given in (14). The above non-linear Riccati type equation can be solved in terms of a confluent hypergeometric Whittaker function as discussed by Khan [19]. However, we restrict ourselves to the zero-order solution, and similarly, to heat and mass transport equations.

4.2 Solution of heat transfer equation

Using the zero-order approximations of f and f_η and further introducing a new variable

$$\xi = -\frac{Pr}{s_0^2}e^{-s_0\eta}, \tag{34}$$

Equation (12) and the thermal boundary conditions (15) take the form

$$\left(1 + \frac{4}{3}K\right)\xi\theta_{\xi\xi} + \left(1 + \frac{4}{3}K - Pr^* - \xi\right)\theta_\xi + 4\theta = -\frac{Gb}{Pr}s_0^2(M + s_0^2)\xi, \tag{35}$$

$$\theta(-Pr^*) = 1, \qquad \theta(0^-) \to 0, \tag{36}$$

where $Pr^* = Pr/s_0^2$ is the modified Prandtl number. The solution of Equation (35) is assumed in the form of

$$\theta(\xi) = \theta_c(\xi) + \theta_p(\xi),$$

where $\theta_c(\xi)$ is the complementary solution and $\theta_p(\xi)$ is the particular solution. The complementary solution of Equation (35) is obtained in terms of confluent hypergeometric function in the following form:

$$\theta_c(\xi) = C_0 \xi^{\alpha} M\left[\alpha - 4, \alpha + 1, \frac{-\xi}{1 + \frac{4}{3}K}\right], \tag{37}$$

where

$$M[a, b, z] = \sum_{r=0}^{\infty} \frac{a(a+1)\cdots(a+r-1)}{b(b+1)\cdots(b+r-1)} \frac{z}{r!}$$

is Kummer's function (see Abramowitz and Stegun [39]) and

$$\alpha = \frac{Pr^*}{1 + \frac{4}{3}K}.$$

The particular solution is obtained as

$$\theta_p(\xi) = a_0 \xi^2 + a_1 \xi^3 + a_2 \xi^4, \tag{38}$$

where

$$a_0 = -\left(\frac{Gb}{Pr^*}\right) \frac{M + s_0^2}{4(1 + \frac{4}{3}K) - 2Pr^*},$$

$$a_1 = \frac{-2a_0}{9(1 + \frac{4}{3}K) - 3Pr^*},$$

$$a_2 = \frac{-a_1}{16(1 + \frac{4}{3}K) - 4Pr^*}.$$

Now, the complete solution can be written as

$$\theta(\xi) = \theta_c(\xi) + \theta_p(\xi). \tag{39}$$

Making use of the boundary conditions (36) and rewriting the solution in terms of the variable η, we get

$$\theta(\eta) = C_1 \frac{e^{-s_0\eta\alpha} M[\alpha - 4, \alpha + 1, -\alpha e^{-s_0\eta}]}{M[\alpha - 4, \alpha + 1, -\alpha]} + a_0 Pr^{*2} e^{-2s_0\eta} - a_1 Pr^{*3} e^{-3s_0\eta} + a_2 Pr^{*4} e^{-4s_0\eta}, \tag{40}$$

where

$$C_1 = 1 - a_0 Pr^{*2} + a_1 Pr^{*3} - a_2 Pr^{*4}.$$

4.3 Solution of mass transfer equation

Using the zero-order approximation of f and f_η and further introducing a new variable

$$\zeta = -\frac{Sc}{s_0^2} e^{-s_0 \eta}, \tag{41}$$

Equation (13) and the thermal boundary conditions in (16) take the form

$$\zeta \phi_{\zeta\zeta} + (1 - Sc^* - \zeta)\phi_\zeta + 4\phi = 0, \tag{42}$$

$$\phi(-Sc^*) = 1, \qquad \phi(0^-) \to 0, \tag{43}$$

where $Sc^* = Sc/s_0^2$ is the modified Schmidt number. Following the solution procedure discussed in the case of the energy equation, the solution of Equation (42) is obtained in terms of confluent hypergeometric function as

$$\phi(\eta) = \frac{e^{-s_0 Sc^* \eta} M[Sc^* - 4, Sc^* + 1, -Sc^* e^{-s_0 \eta}]}{M[Sc^* - 4, Sc^* + 1, -Sc^*]}. \tag{44}$$

5 Solution procedure

The set of non-linear differential Equations (11)-(13) subject to the boundary conditions (14)-(16) were solved numerically using an efficient Runge-Kutta-Fehlberg method with a shooting technique, which is described in Pal and Shivakumara [40]. The most important step in this method is to choose an appropriate finite value of $\eta \to \infty$. In order to determine $\eta \to \infty$ for the boundary value problem described by Equations (11)-(13), we start with initial guess values for a particular set of physical parameters to obtain $f''(0)$, $\theta'(0)$ and $\phi'(0)$. The solution procedure is repeated with another large value of $\eta \to \infty$ until two successive values of $f''(0)$, $\theta'(0)$ and $\phi'(0)$ differ only by a specified significant digit. The value of η may change for a different set of physical parameters. Once the appropriate value of η is determined, the coupled boundary value problem given by Equations (11)-(13) is solved numerically using the method of superposition. In this method, third-order non-linear Equation (11), second-order Equations (12) and (13) have been reduced to five ordinary differential equations as follows:

$$\begin{aligned}
f_1' &= f_2, \qquad f_2' = f_3, \\
f_3' &= 2f_2^2 + Mf_2 - f_1 f_3, \\
f_4' &= f_5, \\
f_5' &= -\frac{Pr}{(1 + \frac{4}{3}K)}\left[f_1 f_5 - 4f_2 f_4 + Gb\left(Mf_2^2 + f_3^2\right)\right], \\
f_6' &= f_7, \\
f_7' &= Sc(4f_2 f_6 - f_1 f_7),
\end{aligned} \tag{45}$$

where

$$f_1 = f, \quad f_2 = f', \quad f_3 = f'', \quad f_4 = \theta, \quad f_5 = \theta', \quad f_6 = \phi, \quad f_7 = \phi', \tag{46}$$

and a prime denotes differentiation with respect to η. The boundary conditions now become

$$\begin{aligned} &f_1 = 0, \quad f_2 = 1, \quad f_3 = s_1, \quad f_4 = 1, \\ &f_5 = s_2, \quad f_6 = 1, \quad f_7 = s_3 \quad \text{at } \eta \to 0, \end{aligned} \tag{47}$$

$$f_2 = 0, \quad f_4 = 0, \quad f_6 = 0 \quad \text{as } \eta \to \infty, \tag{48}$$

where s_1, s_2 and s_3 are determined such that $f_2(\infty) = 0$, $f_4(\infty) = 0$ and $f_6(\infty) = 0$. Thus, to solve this system, we require six initial conditions. However, since we have only three initial conditions for f and two initial conditions for θ and ϕ, the conditions $f''(0)$, $\theta'(0)$, $\phi'(0)$ are to be determined by the shooting method using the initial guess values s_1, s_2 and s_3 until the conditions $f_2(\infty) = 0$, $f_3(\infty) = 0$ and $f_5(\infty) = 0$ are satisfied. In this paper, we employed the shooting technique with the Runge-Kutta-Fehlberg scheme to determine two more unknowns in order to convert the boundary value problem to an initial value problem. Once all the six initial conditions were determined, the resulting differential equations were integrated using an initial value solver. For this purpose, the fifth-order Runge-Kutta-Fehlberg integration scheme was used.

6 Results and discussion

Analytical and numerical solutions were obtained for the effects of radiation and viscous dissipation for the MHD flow over an exponentially stretching sheet. Similarity transformations were used to transform the governing partial differential equations of flow, heat and mass transfer into a system of non-linear ordinary differential equations. The zero-order approximate solution for the dimensionless stream function f has been obtained analytically. Solutions of the energy and species equations were obtained in terms of confluent hypergeometric functions. The accuracy of the method was established by comparing the analytical solution with the numerical solution obtained by a shooting method together with Runge-Kutta-Fehlberg and Newton-Raphson schemes. The skin friction, heat and mass transfer coefficients are tabulated in Tables 1-3. The effects of magnetic, radiation and viscous dissipation parameters on the velocity $f'(\eta)$, temperature $\theta(\eta)$ and concentration $\phi(\eta)$ profiles are shown in Figures 2-6.

Table 1 provides values of the skin friction coefficient for different values of the magnetic parameter M. Increasing values of M result in considerable opposition to the flow in the

Table 1 A comparison of $-f''(0)$ obtained by the analytical method with the shooting technique for different values of M

M	$-f''(0)$	
	Analytical	Numerical
0	1.22474	1.281809
1	1.58114	1.629178
2	1.87083	1.912620
3	2.12132	2.158736
5	2.54951	2.581130
10	3.39116	3.41529

Table 2 A comparison of $-\theta'(0)$ obtained by the analytical method with the shooting technique for different values of M, Gb and K for fixed values of $Pr = 7$

M	K	Gb	$-\theta'(0)$	
			Analytical	Numerical
0	0.5	0.2	3.82684	3.822508
1			3.48576	3.483155
2			3.19181	3.191131
3			2.92781	2.928577
1	0	0.2	4.56379	4.556219
	0.5		3.48576	3.483155
	1		2.90556	2.905805
	2		2.25649	2.260503
	3		1.88314	1.889815
1	0.5	0	3.94905	3.946604
		0.1	3.71740	3.714879
		0.2	3.48576	3.483155
		0.5	2.79082	2.787982
		1	1.63260	1.629360

Table 3 A comparison of $-\phi'(0)$ obtained by the analytical method with the shooting technique for different values of M, Sc

M	Sc	$-\phi'(0)$	
		Analytical	Numerical
0	1	1.79791	1.805684
1		1.69115	1.699309
2		1.60312	1.611410
3		1.52781	1.535984
1	1	1.69115	1.699309
	2	2.58672	2.589044
	5	4.34813	4.344825
	10	6.32456	6.318568

form of a Lorenz drag which enhances the values of the skin friction coefficient. Table 2 highlights the effect of the magnetic field, radiation and dissipation on the dimensionless wall temperature gradient. It is evident that all the three parameters reduce the values of the wall temperature gradient. Table 3 shows that the increase in Schmidt numbers leads to the increase in the dimensionless wall concentration gradient, while the opposite trend is observed in the case of the magnetic parameter. The results confirm a good agreement between analytical and numerical results.

The skin friction coefficients are shown in Table 4 for different values of the magnetic parameter in the absence of the physical parameters (*i.e.*, $Pr = Sc = K = Gb = 0$). We observe that skin friction coefficient increases with an increase in the magnetic parameter. It is interesting to note that the value of the wall skin-friction coefficient in the non-magnetic ($M = 0$) and magnetic ($M = 1$) cases are in good agreement with the results presented by Reddy and Reddy [33].

Figure 2 shows the variation of the velocity profile against the magnetic parameter. We notice that the effect of the magnetic parameter is to reduce the velocity of the fluid in the boundary layer region. This is due to an increase in the Lorentz force, similar to Darcy's drag observed in the case of flow through a porous medium. This adverse force is responsible for slowing down the motion of the fluid in the boundary layer region. These results are similar to the results obtained by Reddy and Reddy [33].

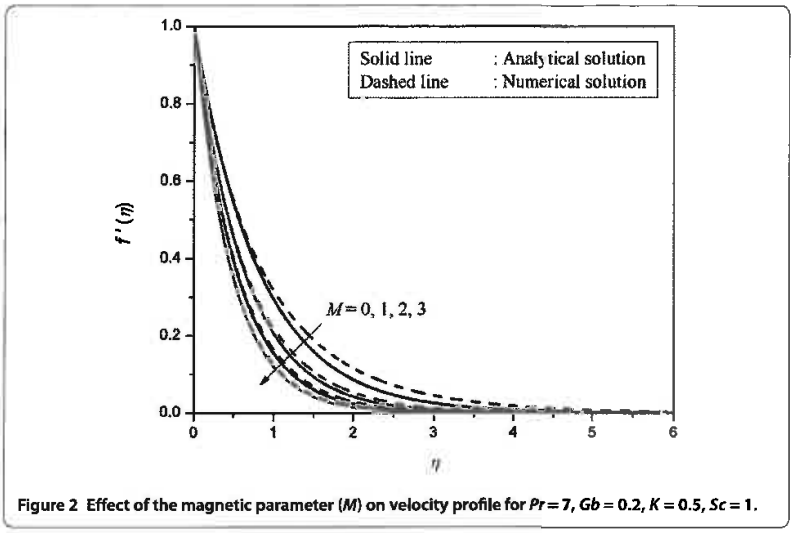

Figure 2 Effect of the magnetic parameter (*M*) on velocity profile for *Pr* = 7, *Gb* = 0.2, *K* = 0.5, *Sc* = 1.

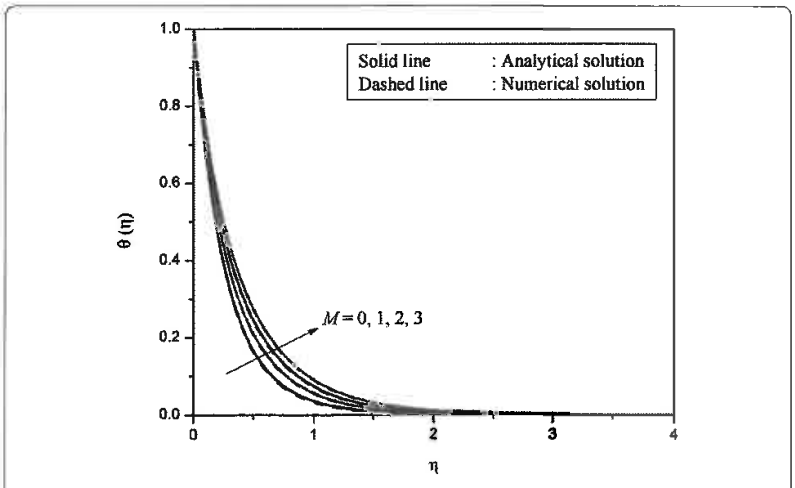

Figure 3 Effect of *M* on temperature profile for *Pr* = 7, *Gb* = 0.2, *K* = 0.5, *Sc* = 1.

The variation of the temperature distribution with the magnetic parameter is shown in Figure 3. The thermal boundary layer thickness increases with increasing values of the magnetic parameter. The opposing force introduced in the form of the Lorentz drag contributes in increasing the frictional heating between the fluid layers, and hence energy is released in the form of heat. This results in thickening of the thermal boundary layer.

The effect of the magnetic parameter on the concentration profile is shown in Figure 4. It is observed that increases in the values in M result in thickening of the species boundary layer.

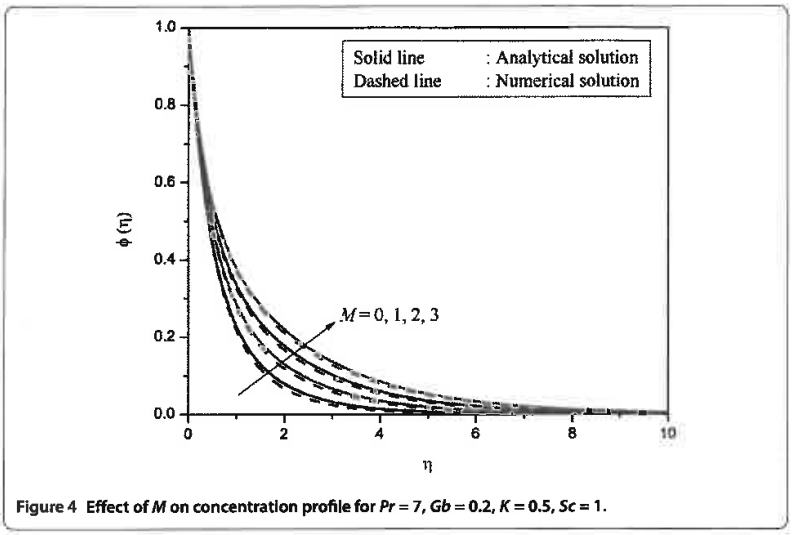

Figure 4 Effect of *M* on concentration profile for *Pr* = 7, *Gb* = 0.2, *K* = 0.5, *Sc* = 1.

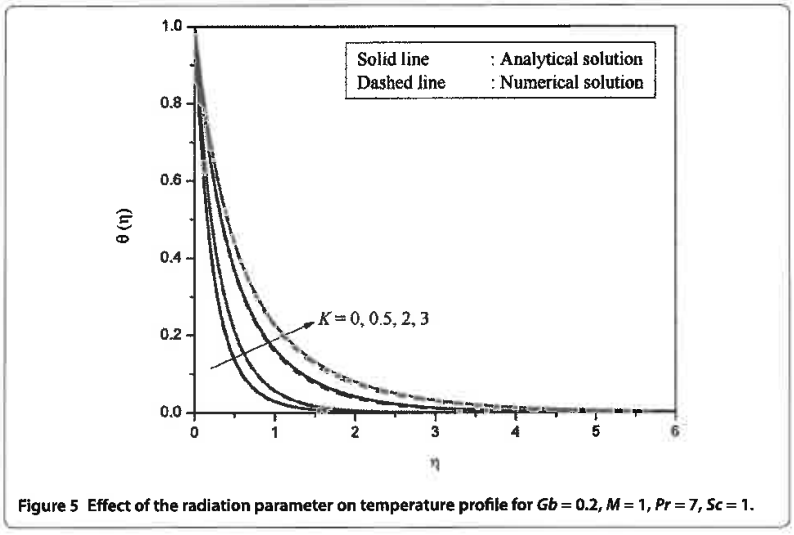

Figure 5 Effect of the radiation parameter on temperature profile for *Gb* = 0.2, *M* = 1, *Pr* = 7, *Sc* = 1.

The influence of the thermal radiation parameter K on temperature is shown in Figure 5. It is clear that thermal radiation enhances the temperature in the boundary layer region. Thus radiation should be kept at its minimum in order to facilitate better cooling environment. The radiation parameter K defines the relative contribution of conduction heat transfer to thermal radiation transfer.

The effect of the Gebhart number Gb on the heat transfer is shown in Figure 6. It is clear that the temperature in the boundary layer region increases with an increase in the viscous dissipation parameter. We also note that since the energy equation is partially decoupled from the momentum and species conservation equations, the parameters affecting the

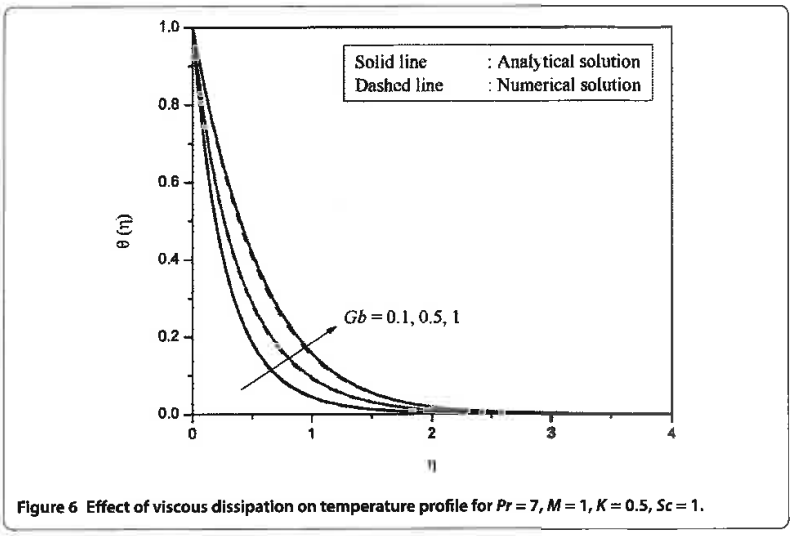

Figure 6 Effect of viscous dissipation on temperature profile for $Pr = 7$, $M = 1$, $K = 0.5$, $Sc = 1$.

Table 4 A comparison of $-f''(0)$ for different values of M for fixed values of $Pr = Sc = K = Gb = 0$

M	$-f''(0)$	
	Reddy and Reddy [33]	Present
0	1.28213	1.28181
1	1.62918	1.62918
2	-	1.91262
3	-	2.15874
4	-	2.37937

energy equation, namely, the Prandtl number, the radiation parameter and the Gebhart number, do not alter velocity and concentration profiles. We also observe a good agreement between the analytical and numerical solutions through Figures 2-6.

7 Conclusions

The problem of hydromagnetic Newtonian liquid flow due to an exponentially stretching sheet in the presence of radiation and viscous dissipation effects has been analyzed. Exact solutions were found in terms of hypergeometric functions, and a comparison of analytical and numerical results was shown. We found that the effect of the magnetic parameter is to reduce the velocity of the fluid in the boundary layer region. It was also observed that the increase in values of M results in thickening of the species boundary layer. The combined and individual effects of the magnetic parameter M, the radiation parameter K, and the viscous dissipation parameter Gb are to increase the heat transfer rates. Under some limiting conditions when the parameters Pr, Sc, K, Gb are zero, the current results agree well with available results in the literature.

Competing interests
The authors declare that they have no competing interests.

Authors' contributions
The problem was conceived in discussions by the authors. PKK and MN carried out the analytical and numerical computations, while GM and PS participated in the design of the study and drafted the manuscript.

Acknowledgements
The authors are grateful to the National Research Foundation (NRF) and the University of KwaZulu-Natal for financial support.

Received: 25 May 2012 Accepted: 23 August 2012 Published: 2 October 2012

References

1. Crane, LJ: Flow past a stretching plate. Z. Angew. Math. Phys. **21**, 645-647 (1970)
2. Gupta, PS, Gupta, AS: Heat and mass transfer on a stretching sheet with suction or blowing. Can. J. Chem. Eng. **55**, 744-746 (1977)
3. Grubka, LG, Bobba, KM: Heat transfer characteristics of a continuous stretching surface with variable temperature. J. Heat Transf. **107**, 248-250 (1985)
4. Dutta, BK, Gupta, AS: Cooling of a stretching sheet in a various flow. Ind. Eng. Chem. Res. **26**, 333-336 (1987)
5. Siddappa, B, Abel, MS: Non-Newtonian flow past a stretching plate. Z. Angew. Math. Phys. **36**, 47-54 (1985)
6. Chen, CK, Char, MI: Heat transfer of a continuous stretching surface with suction or blowing. J. Math. Anal. Appl. **135**, 568-580 (1988)
7. Laha, MK, Gupta, PS, Gupta, AS: Heat transfer characteristics of the flow of an incompressible viscous fluid over a stretching sheet. Wärme-Stoffübertrag. **24**, 151-153 (1989)
8. Chakarabarti, A, Gupta, AS: Hydromagentic flow and heat transfer over a stretching sheet. Q. Appl. Math. **37**, 73-78 (1979)
9. Andersson, HI, Bech, KH, Dandapat, BS: Magnetohydrodynamic flow of a power-law fluid over a stretching sheet. Int. J. Non-Linear Mech. **27**, 929-936 (1992)
10. Siddheshwar, PG, Mahabaleswar, US: Effects of radiation and heat source on MHD flow of a viscoelastic liquid and heat transfer over a stretching sheet. Int. J. Non-Linear Mech. **40**, 807-820 (2005)
11. Abel, MS, Mahesha, N: Heat transfer in MHD viscoelastic fluid flow over a stretching sheet with variable thermal conductivity, non-uniform heat source and radiation. Appl. Math. Model. **32**, 1965-1983 (2008)
12. Abel, MS, Siddheshwar, PG, Mahesha, N: Effects of thermal buoyancy and variable thermal conductivity on the MHD flow and heat transfer in a power-law fluid past a vertical stretching sheet in the presence of a non-uniform heat source. Int. J. Non-Linear Mech. **44**, 1-12 (2009)
13. Elbashbeshy, EMA: Heat transfer over an exponentially stretching continuous surface with suction. Arch. Mech. **53**(6), 643-651 (2001)
14. Ishak, A: MHD boundary layer flow due to an exponentially stretching sheet with radiation effect. Sains Malays. **40**(4), 391-395 (2011)
15. Magyari, E, Keller, B: Heat and mass transfer in the boundary layers on an exponentially stretching continuous surface. J. Phys. D, Appl. Phys. **32**, 577-585 (1999)
16. Sanjayanand, E, Khan, SK: On heat and mass transfer in a viscoelastic boundary layer flow over an exponentially stretching sheet. Int. J. Therm. Sci. **45**, 819-828 (2006)
17. Partha, MK, Murthy, PVSN, Rajasekhar, GP: Effect of viscous dissipation on the mixed convection heat transfer from an exponentially stretching surface. Heat Mass Transf. **41**, 360-366 (2005)
18. Sajid, M, Hayat, T: Influence of thermal radiation on the boundary layer flow due to an exponentially stretching sheet. Int. Commun. Heat Mass Transf. **35**, 347-356 (2008)
19. Khan, SK: Boundary layer viscoelastic fluid flow over an exponentially stretching sheet. Int. J. Appl. Mech. Eng. **11**(2), 321-335 (2006)
20. Steenbeck, M: Wissen. Veroff. Siemens **15**(2), 1 (1936)
21. Tonks, L: Theory of magnetic effects in the plasma of an arc. Phys. Rev. **56**, 360-373 (1939)
22. Pavlov, KB: Magnetohydromagnetic flow of an incompressible viscous fluid caused by deformation of a surface. Magn. Gidrodin. **4**, 146-147 (1974)
23. Sarpkaya, T: Flow of non-Newtonian fluids in a magnetic field. AIChE J. **7**, 324-328 (1961)
24. Andersson, HI: MHD flow of a viscoelastic fluid past a stretching surface. Acta Mech. **95**, 227-230 (1992)
25. Lawrence, PS, Rao, BN: The non-uniqueness of the MHD flow of a viscoelastic fluid past a stretching sheet. Acta Mech. **112**, 223-228 (1995)
26. Abel, MS, Joshi, A, Sonth, RM: Heat transfer in MHD viscoelastic fluid flow over a stretching surface. Z. Angew. Math. Mech. **81**, 691-698 (2001)
27. Cortell, R: Flow and heat transfer of an electrically conducing fluid of second grade over a stretching sheet subject to suction and to a transverse magnetic field. Int. J. Heat Mass Transf. **49**, 1851-1856 (2006)
28. Reddy, PBA, Reddy, NB, Suneetha, S: Radiation effects on MHD flow past an exponentially accelerated isothermal vertical plate with uniform mass diffusion in the presence of heat source. J. Appl. Fluid Mech. **5**(3), 119-126 (2012)
29. Raptis, A: Radiation and viscoelastic flow. Int. Commun. Heat Mass Transf. **26**(6), 889-895 (1999)
30. Raptis, A, Perdikis, C: Viscoelastic flow by the presence of radiation. Z. Angew. Math. Mech. **78**, 277-279 (1998)
31. Bidin, B, Nazar, R: Numerical solution of the boundary layer flow over an exponentially stretching sheet with thermal radiation. Eur. J. Sci. Res. **33**(4), 710-717 (2009)
32. Elbashbeshy, EMA, Dimian, MF: Effect of radiation on the flow and heat transfer over a wedge with variable viscosity. Appl. Math. Comput. **132**, 445-454 (2002)
33. Reddy, PBA, Reddy, NB: Thermal radiation effects on hydromagnetic flow due to an exponentially stretching sheet. Int. J. Appl. Math. Comput. **3**(4), 300-306 (2011)
34. Raptis, A, Perdikis, C, Takhar, HS: Effect of thermal radiation on MHD flow. Int. J. Heat Mass Transf. **153**, 645-649 (2004)
35. Hayat, T, Abbas, Z, Sajid, M, Asghar, S: The influence of thermal radiation on MHD flow of a second grade fluid. Int. J. Heat Mass Transf. **50**, 931-941 (2007)
36. Gebhart, B: Effect of viscous dissipation in natural convection. J. Fluid Mech. **14**, 225-232 (1962)
37. Gebhart, B, Mollendorf, J: Viscous dissipation in external natural convection flows. J. Fluid Mech. **38**, 97-107 (1969)
38. Vajravelu, K, Hadjinicolaou, A: Heat transfer in a viscous fluid over a stretching sheet with viscous dissipation and internal heat generation. Int. Commun. Heat Mass Transf. **20**, 417-430 (1993)

39. Abramowitz, M, Stegun, LA: Handbook of Mathematical Functions. National Bureau of Standards, AMS, vol. 55 (1972)
40. Pal, D, Shivakumara, IS: Mixed convection heat transfer from a vertical plate embedded in a sparsely packed porous medium. Int. J. Appl. Mech. Eng. 11(4), 929-939 (2006)

doi:10.1186/1687-2770-2012-105
Cite this article as: Kameswaran et al.: **On radiation effects on hydromagnetic Newtonian liquid flow due to an exponential stretching sheet.** *Boundary Value Problems* 2012 **2012**:105.

Appendix B

Hindawi Publishing Corporation
Mathematical Problems in Engineering
Volume 2013, Article ID 934712, 11 pages
http://dx.doi.org/10.1155/2013/934712

Research Article

Natural Convection of Viscoelastic Fluid from a Cone Embedded in a Porous Medium with Viscous Dissipation

Gilbert Makanda,[1] O. D. Makinde,[2] and Precious Sibanda[1]

[1] *School of Mathematical Sciences, University of KwaZulu-Natal, Private Bag X01, Scottsville, Pietermaritzburg 3209, South Africa*
[2] *Faculty of Military Science, Stellenbosch University, Private Bag X2, Saldanha 7395, South Africa*

Correspondence should be addressed to Gilbert Makanda; gilbertmakanda@yahoo.com

Received 11 March 2013; Accepted 9 September 2013

Academic Editor: Anders Eriksson

We study natural convection from a downward pointing cone in a viscoelastic fluid embedded in a porous medium. The fluid properties are numerically computed for different viscoelastic, porosity, Prandtl and Eckert numbers. The governing partial differential equations are converted to a system of fourth order ordinary differential equations using the similarity transformations and then solved together by using the successive linearization method (SLM). Many studies have been carried out on natural convection from a cone but they did not consider a cone embedded in a porous medium with linear surface temperature. The results in this work are validated by the comparison with other authors.

1. Introduction

Natural convection of viscoelastic fluid in a porous medium with viscous dissipation is the transfer of heat due to density differences caused by temperature gradients through a permeable medium and heat generated due to the interaction of fluid molecules is considered. There are examples in practical application such as thermal insulation, extraction of petroleum resources and the so-called fracking, metal processing, performance of lubricants, application of paints, and extrusion of plastic sheets. The study of second grade fluids has been studied but there is no single constitutive equation that can fully describe non-Newtonian fluids [1]; due to this fact many authors did not consider the appropriate constitutive energy equation for second grade fluids.

Natural convection on a cone geometry has been studied by among others Alim et al. [2], Awad et al. [3], Cheng [4, 5], and Kairi and Murthy [6]. Studies have been done on other geometries such as flow over a flat plate, cylinders, vertical surfaces, stretching sheets, and inclined surfaces by, among others, Abbas et al. [7] who considered unsteady second grade fluid flow on an unsteady stretching sheet; they did not consider the energy equation mainly due to difficulties in its characterization. Anwar et al. [8] studied mixed convection boundary layer flow of a viscoelastic fluid over a horizontal circular cylinder; they solved the fourth order ordinary differential equations by considering the insufficiency of the boundary conditions by taking the zeroth, first, and second order of the viscoelastic parameter and coming up with three systems of ordinary differential equations. Cortell [9] investigated flow and heat transfer of a viscoelastic fluid over a stretching sheet. Damseh et al. [10] studied the transient mixed convection flow of a second grade viscoelastic fluid over a vertical surface. They used McCormack's method to solve their differential equations. Hayat et al. [11] studied mixed convection in a stagnation point flow adjacent to a vertical surface in a viscoelastic fluid.

The model in this work has been originally developed from the work of Ece [5] who studied heat and mass transfer from a downward pointing cone in a Newtonian fluid. In this paper the work of Ece [5] is extended to take into account the flow of a second grade fluid in a porous medium and the effect of viscous dissipation is considered. Several other studies have been done in natural convection in a viscoelastic fluid by among others Hsiao [12] who studied mixed convection for viscoelastic fluid past a porous wedge. Kasim et al. [13] investigated free convection boundary layer flow of a viscoelastic fluid in the presence of heat generation. Massoudi et al. [14]

studied natural convection flow of generalized second grade fluid between two vertical walls. Olajuwon [15] studied the convection heat and mass transfer in a hydromagnetic flow of a second grade fluid in the presence of thermal radiation and thermal diffusion; it was shown that increasing the second grade parameter causes reduction in the rate of the fluid flow and mass transfer, but heat transfer increases. Sajid et al. investigated fully developed mixed convection flow of a viscoelastic fluid between permeable parallel vertical plates [16].

Studies for viscous dissipation in a second grade fluid have been done by many authors but some assumed that fluids are more viscous than elastic resulting in the energy equation without the elastic term. Viscous dissipation has been studied by among others Subhas Abel et al. [17] who studied viscoelastic MHD flow and heat transfer over a stretching sheet with viscous and ohmic dissipations and [18] in which a Newtonian fluid was considered. The viscous dissipation term which they used in [17] assumes that the fluid is more viscous in nature than elastic. Jha [19] investigated the effects of viscous dissipation on natural convection flow between parallel plates with time periodic boundary conditions. Chen [20] studied the analytic solution of MHD flow and heat transfer for two types of viscoelastic fluids over a stretching sheet with energy dissipation, internal heat source, and thermal radiation. Cortell [21] worked on viscous dissipation and thermal radiation effects on the flow and heat transfer of a power law fluid past an infinite porous plate. Hsiao [22] investigated multimedia physical feature for unsteady MHD mixed convection viscoelastic fluid over a vertical stretching sheet with viscous dissipation. Kameswaran et al. [23] studied hydromagnetic nanofluid flow due to a stretching sheet or shrinking sheet with viscous dissipation and chemical reaction effects.

Studies have been done in porous media by among others Awad et al. [3, 4, 6, 24] and Singh and Agarwal [25] who studied heat transfer in a second grade fluid over an exponentially stretching sheet through porous medium with thermal radiation and elastic deformation under the effect of magnetic field.

An investigation of available literature shows that, to the best of our knowledge, no analysis has been done on natural convection of a viscoelastic fluid embedded in a porous medium with viscous dissipation under the given boundary conditions. The study takes into consideration a temperature that changes linearly along the surface of the cone (see Ece [5]).

2. Mathematical Formulation

A cone in a viscoelastic fluid embedded in a porous medium is heated and maintained at a linearly changing temperature T ($> T_\infty$), and the ambient conditions are maintained at T_∞; the fluid has a constant viscosity ν. The vertex angle of the cone is 2ϕ. The velocity components u and v are in the directions of x and y, respectively, with the x-axis being inclined at an angle ϕ to the vertical. A sketch of the system and coordinate axis is illustrated in Figure 1.

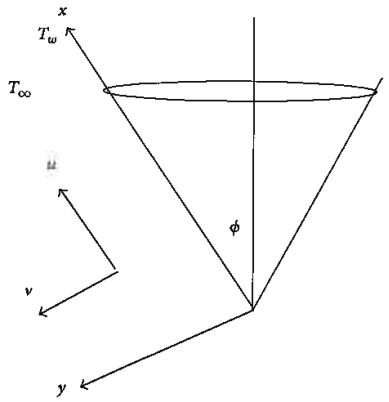

Figure 1: Physical model and coordinate system.

The governing equations in this buoyant-driven flow are given by

$$\frac{\partial}{\partial x}(ru) + \frac{\partial}{\partial y}(rv) = 0,$$

$$u\frac{\partial u}{\partial x} + v\frac{\partial u}{\partial y} = \nu\frac{\partial^2 u}{\partial y^2} - \frac{\nu}{K}u - k_o\left\{u\frac{\partial^3 u}{\partial x \partial y^2} + v\frac{\partial^3 u}{\partial y^3} + \frac{\partial u}{\partial x}\frac{\partial^2 u}{\partial y^2} - \frac{\partial^2 u}{\partial x \partial y}\frac{\partial u}{\partial y}\right\} + g\beta(T - T_\infty)\cos\phi,$$

$$u\frac{\partial T}{\partial x} + v\frac{\partial T}{\partial y} = \alpha\frac{\partial^2 T}{\partial y^2} + \frac{\nu}{C_p}\left(\frac{\partial u}{\partial y}\right)^2 + \frac{k_0}{\rho C_p}\left(u\frac{\partial^2 u}{\partial x \partial y}\frac{\partial u}{\partial y} + v\frac{\partial^2 u}{\partial y^2}\frac{\partial u}{\partial y}\right). \tag{1}$$

where $r = x\sin\phi$, g is the acceleration due to gravity, ν is the kinematic viscosity for the fluid, k_o is the non-Newtonian parameter of the viscoelastic fluid, β is the coefficient of thermal expansion, α is the thermal diffusivity, C_p is the specific heat capacity for the fluid, ρ is the density of the fluid, and K is the permeability coefficient of the porous medium. The boundary conditions are given as

$$u = v = 0, \quad T = T_w(x) = T_\infty + A\left(\frac{x}{L}\right) \quad \text{at } y = 0,$$
$$\frac{\partial u}{\partial y}, \quad u \longrightarrow 0, \quad T \longrightarrow T_\infty, \quad \text{as } y \longrightarrow \infty, \tag{2}$$

where $A > 0$ is a constant, $L > 0$ is the characteristic length, and the subscript ∞ refers to the ambient condition.

We introduce the nondimensional variables:

$$X = \frac{x}{L}, \quad Y = \frac{\mathrm{Gr}^{1/4} y}{L}, \quad R = \frac{r}{L},$$
$$U = \frac{u}{U_0}, \quad V = \frac{\mathrm{Gr}^{1/4} v}{U_0}, \tag{3}$$
$$\overline{T} = \frac{T - T_\infty}{T_w - T_\infty}, \quad \mathrm{Gr} = \left(\frac{U_0 L}{\nu}\right)^2,$$

where $U_0 = [g\beta \cos\phi L(T_w - T_\infty)]^{1/2}$. Using (3) in (1) gives the following equations:

$$\frac{\partial}{\partial X}(RU) + \frac{\partial}{\partial Y}(RV) = 0,$$
$$U\frac{\partial U}{\partial X} + V\frac{\partial U}{\partial Y} = \frac{\partial^2 U}{\partial Y^2} - \frac{\nu U}{K} - \Lambda\left\{U\frac{\partial^3 U}{\partial X \partial Y^2} + V\frac{\partial^3 U}{\partial Y^3} + \frac{\partial U}{\partial X}\frac{\partial^2 U}{\partial Y^2} - \frac{\partial^2 U}{\partial X \partial Y}\frac{\partial U}{\partial Y}\right\} + \overline{T},$$
$$U\frac{\partial \overline{T}}{\partial X} + V\frac{\partial \overline{T}}{\partial Y} = \frac{1}{\mathrm{Pr}}\frac{\partial^2 \overline{T}}{\partial Y^2} + \mathrm{Ec}\left(\frac{\partial U}{\partial Y}\right)^2 + \Lambda \mathrm{Ec}\left(U\frac{\partial^2 U}{\partial X \partial Y}\frac{\partial U}{\partial Y} + V\frac{\partial^2 U}{\partial Y^2}\frac{\partial U}{\partial Y}\right), \tag{4}$$

where $R = X\sin\phi$, $\Lambda = (k_0 U_0/\nu L)$ is the viscoelastic parameter known as the Deborah number, Gr is the Grashof number, $\mathrm{Pr} = \nu/\alpha$ is the Prandtl number, and $\mathrm{Ec} = (U_0^2/C_p A)$ is the Eckert number. The corresponding boundary conditions are given as

$$U = V = 0, \quad \overline{T} = X \quad \text{at } Y = 0,$$
$$\frac{\partial U}{\partial Y}, \quad U \longrightarrow 0, \quad \overline{T} \longrightarrow 0 \quad \text{as } Y \longrightarrow \infty. \tag{5}$$

We now introduce the stream functions $\psi = XRf(Y)$ and $\overline{T} = X\theta(Y)$ defined by

$$U = \frac{1}{R}\frac{\partial \psi}{\partial Y}, \quad V = -\frac{1}{R}\frac{\partial \psi}{\partial X}. \tag{6}$$

Substituting (6) and the similarity variables in (4) gives the following ordinary differential equations:

$$f''' + 2ff'' - (f')^2 + \theta - \gamma f' - \Lambda\left(2f'f''' - 2ff^{iv} - (f'')^2\right) = 0, \tag{7}$$
$$\theta'' + \mathrm{Pr}\left(2f\theta' - f'\theta\right) + \mathrm{Pr}\,\mathrm{Ec}\,f''^2 + \Lambda \mathrm{Pr}\,\mathrm{Ec}\left(f'f''^2 - ff''f'''\right) = 0. \tag{8}$$

With boundary conditions,

$$f(0) = f'(0) = 0, \quad \theta(0) = 1, \tag{9}$$
$$f'(\infty) \longrightarrow 0, \quad f''(\infty) \longrightarrow 0, \quad \theta(\infty) \longrightarrow 0. \tag{10}$$

It is of interest to discuss the skin friction and the heat transfer coefficient in this context. The shear stress at the surface of the cone is defined as (see Olajuwon [15])

$$\tau_w = \mu\left[\frac{\partial u}{\partial y}\right]_{y=0} + k_0\left[u\frac{\partial^2 u}{\partial x \partial y} - 2\frac{\partial u}{\partial x}\frac{\partial u}{\partial y}\right]_{y=0}, \tag{11}$$

where μ is the coefficient of viscosity. The skin friction is defined as

$$c_f = \frac{\tau_w}{(1/2)\rho U_\infty^2},$$
$$c_f = \frac{2X}{\mathrm{Gr}^{1/4}} f''(0)\left(1 + 3\Lambda f'(0)\right). \tag{12}$$

The skin friction coefficient can be expressed as

$$\frac{C_f \mathrm{Gr}^{1/4}}{2X} = f''(0). \tag{13}$$

The heat transfer rate at the surface of the cone is given by

$$q_w = -\frac{k}{X}\left[\frac{\partial T}{\partial y}\right]_{y=0}. \tag{14}$$

The Nusselt number can be expressed as

$$\mathrm{Nu} = \frac{L q_w}{k(T_w - T_\infty)}. \tag{15}$$

Using the nondimensional variables (9)-(10), the dimensionless wall heat rate is given by

$$\mathrm{Nu}\,\mathrm{Gr}^{-1/4} = -\theta'(0). \tag{16}$$

3. Method of Solution

In this study, (7)–(10) were solved using the successive linearization method. The inclusion of the non-Newtonian term brings about the fourth order ordinary differential equation for the momentum equation. The given boundary conditions are insufficient to obtain a unique solution. To overcome this problem the system is decomposed into the zeroth, first, and second order systems of the viscoelastic parameter. Subhas Abel et al. [17] showed that if this method is applied small values of the viscoelastic parameter can be used without difficulty in convergence. It is also noticed in this study that the direct application of the successive linearization method has difficulties in convergence for small values of the viscoelastic parameter. Anwar et al. [8] also confirmed the same observation and solved a system of differential equations simultaneously and obtained better convergence for small values of the viscoelastic parameter. In this work we solve the system using the successive linearization method. To solve the equations we seek the series solution of the form

$$\begin{aligned} f(y) &= f_0(y) + \Lambda f_1(y) + \Lambda^2 f_2(y) + \cdots, \\ \theta(y) &= \theta_0(y) + \Lambda\theta_1(y) + \Lambda^2\theta_2(y) + \cdots. \end{aligned} \tag{17}$$

The skin friction can be computed using

$$f''(0) = f_0''(0) + \Lambda f_1''(0) + \Lambda^2 f_2''(0) + \cdots. \tag{18}$$

Then substituting (17) into the system (7)–(10). We then take the zeroth, first, and second order of the viscoelastic parameter Λ. We obtain the following system.

Zeroth order:

$$f_0''' + 2f_0f_0'' - f_0'^2 + \theta_0 - \gamma f_0' = 0, \tag{19}$$

$$\theta'' + 2\Pr f_0\theta_0' - \Pr f_0'\theta_0 + \Pr \mathrm{Ec} f_0''^2 = 0, \tag{20}$$

$$f_0(0) = 0, \qquad f_0'(0) = 0, \qquad \theta_0(0) = 1, \tag{21}$$

$$f_0'(\infty) = 0, \qquad \theta_0(\infty) = 0. \tag{22}$$

First order:

$$\begin{aligned} &f_1''' + 2f_0f_1'' + 2f_1f_0'' - 2f_0'f_1' + \theta_1 \\ &\quad - \gamma f_1' - 2f_0'f_0''' + 2f_0f_0^{iv} + f_0''^2 = 0, \end{aligned} \tag{23}$$

$$\begin{aligned} &\theta_1'' + 2\Pr f_0\theta_1 + 2\Pr f_1\theta_0' - \Pr f_0'\theta_1 - \Pr f_1'\theta_0 \\ &\quad + 2\Pr \mathrm{Ec} f_0'' f_1'' + \Pr \mathrm{Ec} f_0' f_0''^2 - \Pr \mathrm{Ec} f_0 f_0'' f_0''' = 0, \end{aligned} \tag{24}$$

$$f_1(0) = 0, \qquad f_1'(0) = 0, \qquad f_1'(\infty) = 0, \tag{25}$$

$$\theta_1(0) = 0, \qquad \theta_1(\infty) = 0. \tag{26}$$

Second order:

$$\begin{aligned} &f_2''' + 2f_0f_2'' + 2f_1f_1'' + 2f_2'f_0'' - 2f_0'f_2' - f_1'^2 + \theta_2 - \gamma f_2' \\ &\quad - 2f_0'f_1''' - 2f_1'f_0''' + 2f_0f_1^{iv} + 2f_1f_0^{iv} + 2f_0''f_1'' = 0, \end{aligned} \tag{27}$$

$$\begin{aligned} &\theta_2'' + 2\Pr f_0\theta_2' + 2\Pr f_1\theta_1' + 2\Pr f_2\theta_0' - \Pr f_0'\theta_2 - \Pr f_1'\theta_1 \\ &\quad + \Pr \mathrm{Ec}\left(2f_0''f_2'' + f_1''^2 + 2f_0'f_0''f_1'' + f_1'f_0''^2 + f_2'f_0''^2\right. \\ &\quad \left. + f_0f_0''f_1''' + f_0f_1''f_0''' + f_1f_0''f_0'''\right) = 0, \end{aligned} \tag{28}$$

$$f_2(0) = 0, \qquad f_2'(0) = 0, \qquad f_2'(\infty) = 0, \tag{29}$$

$$\theta_2(0) = 0, \qquad \theta_2(\infty) = 0. \tag{30}$$

The functions in the system (19)–(30) may be expanded in series form as

$$\begin{aligned} f_0(y) &= f_{0i}(y) + \sum_{m=0}^{i-1} f_{0m}(y), \\ \theta_0(y) &= \theta_{0i}(y) + \sum_{m=0}^{i-1} \theta_{0m}(y), \\ f_1(y) &= f_{1i}(y) + \sum_{m=0}^{i-1} f_{1m}(y), \\ \theta_1(y) &= \theta_{1i}(y) + \sum_{m=0}^{i-1} \theta_{1m}(y), \\ f_2(y) &= f_{2i}(y) + \sum_{m=0}^{i-1} f_{2m}(y), \\ \theta_2(y) &= \theta_{2i}(y) + \sum_{m=0}^{i-1} \theta_{2m}(y), \end{aligned} \tag{31}$$

where f_{0i}, f_{1i}, and f_{2i} and θ_{0i}, θ_{1i}, and θ_{2i} $(i = 1, 2, 3, \ldots)$ are unknown functions and f_{0m}, f_{1m}, and f_{2m} and θ_{0m}, θ_{1m}, and θ_{2m} are approximations that are found by successively solving the linear part of equations that are obtained after substituting (31) into system (19)–(30). These linear equations have the form

$$f_{0i}''' + a_{01,i-1}f_{0i}'' + a_{02,i-1}f_{0i}' + a_{03,i-1}f_{0i} + a_{04,i-1}\theta_{0i} = r_{01,i-1}, \tag{32}$$

$$\begin{aligned} &\theta_{0i}'' + b_{01,i-1}\theta_{0i}' + b_{02,i-1}\theta_{0i} + b_{03,i-1}f_{0i}'' \\ &\quad + b_{04,i-1}f_{0i}' + b_{05,i-1}f_{0i} = r_{02,i-1}, \end{aligned} \tag{33}$$

$$f_{0i}(0) = 0, \qquad f_{0i}'(0) = 0, \qquad \theta_{0i}(0) = 0, \tag{34}$$

$$f_{0i}'(\infty) = 0, \qquad \theta_{0i}(\infty) = 0, \qquad f_{0i}''(\infty) = 0, \tag{35}$$

$$f_{1i}''' + a_{11,i-1} f_{1i}'' + a_{12,i-1} f_{1i}' + a_{13,i-1} f_{1i} + a_{14,i-1} \theta_{1i} = r_{11,i-1}, \tag{36}$$

$$\theta_{1i}'' + b_{11,i-1} \theta_{1i}' + b_{12,i-1} \theta_{1i} + b_{13,i-1} f_{1i}'' + b_{14,i-1} f_{1i}' + b_{15,i-1} f_{1i} = r_{12,i-1}, \tag{37}$$

$$f_{1i}(0) = 0, \quad f_{1i}'(0) = 0, \quad \theta_{1i}(0) = 0, \tag{38}$$

$$f_{1i}'(\infty) = 0, \quad \theta_{1i}(\infty) = 0, \quad f_{1i}''(\infty) = 0, \tag{39}$$

$$f_{2i}''' + a_{21,i-1} f_{2i}'' + a_{22,i-1} f_{2i}' + a_{23,i-1} f_{2i} + a_{24,i-1} \theta_{2i} = r_{21,i-1}, \tag{40}$$

$$\theta_{2i}'' + b_{21,i-1} \theta_{2i}' + b_{22,i-1} \theta_{2i} + b_{23,i-1} f_{2i}'' + b_{24,i-1} f_{2i}' + b_{25,i-1} f_{2i} = r_{22,i-1}, \tag{41}$$

$$f_{2i}(0) = 0, \quad f_{2i}'(0) = 0, \quad \theta_{2i}(0) = 0, \tag{42}$$

$$f_{2i}'(\infty) = 0, \quad \theta_{2i}(\infty) = 0, \quad f_{2i}''(\infty) = 0. \tag{43}$$

The coefficients $a_{jk,i-1}, b_{jk,i-1}$ $(j = 0, 1, 2,\ k = 1, \ldots, 5)$, $r_{j1,i-1}$, and $r_{j2,i-1}$ are defined as

$$a_{01,i-1} = a_{11,i-1} = a_{21,i-1} = 2\sum_{m=0}^{i-1} f_{0m},$$

$$a_{02,i-1} = a_{12,i-1} = a_{22,i-1} = -\left(2\sum_{m=0}^{i-1} f_{0m}' + \gamma\right),$$

$$a_{03,i-1} = a_{13,i-1} = a_{23,i-1} = 2\sum_{m=0}^{i-1} f_{0m}'',$$

$$a_{04,i-1} = a_{14,i-1} = a_{24,i-1} = \mathrm{I},$$

$$b_{01,i-1} = b_{11,i-1} = b_{21,i-1} = 2\mathrm{Pr}\sum_{m=0}^{i-1} f_{0m},$$

$$b_{02,i-1} = b_{12,i-1} = b_{22,i-1} = -\mathrm{Pr}\sum_{m=0}^{i-1} f_{0m}',$$

$$b_{03,i-1} = b_{13,i-1} = b_{23,i-1} = \mathrm{Pr\,Ec}\sum_{m=0}^{i-1} f_{0m}'',$$

$$b_{04,i-1} = b_{14,i-1} = b_{24,i-1} = -\mathrm{Pr}\sum_{m=0}^{i-1} \theta_{0m},$$

$$b_{05,i-1} = b_{15,i-1} = b_{25,i-1} = 2\mathrm{Pr}\sum_{m=0}^{i-1} \theta_{0m}',$$

$$r_{01,i-1} = -\left[\sum_{m=0}^{i-1} f_{0m}''' + 2\sum_{m=0}^{i-1} f_{0m}\sum_{m=0}^{i-1} f_{0m}'' - \left(\sum_{m=0}^{i-1} f_{0m}'\right)^2 - \sum_{m=0}^{i-1} \theta_{0m} - \gamma\sum_{m=0}^{i-1} f_{0m}'\right],$$

$$r_{02,i-1} = -\left[\sum_{m=0}^{i-1} \theta_{0m}'' + 2\mathrm{Pr}\sum_{m=0}^{i-1} f_{0m}\sum_{m=0}^{i-1} \theta_{0m}' - \mathrm{Pr}\sum_{m=0}^{i-1} f_{0m}'\sum_{m=0}^{i-1} \theta_{0m} + \mathrm{Pr\,Ec}\left(\sum_{m=0}^{i-1} f_{0m}''\right)^2\right],$$

$$r_{11,i-1} = -\left[\sum_{m=0}^{i-1} f_{1m}''' + 4\sum_{m=0}^{i-1} f_{0m}\sum_{m=0}^{i-1} f_{1m}' + 4\sum_{m=0}^{i-1} f_{1m}\sum_{m=0}^{i-1} f_{0m}'' - 6\sum_{m=0}^{i-1} f_{0m}''\sum_{m=0}^{i-1} - \gamma\sum_{m=0}^{i-1} f_{0m}' + 3\left(\sum_{m=0}^{i-1} f_{0m}''\right)^2 + 6\sum_{m=0}^{i-1} f_{0m}\sum_{m=0}^{i-1} f_{0m}^{iv} - 6\sum_{m=0}^{i-1} f_{0m}'\sum_{m=0}^{i-1} f_{0m}''' + \sum_{m=0}^{i-1}\right],$$

$$r_{12,i-1} = -\left[\sum_{m=0}^{i-1} \theta_{1m}'' + 4\mathrm{Pr}\sum_{m=0}^{i-1} f_{0m}\sum_{m=0}^{i-1} \theta_{1m}' - 2\mathrm{Pr}\sum_{m=0}^{i-1} f_{0m}'\sum_{m=0}^{i-1} \theta_{1m} - 2\mathrm{Pr}\sum_{m=0}^{i-1} f_{1m}'\sum_{m=0}^{i-1} \theta_{0m} + 4\mathrm{Pr}\sum_{m=0}^{i-1} f_{1m}\sum_{m=0}^{i-1} \theta_{0m}' + 4\mathrm{Pr\,Ec}\sum_{m=0}^{i-1} f_{0m}''\sum_{m=0}^{i-1} f_{1m}'' + 4\mathrm{Pr\,Ec}\sum_{m=0}^{i-1} f_{0m}'\left(\sum_{m=0}^{i-1} f_{0m}\right)^2 - 4\mathrm{Pr\,Ec}\sum_{m=0}^{i-1} f_{0m}\sum_{m=0}^{i-1} f_{0m}''\sum_{m=0}^{i-1} f_{0m}'''\right],$$

$$r_{21,i-1} = -\left[\sum_{m=0}^{i-1} f_2''' + 4\sum_{m=0}^{i-1} f_{0m}\sum_{m=0}^{i-1} f_{2m}'' + 6\sum_{m=0}^{i-1} f_{1m}\sum_{m=0}^{i-1} f_{1m}'' - 4\sum_{m=0}^{i-1} f_{2m}\sum_{m=0}^{i-1} f_{0m}'' - 4\sum_{m=0}^{i-1} f_{2m}'\sum_{m=0}^{i-1} f_{0m}' - 3\left(\sum_{m=0}^{i-1} f_{1m}'\right)^2 - \gamma\sum_{m=0}^{i-1} f_{2m}' + \sum_{m=0}^{i-1} \theta_{2m} - 6\sum_{m=0}^{i-1} f_{1m}'''\sum_{m=0}^{i-1} f_{0m}' - 6\sum_{m=0}^{i-1} f_{0m}'''\sum_{m=0}^{i-1} f_{1m}' + 6\sum_{m=0}^{i-1} f_{1m}^{iv}\sum_{m=0}^{i-1} f_{0m} + 6\sum_{m=0}^{i-1} f_{0m}^{iv}\sum_{m=0}^{i-1} f_{1m} + 6\sum_{m=0}^{i-1} f_{1m}''\sum_{m=0}^{i-1} f_{1m}''\right],$$

$$r_{22,i-1} = -\left[\sum_{m=0}^{i-1} \theta_{2m}'' + 4\mathrm{Pr}\sum_{m=0}^{i-1} f_{0m}\sum_{m=0}^{i-1} \theta_{2m}'\right.$$

$$
\begin{aligned}
&- 6\mathrm{Pr}\sum_{m=0}^{i-1} f'_{1m}\sum_{m=0}^{i-1}\theta'_{1m} - 6\mathrm{Pr}\sum_{m=0}^{i-1} f_{1m}\sum_{m=0}^{i-1}\theta'_{1m} \\
&+ 4\mathrm{Pr}\sum_{m=0}^{i-1} f_{2m}\sum_{m=0}^{i-1} f'_{0m} - 2\mathrm{Pr}\sum_{m=0}^{i-1}\theta_{2m}\sum_{m=0}^{i-1} f'_{0m} \\
&- 3\mathrm{Pr}\sum_{m=0}^{i-1}\theta_{1m}\sum_{m=0}^{i-1} f'_{1m} \\
&+ 10\mathrm{Pr}\,\mathrm{Ec}\sum_{m=0}^{i-1} f'_{0m}\sum_{m=0}^{i-1} f''_{0m}\sum_{m=0}^{i-1} f'_{1m} \\
&+ 2\left(\sum_{m=0}^{i-1} f''_{0m}\right)^2\sum_{m=0}^{i-1} f'_{1m} + 4\left(\sum_{m=0}^{i-1} f''_{0m}\right)^2\sum_{m=0}^{i-1} f'_{2m} \\
&+4\sum_{m=0}^{i-1} f_{0m}\sum_{m=0}^{i-1} f''_{0m}\sum_{m=0}^{i-1} f'''_{1m}+4\sum_{m=0}^{i-1} f_{0m}\sum_{m=0}^{i-1} f''_{1m}\sum_{m=0}^{i-1} f'''_{0m} \\
&+4\sum_{m=0}^{i-1} f''_{0m}\sum_{m=0}^{i-1} f'''_{0m}\sum_{m=0}^{i-1} f_{1m}\Bigg]
\end{aligned}
\tag{44}
$$

Equations (32)–(43) must be solved simultaneously subject to certain initial approximations f_0 and θ_0. We choose these initial approximations so that they satisfy the given boundary conditions. In this case suitable initial approximations are

$$f_0(Y) = 1 - e^{-Y} - Ye^{-Y}, \qquad \theta_0(Y) = e^{-Y}. \tag{45}$$

We note that when f_i and θ_i $(i > 1)$ have been found, the approximate solutions $f(Y)$ and $\theta(Y)$ are obtained as

$$f(Y) \approx \sum_{n=0}^{M} f_n(Y), \qquad \theta(Y) \approx \sum_{n=0}^{M} \theta_n(Y), \tag{46}$$

where M is the order of the SLM approximation. Equations (32) and (43) can be solved by any numerical method. In this work the equations have been solved by the Chebyshev spectral collocation method. The method of solution is fully described in Awad et al. [3]. The system of differential equations is solved simultaneously using the MATLAB SLM code.

3.1. Results and Discussion. The problem that is investigated in this study is the steady laminar flow and natural convection from a cone in a viscoelastic fluid in the presence of viscous dissipation in a porous medium. The coupled nonlinear differential equations (7)–(10) were solved numerically using the successive linearisation method (SLM). In this section we discuss the effects of the viscoelastic parameter (Λ), porosity parameter (γ), Prandtl number (Pr), and Eckert numbers (Ec) on both the velocity and temperature profiles.

In Table 1 the comparison between our results for the local skin friction and Nusselt numbers and those of Ece [5] who used the Thomas algorithm shows that our method gives satisfactory results, thus confirming that the method is accurate.

Table 1: Comparison of the values of $f''(0)$ obtained by SLM against the Thomas algorithm of Ece [5] when $\Lambda = 0$.

Pr	Ece [5]		Present	
	$f''(0)$	$-\theta'(0)$	$f''(0)$	$-\theta'(0)$
1	0.681483	0.638855	0.68148334	0.63885473
10	0.433268	1.275499	0.43327820	1.27552877

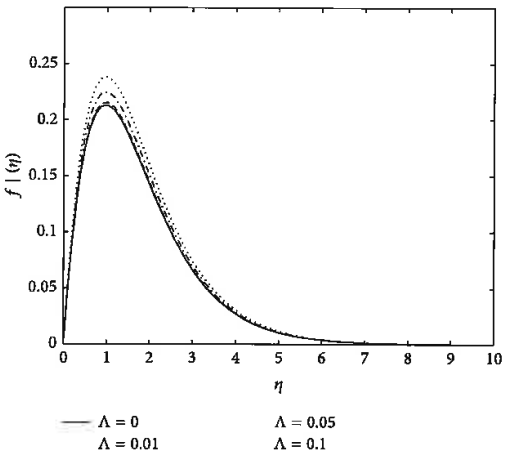

Figure 2: Velocity profiles for different values of the viscoelastic parameter Λ at Pr = 1, Ec = 0.1, and $\gamma = 1$.

To get a clear understanding of natural convection effects on the physics of the problem of a flow from a cone in a viscoelastic fluid with viscous dissipation, the investigation has been carried out for different viscoelastic numbers Λ, porosity parameter γ, the Eckert number Ec, and the Prandtl number Pr. The results for the skin friction and heat transfer coefficients are depicted in Tables 1 and 2.

In Table 2 the effect of increasing the viscoelastic parameter increases the skin friction coefficient and the opposite effect is noted on the Nusselt number in the presence of the porous medium and viscous dissipation. Cortell [9] noted the same result. A faster increase is noted in the absence of the porous medium and the Eckert number. Increasing the porosity parameter reduces local skin friction and the same trend is noted on the Nusselt number. Skin friction increases with increasing Eckert number and the opposite trend is noted on the Nusselt number. The skin friction decreases with increasing Prandtl number, and the opposite trend is noted on the Nusselt number.

Figures 2–9 show the effects of various fluid properties on the velocity and temperature profiles.

Figure 2 shows that increasing the viscoelastic parameter increases the velocity across the boundary layer (see Butt et al. [24]).

Increasing the Prandtl number decreases the velocity profile in the boundary layer as shown in Figure 3; This is

Table 2: Effect of the viscoelastic and porosity parameters and Eckert number Λ, γ, and Ec on the local skin friction and heat transfer for Pr = 1.

Λ	γ	Ec	Pr	$f''(0)$	$-\theta'(0)$
−0.1	1	0.1	1	0.51437649	0.64214087
−0.05	1	0.1	1	0.53489736	0.59964040
−0.01	1	0.1	1	0.55491411	0.56204002
0	1	0.1	1	0.56041829	0.55213993
0.01	1	0.1	1	0.56612247	0.54203983
0.05	1	0.1	1	0.59093920	0.49963495
0.1	1	0.1	1	0.62646010	0.44213898
0.01	0	0.1	1	0.68990728	0.61800108
0.01	1	0.1	1	0.56612247	0.54203983
0.01	2	0.1	1	0.49213165	0.48868800
0.01	3	0.1	1	0.44155007	0.44852699
0.01	1	0.1	1	0.56612247	0.54203983
0.01	1	0.2	1	0.56678919	0.53544933
0.01	1	0.3	1	0.56745956	0.52882111
0.01	1	0.4	1	0.56813364	0.52215479
0.01	1	0.1	0.7	0.59466242	0.47714847
0.01	1	0.1	1	0.56612247	0.54203983
0.01	1	0.1	2	0.50981746	0.68640396
0.01	1	0.1	10	0.38403617	1.13367723

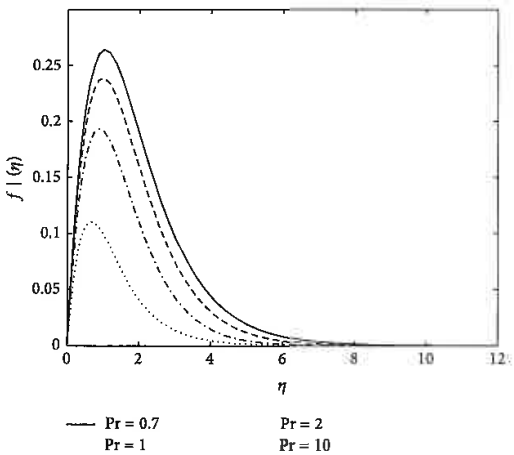

Figure 3: Velocity profiles for different values of the Prandtl number Pr at Ec = 0.1, γ = 1, and Λ = 0.1.

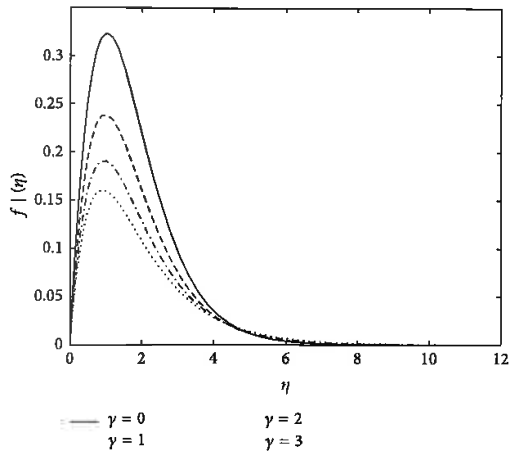

Figure 4: Velocity profiles for different values of the porosity parameter γ at Pr = 1, Ec = 0.1, and Λ = 0.1.

because when the Prandtl number is increased the conduction process is more enhanced than convection suggesting lower molecular motion causing fluid velocity to decrease.

Figure 4 shows the variation of the porosity parameter with velocity profile for the linear surface temperature. Increasing porosity parameter reduces the velocity profile across the boundary layer. The fluid particles move slower as the medium becomes less porous (see Singh and Agarwal [25]).

Figure 5 shows the variation of the Eckert number with velocity profile across the boundary layer. Increasing the Eckert number increases the velocity profile; this is caused by the increase in the kinetic energy caused by viscous dissipation in the boundary layer which leads to a small temperature gradient.

Figure 6 shows the effect of increasing the viscoelastic parameter on the temperature profiles. Increasing the viscoelastic parameter increases the temperature profile.

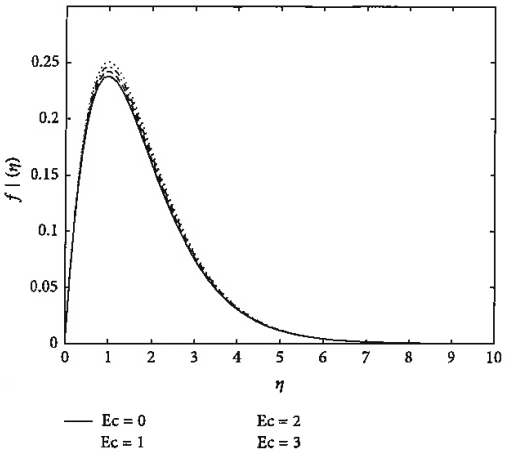

FIGURE 5: Velocity profiles for different values of the Eckert number Ec at Pr = 1, γ = 1, and Λ = 0.1.

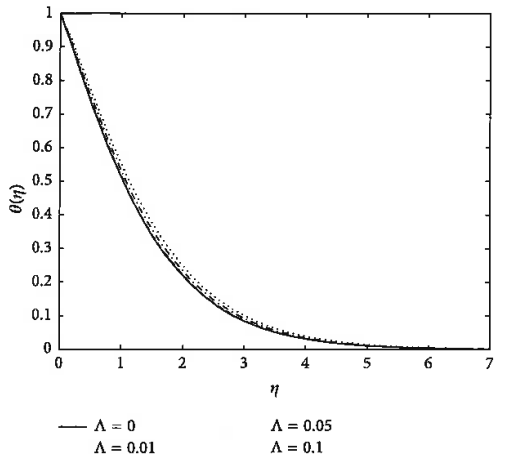

FIGURE 6: Temperature profiles for different values of the viscoelastic parameter Λ at Pr = 1, γ = 1, and Ec = 0.1.

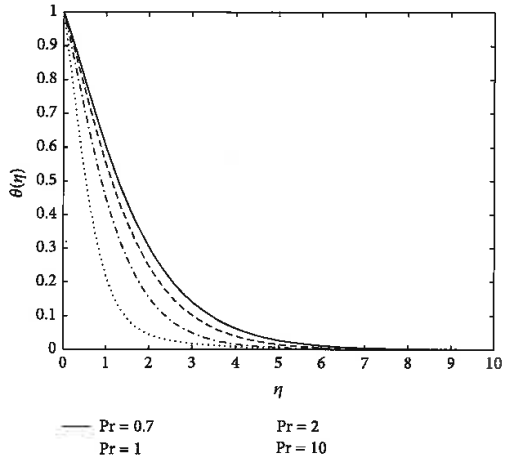

FIGURE 7: Temperature profiles for different values of the Prandtl number Pr at Ec = 0.1, γ = 0.1, and Λ = 0.1.

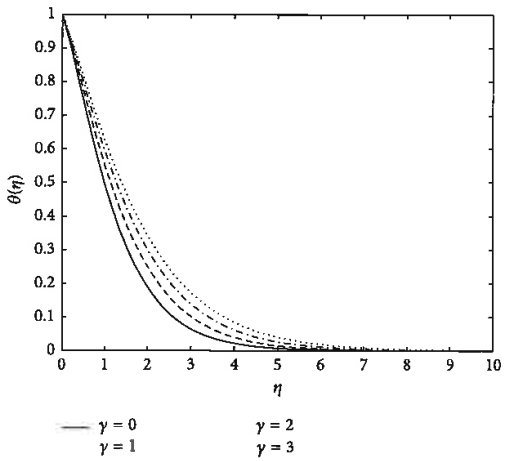

FIGURE 8: Temperature profiles for different values of the porosity parameter γ at Pr = 1, Λ = 0.1, and Ec = 0.1.

Figure 7 depicts the variation of the Prandtl number with temperature profiles. Increasing the Prandtl number decreases the temperature profile; The thermal diffusivity becomes smaller than the viscous diffusion rate causing smaller temperature profiles.

Figure 8 shows the variation of the porosity parameter with the temperature profile. Increasing the porosity parameter increases the temperature profile; when the fluid moves much slower due to the reduction in porosity heat transfer becomes more rapid.

In Figure 9 increasing the Eckert number increases the temperature profile; the heat produced due to viscous dissipation increases the temperature across the boundary layer.

Figure 10 shows the variation of the skin friction with the viscoelastic parameter at different values of the porosity parameter. Skin friction increases with increasing viscoelastic parameter and increasing the porosity parameter reduces skin friction.

Figure 11 shows the variation of the Nusselt number with the viscoelastic parameter; increasing the viscoelastic parameter reduces Nusselt number and increasing the porosity parameter reduces the Nusselt number.

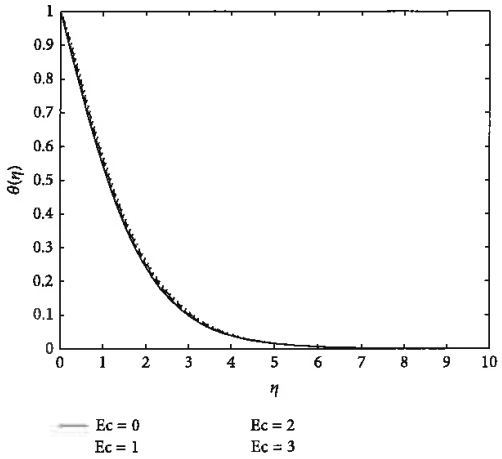

FIGURE 9: Temperature profiles for different values of the Eckert number Ec at Pr = 1, $\gamma = 1$, and $\Lambda = 0.1$.

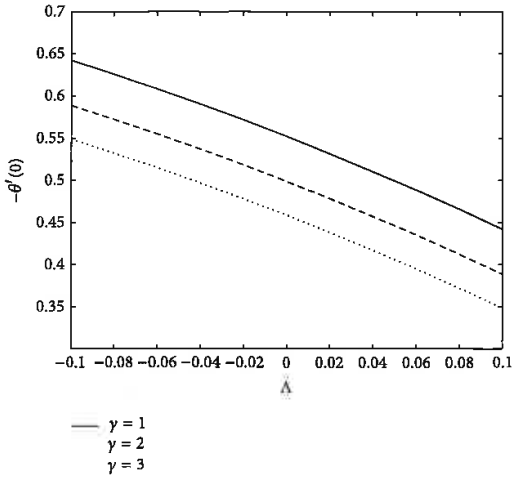

FIGURE 11: Nusselt number $-\theta'(0)$ versus viscoelastic parameter Λ for different values of porosity parameter.

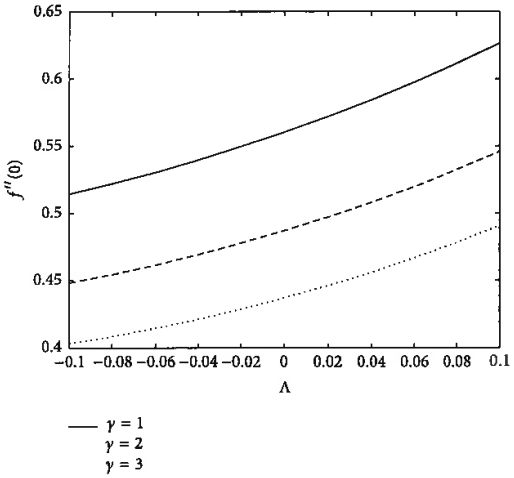

FIGURE 10: Skin friction $f''(0)$ versus viscoelastic parameter Λ for different values of porosity parameter.

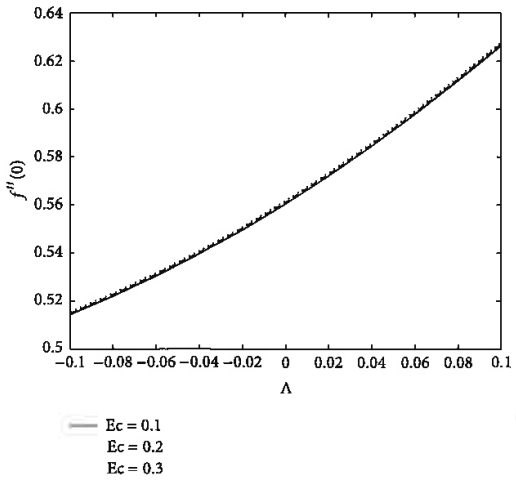

FIGURE 12: Skin friction $f''(0)$ versus viscoelastic parameter Λ for different values of Eckert numbers.

Figure 12 shows the effect of increasing the Eckert number on the skin friction and viscoelastic parameter. Increasing viscoelastic parameter increases skin friction and increasing the Eckert number increases the skin friction.

In Figure 13 the increase of viscoelastic parameter reduces the Nusselt number and increasing the Eckert number reduces the Nusselt number.

Figure 14 shows that generally increasing the viscoelastic parameter increases the skin friction and increasing the Prandtl number reduces skin friction.

In Figure 15 increasing the viscoelastic parameter reduces the Nusselt number and increasing the Prandtl number increases the Nusselt number.

4. Conclusion

This study presented an analysis of flow and heat transfer in natural convection of viscoelastic fluid from a cone embedded in a porous medium with viscous dissipation. The nonlinear coupled governing equations were solved using the successive linearization method (SLM). The equations

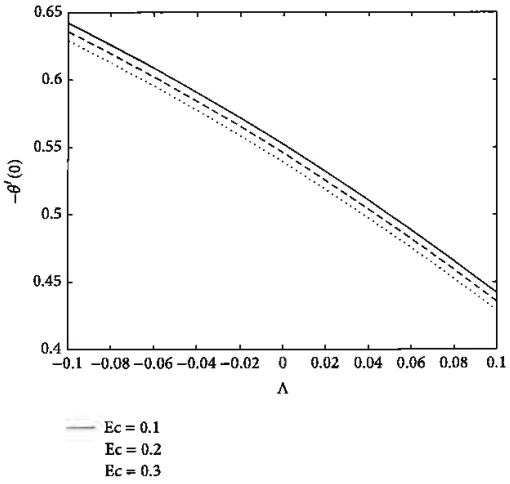

FIGURE 13: Nusselt number $-\theta'(0)$ versus viscoelastic parameter Λ for different values of Eckert numbers.

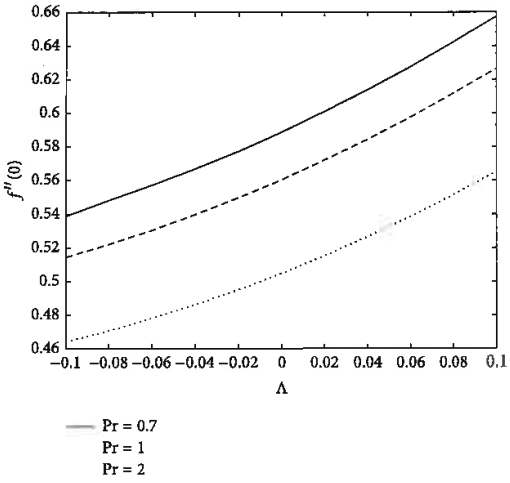

FIGURE 14: Skin friction $f''(0)$ versus viscoelastic parameter Λ for different values of the Prandtl numbers.

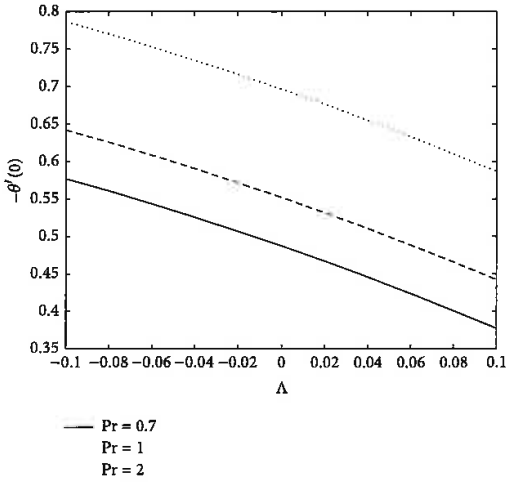

FIGURE 15: Nusselt number $-\theta'(0)$ versus viscoelastic parameter Λ for different values of Prandtl numbers.

were first split into the zeroth, first, and second order of the viscoelastic parameter and solved together under the linear surface boundary conditions. The velocity and temperature profiles together with local skin friction and local Nusselt numbers were presented and investigated. It was found that increasing the viscoelastic parameter increased the skin friction, reduced the Nusselt number, and increased the velocity and temperature profiles. Increasing the porosity parameter decreased the skin friction and Nusselt number and decreased the velocity profile and the opposite effect was noted in the temperature profile. Increasing the Eckert number increased both velocity and temperature profiles and decreased the Nusselt number and the opposite was noted on the skin friction. The results compared well with those of Ece [5] in case when $\gamma = \Lambda = \mathrm{Ec} = 0$.

References

[1] O. D. Makinde, "On thermal stability of a reactive third-grade fluid in a channel with convective cooling the walls," *Applied Mathematics and Computation*, vol. 213, no. 1, pp. 170–176, 2009.

[2] M. A. Alim, M. Alam, and M. K. Chowdhury, "Pressure work effect on natural convection flow from a vertical circular cone with suction and non-uniform surface temperature," *Journal of Mechanical Engineering*, vol. 36, pp. 6–11, 2006.

[3] F. G. Awad, P. Sibanda, S. S. Motsa, and O. D. Makinde, "Convection from an inverted cone in a porous medium with cross-diffusion effects," *Computers & Mathematics with Applications*, vol. 61, no. 5, pp. 1431–1441, 2011.

[4] C. Cheng, "Soret and Dufour effects on natural convection boundary layer flow over a vertical cone in a porous medium with constant wall heat and mass fluxes," *International Communications in Heat and Mass Transfer*, vol. 38, no. 1, pp. 44–48, 2011.

[5] M. C. Ece, "Free convection flow about a cone under mixed thermal boundary conditions and a magnetic field," *Applied Mathematical Modelling*, vol. 29, no. 11, pp. 1121–1134, 2005.

[6] R. R. Kairi and P. V. S. N. Murthy, "Effect of viscous dissipation on natural convection heat and mass transfer from vertical cone in a non-Newtonian fluid saturated non-Darcy porous medium," *Applied Mathematics and Computation*, vol. 217, no. 20, pp. 8100–8114, 2011.

[7] Z. Abbas, T. Hayat, and I. Pop, "Unsteady flow of a second grade fluid film over an unsteady stretching sheet," *Mathematical and Computer Modelling*, vol. 48, no. 3-4, pp. 518–526, 2008.

[8] I. Anwar, N. Amin, and I. Pop, "Mixed convection boundary layer flow of a viscoelastic fluid over a horizontal circular

cylinder," *International Journal of Non-Linear Mechanics*, vol. 43, no. 9, pp. 814–821, 2008.

[9] R. Cortell, "A note on flow and heat transfer of a viscoelastic fluid over a stretching sheet," *International Journal of Non-Linear Mechanics*, vol. 41, no. 1, pp. 78–85, 2006.

[10] R. A. Damseh, A. S. Shatnawi, A. J. Chamka, and H. M. Duwairi, "Transient mixed convection flow of a second grade visco-Elastic fluid over a vertical surface," *Nonlinear Analysis: Modelling and Control*, vol. 13, no. 2, pp. 169–179, 2008.

[11] T. Hayat, Z. Abbas, and I. Pop, "Mixed convection in the stagnation point flow adjacent to a vertical surface in a viscoelastic fluid," *International Journal of Heat and Mass Transfer*, vol. 51, no. 11-12, pp. 3200–3206, 2008.

[12] K. Hsiao, "MHD mixed convection for viscoelastic fluid past a porous wedge," *International Journal of Non-Linear Mechanics*, vol. 46, no. 1, pp. 1–8, 2011.

[13] A. R. M. Kasim, M. A. Admon, and S. Shafie, "Free convection boundary layer flow of a viscoelastic fluid in the presence of heat generation," *World Academy of Science, Engineering and Technology*, vol. 75, pp. 492–499, 2011.

[14] M. Massoudi, A. Vaidya, and R. Wulandana, "Natural convection flow of a generalized second grade fluid between two vertical walls," *Nonlinear Analysis: Real World Applications*, vol. 9, no. 1, pp. 80–93, 2008.

[15] B. I. Olajuwon, "Convection heat and mass transfer in a hydromagnetic flow of a second grade fluid in the presence of thermal radiation and thermal diffusion," *International Communications in Heat and Mass Transfer*, vol. 38, no. 3, pp. 377–382, 2011.

[16] M. Sajid, I. Pop, and T. Hayat, "Fully developed mixed convection flow of a viscoelastic fluid between permeable parallel vertical plates," *Computers & Mathematics with Applications*, vol. 59, no. 1, pp. 493–498, 2010.

[17] M. Subhas Abel, E. Sanjayanand, and M. M. Nandeppanavar, "Viscoelastic MHD flow and heat transfer over a stretching sheet with viscous and ohmic dissipations," *Communications in Nonlinear Science and Numerical Simulation*, vol. 13, no. 9, pp. 1808–1821, 2008.

[18] M. S. Abel, N. Mahesha, and J. Tawade, "Heat transfer in a liquid film over an unsteady stretching surface with viscous dissipation in presence of external magnetic field," *Applied Mathematical Modelling*, vol. 33, no. 8, pp. 3430–3441, 2009.

[19] B. K. Jha and A. O. Ajibade, "Effect of viscous dissipation on natural convection flow between vertical parallel plates with time-periodic boundary conditions," *Communications in Nonlinear Science and Numerical Simulation*, vol. 17, no. 4, pp. 1576–1587, 2012.

[20] C. Chen, "On the analytic solution of MHD flow and heat transfer for two types of viscoelastic fluid over a stretching sheet with energy dissipation, internal heat source and thermal radiation," *International Journal of Heat and Mass Transfer*, vol. 53, no. 19-20, pp. 4264–4273, 2010.

[21] R. Cortell, "Suction, viscous dissipation and thermal radiation effects on the flow and heat transfer of a power-law fluid past an infinite porous plate," *Chemical Engineering Research and Design*, vol. 89, no. 1, pp. 85–93, 2011.

[22] K. L. Hsiao, "Multimedia physical feature for unsteady MHD mixed convection viscoelastic fluid over a vertical stretching sheet with viscous dissipation," *International Journal of the Physical Sciences*, vol. 7, no. 17, pp. 2515–2524, 2012.

[23] P. K. Kameswaran, M. Narayana, P. Sibanda, and P. V. S. N. Murthy, "Hydromagnetic nanofluid flow due to a stretching sheet or shrinking sheet with viscous dissipation and chemical reaction effects," *International Journal of Heat and Mass Transfer*, vol. 55, no. 25-26, pp. 7587–7595, 2012.

[24] A. S. Butt, S. Munawar, A. Mehmood, and A. Ali, "Effect of viscoelasticity on Entropy generation in a porous medium over a stretching plate," *World Applied Sciences Journal*, vol. 17, no. 4, pp. 516–523, 2012.

[25] V. Singh and S. Agarwal, "Heat transfer in a second grade fluid over an exponentially stretching sheet through porous medium with thermal radiation and elastic deformation under the effect of magnetic field," *International Jornal of Applied Mathematics and Mechanics*, vol. 8, no. 4, pp. 41–63, 2012.

Appendix C

Hindawi Publishing Corporation
Mathematical Problems in Engineering
Article ID 724596

Research Article

Diffusion of Chemically Reactive Species in Casson Fluid Flow over an Unsteady Stretching Surface in Porous Medium in the Presence of a Magnetic Field

Gilbert Makanda, Sachin Shaw, and Precious Sibanda

School of Mathematics, Statistics and Computer Science, University of KwaZulu-Natal, Private Bag X01, Scottsville, Pietermaritzburg 3209, South Africa

Correspondence should be addressed to Precious Sibanda; sibandap@ukzn.ac.za

Received 31 July 2014; Accepted 14 September 2014

Academic Editor: Stanford Shateyi

A study is performed on two-dimensional flow and diffusion of chemically reactive species of Casson fluid from an unsteady stretching surface in porous medium in the presence of a magnetic field. The boundary layer velocity, temperature, and concentration profiles are numerically computed for different governing parameters. The paper intends to show unique results of a combination of heat transfer and chemical reaction in Casson fluid flow. The resulting partial differential equations are converted to a system of ordinary differential equations using the appropriate similarity transformation, which are solved by using the Runge-Kutta-Fehlberg numerical scheme. The results in this work are validated by the comparison with other authors.

1. Introduction

The study of Casson fluid has attracted attention to many researchers due to its application in the field of metallurgy, food processing, drilling operations, and bioengineering operations. Its application extends to the manufacturing of pharmaceutical products, coal in water, china clay, paints, synthetic lubricants, and biological fluids such as synovial fluids, sewage sludge, jelly, tomato sauce, honey, soup, and blood due to its contents such as plasma, fibrinogen, and protein, making the study of Casson fluid important in fluid dynamics. Casson fluid is classified as a non-Newtonian fluid due to its rheological characteristics. These characteristics show shear stress-strain relationships that are significantly different from Newtonian fluids. The study of non-Newtonian fluids has not been thoroughly covered due to the complex representation of their constitutive equations. It is therefore important to undertake this study of Casson fluid. Most studies have concentrated on viscoelastic fluids in which different constitutive equations have been suggested. This work can be applied to chemical processing equipment in which some fluids react chemically with some ingredients present in them.

The driving force for mass transfer is a combination of temperature and concentration gradients. In this study the effect of chemical reaction on the fluid is considered as in Mukhopadhyay and Vajravelu [1]. The study of boundary layer flow over a stretching sheet has been studied by Mukhopadhyay et al. [2], among others, who investigated Casson fluid flow over an unsteady stretching surface. In their work they did not consider mass transfer and they considered a different wall temperature expression. Abd El-Aziz [3] studied mixed convection flow of a micropolar fluid from an unsteady stretching surface with viscous dissipation. In this work he considered a similar stretching velocity, wall temperature, and wall concentration distribution. We extended the work of Grubka and Bobba [4] who investigated heat transfer characteristics of a continuous stretching surface with variable temperature in which we introduced the MHD and porous medium source terms and chemical reaction effects. Sharidan et al. [5] studied similarity solutions for the unsteady boundary layer flow and heat transfer due to a stretching sheet; Nadeem et al. [6, 7] and Ahmed and Nazar [8] also studied Casson fluid over a stretching sheet and in their paper they assumed that the velocity of the stretching

surface is linearly proportional to the distance from fixed origin.

In the study of non-Newtonian fluids many authors have studied the flow of blood as Casson fluid. The studies were carried out by Rohlf and Tenti [9], among others, who investigated the role of Womersley number in pulsatile blood flow, a theoretical study of the Casson model; Sankar and Lee [10, 11] investigated two-fluid nonlinear model for flow in catheterized blood vessels and two-fluid Casson model for pulsatile blood flow through stenosed arteries, respectively. Shaw et al. [12] studied pulsatile Casson fluid flow through stenosed bifurcated artery. In relation to blood flow there are other research works that were done in different geometries such as flows in microslit channels, slightly curved channels, and peristaltic transport as in [13–15].

The study of Casson fluid in porous media was also studied by Nadeem et al. [16] who considered MHD three-dimensional Casson fluid flow past a porous linearly stretching sheet. Dash et al. [17] studied Casson fluid flow in a pipe filled with homogeneous porous medium. Tripathi [18] investigated the transient peristaltic heat flow through a finite porous channel. Pramanik [19] studied Casson fluid flow and heat transfer past an exponentially porous stretching surface in the presence of thermal radiation. Ramachandra et al. [20] investigated flow and heat transfer of Casson fluid from a horizontal circular cylinder with partial slip in a non-Darcy porous medium. In their work they considered slip conditions on the wall.

There are many studies that investigated fluid flow with chemical reactions. Kameswaran et al. [21] investigated homogeneous-heterogeneous reactions in a nanofluid flow due to a porous stretching sheet, Shaw et al. [22] studied homogeneous-heterogeneous reactions in a nanofluid flow due to a porous stretching sheet, and Chamkha et al. [23] investigated similarity solutions for unsteady heat and mass transfer from a stretching surface embedded in a porous medium with suction/injection and chemical reaction effects.

Although there are many applications and use of non-Newtonian fluids in industry, the study of Casson fluid has not been thoroughly investigated for heat and mass transfer past a stretching surface. In this work we extend the work of Mukhopadhyay and Vajravelu [1] and Grubka and Bobba [4] in which the energy equation, the source terms for porous medium, and magnetic field are introduced. Similarity transformations are used to convert the partial differential equations into ordinary differential equations which are then solved by using Runge-Kutta-Fehlberg integration scheme and the successive linearization method described by Makanda et al. [24]. In this work we investigate the effect of varying unsteadiness parameter, Casson, Schmidt, and Prandtl numbers, and the reaction rate parameter on the velocity, temperature, and concentration profiles with the depiction of graphical illustrations.

2. Mathematical Formulation

Consider two-dimensional laminar boundary layer flow, temperature, and mass transfer of an incompressible Casson fluid flow over an unsteady stretching sheet. The flow of heat and mass transfer starts at $t = 0$. The sheet is pulled out of the slit at the origin ($x = 0, y = 0$) and moves with velocity $U(x,t) = ax/(1-\alpha t)$, $a > 0$, $\alpha \geq 0$ are constants, and a is the initial stretching rate. The rheological equation of state for an isotropic and incompressible flow of a Casson fluid is given as in [1, 2, 20] by

$$\tau_{ij} = \begin{cases} 2\left(\mu_B + \dfrac{P_y}{\sqrt{2\pi}}\right)e_{ij}, & \pi > \pi_c \\ 2\left(\mu_B + \dfrac{P_y}{\sqrt{2\pi_c}}\right)e_{ij}, & \pi < \pi_c, \end{cases} \tag{1}$$

where $\pi = e_{ij}e_{ij}$ and e_{ij} is the (i,j)th component of the deformation rate, π is the product of the deformation rate with itself, π_c is a critical value of this product based on the non-Newtonian model, μ_B is the plastic dynamic viscosity of the non-Newtonian fluid, and P_y is the yield stress of the fluid. Given that T_w and C_w are, respectively, the temperature and concentration at the sheet and T_∞ and C_∞ are, respectively, the ambient conditions, the positive x coordinate is measured along the stretching sheet and the positive y coordinate is measured perpendicular to the sheet. It is assumed that both temperature and concentration at the surface vary with distance from the origin and time. The temperature T_w and concentration C_w at the surface are therefore given by

$$T_w(x,t) = T_\infty + \frac{bx}{(1-\alpha t)^2}, \qquad C_w(x,t) = C_\infty + \frac{cx}{(1-\alpha t)^2}, \tag{2}$$

where b and c are constants. The surface temperature and surface concentration increase if b and c are positive and reduce if they are negative from T_∞ and C_∞ at the origin to x and the temperature and concentration increase/decrease along the sheet. It is assumed that radiation effects and viscous dissipation are negligible. The expressions $U_w(x,t)$, $T_w(x,t)$, and $C_w(x,t)$ are only valid for $t < \alpha^{-1}$ but not when $\alpha = 0$. Under these assumptions the governing equations in this flow are given as

$$\frac{\partial}{\partial x}(u) + \frac{\partial}{\partial y}(v) = 0, \tag{3}$$

$$\frac{\partial u}{\partial t} + u\frac{\partial u}{\partial x} + v\frac{\partial u}{\partial y} = \nu\left(1 + \frac{1}{\beta}\right)\frac{\partial^2 u}{\partial y^2} - \frac{\nu}{K}u - \frac{\sigma B_0^2}{\rho}u,$$

$$\frac{\partial T}{\partial t} + u\frac{\partial T}{\partial x} + v\frac{\partial T}{\partial y} = \alpha_0\frac{\partial^2 T}{\partial y^2}, \tag{4}$$

$$\frac{\partial C}{\partial t} + u\frac{\partial C}{\partial x} + v\frac{\partial C}{\partial y} = D\frac{\partial^2 C}{\partial y^2} - k(C - C_\infty),$$

where ν is kinematic viscosity of Casson fluid, $\beta = \mu_B\sqrt{2\pi_c}/P_y$ is the non-Newtonian Casson parameter, K is the permeability of the porous medium, σ is the electrical conductivity, B_0 is the strength of the magnetic field, ρ is the density of the Casson fluid, D is the diffusion coefficient of species in the fluid, α_0 is the thermal diffusivity, and $k(t) = k_0/(1-\alpha t)$ is the time dependent reaction rate, where $k > 0$

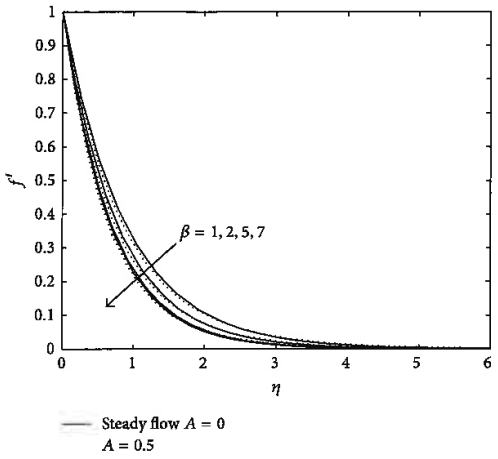

(a) Velocity profiles for different values of the Casson parameter β and unsteadiness parameter A at $\Lambda = 0.5$, $M = 1$, $\Pr = 1$, $\mathrm{Sc} = 1$, and $R = 0.5$

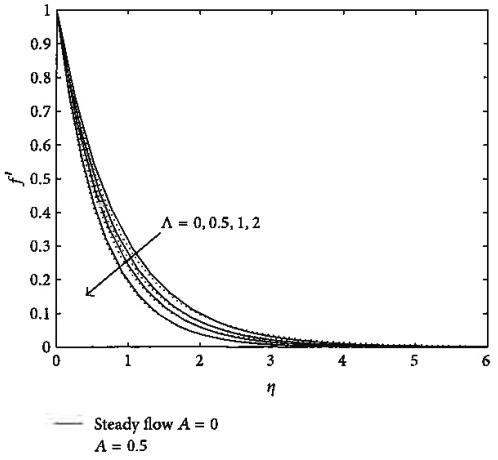

(b) Velocity profiles for different values of the permeability parameter Λ and unsteadiness parameter A at $\beta = 2$, $M = 1$, $\Pr = 1$, $\mathrm{Sc} = 1$, and $R = 0.5$

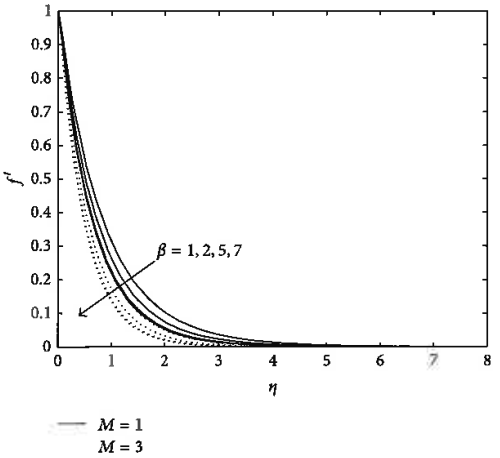

(c) Velocity profiles for different values of the Casson parameter β and magnetic parameter M at $A = 0.5$, $\Lambda = 0.5$, $\Pr = 1$, $\mathrm{Sc} = 1$, and $R = 0.5$

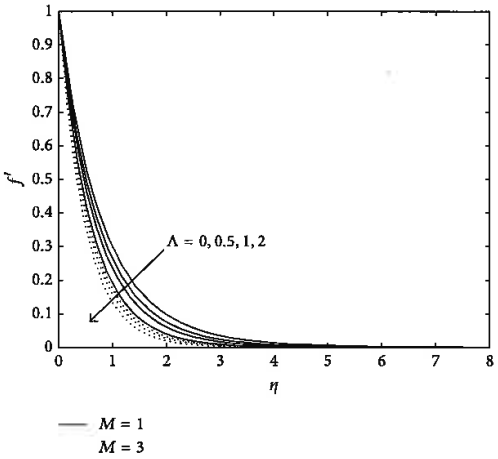

(d) Velocity profiles for different values of the permeability parameter Λ and magnetic parameter M at $\beta = 2$, $A = 0.5$, $\Pr = 1$, $\mathrm{Sc} = 1$, and $R = 0.5$

FIGURE 1: Effects of different parameters on velocity profiles.

represents destructive reaction, $k < 0$ represents constructive reaction, and k_0 is a constant. The boundary conditions are given as

$$\begin{aligned} &u = U(x,t), \quad v = 0, \quad T = T_w(x,t), \\ &C = C_w(x,t), \quad y = 0, \\ &u \longrightarrow 0, \quad T \longrightarrow T_\infty, \quad C \longrightarrow C_\infty, \quad \text{as } y \longrightarrow \infty, \end{aligned} \tag{5}$$

where the subscript ∞ refers to the ambient condition.

We introduce the nondimensional variables

$$\begin{aligned} &u = \frac{\partial \psi}{\partial y}, \quad v = -\frac{\partial \psi}{\partial x}, \\ &\eta = \sqrt{\frac{a}{\nu(1-\alpha t)}}\, y, \quad \psi = \sqrt{\frac{\nu a}{1-\alpha t}}\, x f(\eta), \\ &T_w(x,t) = T_\infty + \frac{bx}{(1-\alpha t)^2}\theta(\eta), \\ &C_w(x,t) = C_\infty + \frac{cx}{(1-\alpha t)^2}\phi(\eta), \end{aligned} \tag{6}$$

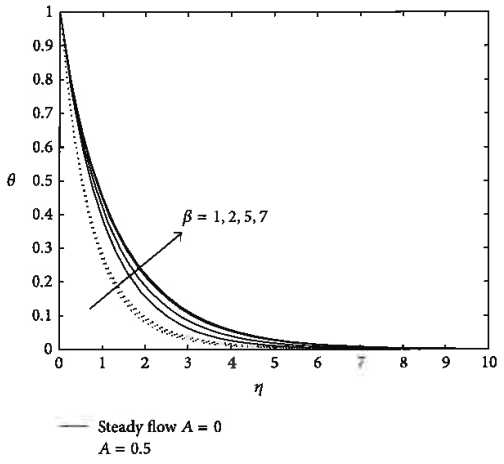

(a) Temperature profiles for different values of the Casson parameter β and unsteadiness parameter A at $\Lambda = 0.5$, $M = 1$, $\Pr = 1$, $\mathrm{Sc} = 1$, and $R = 0.5$

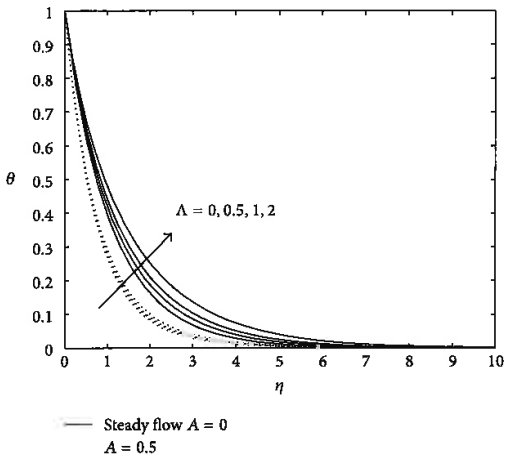

(b) Temperature profiles for different values of the permeability parameter Λ and unsteadiness parameter A at $\beta = 2$, $M = 1$, $\Pr = 1$, $\mathrm{Sc} = 1$, and $R = 0.5$

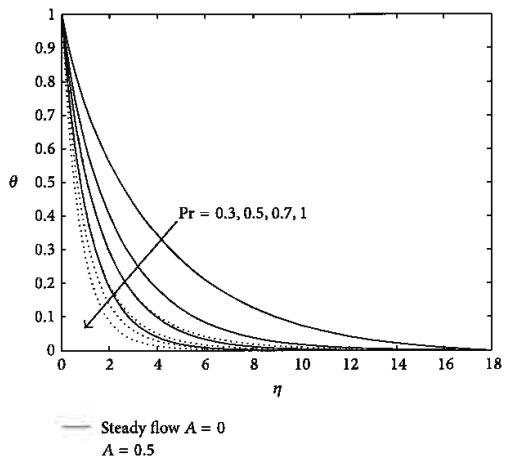

(c) Temperature profiles for different values of the Prandtl numbers Pr and unsteadiness parameter A at $\beta = 2$, $\Lambda = 0.5$, $M = 1$, $\mathrm{Sc} = 1$, and $R = 0.5$

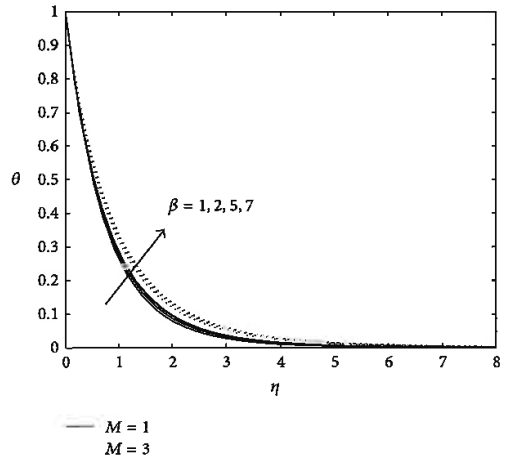

(d) Temperature profiles for different values of the Casson parameter β and magnetic parameter M at $A = 0.5$, $\Lambda = 0.5$, $\Pr = 1$, $\mathrm{Sc} = 1$, and $R = 0.5$

FIGURE 2: Effects of different parameters on temperature profiles.

where $\psi(x, y, t)$ is the stream function which satisfies the continuity equation (3). The velocity components are defined as

$$u = \frac{\partial \psi}{\partial y} = U_w f'(\eta), \qquad v = -\frac{\partial \psi}{\partial x} = -\sqrt{\frac{\nu a}{1 - \alpha t}}. \tag{7}$$

The governing equations reduce to

$$\left(1 + \frac{1}{\beta}\right) f''' + f f'' - f'^2 - \frac{A}{2}\left(2f' + \eta f''\right) - \left(\Lambda + M^2\right) f' = 0,$$

$$\frac{1}{\Pr}\theta'' + f\theta' - f'\theta - \frac{A}{2}\left(4\theta + \eta\theta'\right) = 0,$$

$$\frac{1}{\mathrm{Sc}}\phi'' + f\phi' - f'\phi - \frac{A}{2}\left(4\phi + \eta\phi'\right) - R\phi = 0, \tag{8}$$

with boundary conditions

$$f(0) = 0, \quad f'(0) = 1, \quad \theta(0) = 1, \quad \phi(0) = 1,$$
$$f'(\infty) \longrightarrow 0, \quad \theta(\infty) \longrightarrow 0, \quad \phi(\infty) \longrightarrow 0, \tag{9}$$

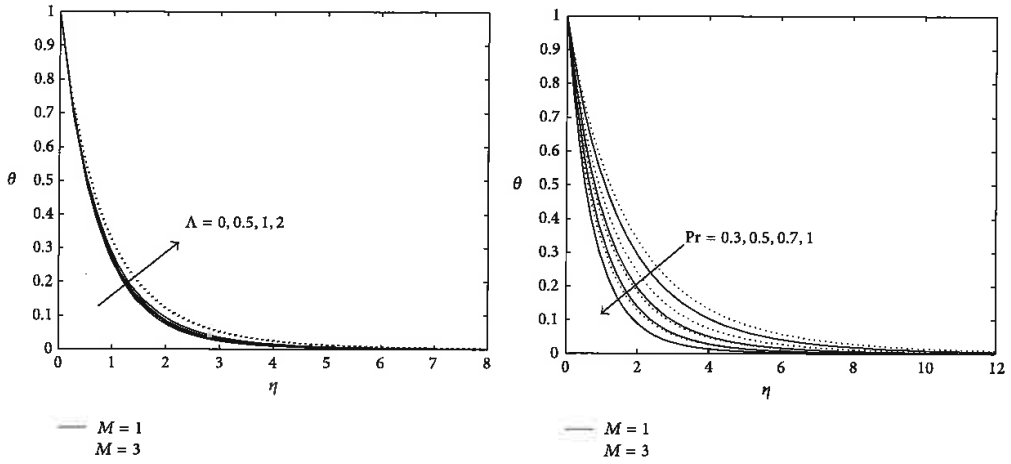

(a) Temperature profiles for different values of the permeability parameter Λ and magnetic parameter M at $\beta = 2$, $A = 0.5$, Pr = 1, Sc = 1, and $R = 0.5$

(b) Temperature profiles for different values of the Prandtl number Pr and magnetic parameter M at $\beta = 2$, $A = 0.5$, $\Lambda = 0.5$, Sc = 1, and $R = 0.5$

FIGURE 3: Effects of different parameters on temperature profiles.

where $A = \alpha/a$ is the unsteadiness parameter, $\Pr = \nu/\alpha_0$ is the Prandtl number, $\mathrm{Sc} = \nu/D$ is the Schmidt number, and $R = k_0/a$ is the reaction parameter. $\Lambda = \nu(1 - \alpha t)/aK$ is the permeability parameter; $M^2 = \sigma B_0^2(1 - \alpha t)/\rho a$ is the magnetic parameter. The nondimensional temperature and concentration are, respectively, given by $\theta = (T - T_\infty)/(T_w - T_\infty)$ and $\phi = (C - C_\infty)/(C_w - C_\infty)$.

The parameters of engineering interests are the local skin friction and the Nusselt and Sherwood numbers which are defined as

$$C_{fx} = 2\left(1 + \frac{1}{\beta}\right)\mathrm{Re}_x^{-1/2} f''(0). \tag{10}$$

The local Nusselt and Sherwood numbers are defined as

$$\mathrm{Nu}_x = \frac{x}{\alpha_0}\frac{q_w}{(T_w - T_\infty)}, \qquad \mathrm{Sh}_x = \frac{x}{D}\frac{J_w}{(C_w - C_\infty)}, \tag{11}$$

$$q_w = -\alpha_0\left[\frac{\partial T}{\partial y}\right]_{y=0}, \qquad J_w = -D\left[\frac{\partial C}{\partial y}\right]_{y=0}. \tag{12}$$

Using expressions (11) and (6),

$$\mathrm{Nu}_x = -\mathrm{Re}_x^{1/2}\theta'(0), \qquad \mathrm{Sh}_x = -\mathrm{Re}_x^{1/2}\phi'(0), \tag{13}$$

where Re_x is the Reynolds number defined as $\mathrm{Re}_x = U_w x/\nu$. It is important at this stage to mention that the system of equations (8)-(9) reduce to those of Grubka and Bobba [4] when $(1/\beta \to 0)$, $A = \lambda = M = \mathrm{Sc} = 0$. The present problem reduces to that of Grubka and Bobba [4], $A = 0$ denote steady flow, and in their paper they obtained an exact solution in terms of Kummer's functions written in terms of the confluent hypergeometric functions.

The solution of the boundary value problem (8)-(9) was solved using the Runge-Kutta-Fehlberg integration scheme. In the method we choose finite values of $\eta \to \infty$. This value is the boundary layer thickness given by η_∞. We begin by choosing an initial guess of η_∞ to obtain the values $f''(0)$, $-\theta'(0)$, and $-\phi'(0)$. The solution is repeated with new values until two consecutive values differ by 10^{-6}.

3. Results and Discussion

To obtain a clear understanding of the flow of Casson fluid, we discuss the physics of the problem by studying the effects of the unsteadiness (A), permeability (Λ), magnetic (M), Prandtl (Pr), Schmidt (Sc), and reaction rate (R) numbers on velocity, temperature, and concentration profiles. We also study the variation of skin friction, the local Nusselt number, and the Sherwood number with unsteadiness parameter. For validation of the numerical method used in this study, results for the Nusselt number $-\theta(0)$ for the Newtonian fluid were compared to those of Abd El-Aziz [3] and Grubka and Bobba [4] for the unsteadiness parameter $A = \Lambda = M = \mathrm{Sc} = 0$. The comparison is shown in Table 1 and it is found to be in agreement with at least four decimal places. To further verify the accuracy of the numerical scheme used, the successive linearization method (SLM) was used and there was agreement with Runge-Kutta-Fehlberg integration scheme.

To get a clear understanding of the behavior of velocity, temperature, and concentration profiles of Casson fluid, a detailed numerical calculation is done for different parameter values that describe the nature of flow and the results are depicted through Figures 1–5.

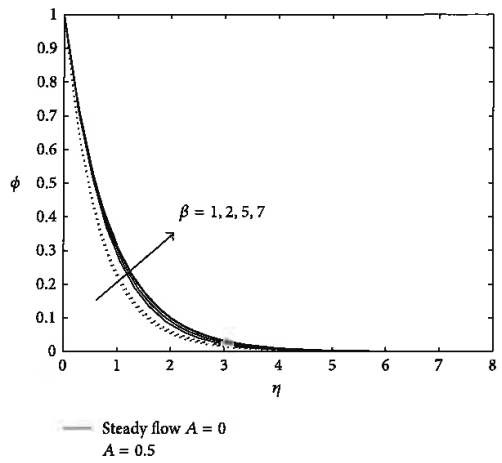

(a) Concentration profiles for different values of the Casson parameter β and unsteadiness parameter A at $\Lambda = 0.5$, $M = 1$, $\Pr = 1$, $\mathrm{Sc} = 1$, and $R = 0.5$

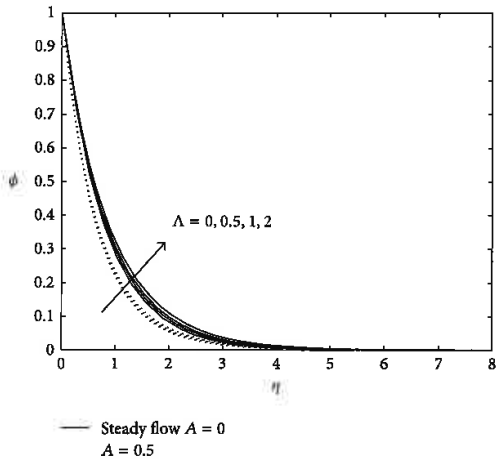

(b) Concentration profiles for different values of the permeability parameter Λ and unsteadiness parameter A at $\beta = 2$, $M = 1$, $\Pr = 1$, $\mathrm{Sc} = 1$, and $R = 0.5$

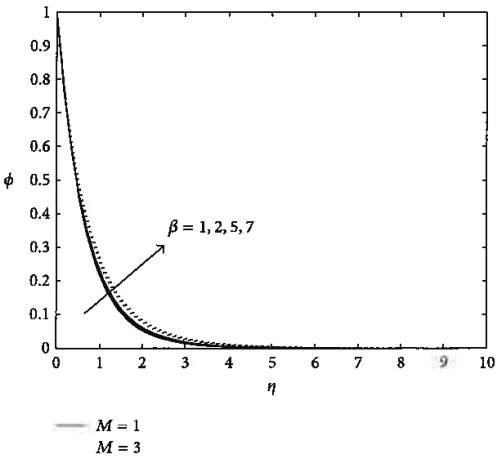

(c) Concentration profiles for different values of the Casson parameter β and magnetic parameter M at $A = 0.5$, $\Lambda = 0.5$, $\Pr = 1$, $\mathrm{Sc} = 1$, and $R = 0.5$

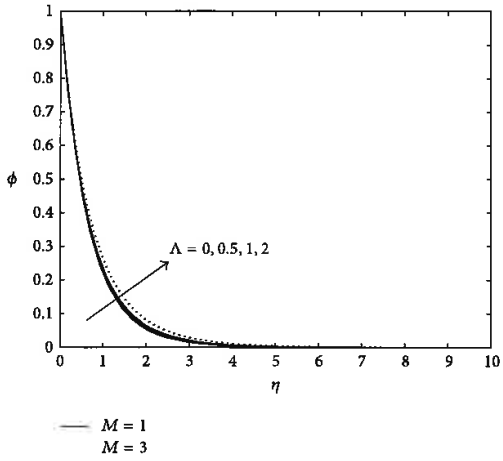

(d) Concentration profiles for different values of the permeability parameter Λ and magnetic parameter M at $A = 0.5$, $\beta = 2$, $\Pr = 1$, $\mathrm{Sc} = 1$, and $R = 0.5$

FIGURE 4: Effects of different parameters on concentration profiles.

TABLE 1: Comparison of the values of $-\theta(0)$ for $\Lambda = M = \mathrm{Sc} = 0$ and various values of A and Pr with previously published data.

A	Pr	Grubka and Bobba [4]	Abd El-Aziz [3]	SLM	Present results
0	0.72	0.8086	0.80873135	0.80873007	0.80863761
	1	1.0000	1.00000000	1.00000000	1.00000006
	3	1.9237	1.92368255	1.92367361	1.92367736
	10	3.7207	3.72067395	3.72066225	3.72066701

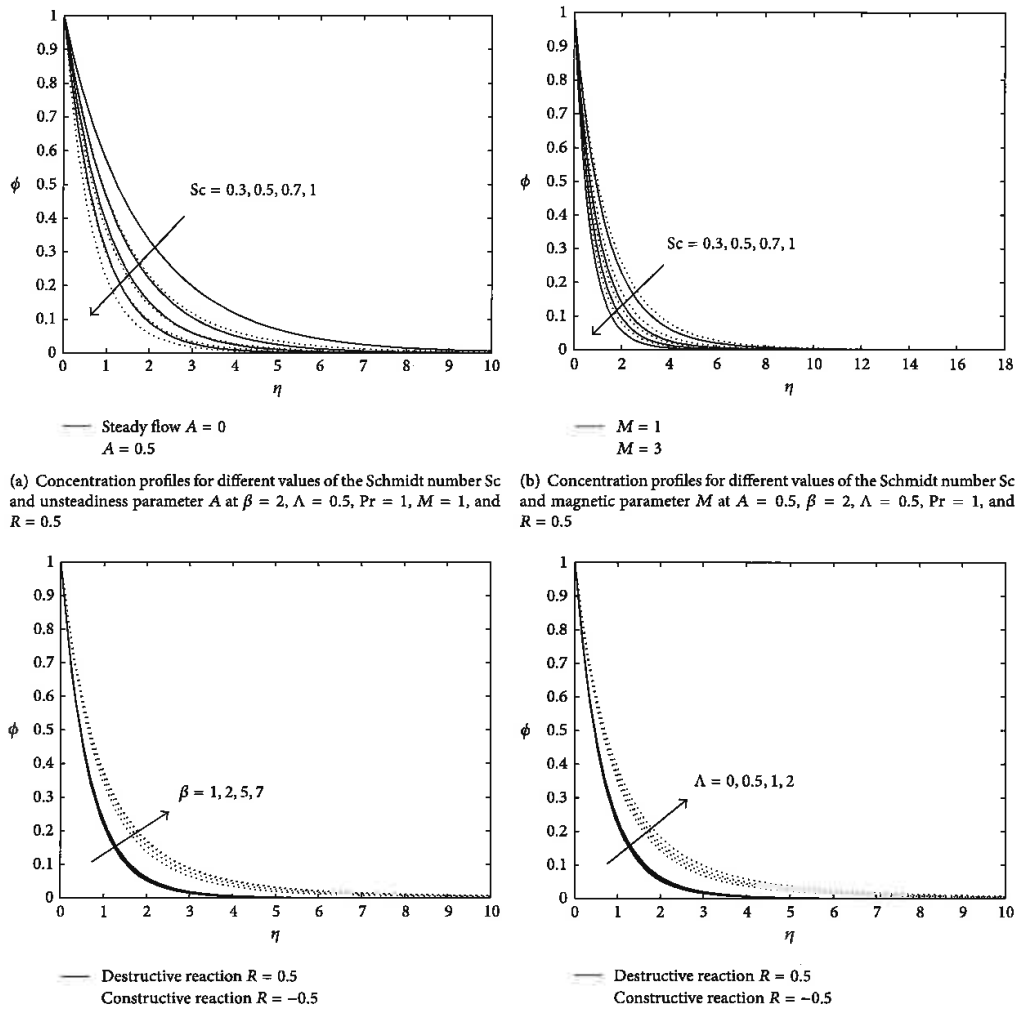

(a) Concentration profiles for different values of the Schmidt number Sc and unsteadiness parameter A at $\beta = 2$, $\Lambda = 0.5$, Pr = 1, $M = 1$, and $R = 0.5$

(b) Concentration profiles for different values of the Schmidt number Sc and magnetic parameter M at $A = 0.5$, $\beta = 2$, $\Lambda = 0.5$, Pr = 1, and $R = 0.5$

(c) Concentration profiles for different values of the Casson parameter β and reaction rate R at $A = 0.5$, $M = 1$, $\Lambda = 0.5$, Pr = 1, and Sc = 1

(d) Concentration profiles for different values of the permeability parameter Λ and reaction rate R at $A = 0.5$, $\beta = 2$, $M = 1$, Pr = 1, and Sc = 1

FIGURE 5: Effects of different parameters on concentration profiles.

Figure 1 shows that increasing the Casson parameter β and the permeability parameter Λ decreases velocity profiles. Both situations retard fluid motion across the boundary layer as shown in Figures 1(a) to 1(d). The velocity profiles for unsteady flow become similar to steady flow far away from the boundary at $\eta > 2$. This indicates that for $A = 0.5$ the flow away from the boundary is steady. Increasing A retards velocity profiles across the boundary layer as shown in Figures 1(a) and 1(b). In Figure 1(b) it is noted that increasing A reduces velocity profiles and the reverse effect is noted around $\eta = 2.5$ indicating slightly steady flow far away from the boundary. A slightly different observation is noted if the magnetic parameter is increased from $M = 1$ to $M = 3$; the velocity profiles decrease significantly reducing the momentum boundary layer thickness as shown in Figures 1(c) and 1(d).

Figure 2 shows the variation of different parameters with temperature profiles. Increasing the Casson parameter increases temperature profiles; this decreases the yield stress. The fluid behaves as Newtonian as β increases; this retards fluid motion. The effect of increasing β leads to enhancing the temperature profiles for both steady and unsteady flows

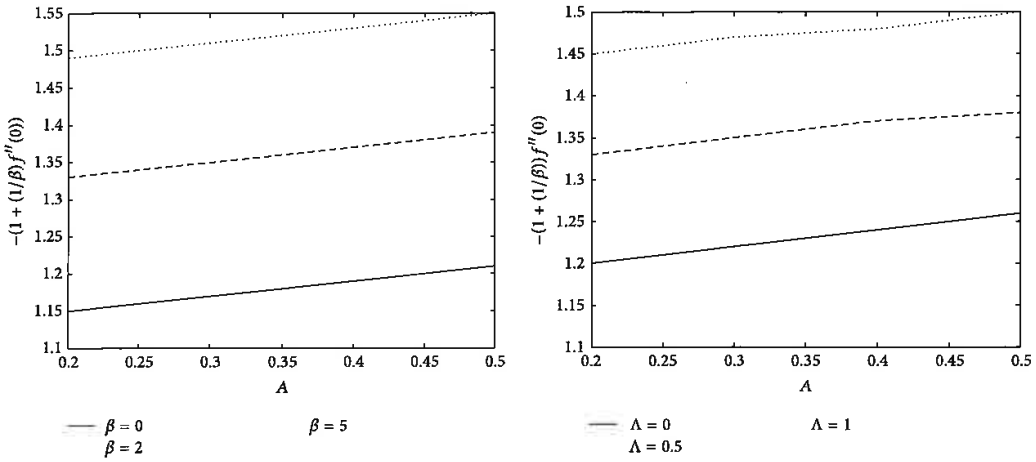

(a) Skin friction versus unsteadiness parameter at different values of the Casson parameter β at $M = 1$, $\Lambda = 0.5$, $\mathrm{Pr} = 1$, $\mathrm{Sc} = 1$, and $R = 0.5$

(b) Skin friction versus unsteadiness parameter at different values of the permeability parameter Λ at $M = 1$, $\beta = 2$, $\mathrm{Pr} = 1$, $\mathrm{Sc} = 1$, and $R = 0.5$

FIGURE 6: Variation of (a) skin friction coefficient with unsteadiness parameter for different β values and (b) with different Λ values.

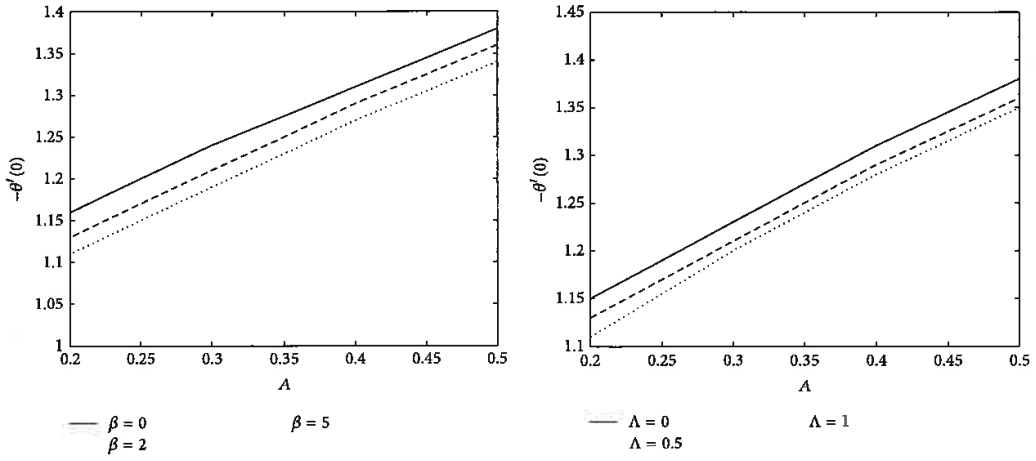

(a) Heat transfer coefficient versus unsteadiness parameter at different values of the Casson parameter β at $M = 1$, $\Lambda = 0.5$, $\mathrm{Pr} = 1$, $\mathrm{Sc} = 1$, and $R = 0.5$

(b) Heat transfer coefficient versus unsteadiness parameter at different values of the permeability parameter Λ at $M = 1$, $\beta = 0.5$, $\mathrm{Pr} = 1$, $\mathrm{Sc} = 1$, and $R = 0.5$

FIGURE 7: Variation of (a) heat transfer coefficient with unsteadiness parameter for different β values and (b) with different Λ values.

as shown in Figure 2(a). The same observation is noted in Figure 2(d). Increasing the permeability parameter Λ enhances temperature profiles. High values of Λ lead to the reduction of fluid velocity enhancing temperature profiles. This effect is more pronounced in steady flow and the thickening of the thermal boundary layer increases as Λ increases. In Figure 2(c) increasing the Prandtl number Pr reduces temperature profiles; Pr is inversely proportional to the thermal diffusivity which is low for Casson fluid. In Figures 2(d), 3(a), and 3(b), increasing M increases temperature profiles; the slowing down of fluid flow leads to the buildup of heat. It is more pronounced in low values of M. Increasing A leads to the reduction of temperature profiles; less heat is transferred from the sheet to the fluid; hence, temperature decreases as depicted in Figures 2(a), 2(b), and 2(c).

In Figure 4, increasing the Casson parameter β results in the increase of the solute concentration; as the fluid

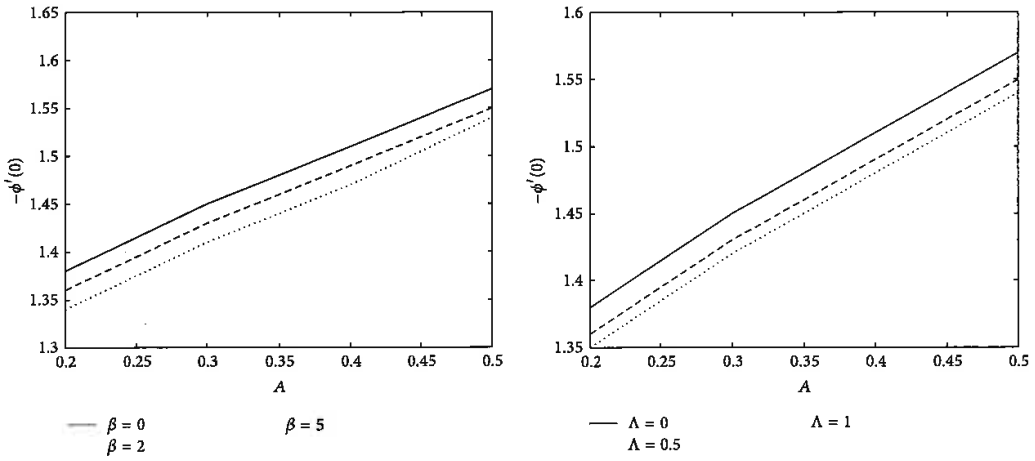

(a) Mass transfer coefficient versus unsteadiness parameter at different values of the Casson parameter β at $M = 1$, $\Lambda = 0.5$, Pr = 1, Sc = 1, and $R = 0.5$

(b) Heat transfer coefficient versus unsteadiness parameter at different values of the permeability parameter Λ at $M = 1$, $\beta = 2$, Pr = 1, Sc = 1, and $R = 0.5$

FIGURE 8: Variation of (a) mass transfer coefficient with unsteadiness parameter for different β values and (b) with different Λ values.

becomes Newtonian, solute transfer is enhanced as shown in Figures 4(a), 4(d), and 5(c). This is more pronounced in steady flow. The opposite effect is noted in increasing A which reduces solute concentration. Increasing Λ increases concentration profiles; since this reduces fluid motion, it leads to the buildup of solute concentration as shown in Figures 4(b), 4(d), and 5(d). Increasing Sc decreases concentration profiles; the diffusion rate is smaller in Casson fluid and hence reducing solute concentration as depicted in Figures 5(a) and 5(b). In Figures 4(c), 4(d), and 5(b), increasing M increases profiles; the slowing down of fluid flow leads to the buildup of mass. It is more pronounced in low values of M.

Figures 5(c) and 5(d) show the effects of reaction rate R on the concentration profiles in Casson fluid in porous medium. Increasing the absolute value of R decreases the concentration profiles. The reaction rate is in general a destructive agent which leads to the reduction of the solute boundary layer. It shows the increase of solute boundary layer in the case of constructive reaction $R < 0$ and the decrease of solute boundary layer in the case of destructive reaction $R > 0$. The effect of increasing β and Λ is more pronounced in unsteady flow.

Figures 6(a) and 6(b) show effects of Casson parameter β and permeability parameter Λ on velocity gradient at the wall with unsteadiness parameter. The magnitude of $f''(0)$ related to skin friction decreases with increasing unsteadiness parameter A and also with Casson parameter β and permeability parameter Λ. The magnitude of the heat transfer rate at the surface $-\theta'(0)$ decreases with increasing β and Λ and increases with A as shown in Figure 7. The mass transfer coefficient at the surface $-\phi'(0)$ decreases with increasing β and Λ and increases with A as shown in Figure 8.

4. Conclusion

The study presented in this analysis of diffusion of chemically reactive species in Casson fluid flow over an unsteady stretching surface in a porous medium in the presence of a magnetic field provides numerical solutions for the boundary layer flow and heat and mass transfer. The coupled nonlinear governing equations were solved using the Runge-Kutta-Fehlberg integration scheme. Increasing the unsteadiness parameter decreases velocity profiles. Increasing the Casson parameter decreases the velocity profiles. The presence of heat transfer does not seem to significantly change the results obtained by Mukhopadhyay and Vajravelu [1]; the main difference is noted in the presence of magnetic and permeability parameters which they did not consider. In this study it is generally noted that increasing the magnetic parameter and permeability parameter decreases the velocity profiles but increases the skin friction; it then decreases the coefficient of heat transfer and the concentration profiles.

Conflict of Interests

The authors declare that there is no conflict of interests regarding the publication of this paper.

References

[1] S. Mukhopadhyay and K. Vajravelu, "Diffusion of chemically reactive species in Casson fluid flow over an unsteady permeable stretching surface," *Journal of Hydrodynamics*, vol. 25, no. 4, pp. 591–598, 2013.

[2] S. Mukhopadhyay, P. R. de, K. Bhattacharyya, and G. C. Layek, "Casson fluid flow over an unsteady stretching surface," *Ain Shams Engineering Journal*, vol. 4, no. 4, pp. 933–938, 2013.

[3] M. Abd El-Aziz, "Mixed convection flow of a micropolar fluid from an unsteady stretching surface with viscous dissipation," *Journal of the Egyptian Mathematical Society*, vol. 21, no. 3, pp. 385–394, 2013.

[4] L. J. Grubka and K. M. Bobba, "Heat transfer characteristics of a continuous stretching surface with variable temperature," *Journal of Heat Transfer*, vol. 107, no. 1, pp. 248–250, 1985.

[5] S. Sharidan, T. Mahmood, and I. Pop, "Similarity solutions for the unsteady boundary layer flow and heat transfer due to a stretching sheet," *International journal of Applied Mechanical Engineering*, vol. 11, pp. 647–654, 2006.

[6] S. Nadeem, R. Ul Haq, and C. Lee, "MHD flow of a Casson fluid over an exponentially shrinking sheet," *Scientia Iranica*, vol. 19, no. 6, pp. 1550–1553, 2012.

[7] S. Nadeem, R. U. Haq, and Z. H. Khan, "Numerical study of MHD boundary layer flow of a Maxwell fluid past a stretching sheet in the presence of nanoparticles," *Journal of the Taiwan Institute of Chemical Engineers*, vol. 45, no. 1, pp. 121–126, 2014.

[8] K. Ahmed and R. Nazar, "Magnetohydrodynamic three dimensional flow and heat transfer over a stretching surface in a viscoelastic fluid," *Journal of Science and Technology*, vol. 3, no. 1, pp. 33–46, 2011.

[9] K. Rohlf and G. Tenti, "The role of the Womersley number in pulsatile blood flow a theoretical study of the Casson model," *Journal of Biomechanics*, vol. 34, no. 1, pp. 141–148, 2001.

[10] D. S. Sankar and U. Lee, "Two-fluid non-linear model for flow in catheterized blood vessels," *International Journal of Non-Linear Mechanics*, vol. 43, no. 7, pp. 622–631, 2008.

[11] D. S. Sankar and U. Lee, "Two-fluid Casson model for pulsatile blood flow through stenosed arteries: a theoretical model," *Communications in Nonlinear Science and Numerical Simulation*, vol. 15, no. 8, pp. 2086–2097, 2010.

[12] S. Shaw, R. S. R. Gorla, P. V. S. N. Murthy, and C.-O. Ng, "Pulsatile casson fluid flow through a stenosed bifurcated artery," *International Journal of Fluid Mechanics Research*, vol. 36, no. 1, pp. 43–63, 2009.

[13] A. V. Mernone, J. N. Mazumdar, and S. K. Lucas, "A mathematical study of peristaltic transport of a Casson fluid," *Mathematical and Computer Modelling*, vol. 35, no. 7-8, pp. 895–912, 2002.

[14] B. Das and R. L. Batra, "Secondary flow of a Casson fluid in a slightly curved tube," *International Journal of Non-Linear Mechanics*, vol. 28, no. 5, pp. 567–577, 1993.

[15] C.-O. Ng, "Combined pressure-driven and electroosmotic flow of Casson fluid through a slit microchannel," *Journal of Non-Newtonian Fluid Mechanics*, vol. 198, pp. 1–9, 2013.

[16] S. Nadeem, R. Ul Haq, N. S. Akbar, and Z. H. Khan, "MHD three-dimensional Casson fluid flow past a porous linearly stretching sheet," *Alexandria Engineering Journal*, vol. 52, no. 4, pp. 577–582, 2013.

[17] R. K. Dash, K. N. Mehta, and G. Jayaraman, "Casson fluid flow in a pipe filled with a homogeneous porous medium," *International Journal of Engineering Science*, vol. 34, no. 10, pp. 1145–1156, 1996.

[18] D. Tripathi, "Study of transient peristaltic heat flow through a finite porous channel," *Mathematical and Computer Modelling*, vol. 57, no. 5-6, pp. 1270–1283, 2013.

[19] S. Pramanik, "Casson fluid flow and heat transfer past an exponentially porous stretching surface in presence of thermal radiation," *Ain Shams Engineering Journal*, vol. 5, no. 1, pp. 205–212, 2014.

[20] P. V. Ramachandra, R. A. Subba, and B. O. Anwa, "Flow and heat transfer of casson fluid from a horizontal cylinder with partial slip in non-darcy porous medium," *Applied and computational Mathematics*, vol. 2, article 2, 2013.

[21] P. K. Kameswaran, S. Shaw, P. Sibanda, and P. V. S. N. Murthy, "Homogeneous-heterogeneous reactions in a nanofluid flow due to a porous stretching sheet," *International Journal of Heat and Mass Transfer*, vol. 57, no. 2, pp. 465–472, 2013.

[22] S. Shaw, P. K. Kameswaran, and P. Sibanda, "Homogeneous-heterogeneous reactions in micropolar fluid flow from a permeable stretching or shrinking sheet in a porous medium," *Boundary Value Problems*, vol. 2013, article 77, 2013.

[23] A. J. Chamkha, A. M. Aly, and M. A. Mansour, "Similarity solution for unsteady heat and mass transfer from a stretching surface embedded in a porous medium with suction/injection and chemical reaction effects," *Chemical Engineering Communications*, vol. 197, no. 6, pp. 846–858, 2010.

[24] G. Makanda, O. D. Makinde, and P. Sibanda, "Natural convection of viscoelastic fluid from a cone embedded in a porous medium with viscous dissipation," *Mathematical Problems in Engineering*, vol. 2013, Article ID 934712, 11 pages, 2013.

Appendix D

Makanda et al. *Boundary Value Problems* (2015) 2015:75
DOI 10.1186/s13661-015-0333-5

Boundary Value Problems
a SpringerOpen Journal

RESEARCH Open Access

Effects of radiation on MHD free convection of a Casson fluid from a horizontal circular cylinder with partial slip in non-Darcy porous medium with viscous dissipation

Gilbert Makanda*, Sachin Shaw and Precious Sibanda

*Correspondence:
gilbertmakanda@yahoo.com
School of Mathematics, Statistics and Computer Science, University of KwaZulu-Natal, Private Bag X01, Scottsville, Pietermaritzburg, 3209, South Africa

Abstract

In the present study, the effects of radiation on MHD free convection from a cylinder with partial slip in a Casson fluid in non-Darcy porous medium is investigated. The surface of the cylinder is heated under constant surface temperature with partial slip. Partial slip factors are considered on the surface for both velocity and temperature. The boundary layer equations are normalized into a system of non-similar partial differential equations and are then solved using a bi-variate quasilinearization method (BQLM). The boundary layer velocity and temperature profiles are computed for different values of the physical parameters. Increasing the Forchheimer parameter decreases the temperature profiles. The decrease of the velocity profiles with the increase in magnetic parameter is more enhanced in the presence of the velocity slip factor. Increasing the Eckert number increases the temperature profiles in both suction and blowing cases. This study considers the unique problem of the effect of transpiration in a Casson fluid in the presence of radiation, a magnetic field, and viscous dissipation. The results obtained in this study are compared with other numerical methods and were found to be in excellent agreement.

Keywords: Casson fluid; partial slip; viscous dissipation; bi-variate quasilinearization method

1 Introduction

The flow of non-Newtonian fluids is applied in many situations in industry such as processing of materials and chemical engineering. These fluids show different characteristics from the Newtonian fluids which cannot be fully represented by the Navier-Stokes equations. To represent these non-Newtonian fluids some modifications to the Navier-Stokes equations are used and these are seen in many research works which studied viscoelastic and micropolar fluids [1, 2]. These fluids are categorized as viscoelastic, thixotropic, and power-law fluids. The constitutive equations of such fluids cannot fully represent the actual behavior of these fluids. These fluids include contaminated lubricants, molten metal, synovial fluids, *etc.*

The study of radiation effects on MHD free convection of a Casson fluid in porous medium with partial slip is an important aspect due to its practical application in the

design of automatic cooking machines and the design of internal engine parts in mechanical engineering. Other examples arise in petroleum production, multiphase mixtures, pharmaceutical formulations, coal in water, paints, lubricants, jams, sewage, soup, blood. There has been a significant improvement in the study of non-Newtonian fluids in which many different situations have been considered. Studies in a Casson fluid include work by among others Mukhopadhyay *et al.* [3] and Nadeem *et al.* [4].

Several research workers have studied radiation effects, these include Kameswaran *et al.* [5] who studied radiation effects on hydromagnetic Newtonian liquid flow due to an exponentially stretching sheet. They studied radiation effects in the presence of a magnetic field, advancing the studies of radiation effects in Newtonian fluids. Shateyi and Marewo [6] investigated numerical analysis of MHD stagnation point flow of a Casson fluid, they considered thermal radiation in their work. Chamkha *et al.* [7] studied thermal radiation effects on MHD forced convection flow adjacent to a non-isothermal wedge in the presence of a heat source or sink. Pramanik [8] studied Casson fluid flow and heat transfer past an exponentially porous stretching surface in the presence of thermal radiation.

The study of fluid flow in the presence of a magnetic fluid has also been performed by many authors, among others Ece [9], who investigated free convection flow about a cone under mixed thermal boundary conditions and a magnetic field. Narayana *et al.* [10] studied free magnetohydrodynamic flow and convection from a vertical spinning cone with cross diffusion effects. Nadeem *et al.* [11] studied numerically MHD boundary layer flow of a Maxwell fluid past a stretching sheet in the presence of nanoparticles. Chen [12] investigated the combined heat and mass transfer in MHD free convection from a vertical surface with ohmic heating and viscous dissipation.

The study of fluid flow past a cylindrical geometry was performed by among others Anwa *et al.* [13], who studied mixed convection boundary layer flow of a viscoelastic fluid over a horizontal cylinder. Deka *et al.* [14] investigated transient free convection flow past an accelerated vertical cylinder in a rotating cylinder. Ribeiro *et al.* [15] studied viscoelastic flow past a confined cylinder with three dimensional effects and stability. Patel and Chhabra [16] studied steady flow of Bingham plastic fluids past an elliptical cylinder.

Studies in porous media and viscous dissipation have been carried out by among others, Awad *et al.* [17] who studied natural convection of viscoelastic fluid from a cone embedded in a porous medium with viscous dissipation. Awad *et al.* [17] investigated convection from an inverted cone in a porous medium with cross diffusion effects. Hayat *et al.* [18] studied heat and mass transfer for Soret and Dufour effects on mixed convection boundary layer flow over a stretching vertical surface in a porous medium filled with a viscoelastic fluid. Cheng [19] studied Soret and Dufour effects on free convection boundary layer over a vertical cylinder in a saturated porous medium. Chamkha and Rashad [20] investigated natural convection from a vertical permeable cone in nanofluid saturated porous media for uniform heat and nanoparticles volume fraction fluxes.

In this study we investigate the effects of radiation in MHD free convection of a Casson fluid from a horizontal circular cylinder with partial slip in non-Darcy porous medium with viscous dissipation. The surface of the cylinder is perforated in which we have the effects of transpiration which acts transversely in the direction ξ. The force which causes transpiration is sometimes called the Forchheimer drag force term $-\xi \Lambda f'^2$, which appears in the momentum equation (12). This term is also associated with the geometry of the porous medium. In this work we extended the work of Ramachandra *et al.* [1] in which we

introduced magnetic field, radiation effects and viscous dissipation. We also solved the system of the resulting partial differential equations by the bi-variate quasilinearization method (BQLM). The method is described in detail in Motsa *et al.* [21]. We study the effects of the magnetic field, radiation. and the Eckert number on velocity and temperature profiles for different values of the Casson parameter β, the local inertia (Forchheimer parameter) Λ, and the Darcian drag force coefficient Λ_1. The results of this work are validated by comparison with other methods, which are the successive linearization method (SLM) and MATLAB's routine 'bvp4c'.

2 Mathematical formulation

The steady, laminar, two dimensional MHD free convection of a Casson fluid flow from a horizontal circular cylinder with partial slip in a non-Darcy porous medium, with viscous dissipation and radiation effects, is considered. The fluid is maintained at a uniform temperature T_w ($> T_\infty$), the transpiration velocity V_w is in the direction ξ. x is the tangential coordinate of the circle and y is the radial coordinate of the circle. u and v are the velocity components in the x and y directions, respectively, as shown in Figure 1.

The rheological equation of state for an isotropic and incompressible flow of a Casson fluid is given as in [1–3] by

$$\tau_{ij} = \begin{cases} 2(\mu_B + \frac{P_y}{\sqrt{2\pi}})e_{ij}, & \pi > \pi_c, \\ 2(\mu_B + \frac{P_y}{\sqrt{2\pi_c}})e_{ij}, & \pi < \pi_c, \end{cases} \tag{1}$$

$\pi = e_{ij}e_{ij}$ and e_{ij} is the (i,j)th component of the deformation rate, π is the product of the deformation rate with itself, π_c is a critical value of this product based on the non-Newtonian model, μ_B is the plastic dynamic viscosity of the non-Newtonian fluid, P_y is the yield stress of the fluid.

The governing equations in this flow are given as

$$\frac{\partial}{\partial x}(ru) + \frac{\partial}{\partial y}(rv) = 0, \tag{2}$$

$$u\frac{\partial u}{\partial x} + v\frac{\partial u}{\partial y} = \nu\left(1+\frac{1}{\beta}\right)\frac{\partial^2 u}{\partial y^2} + \bar{g}\beta_T(T-T_\infty)\sin\left(\frac{x}{a}\right) - \Gamma u^2 - \frac{\nu}{\bar{K}}u - \frac{\sigma B_0^2}{\rho}u, \tag{3}$$

$$u\frac{\partial T}{\partial x} + v\frac{\partial T}{\partial y} = \alpha\frac{\partial^2 T}{\partial y^2} - \frac{1}{\rho C_p}\frac{\partial q_r}{\partial y} + \frac{\nu}{\rho C_p}\left(1+\frac{1}{\beta}\right)\left(\frac{\partial u}{\partial y}\right)^2 + \frac{\sigma B_0^2 u^2}{\rho C_p}, \tag{4}$$

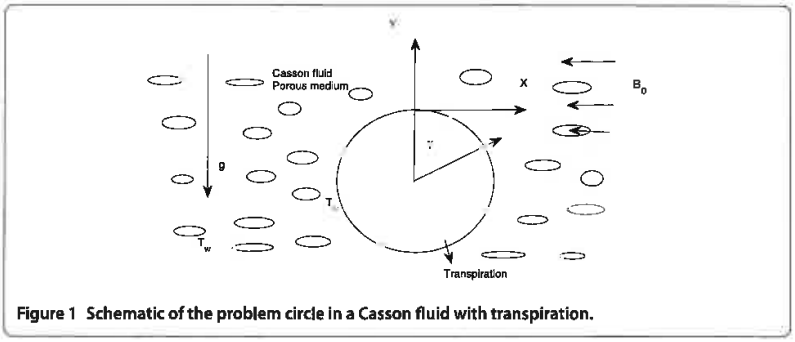

Figure 1 Schematic of the problem circle in a Casson fluid with transpiration.

where u and v are the velocity components in the x and y directions, respectively, a is the radius of the cylinder, ν is the kinematic viscosity of the Casson fluid, $\beta = \mu_B\sqrt{2\pi_c}/P_y$ is the non-Newtonian Casson parameter, $\alpha = \kappa/\rho C_p$ is the thermal diffusivity, κ is thermal conductivity of the fluid, q_r is the radiative heat flux, C_p is the specific heat, $\bar{g}$ is the acceleration due to gravity, β_T is the coefficient of thermal expansions, and T is the temperature of the fluid. T_∞ is the free stream temperature, ρ is the fluid density, $\bar{K}$ and Γ are the permeability and inertia coefficients respectively. σ is the electric conductivity and B_0 is the magnetic flux density. The Rosseland approximation for radiation may be written as follows:

$$q_r = -\frac{4\sigma^*}{3k^*}\frac{\partial T^4}{\partial y}, \tag{5}$$

where σ^* is the Stefan-Boltzmann constant and k^* is the absorption coefficient. If the temperature difference within the flow is such that T^4 may be expanded in a Taylor series about T_∞ and neglecting higher powers, we obtain $T^4 - 4T_\infty^3 - 3T_\infty^4$ and therefore (4) can be written as

$$u\frac{\partial T}{\partial x} + v\frac{\partial T}{\partial y} = \alpha\frac{\partial^2 T}{\partial y^2} + \frac{16\sigma^* T_\infty^3}{3\rho C_p k^*}\frac{\partial^2 T}{\partial y^2} + \frac{\nu}{\rho C_p}\left(1+\frac{1}{\beta}\right)\left(\frac{\partial u}{\partial y}\right)^2 + \frac{\sigma B_0^2 u^2}{\rho C_p}. \tag{6}$$

The boundary conditions are given as

$$u = N_0\left(1+\frac{1}{\beta}\right)\frac{\partial u}{\partial y}, \qquad v = -V_w, \qquad T = T_w + K_0\frac{\partial T}{\partial Y}, \qquad y = 0, \tag{7}$$

$$u \to 0, \qquad T \to T_\infty, \quad \text{as } y \to \infty, \tag{8}$$

where N_0 is the velocity slip factor, K_0 is the thermal slip factor. $N_0 = K_0 = 0$ corresponds to no-slip conditions. The subscripts w and ∞ refer to surface and ambient conditions, respectively.

We introduce the non-dimensional variables

$$\left.\begin{aligned} &\xi = \frac{x}{a}, \qquad \eta = \frac{y}{a}Gr^{\frac{1}{4}}, \qquad Pr = \frac{\nu}{\alpha}, \\ &Gr = \frac{g\beta_T(T_w - T_\infty)a^3}{\nu^2}, \qquad \beta_c = \mu_B\frac{\sqrt{2\pi_c}}{P_y}, \\ &\Lambda = \Gamma a, \qquad \Lambda_1 = \frac{1}{DaGr^{\frac{1}{2}}}, \qquad Da = \frac{\bar{K}}{a^2}, \qquad f_w = -\frac{V_w a}{\nu Gr^{\frac{1}{4}}}, \qquad U_0 = \frac{\nu Gr^{\frac{1}{2}}}{a}. \end{aligned}\right\} \tag{9}$$

Introducing the stream function ψ and similarity variables

$$u = \frac{\partial\psi}{\partial y} \quad \text{and} \quad v = -\frac{\partial\psi}{\partial x}, \tag{10}$$

$$f(\xi,\eta) = \frac{\psi}{\nu\xi Gr^{\frac{1}{4}}}, \qquad \theta(\xi,\eta) = \frac{T - T_\infty}{T_w - T_\infty}, \tag{11}$$

using the stream function defined in (10) and the similarity variable in (11), (2)-(6) together with the boundary conditions (7) and (8) reduce to the following system of partial

differential equations:

$$\left(1+\frac{1}{\beta}\right)f'''+ff''-(1+\Lambda\xi)f'^2-\left(\Lambda_1+M^2\right)f'+\frac{\sin(\xi)}{\xi}\theta=\xi\left(f'\frac{\partial f'}{\partial\xi}-f''\frac{\partial f}{\partial\xi}\right), \tag{12}$$

$$\frac{1}{Pr}\left(1+\frac{4}{3}K\right)\theta''+f\theta'+\xi^2Ec\left[\left(1+\frac{1}{\beta}\right)f''^2+M^2\left(f'\right)^2\right]=\xi\left(f'\frac{\partial\theta}{\partial\xi}-\theta'\frac{\partial f}{\partial\xi}\right) \tag{13}$$

with boundary conditions

$$\eta=0,\qquad f=f_w,\qquad f'=\left(1+\frac{1}{\beta}\right)S_f f'',\qquad \theta=1+S_T\theta', \tag{14}$$

$$\eta\to\infty,\qquad f'\to 0,\qquad \theta\to 0, \tag{15}$$

where β is the Casson parameter, Λ is the Forchheimer parameter, Λ_1 is the Darcian drag coefficient, M is the magnetic field parameter, K is the radiation parameter, Pr is the Prandtl number, Ec is the Eckert number, $f_w > 0$ corresponds to suction, and $f_w < 0$ corresponds to blowing, $S_f = N_0 Gr^{\frac{1}{4}}/L$ is the velocity slip factor, and $S_T = kGr^{\frac{1}{4}}/L$ is the thermal slip factor. In the above equations the primes refer to the derivative with respect to η. The engineering parameters of interest are the local skin friction and the local Nusselt numbers, which are defined as follows.

The shear stress at the surface of the cone is given by

$$\tau_w=\mu\left[\left(1+\frac{1}{\beta}\right)\frac{\partial u}{\partial y}\right]_{y=0}=\frac{\mu(1+\frac{1}{\beta})\nu\xi Gr^{\frac{3}{4}}}{a^2}f''(0), \tag{16}$$

where μ is the coefficient of viscosity. The skin friction coefficient is given by

$$C_f=\frac{\tau_w}{\frac{1}{2}\rho U_0^2}. \tag{17}$$

Using (16) and (17) together with (10) and (11) give

$$C_f Gr^{-\frac{3}{4}}=\left(1+\frac{1}{\beta}\right)\xi f''(0). \tag{18}$$

The heat transfer from the surface of the circle into the fluid is given by

$$q_w=-k\left[\frac{\partial T}{\partial y}\right]_{y=0}=\frac{-k(T_w-T_\infty)}{aGr^{-\frac{1}{4}}}X\theta'(0), \tag{19}$$

k is the thermal conductivity of the fluid. The Nusselt number under LST is given by

$$Nu=\frac{a}{k}\frac{q_w}{T_w-T_\infty}. \tag{20}$$

Equations (19) and (20) together with (10) and (11) give

$$NuGr^{-\frac{1}{4}}=-\theta'(0). \tag{21}$$

3 Solution method

In this section we describe the implementation of the bi-variate quasilinearization method (BQLM) which is based on the quasilinearization method (QLM) which is described in detail in Motsa *et al.* [21]. We apply the quasilinearization method (QLM) first proposed by Bellman and Kalaba [22] to (12)-(13), which is based on the Taylor series expansion with the assumption that the differences $(f_{r+1} - f_r)$, $(\theta_{r+1} - \theta_r)$, and all the derivatives are small. We obtain the following equations:

$$\left(1+\frac{1}{\beta}\right)f'''_{r+1} + a_{1,r}(\eta,\xi)f''_{r+1} + a_{2,r}(\eta,\xi)f'_{r+1} + a_{3,r}(\eta,\xi)f_{r+1} + a_{4,r}(\eta,\xi)\frac{\partial f'_{r+1}}{\partial \xi} + a_{5,r}(\eta,\xi)\frac{\partial f_{r+1}}{\partial \xi} = a_{6,r}(\eta,\xi), \tag{22}$$

$$\frac{1}{Pr}\left(1+\frac{4}{3}K\right)\theta''_{r+1} + b_{1,r}(\eta,\xi)\theta'_{r+1} + b_{2,r}(\eta,\xi)\frac{\partial \theta_{r+1}}{\partial \xi} = b_{3,r}(\eta,\xi), \tag{23}$$

where

$$a_{1,r} = f_r + \xi\frac{\partial f_r}{\partial \xi}, \tag{24}$$

$$a_{2,r} = -\left[2(1+\Lambda\xi)f'_r + \Lambda_1 + M^2 + \xi\frac{\partial f'_r}{\partial \xi}\right], \tag{25}$$

$$a_{3,r} = f''_r, \tag{26}$$

$$a_{4,r} = -\xi f'_r, \tag{27}$$

$$a_{5,r} = \xi f''_r, \tag{28}$$

$$a_{6,r} = f_r f''_r - (1+\Lambda\xi)(f'_r)^2 - \frac{\sin\xi}{\xi}\theta_r - \xi\left(\frac{\partial f'_r}{\partial \xi} - f''_r\frac{\partial f_r}{\partial \xi}\right), \tag{29}$$

$$b_{1,r} = f_r + \xi\frac{\partial f_r}{\partial \xi}, \tag{30}$$

$$b_{2,r} = -\xi f', \tag{31}$$

$$b_{3,r} = -Ec\xi^2\left[\left(1+\frac{1}{\beta}\right)(f''_r)^2 + M^2(f'_r)^2\right]. \tag{32}$$

The solution for the now linear partial differential equations (22)-(23) is obtained by approximating the exact solutions of $f(\eta,\xi)$ and $\theta(\eta,\xi)$ by the Lagrange form of polynomial $F(\eta,\xi)$ and $\Theta(\eta,\xi)$ at the selected collocation points,

$$0 = \xi_0 < \xi_1 < \xi_2 < \cdots < \xi_{N_\xi} = 1.$$

The approximation for $f(\eta,\xi)$ and $\theta(\eta,\xi)$ has the form

$$f(\eta,\xi) \approx \sum_{j=0}^{N_\xi} F(\eta,\xi)L_j(\xi) = \sum_{j=0}^{N_\xi} F_j(\eta)L_j(\xi), \tag{33}$$

$$\theta(\eta,\xi) \approx \sum_{j=0}^{N_\xi} \Theta(\eta,\xi)L_j(\xi) = \sum_{j=0}^{N_\xi} \Theta_j(\eta)L_j(\xi), \tag{34}$$

where $F_j(\eta) = F(\eta, \xi)$ and $\Theta_j(\eta) = \Theta(\eta, \xi)$, L_j is the characteristic Lagrange cardinal polynomial defined as

$$L_j(\xi) = \prod_{k=0, k\neq j}^{M} \frac{\xi - \xi_k}{\xi_j - \xi_k}, \tag{35}$$

which obey the Kronecker delta equation

$$L_j(\xi_k) = \delta_{jk} = \begin{cases} 0 & \text{if } j \neq k, \\ 1 & \text{if } j = k. \end{cases} \tag{36}$$

The equations for the solution of $F_j(\eta)$ and $\Theta_j(\eta)$ are obtained by substituting (33)-(34) into (22)-(23) and letting the equations be satisfied at the points ξ_i, $i = 0, 1, 2, \ldots, N_\xi$. To compute the derivatives of the Lagrange polynomial analytically we transform $\xi \in [0, L_\xi]$ to $\zeta \in [-1, 1]$, and then we choose Chebyshev-Gauss-Lobatto points $\zeta_i = \cos \frac{i\pi}{N_\xi}$. After using the linear transformation $\xi = L_\xi(\zeta + 1)/2$, the derivatives of f' with respect to the collocation points ζ_j are computed as

$$\left.\frac{\partial f'}{\partial \xi}\right|_{\xi=\xi_i} = 2\sum_{j=0}^{N_\xi} F'_j(\eta)\frac{dL_j}{d\zeta}(\zeta_i) = \sum_{j=0}^{N_\xi} \mathbf{d}_{i,j} F'_j(\eta), \quad i = 0, 1, 2, \ldots, N_\xi, \tag{37}$$

where $\mathbf{d}_{i,j} = \frac{dL_j}{d\zeta}(\zeta_i)$ $(i = 0, 1, \ldots, N_\xi)$ are entries of the standard Chebyshev differentiation matrix, $\mathbf{d} = \frac{2}{L_\xi} d$. We now apply the collocation (η, ξ_i) in (22)-(23) we obtain

$$\begin{aligned} &\left(1 + \frac{1}{\beta}\right) F'''_{r+1,i}(\eta) + a^{(i)}_{1,r} F''_{r+1,i}(\eta) + a^{(i)}_{2,r} F'_{r+1,i}(\eta) + a^{(i)}_{3,r} F_{r+1,i}(\eta) \\ &\quad + a^{(i)}_{4,r} \sum_{j=0}^{N_\xi} \mathbf{d}_{i,j} F'_{r+1,i}(\eta) + a^{(i)}_{5,r} \sum_{j=0}^{N_\xi} \mathbf{d}_{i,j} F_{r+1,i}(\eta) = a^{(i)}_{6,r}, \end{aligned} \tag{38}$$

$$\frac{1}{Pr}\left(1 + \frac{4}{3}K\right)\Theta''_{r+1,i}(\eta) + b^{(i)}_{1,r}\Theta'_{r+1,i}(\eta) + b^{(i)}_{2,r}\sum_{j=0}^{N_\xi} \mathbf{d}_{i,j}\Theta_{r+1,i}(\eta) = b^{(i)}_{3,r}, \tag{39}$$

where $a^{(i)}_{k,r} = a_{k,r}(\eta, \xi_i)$ $(k = 1, 2, 3, 4, 5, 6)$ and $b^{(i)}_{k,r} = b_{k,r}(\eta, \xi_i)$ $(k = 1, 2, 3)$. Since the solution at $\xi = 0$ $(\zeta = \zeta_{N_\xi})$ is known, we evaluate (38)-(39) for $i = 0, 1, \ldots, N_\xi - 1$ and the system becomes

$$\begin{aligned} &\left(1 + \frac{1}{\beta}\right) F'''_{r+1,i} + a^{(i)}_{1,r} F''_{r+1,i} + a^{(i)}_{2,r} F'_{r+1,i} + a^{(i)}_{3,r} F_{r+1,i} + a^{(i)}_{4,r} \sum_{j=0}^{N_\xi - 1} \mathbf{d}_{i,j} F'_{r+1,i} \\ &\quad + a^{(i)}_{5,r} \sum_{j=0}^{N_\xi - 1} \mathbf{d}_{i,j} F_{r+1,i} = a^{(i)}_{6,r} - a^{(i)}_{4,r} \mathbf{d}_{i,N_\xi} F'_{r+1,N_\xi} - a^{(i)}_{5,r} \mathbf{d}_{i,N_\xi} F_{r+1,N_\xi}, \end{aligned} \tag{40}$$

$$\begin{aligned} &\frac{1}{Pr}\left(1 + \frac{4}{3}K\right)\Theta''_{r+1,i} + b^{(i)}_{1,r}\Theta'_{r+1,i} + b^{(i)}_{2,r}\sum_{j=0}^{N_\xi - 1} \mathbf{d}_{i,j}\Theta_{r+1,i} \\ &\quad = b^{(i)}_{3,r} - b^{(i)}_{2,r}\mathbf{d}_{i,N_\xi}\Theta_{r+1,N_\xi}. \end{aligned} \tag{41}$$

For each ξ_i, (40)-(41) forms a system of linear ordinary differential equations with variable coefficients. In this system we apply the Chebyshev spectral collocation independently in the η direction by choosing $N_\eta + 1$ Chebyshev-Gauss-Lobatto points $0 = \eta_0 < \eta_1 < \eta_2 < \cdots < \eta_{N_\eta} = \eta_e$, where η_e is a finite value that is chosen to be adequately large to approximate the conditions at ∞. We now implement the collocation in the interval $[0, \eta_e]$ on the η-axis, which is then transformed into the interval $[-1, 1]$ using a linear transformation $\eta = \eta_e(\tau + 1)/2$. The collocation points are chosen as $\tau_j = \cos\frac{j\pi}{N_\eta}$. The derivatives with respect to η are defined in terms of the Chebyshev differentiation matrix as

$$\left.\frac{d^p F'_{r+1,i}}{d\eta^p}\right|_{\eta=\eta_j} = \left(\frac{2}{\eta_e}\right)^p \sum_{k=0}^{N_\eta} D^p_{j,k} F_{r+1,i}(\tau_k) = \left[\mathbf{D}^p \mathbf{F}_{r+1,i}\right]_j, \tag{42}$$

where p is the order of the derivative, $\mathbf{D} = \frac{2}{\eta_e} D$ $(j, k = 0, 1, 2, \ldots, N_\eta)$ with D being an $(N_\eta + 1) \times (N_\eta + 1)$ Chebyshev derivative matrix, and the vector $\mathbf{F}_{r+1,i}$ is defined as

$$\mathbf{F}_{r+1,i} = \left[F_{r+1,1}(\tau_0), F_{r+1,1}(\tau_1), \ldots, F_{r+1,1}(\tau_{N_\eta})\right]^T, \tag{43}$$

$$\mathbf{\Theta}_{r+1,i} = \left[\Theta_{r+1,i}(\tau_0), \Theta_{r+1,i}(\tau_1), \ldots, \Theta_{r+1,i}(\tau_{N_\eta})\right]^T, \tag{44}$$

substituting (42) into (40) we get

$$\mathbf{A}^{(i)}\mathbf{F}_{r+1,i} + \mathbf{a}^{(i)}_{4,r} \sum_{j=0}^{N_\xi - 1} d_{i,j}\mathbf{D}\mathbf{F}_{r+1,j} + \mathbf{a}^{(i)}_{5,r} \sum_{j=0}^{N_\xi - 1} d_{i,j}\mathbf{F}_{r+1,j} = R^{(i)}_1, \tag{45}$$

$$\mathbf{A}^{(i)} = \left(1 + \frac{1}{\beta}\right)\mathbf{D}^3 + \mathbf{a}^{(i)}_{1,r}\mathbf{D}^2 + a^{(i)}_{2,r}\mathbf{D} + \mathbf{a}^{(i)}_{2,r}, \tag{46}$$

$$\mathbf{R}^{(i)}_1 = \mathbf{a}^{(i)}_{6,r} - \mathbf{a}^{(i)}_{4,r} d_{i,N_\xi}\mathbf{D}\mathbf{F}_{r+1,N_\xi} - \mathbf{a}^{(i)}_{5,r} d_{i,N_\xi}\mathbf{F}_{r+1,N_\xi} \tag{47}$$

$$\mathbf{B}^{(i)}\mathbf{\Theta}_{r+1,i} + \mathbf{b}^{(i)}_{2,r} \sum_{j=0}^{N_\xi - 1} d_{i,j}\mathbf{\Theta}_{r+1,j} = R^{(i)}_2, \tag{48}$$

$$\mathbf{B}^{(i)} = \frac{1}{Pr}\left(1 + \frac{4}{3}K\right)\mathbf{D}^2 + \mathbf{b}^{(i)}_{1,r}\mathbf{D}, \tag{49}$$

$$\mathbf{R}^{(i)}_2 = \mathbf{b}^{(i)}_{3,r} - \mathbf{b}^{(i)}_{2,r} d_{i,N_\xi}\mathbf{\Theta}_{r+1,N_\xi}. \tag{50}$$

$\mathbf{a}_{k,r}$ $(k = 1, 2, 3, 4, 5, 6)$, $\mathbf{b}_{k,r}$ $(k = 1, 2, 3)$ are the diagonal matrices with vectors $[a_{k,r}(\tau_0), a_{k,r}(\tau_1), \ldots, a_{k,r}(\tau_{N_x})]^T$ and $[b_{k,r}(\tau_0), b_{k,r}(\tau_1), \ldots, b_{k,r}(\tau_{N_x})]^T$. We then impose boundary conditions and a matrix system is formed as follows:

$$\mathbf{AA} = \left(\begin{array}{cccc|cccc} A_{0,0} & A_{0,1} & \cdots & A_{0,N_\xi-1} & 0 & 0 & \cdots & 0 \\ A_{1,0} & A_{1,1} & \cdots & A_{1,N_\xi-1} & 0 & 0 & \cdots & 0 \\ \vdots & \vdots & \ddots & \vdots & \vdots & \vdots & \ddots & \vdots \\ A_{N_\xi-1,0} & A_{N_\xi-1,1} & \cdots & A_{N_\xi-1,N_\xi-1} & \vdots & \vdots & \ddots & \vdots \\ \hline 0 & 0 & \cdots & 0 & B_{0,0} & B_{0,1} & \cdots & B_{0,N_\xi-1} \\ 0 & 0 & \cdots & 0 & B_{1,0} & B_{1,1} & \cdots & B_{1,N_\xi-1} \\ \vdots & \vdots & \ddots & \vdots & \vdots & \vdots & \ddots & \vdots \\ 0 & 0 & \cdots & 0 & B_{N_\xi-1,0} & B_{N_\xi-1,1} & \cdots & B_{N_\xi-1,N_\xi-1} \end{array}\right),$$

$$\mathbf{FF} = \begin{pmatrix} \mathbf{F}_{r+1,0} \\ \mathbf{F}_{r+1,1} \\ \vdots \\ \mathbf{F}_{r+1,N_\xi-1} \\ \hline \boldsymbol{\Theta}_{r+1,0} \\ \boldsymbol{\Theta}_{r+1,1} \\ \vdots \\ \boldsymbol{\Theta}_{r+1,N_\xi-1} \end{pmatrix}, \qquad \mathbf{RR} = \begin{pmatrix} R_1^{(0)} \\ R_1^{(1)} \\ \vdots \\ R_1^{(N_\xi-1)} \\ \hline R_2^{(0)} \\ R_2^{(1)} \\ \vdots \\ R_2^{(N_\xi-1)} \end{pmatrix}.$$

The above system is then solved as

$$\mathbf{FF} = \mathbf{AA}^{-1}\mathbf{RR}. \tag{51}$$

We have

$$\begin{aligned} A_{i,i} &= \mathbf{A}^{(i)} + a_{4,r}^{(i)} d_{i,i}\mathbf{D} + a_{5,r}^{(i)} d_{i,i}, \\ B_{i,i} &= \mathbf{B}^{(i)} + b_{2,r}^{(i)} d_{i,i}, \quad i = 0, 1, \ldots, N_\xi - 1, \end{aligned} \tag{52}$$

$$\begin{aligned} A_{i,j} &= a_{4,r}^{(i)} d_{i,j}\mathbf{D} + a_{5,r}^{(i)} d_{i,j}, \quad i \neq j, \\ B_{i,j} &= b_{2,r}^{(i)} d_{i,j}, \quad i \neq j. \end{aligned} \tag{53}$$

4 Results and discussion

In Table 1, we compare the results of the bi-variate quasilinearization method (BQLM) to the successive linearization method (SLM) and MATLAB's 'bvp4c' method. The results of the BQLM are in excellent agreement with these two methods to seven decimal places showing the accuracy of this method.

To understand the behavior of the velocity and temperature profiles the illustrations for the numerical solution obtained are depicted as graphs in Figures 2-8.

Figure 2 shows the influence of Casson parameter β on the velocity and the temperature profiles at different values of the Forchheimer parameter Λ in the case of velocity profiles (see Figure 2(a)), and thermal slip factor S_T in the case of temperature profiles (see Figure 2(b)). Increasing the Casson parameter increases the velocity profiles close to the boundary, as $\beta \to \infty$, $\frac{1}{\beta} \to 0$, the fluid becomes Newtonian. The same result is noted in Ramachandra *et al.* [1]. The difference in these results from those of Ramachandra *et al.* [1] is that there is a reverse effect that is noted further away from the boundary. This is due to the presence of the velocity slip factor which tends to assist flow at the boundary. Increasing the Forchheimer parameter reduce velocity profiles, this is caused by the transpiration effect taking place at the surface of the circle. Increasing the Casson parameter β reduces temperature profiles (see [1–3]). In the case of no thermal slip factor,

Table 1 Comparison of the values of the skin friction coefficient and heat transfer coefficient obtained by BQLM against the SLM and bvp4c for $\beta \to \infty$, $\Lambda = \Lambda_1 = M = \xi = K = f_w = S_f = S_T = 0$

Pr	SLM		bvp4c		Present	
	$f''(0)$	$-\theta'(0)$	$f''(0)$	$-\theta'(0)$	$f''(0)$	$-\theta'(0)$
1	0.87100777	0.42143140	0.81700776	0.42143144	0.81700776	0.42143144
10	0.54471433	0.88046306	0.54471423	0.88046307	0.54471422	0.88046307

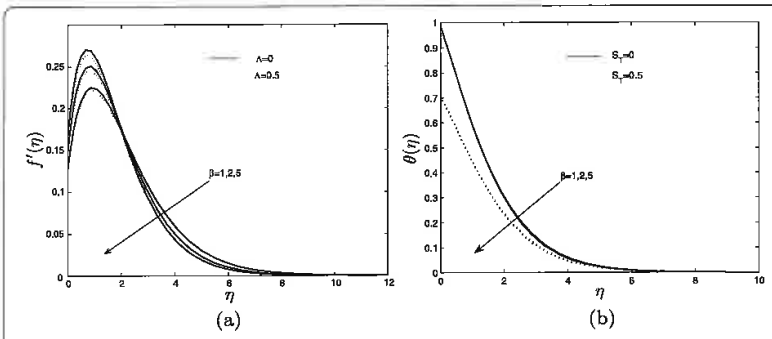

Figure 2 Effects of Casson parameter on (a) velocity and (b) temperature profiles for different Λ and S_T, at $\Lambda_1 = 0.5$, $K = 0.5$, $Pr = 1$, $Ec = 1$, $M = 1$, $f_w = 0.5$, $S_f = 0.5$.

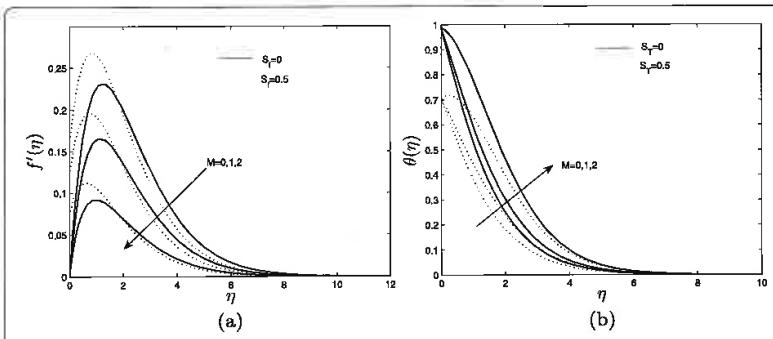

Figure 3 Effects of magnetic parameter on (a) velocity and (b) temperature profiles for different S_f and S_T, at $\Lambda_1 = 0.5$, $K = 0.5$, $Pr = 1$, $Ec = 1$, $f_w = 0.5$, $\Lambda = 0.5$, $\beta = 2$.

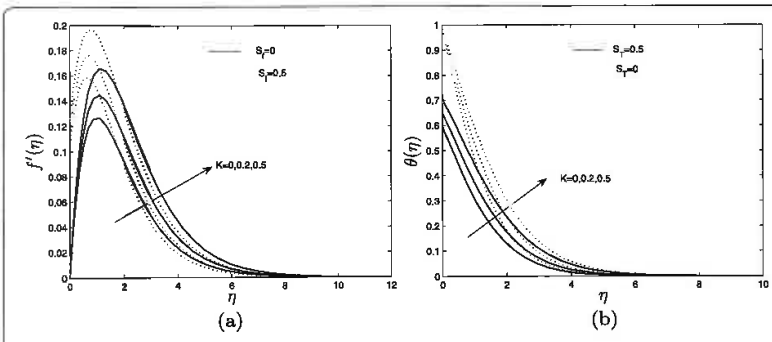

Figure 4 Effects of radiation parameter on (a) velocity and (b) temperature profiles for different S_f and S_T, at $\beta = 2$, $\Lambda_1 = 0.5$, $K = 0.5$, $Pr = 1$, $Ec = 1$, $M = 1$, $f_w = 0.5$, $\Lambda = 0.5$.

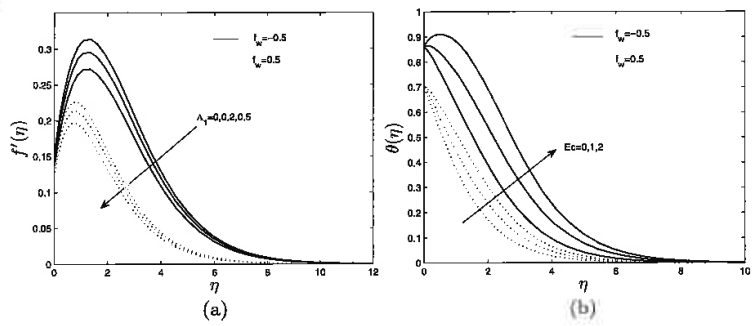

Figure 5 Effects of Λ_1 and *Ec* on (a) velocity and (b) temperature profiles for different f_w, at $\beta = 2$, $\Lambda = 0.5$, $K = 0.5$, $M = 1$, $K = 0.5$, $Pr = 1$, $S_T = 0.5$.

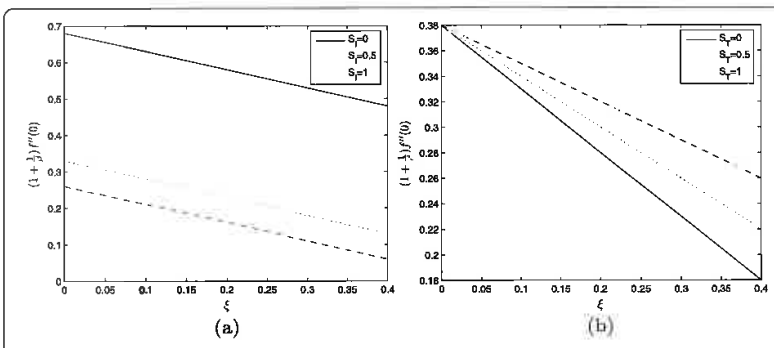

Figure 6 Skin friction coefficient *vs.* ξ for different S_f (a) and skin friction coefficient *vs.* ξ for different S_T (b) at $\beta = 2$, $\Lambda_1 = 0.5$, $K = 0.5$, $M = 1$, $Pr = 1$, $Ec = 1$, $f_w = 0.5$, $\Lambda = 0.5$.

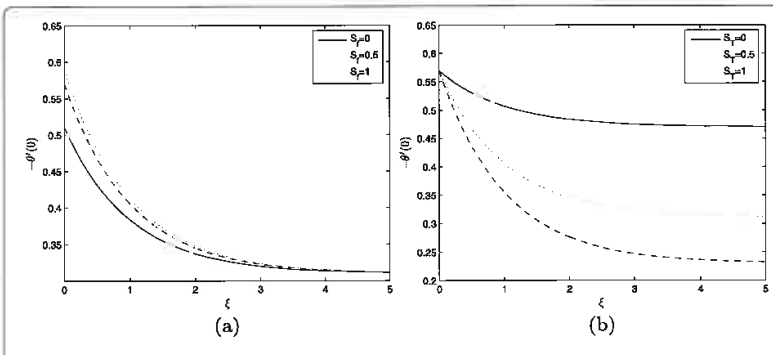

Figure 7 Heat transfer coefficient *vs.* ξ for different S_f (a) and skin friction coefficient *vs.* ξ for different S_T (b) at $\beta = 2$, $\Lambda_1 = 0.5$, $K = 0.5$, $M = 1$, $Pr = 1$, $Ec = 1$, $f_w = 0.5$, $\Lambda = 0.5$.

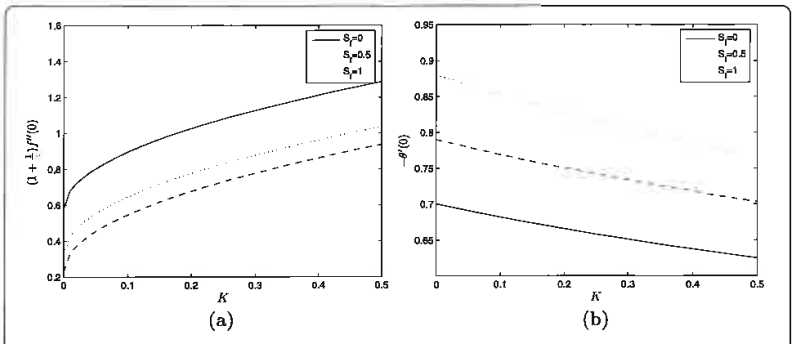

Figure 8 Skin friction coefficient *vs.* K for different S_f (a) and skin friction coefficient *vs.* ξ for different S_T (b) at $\beta = 2$, $\Lambda_1 = 0.5$, $M = 1$, $Pr = 1$, $Ec = 1$, $f_w = 0.5$, $\Lambda = 0.5$.

higher temperature profiles are noticed and lower temperature profiles are noticed in the presence of the thermal slip factor, as shown in Figure 2(b).

Figure 3 depicts the effect of the magnetic parameter M on the velocity and temperature profiles at different values of the velocity slip factor S_f in the case of velocity profiles (see Figure 3(a)), and thermal slip factor in the case of temperature profiles (see Figure 3(b)). M suppress velocity profiles. A magnetic field incident across a flowing fluid retards the velocity of the flow as noted in [4, 12]. The velocity profiles in the case of no-slip conditions resemble those of Narayana *et al.* [10]. It is noted that the velocity profiles are increased with the increase in the velocity slip factor as expected on a lubricated surface. In Figure 3(b) the temperature profiles are increased with increasing magnetic parameter and are decreased by the increase in the Forchheimer parameter Λ. Increasing the inertia causes more friction on the surface changing surface temperature, thereby causing the observed thermal slip.

Figure 4 shows the effect of the radiation parameter K on the velocity and temperature profiles at different values of the velocity slip factor S_f in the case of velocity profiles (see Figure 4(a)), and thermal slip factor in the case of temperature profiles (see Figure 4(b)). The same observation is noted in Figure 4(b); increasing K increases the temperature profiles.

Figure 5 illustrates the velocity response to the change in the Darcian drag force term Λ_1 at different values of the suction/injection parameter f_w (see Figure 5(a)), and the effect of the Eckert number Ec at different values of the suction/injection parameter f_w (see Figure 5(b)). In this case the Λ_1 is inversely proportional to the Darcy number, Da (also inversely proportional to the permeability of the medium). Increasing Λ_1 decreases the velocity profiles. It is noted that the case $f_w < 0$ (blowing) assists the flow, while the case $f_w > 0$ (suction) retards the velocity profiles. The differences of these results to those of Ramachandra *et al.* [1] are shown in the presence of a magnetic field which generally tend to suppress velocity profiles. The presence of viscous dissipation is also noted in the increase in the temperature profiles. In Figure 5(b) increasing the Eckert number results in the increase in the temperature profiles.

Figure 6 shows the plot of the skin friction coefficient *versus* ξ for different values of both the velocity slip factor S_f (see Figure 6(a)), and the thermal slip factor S_T (see Figure 6(b)). The skin friction coefficient decreases with increasing velocity slip factor and

also decreases with increasing ξ. In Figure 6(b) the skin friction coefficient decreases with increasing thermal slip factor.

Figure 7 shows the plot of the heat transfer coefficient *versus* ξ for different values of both the velocity slip factor S_f (see Figure 7(a)), and the thermal slip factor S_T (see Figure 7(b)). It is noted that, at the surface of the circle, there is a more significant change in heat transfer than further away from the surface of the circle. In Figure 7(b) increasing the velocity slip factor does not change the heat transfer at the surface. It is noticed that there is a large difference in the heat transfer further away from the circle surface.

Figure 8 shows the plot of the skin friction coefficient *versus* K for different values of both the velocity slip factor S_f (see Figure 8(a)), and the Nusselt number *versus* thermal slip factor S_T (see Figure 8(b)). In Figure 8(a) the skin friction coefficient increases with increasing thermal radiation K and decreases with increasing velocity slip factor, which is expected on a lubricated surface. There is a noticeable difference in the skin friction coefficient at different values of the velocity slip factor. In Figure 8(b) increasing the thermal radiation decreases the heat transfer coefficient. Increasing the thermal slip factor increases the heat transfer coefficient.

5 Conclusion

The study presented in this analysis of effects of radiation on MHD free convection of a Casson fluid from a horizontal circular cylinder with partial slip in non-Darcy porous medium with viscous dissipation provides numerical solutions for the boundary layer flow and heat transfer. The coupled nonlinear governing partial differential equations were solved using the bi-variate quasilinearization method (BQLM) and validated by the successive linearization method (SLM) and MATLAB's 'bvp4c'. This paper also describes the BQLM numerical method which uses collocation methods in both directions η (direction of increasing boundary layer thickness) and ξ (radial transpiration direction). The most important results are those reflected in the presence of a magnetic field and viscous dissipation in a Casson fluid, which were never reported before.

Competing interests
The authors declare that they have no competing interests.

Authors' contributions
GM conceptualized the idea of research, formulation of the problem and computed the results for the bi-variate quasilinearization method (BQLM), SS computed the results for the 'bvp4c' and successive linearization method (SLM), PS edited the paper and confirmed the well-posed-ness of the problem, directed the general setup of the paper. All authors read and approved the final manuscript.

Acknowledgements
The authors would like to thank the University of KwaZulu-Natal, School of Mathematics, Statistics and Computer Science for the funding and support in the development of the paper.

Received: 4 November 2014 Accepted: 14 April 2015 Published online: 06 May 2015

References

1. Ramachandra, PV, Subba, RA, Anwa, BO: Flow and heat transfer of Casson fluid from a horizontal cylinder with partial slip in non-Darcy porous medium. Appl. Comput. Math. 2, 1-2 (2013)
2. Vajravelu, K, Mukhopadhyay, S: Diffusion of chemically reactive species in Casson fluid flow over an unsteady permeable stretching surface. J. Hydrodyn. 25, 591-598 (2013)
3. Mukhopadhyay, S, De, PR, Bhattacharyya, K, Layek, GC: Casson fluid flow over an unsteady stretching surface. Ain Shams Eng. J. 4 933-938 (2013)
4. Nadeem, S, Ul Haq, R, Lee, C: MHD flow of a Casson fluid over an exponentially stretching sheet. Sci. Iran. 19, 1550-1553 (2012)
5. Kameswaran, PK, Narayana, M, Makanda, G, Sibanda, P: On radiation effects on hydromagnetic Newtonian liquid flow due to an exponential stretching sheet. Bound. Value Probl. (2012). doi:10.1186/1687-2770-2012-105

6. Shateyi, S, Marewo, GT: Numerical analysis of MHD stagnation point flow of Casson fluid, heat and mass transfer over a stretching sheet. In: Balicki, J (ed.) Advances in Applied and Pure Mathematics, WSEAS, Proceedings of the 7th International Conference on Finite Diferences, Finite Elements, Finite Volumes, Boundary Elements (F-and-B '14), Gdansk, Poland, pp. 128-132 (2014). ISBN:978-960-474-380-3
7. Chamkha, AJ, Mujtaba, M, Quadri, A, Issa, C: Thermal radiation effects on MHD forced convection flow adjacent to a non-isothermal wedge in the presence of a heat source or sink. Heat Mass Transf. **39**, 305-312 (2003)
8. Pramanik, S: Casson fluid flow and heat transfer past an exponentially porous stretching surface in the presence of thermal radiation. Ain Shams Eng. J. **5**, 205-212 (2014)
9. Ece, CM: Free convection flow about a cone under mixed thermal boundary conditions and a magnetic field. Appl. Math. Model. **29**, 1121-1134 (2005)
10. Narayana, M, Awad, FG, Sibanda, P: Free magnetohydrodynamic flow and convection from a vertical spinning cone with cross diffusion effects. Appl. Math. Model. **37**, 2662-2678 (2013)
11. Nadeem, S, Ul Haq, R, Khan, ZH: Numerical study of MHD boundary layer flow of a Maxwell fluid past a stretching sheet in the presence of nanoparticles. J. Chin. Inst. Chem. Eng. **45**, 121-126 (2014)
12. Chen, CH: Combined heat and mass transfer in MHD free convection from a vertical surface with ohmic heating and viscous dissipation. Int. J. Eng. Sci. **42**, 699-713 (2004)
13. Anwa, I, Amin, N, Pop, I: Mixed convection boundary layer flow of a viscoelastic fluid over a horizontal circular cylinder. Int. J. Non-Linear Mech. **43**, 814-821 (2008)
14. Deka, RK, Paul, A, Chaliha, A: Transient free convection flow past an accelerated vertical cylinder in a rotating fluid. Ain Shams Eng. J. **5**, 505-513 (2014)
15. Ribeiro, VM, Coelo, PM, Pinho, FT, Alves, MA: Viscoelastic flow past a confined cylinder: three dimensional effects and stability. Chem. Eng. Sci. **111**, 364-380 (2014)
16. Patel, SA, Chhabra, RP: Steady flow of Bingham plastic fluids past an elliptical cylinder. J. Non-Newton. Fluid Mech. **165**, 32-53 (2013)
17. Awad, FG, Sibanda, P, Motsa, SS, Makinde, OD: Convection from an inverted cone in a porous medium with cross diffusion effect. Comput. Math. Appl. **61**, 1431-1441 (2011)
18. Hayat, T, Mustafa, M, Pop, I: Heat and mass transfer for Soret and Dufour's effect on mixed convection boundary layer flow over a stretching vertical surface in a porous medium filled with viscoelastic fluid. Commun. Nonlinear Sci. Numer. Simul. **15**, 1183-1196 (2010)
19. Cheng, CY: Soret and Dufour's effects on free convection boundary layer over a vertical cylinder in a saturated porous medium. Int. Commun. Heat Mass Transf. **37**, 796-800 (2010)
20. Chamkha, AJ, Rashad, AM: Natural convection from a vertical permeable cone in a nanofluid saturated porous media for uniform heat and nanoparticles volume fraction fluxes. Int. J. Numer. Methods Heat Fluid Flow **22**, 1073-1085 (2012)
21. Motsa, SS, Magagula, VM, Sibanda, P: A bivariate Chebyshev spectral collocation quasilinearization method for nonlinear parabolic equations. Sci. World J. (2014). doi:10.1155/2014/581987
22. Bellman, RE, Kalaba, RE: Quasilinearization and Nonlinear Boundary Value Problems. Elsevier, New York (1965)

Appendix E

DE GRUYTER OPEN

Open Physics 2015; X (X):1–13

Editorial

Open Access

G. Makanda*, S. Shaw, and P. Sibanda

Numerical analysis of free convection Casson fluid flow from a spinning cone in non-Darcy porous medium with radiation, partial slip, cross diffusion and viscous dissipation effects

Abstract: In the present study, a numerical analysis on free convection Casson fluid flow from a spinning cone in non-Darcy porous medium with radiation, partial slip, cross diffusion and viscous dissipation is considered. The surface of the cone is heated under linear surface heat flux (LSHF). The boundary layer partial differential equations are converted into a system of ordinary differential equations which are then solved using spectral relaxation method (SRM) and the successive linearization method (SLM). The boundary layer velocity, temperature and concentration profiles are computed for different values of the physical parameters. In particular, the effect of the Casson parameter, spin parameter, Eckert number, Soret number, velocity slip factor, thermal slip factor and concentration slip factor on velocity, temperature and concentration profiles is studied. In this study it is shown that increasing the Casson parameter decrease velocity profiles. Increasing the velocity slip factor tend to assist the flow, while increasing the thermal and concentration slip factors tend to reduce temperature and concentration profiles respectively. The results obtained in this study were compared with others in the literature and found to be in excellent agreement.

Keywords: Spectral relaxation method, Casson fluid, partial slip, cross diffusion, viscous dissipation, porous medium

PACS: 01.30.-y; 01.30.Xx; 01.30.Tt

DOI ...

Received July 4, 2015; revised ...; accepted ....

***Corresponding Author: G. Makanda:** School of Mathematics, Statistics and Computer Science, University of KwaZulu-Natal, Private Bag X01, Scottsville, Pietermaritzburg 3209, South Africa, E-mail: gilbert-makanda@yahoo.com

S. Shaw, P. Sibanda: School of Mathematics, Statistics and Computer Science, University of KwaZulu-Natal, Private Bag X01, Scottsville, Pietermaritzburg 3209, South Africa

1 Introduction

The problem of heat transfer in spinning objects is important due to its application in industry. In particular in the design of automatic cooking machinery and movement of automotive parts in engines. These designs incorporate different solid shapes including spinning cones immersed in lubricants. It is important to study how the heat generated at these surfaces, the partial slip due these lubricants, the presence of solid particles affect the ambient fluid. Other examples arise in engineering, where double diffusion is seen in the formation of microstructures, cooling of molten metals and fluid which flows close to shrouded fins [1]. Casson fluid flow can be buoyant driven and this situation is found in many practical applications such as soup simmering in a pot, effect of application of heat on blood and synovial fluid in humans, flow of sewage sludge on heated surfaces. Other applications are found in metallurgy, drilling operations, manufacturing of paints, manufacturing pharmaceutical products [2]. It is therefore necessary to investigate the flow of Casson fluid in different geometries under various conditions such as porous media and viscous dissipation. Partial slip conditions at the boundary are also necessary to investigate since this is mostly characteristic of Casson fluid flow due to their lubrication effects.

The study of free convection from a cone in a Newtonian fluid was studied by Ece [3] who considered flow about a cone under mixed boundary conditions and a magnetic field. This study investigated a flow outside the cone which gave an insight in such flows. Other similar studies of flows past cones were conducted by Cheng [4] -[5], who considered various situations such as Soret and Dufour effects, natural convection flows in viscoelastic fluid. Among others Alim [6] investigated

pressure work effect and free convection from a cone in viscoelastic fluid, Narayana and Sibanda [7] investigated cross diffusion effects and free convection from a cone, they studied heat and mass transfer on this geometry, Awad [8] studied convection from an inverted cone in a porous medium with cross diffusion effects. Other cone studies were conducted by Agarwal [9] who studied flow past a cone at certain angles of attack. Other studies on cone geometry include the works of Anilkumar et al. [10],Takar et al.[11], Saleh et al [12] and Chamkha [13].

The study of Casson fluid flow was conducted by many authors, among others Mukhopadhyay and Vejrravelu [14], Mukhopadhyay et al. [15], Nadeem et al. [16], and Ramachandra et al. [17]. These studies considered the flow of Casson fluid on different geometries such as flow over a stretching sheet and circular surfaces, others considered partial slip conditions. They also considered blowing and suction situations on a circular geometry. These studies also considered diffusion of chemical species, porous media, MHD flows and unsteady flows. This shows the importance of studying this type of flow and most of the studies used the well known Runge-Kutta numerical method solve their systems of equations. All of these studies considered a similar constitutive equation for Casson fluid.

Cross diffusion effects have been studied by among others Hayat et al. [18] investigated heat and mass transfer for Soret and Dufour effect on mixed convection boundary layer flow over a stretching vertical surface in a porous medium filled with viscoelastic fluid. Cheng [19] studied Soret and Dufour effects on free convection boundary layer over a vertical cylinder in a saturated porous medium. None of these studies considered a spinning cone and partial slip on cone geometry. Each of these studies considered different boundary conditions and used either the cubic spline or the homotopy analysis methods.

In the present study we investigate the effects of radiation in natural convection from a spinning cone with partial slip in non-Darcy porous medium and cross diffusion effects in Casson fluid with viscous dissipation. The driving force in caused by temperature differences between the cone surface and the surroundings. The present work is also a further development of the work of Narayana et al. [1] in which the linear surface temperature (LST) and linear surface heat flux (LSHF) are considered. The study of Casson fluid has not been widely investigated for heat transfer past a rotating cone. The Darcian drag force term and the viscous dissipation source terms are introduced in the governing equations. Similarity transformations are used to convert the governing equations into a system of partial differential equations which are then solved by using the Runge-Kutta Felhberg integration scheme. The numerical method used is not only validated by comparison to previous work by other authors, but also by the use of the successive linearization method (SLM). In this work we investigate the effect of varying physical parameters on the velocity, temperature and concentration profiles with the presentation of graphical illustrations.

2 Mathematical formulation

The steady, laminar, viscous and buoyancy driven convection heat and mass transfer flow from a spinning vertical cone with viscous dissipation and radiation effects in a Casson fluid maintained at a non-uniform temperature T_{wa} ($> T_\infty$). The solute concentration is considered to be C_{wa}($> C_\infty$) at the surface of the cone and C_∞ in the ambient fluid. Ω is the angular velocity of the spinning cone, u, v and w are the velocity components in the x, y and z respectively. g is the acceleration due to gravity (see Figure 1).

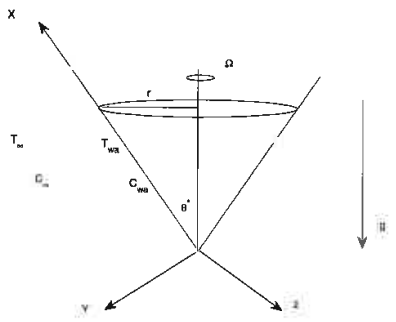

Fig. 1. Schematic diagram of the spinning cone

The rheological equation of state for an isotropic and incompressible flow of a Casson fluid is given as in

[14],[15],[17] by:

$$\tau_{ij} = \begin{cases} 2(\mu_B + \frac{P_y}{\sqrt{2\pi}})e_{ij}, & \pi > \pi_c \\ 2(\mu_B + \frac{P_y}{\sqrt{2\pi_c}})e_{ij}, & \pi < \pi_c \end{cases} \quad (1)$$

$\pi = e_{ij}e_{ij}$ and e_{ij} is the $(i,j)^{th}$ component of the deformation rate, π is the product of the deformation rate with itself, π_c is a critical value of this product based on the non-Newtonian model, μ_B is the plastic dynamic viscosity of the non-Newtonian fluid, P_y is the yield stress of the fluid.

The governing equations in this flow are given as;

$$\frac{\partial}{\partial x}(ru) + \frac{\partial}{\partial y}(rv) = 0, \quad (2)$$

$$u\frac{\partial u}{\partial x} + v\frac{\partial u}{\partial y} - \frac{w^2}{x} = \nu(1+\frac{1}{\beta})\frac{\partial^2 u}{\partial y^2} - \frac{\nu}{K}u + g\beta_T(T-T_\infty)\cos\gamma + g\beta_C(C-C_\infty)\cos\theta^* \quad (3)$$

$$u\frac{\partial w}{\partial x} + v\frac{\partial w}{\partial y} + \frac{uw}{x} = \nu(1+\frac{1}{\beta})\frac{\partial^2 w}{\partial y^2} - \frac{\nu}{K}w \quad (4)$$

$$u\frac{\partial T}{\partial x} + v\frac{\partial T}{\partial y} = \alpha\frac{\partial^2 T}{\partial y^2} + \bar{D}\frac{\partial^2 C}{\partial y^2} - \frac{1}{\rho C_p}\frac{\partial q_r}{\partial y} + \frac{\nu}{\rho C_p}(1+\frac{1}{\beta})\left(\frac{\partial u}{\partial y}\right)^2 \quad (5)$$

$$u\frac{\partial C}{\partial x} + v\frac{\partial C}{\partial y} = D\frac{\partial^2 C}{\partial y^2} + \bar{S}\frac{\partial^2 T}{\partial y^2} \quad (6)$$

where the radius of the cone $r = x\sin\theta^*$, ν is kinematic viscosity of Casson fluid, $\beta = \mu_B\sqrt{2\pi_c}/P_y$ is the non-Newtonian Casson parameter. $\alpha = k/\rho C_p$ is the thermal diffusivity. k is thermal conductivity of the fluid, q_r is the radiative heat flux. C_p is the specific heat. g is the acceleration due to gravity, β_T and β_C are respectively the coefficients of thermal and concentration expansions, T is the temperature of the fluid, C is the solute concentration in the boundary layer, D is the mass diffusivity, $\bar{S}$ and $\bar{D}$ are Soret and Dufour coefficients respectively. The Rosseland approximation for radiation may be written as follows;

$$q_r = -\frac{4\sigma}{3k^*}\frac{\partial T^4}{\partial y} \quad (7)$$

where σ is the Stefan-Boltzman constant and k^* is the absorption coefficient. If the temperature difference within the flow is such that T^4 may be expanded in Taylor series about T_∞ and neglecting higher powers we obtain $T^4 - 4T_\infty^3 - 3T_\infty^4$ and therefore the equation (5) can be written as

$$u\frac{\partial T}{\partial x} + v\frac{\partial T}{\partial y} = \alpha\frac{\partial^2 T}{\partial y^2} + \bar{D}\frac{\partial^2 C}{\partial y^2} + \frac{16\sigma T_\infty^3}{3\rho C_p k^*}\frac{\partial^2 T}{\partial y^2} \quad (8)$$

The boundary conditions are given as

$$\left.\begin{aligned} u = N_0(1+\frac{1}{\beta})\frac{\partial u}{\partial y}, \quad v = -v_{wa}, \\ w = r\Omega + R_0(1+\frac{1}{\beta})\frac{\partial w}{\partial y}, \\ T = T_{wa} + K_0\frac{\partial T}{\partial Y}, \\ C = C_{wa} + F_0\frac{\partial C}{\partial Y} \end{aligned}\right\} \quad y = 0, \quad (9)$$

$$u \to 0, w \to 0, \quad T \to T_\infty, \quad C \to C_\infty \quad \text{as} \quad y \to \infty. \quad (10)$$

where the subscripts wa and ∞ refer to surface the free stream conditions respectively.

We introduce the non-dimensional variables

$$\left.\begin{aligned} (X,Y,R) = \left(\frac{x, yGr^{\frac{1}{4}}, r}{L}\right), \\ (U,V) = \left(\frac{u, vGr^{\frac{1}{4}}}{U_0}\right), \\ W = \frac{w}{\Omega L} \quad \bar{T} = \frac{T-T_\infty}{T_{wa}-T_\infty}, \bar{C} = \frac{C-C_\infty}{C_{wa}-C_\infty}, \\ U_0 = [g\beta_T(T_{wa}-T_\infty)\cos\psi L]^{\frac{1}{2}}, \\ Da = \frac{K}{L^2}, \quad Gr = (\frac{U_0 L}{\nu})^2 \end{aligned}\right\} \quad (11)$$

The governing equations (2) -(6) reduce to

$$\frac{\partial}{\partial X}(RU) + \frac{\partial}{\partial Y}(RV) = 0, \quad (12)$$

$$U\frac{\partial U}{\partial X} + V\frac{\partial U}{\partial Y} - \frac{Re^2}{Gr}\frac{W^2}{X} = \left(1+\frac{1}{\beta}\right)\frac{\partial^2 U}{\partial Y^2} + \bar{T} + N\bar{C} - \left(\frac{1}{DaGr^{\frac{1}{2}}}\right)U, \quad (13)$$

$$U\frac{\partial W}{\partial X} + V\frac{\partial W}{\partial Y} + \frac{UW}{X} = \left(1+\frac{1}{\beta}\right)\frac{\partial^2 W}{\partial Y^2} - \left(\frac{1}{DaGr^{\frac{1}{2}}}\right)W, \quad (14)$$

$$U\frac{\partial \bar{T}}{\partial X} + V\frac{\partial \bar{T}}{\partial Y} = \frac{1}{Pr}\left(\frac{\partial^2 \bar{T}}{\partial Y^2} + D_f\frac{\partial^2 \bar{C}}{\partial Y^2}\right) + \frac{4K}{3Pr}\frac{\partial^2 T}{\partial Y^2} + Ec\left(1+\frac{1}{\beta}\right)\left(\frac{\partial U}{\partial Y}\right)^2, \quad (15)$$

$$U\frac{\partial \bar{C}}{\partial X} + V\frac{\partial \bar{C}}{\partial Y} = \frac{1}{Sc}\left(\frac{\partial^2 \bar{C}}{\partial Y^2} + S_r\frac{\partial^2 \bar{T}}{\partial Y^2}\right). \quad (16)$$

The non dimensional parameters in equations (12)-(16) are the rotational Reynolds number Re, Grashof number Gr, the Darcy number Da, the Prandtl number Pr, Dufour parameter D_f, the Eckert number Ec, the Schmidt number Sc and Soret parameter S_r. These parameters are defined as

$$Re = \frac{\Omega L^2}{\nu}, \quad N = \frac{\beta_C}{\beta_T}\left(\frac{C_{wa}-C_\infty}{T_{wa}-T_\infty}\right), K = \frac{4\sigma^* T_\infty^3}{k^* G r^{\frac{1}{4}}}$$
$$Pr = \frac{\nu}{\alpha}, \quad Sc = \frac{\nu}{D}, \quad Ec = \frac{U_0^2}{C_p(T_{wa}-T_\infty)},$$
$$D_f = \frac{\bar{D}}{\alpha}\left(\frac{C_{wa}-C_\infty}{T_{wa}-T_\infty}\right), \quad S_r = \frac{\bar{S}}{D}\left(\frac{T_{wa}-T_\infty}{C_{wa}-C_\infty}\right).$$

The boundary conditions of system (12)- (16) are given by

$$U = S_f\left(1+\frac{1}{\beta}\right)\frac{\partial U}{\partial Y}, \quad V = V_w,$$
$$W = R + S_g\left(1+\frac{1}{\beta}\right)\frac{\partial W}{\partial Y}, \quad \bar{T} = 1 + S_T\frac{\partial \bar{T}}{\partial Y},$$
$$\bar{C} = 1 + S_{co}\frac{\partial \bar{C}}{\partial Y} \quad \text{at} \quad Y = 0 \tag{17}$$
$$U \to 0, W \to 0, \bar{T} \to 0, \bar{C} \to 0 \quad \text{as} Y \to \infty. \tag{18}$$

Introducing the stream function $\psi(X,Y)$ and similarity variables

$$U = \frac{1}{R}\frac{\partial \psi}{\partial Y} \quad \text{and} \quad V = -\frac{1}{R}\frac{\partial \psi}{\partial X} \tag{19}$$
$$\psi(X,Y) = XRf(Y), \quad W(X,Y) = Rg(Y),$$
$$\bar{T}(X,Y) = X\theta(Y), \quad \bar{C}(X,Y) = X\phi(Y). \tag{20}$$

using the stream function defined in (19) and similarity variable in (20), Eqs. (12)- (16) together with boundary conditions (17) and (18) reduce to the following system of ordinary differential equations.

$$\left(1+\frac{1}{\beta}\right)f''' + 2ff'' - f'^2 + \epsilon g^2 + \theta + N\phi - k_p f' = 0, \tag{21}$$
$$\left(1+\frac{1}{\beta}\right)g'' + 2fg' - 2f'g - k_p g = 0, \tag{22}$$
$$(1+\frac{4}{3}K)\theta'' + Pr(2f\theta' - f'\theta) + D_f\phi'' + EcPr\left(1+\frac{1}{\beta}\right)f''^2 = 0, \tag{23}$$
$$\phi'' + Sc(2f\phi' - f'\phi) + S_r\theta'' = 0 \tag{24}$$

with boundary conditions;

$$Y = 0, \quad f = f_w, \quad f' = \left(1+\frac{1}{\beta}\right)S_f f'',$$
$$g = 1 + \left(1+\frac{1}{\beta}\right)S_g g', \theta = 1 + S_T\theta',$$
$$\phi = 1 + S_{co}\phi', \tag{25}$$
$$Y \to \infty, f' \to 0, g \to 0, \theta \to 0.\phi \to 0. \tag{26}$$

where $k_p = 1/DaGr^{\frac{1}{2}}$ is the Darcian drag force term, β is the Casson parameter and ϵ is the spin parameter. In the bove equations the primes refer to the derivative with respect to Y, $S_f = N_0 Gr^{\frac{1}{4}}/L$, $S_g = M_0 Gr^{\frac{1}{4}}/L$, $S_T = kGr^{\frac{1}{4}}/L$ and $S_{co} = F_0 Gr^{\frac{1}{4}}/L$ are the non dimensional velocity, rotational, thermal and solutal slip parameters respectively. $S_f = S_g = S_T = S_{co} = 0$, corresponds to no-slip conditions. The parameter f_{wa} is the blowing/suction parameter. The case $f_{wa} < 0$ represents blowing and $f_{wa} > 0$ represents suction. The engineering parameters of interest are the local skin friction and the local Nusselt numbers which are defined as follows.

The shear stress at the surface of the cone is given by

$$\tau_{wa} = \mu\left[\left(1+\frac{1}{\beta}\right)\frac{\partial u}{\partial y}\right]_{y=0} = \frac{\mu\left(1+\frac{1}{\beta}\right)U_0}{LGr^{-\frac{1}{4}}}Xf''(0) \tag{27}$$

where μ is the coefficient of viscosity,

the skin friction coefficient is given by

$$C_f = \frac{\tau_{wa}}{\frac{1}{2}\rho U_0^2} \tag{28}$$

Using Eqs.(27) and (28) gives

$$C_f Gr^{\frac{1}{4}} = 2(1+\frac{1}{\beta})Xf''(0). \tag{29}$$

The heat transfer from the cone surface into the fluid is given by

$$q_{wa} = -k\left[\frac{\partial T}{\partial y}\right]_{y=0} = \frac{-k(T_{wa}-T_\infty)}{LGr^{-\frac{1}{4}}}X\theta'(0), \tag{30}$$

k is the thermal conductivity of the fluid,

The Nusselt number under LST is given by

$$Nu = \frac{L}{k}\frac{q_{wa}}{T_{wa}-T_\infty} \tag{31}$$

Eqs.(30) and (31) together with Eqns. (19) and (20) give

$$NuGr^{-\frac{1}{4}} = -X\theta'(0). \tag{32}$$

(33)

The mass flux at the cone surface into the fluid is given by

$$J_{wa} = -D\left[\frac{\partial C}{\partial y}\right]_{y=0} = \frac{-D(C_{wa}-C_\infty)}{LGr^{-\frac{1}{4}}}X\phi'(0), \quad (34)$$

The Sherwood number is given bv

$$Sh = \frac{L}{D}\frac{J_{wa}}{C_{wa}-C_\infty} \quad (35)$$

Eqs.(34) and (35) together with Eqns. (19) and (20) give

$$ShGr^{-\frac{1}{4}} = -X\phi'(0). \quad (36)$$

3 Method of solution

In this section we present the implementation of the spectral relaxation method for the problem of free convection from a spinning cone with partial slip in Casson fluid in non-Darcy porous medium with cross diffusion and viscous dissipation. The method is described in Motsa et al. [20] and implemented in the works of Shateyi [24], Kameswaran [22] and Motsa and Makukula [21]. The method is based on the Gauss-Seidel method normally used to solve a system of linear equations. The system of equations (21)-(24) can be written as a numerical scheme.

$$f'_{r+1} = p_r, \quad (37)$$

$$\left(1+\frac{1}{\beta}\right)p''_{r+1} + 2f_{r+1}p'_{r+1} - k_p p_{r+1} = p_r^2 - \epsilon g_r^2 - \theta - N\phi_r, \quad (38)$$

$$\left(1+\frac{1}{\beta}\right)g''_{r+1} + 2f_{r+1}g'_{r+1} - 2p_{r+1}g_{r+1} - k_p g_{r+1} = 0, \quad (39)$$

$$(1+\frac{4}{3}K)\theta''_{r+1} + Pr(2f_{r+1}\theta' - p_{r+1}\theta_{r+1}) = -D_f\phi''_r - EcPr\left(1+\frac{1}{\beta}\right)(p'_{r+1})^2, \quad (40)$$

$$\phi''_{r+1} + 2Scf_{r+1}\phi'_{r+1} - ScP_{r+1}\phi_{r+1} = -S_r\theta'' \quad (41)$$

with boundary conditions;

$$f(0)_{r+1} = f_w,\ p(0)_{r+1} = \left(1+\frac{1}{\beta}\right)S_f p(0)'_{r+1},$$
$$g(0)_{r+1} = \left(1+\frac{1}{\beta}\right)S_g g(0)'_{r+1},$$
$$\theta(0)_{r+1} = 1 + S_T\theta(0)'_{r+1},$$
$$\phi(0)_{r+1} = 1 + S_{c0}\phi(0)'_{r+1}, \quad (42)$$
$$p_{r+1}(\infty) \to 0,\ g(\infty)_{r+1} \to 0,$$
$$\theta(\infty)_{r+1} \to 0,\ \phi(\infty)_{r+1} \to 0. \quad (43)$$

Applving the Chebyshev pseudo spectral method on (37) - (42) we obtain

$$A_1\mathbf{f}_{r+1} = B_1,\ f(0)_{r+1} = f_w \quad (44)$$

$$A_2\mathbf{p}_{r+1} = B_2,\ p(0)_{r+1} = \left(1+\frac{1}{\beta}\right)S_f p(0)'_{r+1} \quad (45)$$

$$A_3\mathbf{g}_{r+1} = B_3,\ g(0)_{r+1} = \left(1+\frac{1}{\beta}\right)S_g g(0)'_{r+1} \quad (46)$$

$$A_4\theta_{r+1} = B_4,\ \theta(0)_{r+1} = 1 + S_T\theta(0)'_{r+1} \quad (47)$$

$$A_5\phi_{r+1} = B_5,\ \phi(0)_{r+1} = 1 + S_{c0}\phi(0)'_{r+1} \quad (48)$$

where

$$A_1 = \mathbf{D},\ B_1 = \mathbf{p}_r, \quad (49)$$

$$A_2 = \left(1+\frac{1}{\beta}\right)\mathbf{D}^2 + 2\ \mathrm{diag}[\mathbf{f}_{r+1}]\mathbf{D} - k_p\mathbf{I}$$

$$B_2 = \mathbf{p}_r^2 - \epsilon\mathbf{g}_r^2 - \theta_r - N\phi_r, \quad (50)$$

$$A_3 = \left(1+\frac{1}{\beta}\right)\mathbf{D}^2 + 2\ \mathrm{diag}[\mathbf{f}_{r+1}]\mathbf{D} - \left(2\ \mathrm{diag}[\mathbf{p}_{r+1}]\mathbf{g}_{r+1} - k_p\right)\mathbf{I},\ B_3 = \mathbf{0}, \quad (51)$$

$$A_4 = (1+\frac{4}{3}K)\mathbf{D}^2 + 2Pr\ \mathrm{diag}[\mathbf{f}_{r+1}]\mathbf{D} - Pr\ \mathrm{diag}[\mathbf{p}_{r+1}]\mathbf{I}$$

$$B_4 = -D_f\phi''_r - EcPr\left(1+\frac{1}{\beta}\right)(\mathbf{p}'_{r+1})^2, \quad (52)$$

$$A_5 = \mathbf{D}^2 + 2Sc\ \mathrm{diag}[\mathbf{f}_{r+1}]\mathbf{D} - Sc\ \mathrm{diag}[\mathbf{p}_{r+1}]$$

$$B_5 = -S_r\theta'' \quad (53)$$

3.1 Improving the convergence of the spectral relaxation method

In this section we use the concept of successive over-relaxation (SOR) to accelerate the convergence rate of the spectral relaxation method (SRM). If the general SRM scheme is given by equations (44)-(48), then the modified SRM scheme is defined as

$$A_1\mathbf{f}_{r+1} = (1-\omega)A_1\mathbf{f}_r + \omega B_1 \quad (54)$$

$$A_2\mathbf{p}_{r+1} = (1-\omega)A_2\mathbf{p}_r + \omega B_2 \quad (55)$$

$$A_3\mathbf{g}_{r+1} = (1-\omega)A_3\mathbf{g}_r + \omega B_3 \quad (56)$$

$$A_4\boldsymbol{\theta}_{r+1} = (1-\omega)A_4\boldsymbol{\theta}_r + \omega B_4 \quad (57)$$

$$A_5\boldsymbol{\phi}_{r+1} = (1-\omega)A_5\boldsymbol{\phi}_r + \omega B_5 \quad (58)$$

where A_i and B_i are matrices and ω is the convergence controlling parameter. By applying this modified SRM in solving the system (21)-(24). Using the values of the controlling parameter $\omega = 0.9$ (accelerates convergence), $\omega = 1$(usual SRM scheme) and $\omega = 1.1$(slows down convergence). Figure 2 shows the decoupling error E_d against iterations.

4 Results and discussion

In this section we discuss the physics of the problem by studying the effects of the physical parameters on velocity, temperature and concentration profiles. We also study the variation of both skin friction and local Nusselt number with the physical parameters. For validation of the numerical method used in this study, results for the skin friction coefficient $f''(0)$ and heat transfer coefficient $-\theta'(0)$ for the Newtonian fluid were compared to those of Narayana [1] and the SLM, for $1/\beta \to 0, \epsilon = N = K = D_f = S_r = Sc = Ec = 0$ and the Darcian drag force terms $-k_p f' = k_p g = 0$. The comparison is shown in Tables 1 -2 and it is found to be in excellent agreement to five decimal places.

Table 1. Comparison of the values of $f''(0) and -\theta'(0)$ of Narayana [1] with the bvp4c.

Pr	Narayana et al. [1] $f''(0) - \theta'(0)$	Present $f''(0) - \theta'(0)$
1	0.68150212 0.63886614	0.68148625 0.63885897
10	0.43327726 1.27552680	0.43327848 1.27552816

Table 2. Comparison of the values of $f''(0) and -\theta'(0)$ of Narayana [1] with the SLM.

Pr	Narayana et al. [1] $f''(0) - \theta'(0)$	SLM $f''(0) - \theta'(0)$
1	0.68150212 0.63886614	0.68148334 0.63885473
10	0.43327726 1.27552680	0.43327820 1.27552877

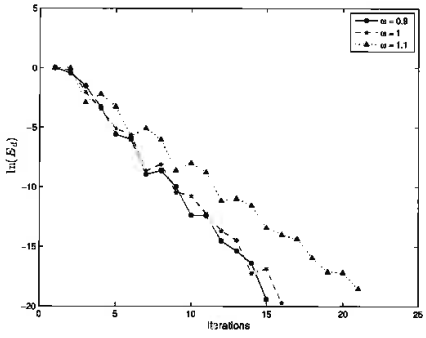

Fig. 2. Effects of the controlling parameter on decoupling error

In Figure 2 the SRM error reduces with the increasing number of iterations, showing the accuracy of the spectral relaxation method (SRM). The decrease in the error shows that the method is convergent and give stable solutions. It is also shown that convergence can be controlled obtaining the results in a fewer number of iterations. The results obtained bv this method are discussed in Tables 3 and 4 and are compared with the results obtained using the successive linearization method (SLM) and were found to be in excellent agreement.

The problem of free convection Casson fluid from a spinning cone in non-Darcy porous medium with radiation, partial slip, cross diffusion and viscous dissipation effects is solved numerically using the spectral relaxation method (SRM). The results depicted in Table 3 are the results generated by the SRM and the bvp4c. A tolerance of 10^{-8} for both methods was used. Comparison of the basic SRM ($\omega = 1$) of the skin friction coefficient against those of the those of SRM with (SOR) ($\omega = 0.9$). The advantage of accelerating convergence is noted in all cases in which the results are obtained accurately in fewer iterations (see also Shateyi and Marewo [23]). The values are generated at selected values of the Darcian drag force term k_p, the Prandtl number Pr and the Casson parameter β. Increasing the k_p and Pr decreases the skin friction coefficient while increasing the Casson parameter increase skin friction coefficient.

Table 3. Comparison of SRM solutions for the skin friction coefficient $f''(0)$ against those of bvp4c.

k_p	Pr	β	SRM(basic) ($\omega = 1$) it	it	SRM(SOR) ($\omega = 0.9$)f"(0)	bvp4c f"(0)
0	1	2	100	47	0.68148334	0.68148334
1	1	2	66	40	0.55974072	0.55974072
2	1	2	46	35	0.48675875	0.48675875
3	1	2	40	33	0.43677770	0.43677770
1	7	2	50	35	0.40562674	0.40562673
1	8	2	48	33	0.39565072	0.39565073
1	9	2	48	33	0.38695722	0.38695722
1	1	2	61	38	0.35629327	0.35629327
1	1	5	62	37	0.43037422	0.43037422
1	1	9	63	39	0.49760348	0.49760348

In Table 4, the heat transfer coefficient decreases with decreasing Darcian drag force term k_p, but increases with increasing both Prandtl Pr and Casson parameter β.

Table 4. Comparison of SRM solutions for the heat transfer coefficient$-\theta'(0)$ against those of bvp4c.

k_p	Pr	β	SRM(basic) $(\omega = 1)$ *it*	it	SRM(SOR) $(\omega = 0.9) - \theta'(0)$	bvp4c f"(0)
0	1	2	91	36	0.59446782	0.5944678
1	1	2	62	37	0.52386360	0.5238636
2	1	2	48	36	0.47594764	0.4759476
3	1	2	42	33	0.44000560	0.4400056
1	7	2	50	33	0.96287011	0.9628701
1	8	2	50	33	1.00136750	1.0013675
1	9	2	49	32	1.03638459	1.0363845
1	1	2	61	37	0.52386360	0.5238636
1	1	5	62	39	0.54308263	0.5430826
1	1	9	63	40	0.54968947	0.5496894

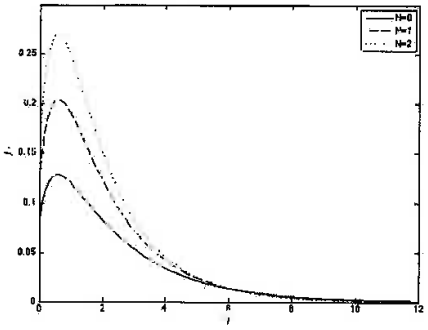

Fig. 4. Effect of buoyancy parameter on velocity profiles for $\beta = 2, \epsilon = 2, Da = 0.1, Gr = 10, K = 0.5, D_f = 0.5, Ec = 1, S_r = 0.5, f_w = 0.5, S_f = 0.5, S_g = 0.5, S_T = 1, S_{co} = 1, Pr = 1, Sc = 0.7$.

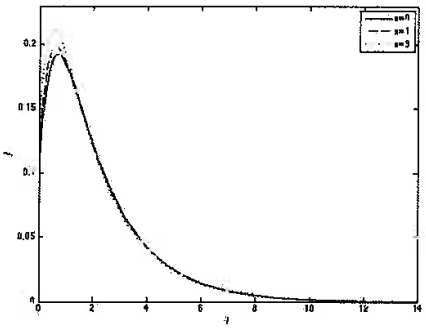

Fig. 3. Effect of spin parameter on velocity profiles for $\beta = 2, N = 1, Da = 0.1, Gr = 10, K = 0.5, D_f = 0.5, Ec = 1, S_r = 0.5, f_w = 0.5, S_f = 0.5, S_g = 0.5, S_T = 1, S_{co} = 1, Pr = 1, Sc = 0.7$.

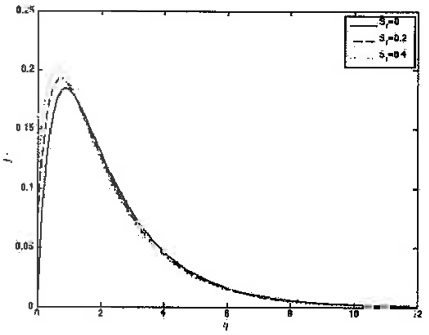

Fig. 5. Effect of velocity slip factor on velocity profiles for $\beta = 2, \epsilon = 2, N = 1, Da = 0.1, Gr = 10, K = 0.5, D_f = 0.5, Ec = 1, S_r = 0.5, f_w = 0.5, S_g = 0.5, S_T = 1, S_{co} = 1, Pr = 1, Sc = 0.7$.

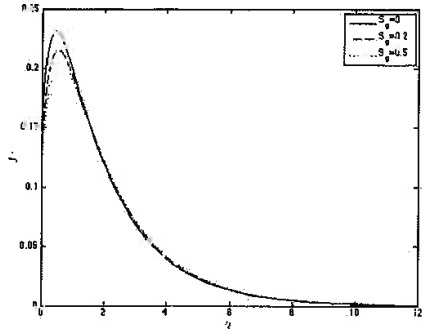

Fig. 6. Effect of rotational slip factor on velocity profiles for $\beta = 2, \epsilon = 2, N = 1, Da = 0.1, Gr = 10, K = 0.5, D_f = 0.5, Ec = 1, S_r = 0.5, f_w = 0.5, S_f = 0.5, S_T = 1, S_{co} = 1, Pr = 1, Sc = 0.7$.

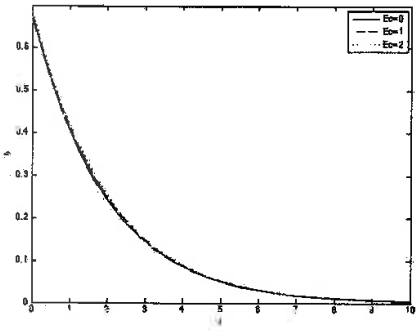

Fig. 8. Effect of Eckert number on temperature profiles for $\beta = 2, \epsilon = 2, N = 1, Da = 0.1, Gr = 10, K = 0.5, D_f = 0.5, S_r = 0.5, f_w = 0.5, S_f = 0.5, S_g = 0.5, S_T = 1, S_{co} = 1, Pr = 1, Sc = 0.7$.

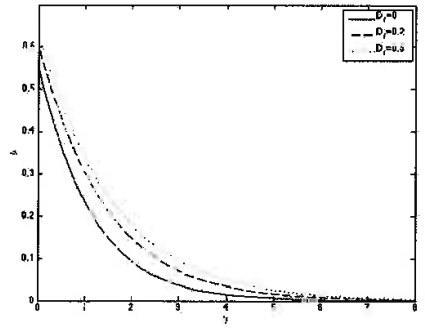

Fig. 7. Effect of Dufour parameter on temperature profiles for $\beta = 2, \epsilon = 2, N = 1, Da = 0.1, Gr = 10, K = 0.5, Ec = 1, S_r = 0.5, f_w = 0.5, S_f = 0.5, S_g = 0.5, S_T = 1, S_{co} = 1, Pr = 1, Sc = 0.7$.

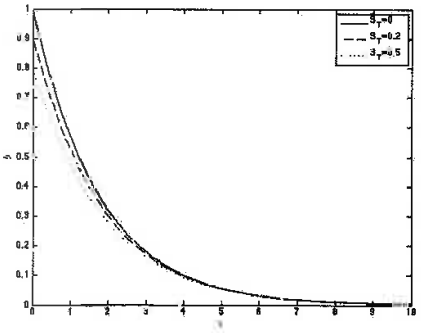

Fig. 9. Effect of thermal slip factor on temperature profiles for $\beta = 2, \epsilon = 2, N = 1, Da = 0.1, Gr = 10, K = 0.5, D_f = 0.5, Ec = 1, S_r = 0.5, f_w = 0.5, S_f = 0.5, S_g = 0.5, S_{co} = 1, Pr = 1, Sc = 0.7$.

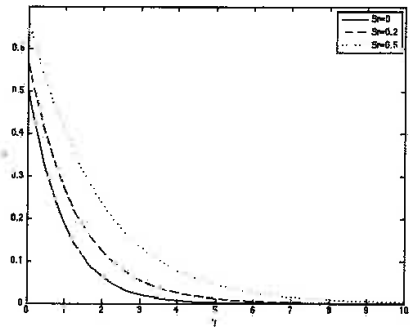

Fig. 10. Effect of Soret parameter on concentration profiles for $\beta = 2, \epsilon = 2, N = 1, Da = 0.1, Gr = 10, K = 0.5, D_f = 0.5, Ec = 1, f_w = 0.5, S_f = 0.5, S_g = 0.5, S_T = 1, S_{co} = 1, Pr = 1, Sc = 0.7.$

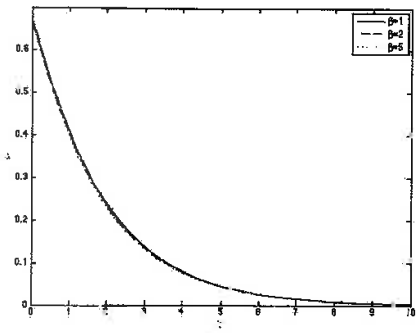

Fig. 12. Effect of Casson parameter on concentration profiles for $\epsilon = 2, N = 1, Da = 0.1, Gr = 10, K = 0.5, D_f = 0.5, Ec = 1, S_r = 0.5, f_w = 0.5, S_f = 0.5, S_g = 0.5, S_T = 1, S_{co} = 1, Pr = 1, Sc = 0.7.$

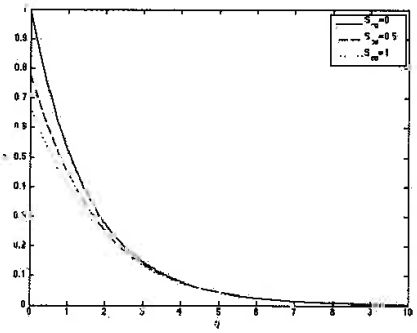

Fig. 11. Effect of solutal slip factor on concentration profiles for $\beta = 2, \epsilon = 2, N = 1, Da = 0.1, Gr = 10, K = 0.5, D_f = 0.5, Ec = 1, S_r = 0.5, f_w = 0.5, S_f = 0.5, S_g = 0.5, S_T = 1, Pr = 1, Sc = 0.7.$

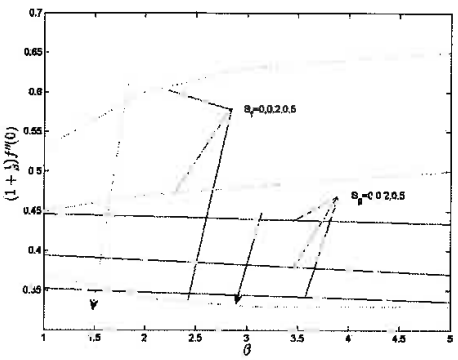

Fig. 13. Plot of skin friction coefficient versus Casson parameter for different values of the velocity and rotational slip factors for $\epsilon = 2, N = 1, Da = 0.1, Gr = 10, K = 0.5, D_f = 0.5, Ec = 1, S_r = 0.5, f_w = 0.5, S_T = 1, S_{co} = 1, Pr = 1, Sc = 0.7.$

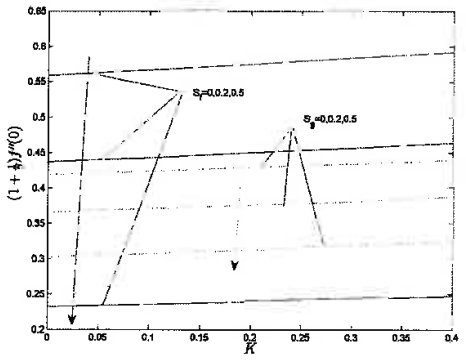

Fig. 14. Plot of skin friction coefficient versus radiation parameter for different values of the velocity and rotational slip factors for $\beta = 2, \epsilon = 2, N = 1, Da = 0.1, Gr = 10, D_f = 0.5, Ec = 1, S_r = 0.5, f_w = 0.5, S_T = 1, S_{co} = 1, Pr = 1, Sc = 0.7$.

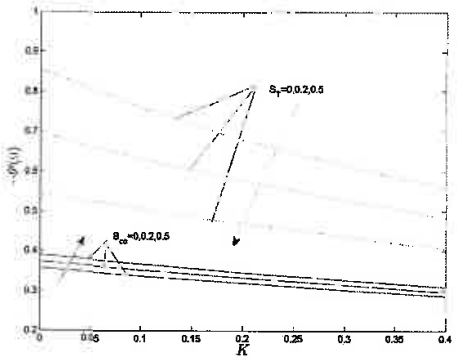

Fig. 16. Plot of heat transfer coefficient versus radiation parameter for different values of the thermal and solutal slip factors for $\beta = 2, \epsilon = 2, N = 1, Da = 0.1, Gr = 10, D_f = 0.5, Ec = 1, S_r = 0.5, f_w = 0.5, S_f = 0.5, S_g = 0.5, Pr = 1, Sc = 0.7$.

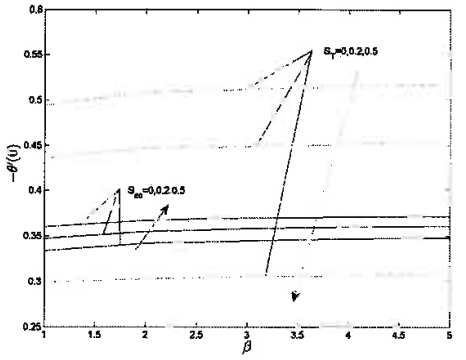

Fig. 15. Plot of heat transfer coefficient versus Casson parameter for different values of the thermal and solutal slip factors for $\epsilon = 2, N = 1, Da = 0.1, Gr = 10, K = 0.5, D_f = 0.5, Ec = 1, S_r = 0.5, f_w = 0.5, S_f = 0.5, S_g = 0.5, Pr = 1, Sc = 0.7$.

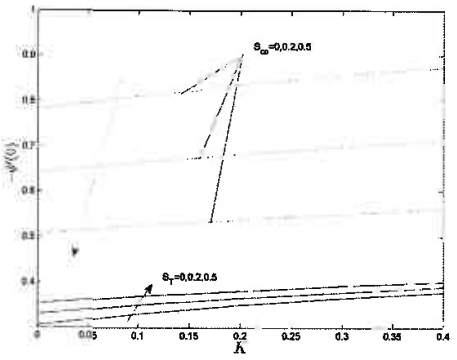

Fig. 17. Plot of mass transfer coefficient versus radiation parameter for different values of the thermal and solutal slip factors for $\beta = 2, \epsilon = 2, N = 1, Da = 0.1, Gr = 10, D_f = 0.5, Ec = 1, S_r = 0.5, f_w = 0.5, S_f = 0.5, S_g = 0.5, Pr = 1, Sc = 0.7$.

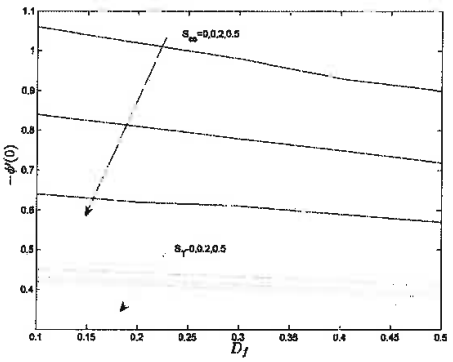

Fig. 18. Plot of mass transfer coefficient versus Dufour parameter for different values of the thermal and solutal slip factors for $\beta = 2, \epsilon = 2, N = 1, Da = 0.1, Gr = 10, K = 0.5, Ec = 1, S_r = 0.5, f_w = 0.5, S_f = 0.5, S_g = 0.5, Pr = 1, Sc = 0.7$.

We study the behavior of velocity, temperature and concentration profiles of free convection of Casson fluid from a spinning cone embedded in porous medium with viscous dissipation, a detailed numerical calculation is done for different parameter values that describe the flow and the results are shown as graphs in Figures 3 - 18. In this study we do not investigate the effects of Darcy number, Grashof number, Prandtl number, Schmidt number, and the suction/blowing parameter on velocity, temperature and concentration profiles. These results are well known and shown in among others Ramachandra et al. [17], Shateyi [24], Narayana et al. [1] and Ece [3].

Figure 3 shows the influence of the spin parameter ϵ on velocity profiles. Increasing the spin parameter assist the flow close to the surface of the cone. A reverse effect is noted further away from the surface, this is due to the Coriolis effect created by the rotation. This effect cause the shrinking of the momentum boundary layer thickness.

Figure 4 shows the effect of buoyancy parameter N on velocity profiles. Increasing the buoyancy parameter assist the flow. The surface of the cone is heated under linear heat flux causing the fluid close to the surface to rise assisting motion. This effect is less enhanced further away from the surface of the cone.

Figure 5 shows the effect of the velocity slip factor S_f on velocity profiles. Increasing the velocity slip factor assist the flow, this is characteristic of the lubricated surface. The case $S_f = 0$ referred to as the no-slip condition shows a velocity profile similar to that reported in Ece [3].

Figure 6 shows the influence of the rotational slip factor S_g on velocity profiles. Increasing the rotational slip factor reduce the velocity profiles. A slip perpendicular to the direction of flow reduce motion in the direction of flow. This effect reduce the momentum boundary layer thickness.

Figure 7 depict the effect of Dufour number D_f on temperature profiles. Increasing the Dufour number increase temperature profiles.

Figure 8 shows the effect of Eckert number Ec on temperature profiles. Increasing the Eckert number increase the temperature profiles, this caused by the heat generated within the fluid increasing the temperature of the fluid.

Figure 9 shows the effect of the thermal slip factor S_T on temperature profiles. Increasing the thermal slip factor decrease temperature profiles. Thermal slip is associated with the sudden temperature drop at the surface of the cone thereby decreasing the thermal boundary layer.

Figure 10 shows the effect of the Soret number Sr on concentration profiles. Increasing the Soret number increase concentration profiles.

Figure 11 shows the effect of the solutal slip parameter S_{co} on concentration profiles. Increasing the solutal slip parameter decrease concentration profiles. Solutal slip is associated with sudden drop of solute at the surface of the cone.

Figure 12 shows the effect of the Casson parameter β on concentration profiles. Increasing the Casson parameter decrease concentration profiles.

In Figure 13 depicts the plot of $(1 + 1/\beta)f''(0)$ related to skin friction coefficient versus the Casson parameter at different values of the velocity and rotational slip factors. In the case of no-slip condition it is noted that skin friction increases with increasing Casson parameter β. Skin friction coefficient reduce with increasing slip factor as expected on a lubricated surface. At higher values of the velocity slip factor the skin friction coefficient decrease with increasing β. As β increases the fluid becomes Newtonian exerting less force on the surface. The same effect is noted on the rotational slip factor S_g. We also note that for no-slip condition we observe a decrease in the skin friction since the rotational slip factor acts perpendicular to the flow.

In Figure 14 increasing the radiation parameter leads to the increase in the skin friction coefficient, when energy transfer is increased in the boundary layer, motion is facilitated exerting more stress on the wall. In-

creasing the velocity and rotational slip factors result in decreasing the skin friction coefficient.

In Figure 15 increasing the Casson parameter does not affect the heat transfer coefficient significantly. It is noted that increasing the thermal slip factor significantly reduce the heat transfer coefficient, and increasing the solutal slip factor increase the heat transfer coefficient. In Figure 16 increasing the thermal slip factor decreases the heat transfer coefficient. Increasing the solutal slip factor increase the heat transfer coefficient. Increasing the thermal radiation reduce the heat transfer coefficient.

In Figure 17 increasing the solutal slip factor reduce the mass transfer coefficient, while increasing the thermal slip factor increase the mass transfer coefficient. Increasing the thermal radiation parameter increase the mass transfer coefficient. In Figure 18 increasing the Dufour number generally decrease the mass transfer coefficient. Increasing both thermal and solutal slip factors decrease the mass transfer coefficient.

5 Conclusion

The investigation presented in this analysis of effects of radiation on free convection from a spinning cone with partial slip in Casson fluid in non-Darcy porous medium with cross diffusion and viscous dissipation provides numerical solutions for the boundary velocity, heat and mass transfer. The coupled nonlinear governing differential equations were solved using the spectral relaxation method (SRM). The interesting results in this work is the consideration of partial slip factors and the effect of spinning. It is generally observed that increasing each of the slip factors, S_f,S_T and S_{co} tend to assist velocity, temperature and concentration profiles respectively. The reverse effects noted in the boundary layer for both velocity and concentration profiles are caused by the presence of the combination of suction, slip factors and spinning effects. This study also presents the effect of slip factors on skin friction, Nusselt and Sherwood numbers. It is generally noted that velocity, thermal and concentration slip factors reduce skin friction, heat transfer and mass transfer coefficients respectively.

References

[1] Narayana, M, Awad, F. G., Sibanda P, Free magnetohydrodynamic flow and convection from a vertical spinning cone with cross diffusion effects, *Applied Mathematical Modelling*, 37, 2662-2678, (2013)

[2] Pramanic S, Casson fluid flow and heat transfer past an exponentially porous stretching surface in the presence of thermal radiation, *Ain Shams Engineering journal*,(2013) .

[3] Ece C.M, Free convection flow about a cone under mixed thermal boundary conditions and a magnetic field, *Applied Mathematical Modelling*, 29 (2005) 1121-1134.

[4] Cheng C.Y, Natural convection boundary layer flow in a micropolar fluid over a vertical permeable cone with variable wall temperature, *International Communications in Heat and Mass Transfer*, 38(2011)429-433.

[5] Cheng C.Y, Natural convection heat transfer of Non-Newtonian fluids in a porous media from a vertical cone under mixed boundary conditions, *International communications in Heat and Mass Transfer*,36(2009)693-697.

[6] Alim M.A, Alam M, Chowdhury M.K, Pressure work effect on Natural convection flow from a vertical circular cone with suction and non uniform surface temperature, *Journal of Mechanical Engineering*,ME36,(2006) 6-11.

[7] Narayana, M., Sibanda, P. (2012) On the solution of double diffusive convective flow due to a cone by a linearization method, *Journal of Applied Mathematics*, **doi**: 10.1155/2012/587357

[8] Awad F.G, Sibanda P, and Motsa S.S, Makinde O.D, Convection from an inverted cone in a porous medium with cross diffusion effects, *Computers and mathematics with applications*,61 (2011) 1431-1441.

[9] Agarwal, R., Rakich, J. V. (1982) Hypersonic laminar viscous flow past spinning cones at angle of attack, *The American Institute of Aeronautics and Astronautics*, **20**, 479-487

[10] Anilkumar D, Roy S, Unsteady mixed convection flow on a rotating cone in a rotating fluid, *Applied Mathematics and computation*, 155 (2004) 545-561.

[11] Takhar H.S, Rama S.B, Williams R.S, Free convection boundary layer flow of a micropolar fluid past a slender cone, *Mechanics research communications*,15(3),(1988)167-176.

[12] Saleh M.A, A numerical study of natural convection heat transfer with variable viscosity and thermal radiation from a cone and wedge in porous media, *Applied Mathematics and computation*, 170(2005)64-75.

[13] Chamkha, A J, Rashad, A M, Natural convection from a vertical permeable cone in a nanofluid saturated porous media for uniform heat and nanoparticles volume fraction fluxes, *International Journal of Numerical Methods for Heat & Fluid Flow*, 22 (8)(2012)1073-1085.

[14] Mukhopadhyay S, Vajrravelu K, Diffusion of chemically reactive species in Casson fluid flow over an unsteady permeable stretching surface,*Journal of Hydrodynamics*, 25-4,(2013) 591-598.

[15] Mukhopadhyay S, De P R, Bhattacharyya K, Layek G.C, Casson fluid flow over an unsteady stretching surface, *Ain Shams Engineering Journal*,(2013).

[16] Nadeem S, Ul Haq R, Lee C, MHD flow of a Casson fluid over an exponentially stretching sheet, *Scientia Iranica B*,19(6)(2012) 1550-1553.

[17] Ramachandra P.V,Subba R.A, Anwa B.O, Flow and heat transfer of Casson fluid from a horizontal cylinder with par-

tial slip in non-Darcy porous medium, *Applied and computational Mathematics*(2013)2:2.

[18] Hayat T, Mustafa M, Pop I, Heat and mass transfer for Soret and Dufour's effect on mixed convection boundary layer flow over a stretching vertical surface in a porous medium filled with viscoelastic fluid, *Commun Nonlinear Sci Numer Simulat*,15(2010) 1183-1196.

[19] Ching-Yang Cheng, Soret and Dufour's effects on free convection boundary layer over a vertical cylinder in a saturated porous medium, *International communications in Heat and Mass Transfer*,37(2010) 796-800.

[20] Motsa S.S, Dlamini P.G, Khumalo M, Spectral relaxation method and spectral quasi-linearization method for solving unsteady boundary layer flows problems, *Advances in Mathematical Physics*, Article ID 341964, 12 pages, **doi**: 10.1155/2014/341964.

[21] Motsa S.S, Makukula Z.G, On spectral relaxation method approach for steady Von-Karman flow of a Reiner-Revlin fluid with Joule heating, viscous dissipation and suction/injection, *Central European Journal of Physics*, 11, (2013) 363-374, **doi**: 10.2478/s11534-013-0182-8.

[22] Kameswaran P.K, Sibanda P, Motsa S, A spectral relaxation method for thermal dispersion and radiation effects in a nanofluid flow, *Boundary Value Problems*, 2013:242 pages 6-18, **doi**: www.boundaryvalueproblems.com/content/2013/242

[23] Shateyi S, Marewo G. T, (2014) "Numerical analysis of MHD stagnation point flow of Casson fluid, heat and mass transfer over a stretching sheet" In Balicki, J. (Ed) *Advances in Applied and Pure Mathematics, WSEAS, Proceedings of the 7th international conference on finite differences, finite elements, finite volumes, boundary elements (F-and-B'14)*, Gdansk, Poland, 128-132, **ISBN**: 978-960-474-380-3

[24] Shateyi, (2014) "On spectral relaxation method for an MHD flow and heat transfer of a Maxwell fluid" In M. Lazrd, O. Martin, P. Majumdar (Ed), *Proceedings of the 2014 international conference on mechanics, fluid mechanics, heat and mass transfer, Recent Advances in Mechanics, Fluid Mechanics, Heat and Mass Transfer*, Interlaken, Switzerland, 102-106, **ISBN**: 978-1-61804-220-0

[25] Datta S. K, The boundary layer flow of the Reiner-Rivlin fluid near a spinning cone, *Applied Scientific Research*, 13, (1964) 194-202.

[26] Dinarvand S., Saber M, Abulhasansari M, Micropolar fluid flow and heat transfer about a spinning cone with Hall current and Ohmic heating, *Journal of Mechanical Engineering Science*, **doi**: 10,1177/0954406213512628

Appendix F

Effects of double dispersion on Casson fluid flow with viscous dissipation and convective boundary conditions

Sachin Shaw[a], Gilbert Makanda[a], Precious Sibanda[a]

[a]*School of Mathematics, Statistics and Computer Science, University of KwaZulu-Natal, Private bag X01, Scottsville 3209, Pietermaritzburg, South Africa*

Abstract

The double diffusion mixed convection Casson fluid flow over vertical plate has been studied and incorporating Soret effect and viscous dissipation with thermal and solutal dispersion. A similarity transformation is used to transform the partial differential equations to a set of non-similar partial differential equations and solved numerically using the bivariate quasi-linearization method (BQLM). The numerical method is validated by comparison to the results obtained by the Matlab `bvp4c` and those previously published in the literature. The unique problem on double dispersion in Casson fluid flow with viscous dissipation under convective boundary conditions is considered. Increasing thermal stratification decreases heat transfer coefficient and increase mass transfer coefficient. Increasing the Casson parameter increases velocity profiles, skin friction coefficient and reduce both temperature and concentration profiles. Increasing the Biot number reduce both temperature profiles and mass transfer coefficient.

Keywords: Casson fluid, double dispersion, Soret effect, viscous dissipation.

1. Introduction

The study of the double dispersion convection in a double stratified medium is gaining interest due to its interesting and important engineering and environmental applications. Engineering application such as underground spreading of chemical wastes and other pollutants, grain storage, evaporation, cooling and solidification, thermal energy storage system such as solar ponds; heat transfer from thermal sources such as condensers of power plants and environmental related application such as heat rejection into lakes, rivers and seas. Narayana and Murthy [1] studied the heat and mass transfer in a double stratified non-Darcy porous medium. Free convection in a thermally stratified non-Darcy porous medium has been investigated by Kairi and Murthy [2]. The effect of the double dispersion in a micropolar fluid has

been studied by Srinivasacharya and RamReddy [3]. Murthy et al. [4] investigate the effect of thermal stratification on nanofluid saturated non-Darcy porous medium. kameswaran and Sibanda [5] studied the thermal dispersion effects on convective heat and mass transfer of Ostwald de Waele nanofluid flow in a porous media.

In industrial applications, non-Newtonian fluids are more appropriate than Newtonian fluids. These fluids have wide range of industrial applications, for example, in the design of thrust bearings and radial diffusers, drag reduction, transpiration cooling, thermal oil recovery, etc. The nonlinear Casson's constitutive equation was derived by Casson [6]. It describes the properties of many polymers over a wide range of shear rates (Vinogradov and Malkin [7]). At low shear rates when blood flows through small vessels, the blood flow is described by the Casson fluid model (McDonald [8]; Shaw et al. [9]).

In all the investigations mentioned above, viscous mechanical dissipation is neglected. A number of authors have considered viscous heating effects on Newtonian flows. Jordan [10] have studied the Dissipation Effects on unsteady free Convection over vertical porous plate. The influence of viscous dissipation on a gray absorbing-emitting fluid flowing past moving vertical plate has been studied by Suneetha et al. [11]. Kameswaran et al. [12]have studied the effect of the viscous dissipation on hydromagnetic nanofluid flow due to a stretching or shrinking sheet.

The aim of the present problem is to study the double stratified Casson fluid flow over vertical plate in the presence of the Soret effect and viscous dissipation. Firstly, using the similarity transformation on the governing equations and then solve numerically using well known bivariate quasi-linearization method described in Motsa et al. [14]. Influence of the different parameters as double stratification, Soret number and viscous dissipation on the flow rheology have been discussed through graphs.

2. Mathematical formulation

Consider steady, incompressible two dimensional flow of a Casson fluid adjacent to a vertical surface. The Cartesian coordinates x and y are along the surface and normal to it, u and v are the respective velocity components. The wall is maintained at constant temperature T_w and concentration C_w, respectively as shown in Figure 1

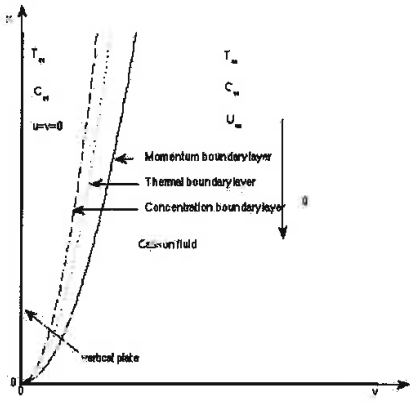

Figure 1: Schematic diagram of vertical plate in Casson fluid

An equation of an isotropic and incompressible flow of Casson fluid is written as (Nakamura and Sawada [13])

$$\tau_{ij} = \begin{cases} \left(\mu + \tau_y/\sqrt{2\pi}\right) 2e_{ij} & \pi > \pi_c \\ \left(\mu + \tau_y/\sqrt{2\pi_c}\right) 2e_{ij} & \pi < \pi_c \end{cases} \tag{1}$$

where μ is plastic dynamics viscosity of the Casson fluid, τ_y is the yield stress of fluid, π is the product of the component of deformation rate with itself, namely, $\pi = e_{ij}e_{ij}$, e_{ij} is the (i,j)-th component of the deformation rate, and π_c is the critical value π.

Taking into account the effect of the thermal and solute dispersion, the double diffusion convection equation of the Casson fluid is written as

$$\frac{\partial u}{\partial x} + \frac{\partial v}{\partial y} = 0, \tag{2}$$

$$u\frac{\partial u}{\partial x} + v\frac{\partial u}{\partial y} = \nu\left(1 + \frac{1}{\beta}\right)\frac{\partial^2 u}{\partial y^2} \pm g\beta_T(T - T_\infty) \pm g\beta_c(C - C_\infty), \tag{3}$$

$$u\frac{\partial T}{\partial x} + v\frac{\partial T}{\partial y} = \frac{\partial}{\partial y}\left(\alpha_y\frac{\partial T}{\partial y}\right) + \frac{\nu}{Cp}\left(1 + \frac{1}{\beta}\right)\left(\frac{\partial u}{\partial y}\right)^2, \tag{4}$$

$$u\frac{\partial C}{\partial x} + v\frac{\partial C}{\partial y} = \frac{\partial}{\partial y}\left(D_y\frac{\partial C}{\partial y}\right) + \frac{D_T}{T_m}\frac{\partial^2 T}{\partial y^2}. \tag{5}$$

and the corresponding boundary conditions are written as

$$u = 0,\ v = 0,\ k_f\frac{\partial T}{\partial y} = h_f(T_f - T),\ \ C = C_w,\quad \text{at } y = 0,$$
$$u \to U,\ T \to T_\infty,\ C \to C_\infty,\ \ \text{as } y \to \infty, \tag{6}$$

where ν is the viscosity of the fluid, $\beta = \mu\sqrt{2\pi_c}/\tau_y$ is the Casson parameter, g is the acceleration due to gravity, β_T and β_C are the coefficients of thermal and solutal expansions, T is the solute temperature, T_∞ is uniform ambient temperature, C is the solute concentration, C_∞ is uniform ambient concentration, $\alpha_y = \alpha + \gamma d\frac{\partial\psi}{\partial y}$ and $D_y = D_{sm} + \zeta d\frac{\partial\psi}{\partial y}$ represent the thermal dispersion and solutal diffusivity, respectively where α is the molecular thermal diffusivity, γ is the mechanical thermal-dispersion coefficient, D_{sm} is the solutal diffusivity and ζ is the mechanical solutal-dispersion coefficient, C_p is the specific heat capacity, is the fluid electrical conductivity, D_T is the thermal diffusivity, T_m is the mean fluid temperature. Introducing the convective boundary condition at the bottom of the surface which is heated by the convection from a hot fluid of temperature T_f and provide a heat transfer coefficient h_f and thermal conductivity k where $T_f > T_w > T_\infty$.

Using the following similarity transformations

$$\xi = \frac{x}{l},\ \eta = \sqrt{\frac{U}{\nu x}}y,\ \psi = \sqrt{\nu U x}f(\xi,\ \eta),\ \theta = \frac{T - T_\infty}{T_f - T_\infty},\ \phi = \frac{C - C_\infty}{C_w - C_\infty}, \tag{7}$$

Using the similarity transformation, the governing equations are written as

$$\left(1 + \frac{1}{\beta}\right)f''' + \frac{1}{2}ff'' \pm \lambda\xi(\theta + N\phi) = \xi\left(f'\frac{\partial f'}{\partial\xi} - f''\frac{\partial f}{\partial\xi}\right), \tag{8}$$
$$\left(\frac{1}{Pr} + R\right)\theta'' + \frac{1}{2}f\theta' + \left(1 + \frac{1}{\beta}\right)Ecf''^2 + \gamma Ra_d\left(f''\theta' + f'\theta''\right) = \xi\left(f'\frac{\partial\theta}{\partial\xi} - \theta'\frac{\partial f}{\partial\xi}\right), \tag{9}$$
$$\frac{1}{Sc}\phi'' + \frac{1}{2}f\phi' + Sr\theta'' + \zeta Ra_d\left(f''\phi' + f'\phi''\right) = \xi\left(f'\frac{\partial\phi}{\partial\xi} - \phi'\frac{\partial f}{\partial\xi}\right), \tag{10}$$

and the boundary conditions are written as

$$f' = 0,\ f + 2\xi\frac{\partial f}{\partial\xi} = 0,\ \theta' = -Bi\left(1 - \theta(0)\right),\ \phi = 1,\quad \text{at } \eta = 0,$$
$$f' \to 1,\ \theta \to 0,\ \phi \to 0,\quad \text{as } \eta \to \infty \tag{11}$$

where 'prime' denoted the differentiation with respect to η. Thermal Grashof number Gr, Reynolds number Re, Solute Grashof number Gr^*, thermal convection parameter λ, solutal

convection parameter λ^*, double diffusion parameter N, stratification parameter Ra_d, radiation parameter R, Eckert number Ec, Schmidt number Sc, Soret number Sr and Biot number Bi defined as

$$Gr = \frac{g\beta_T \Delta T L^3}{\nu^2},\ Re = \frac{UL}{\nu},\ Gr^* = \frac{g\beta_c \Delta C L}{U^2},\ \lambda = \frac{Gr}{Re^2}, \lambda^* = \frac{Gr^*}{Re^2},\ N = \frac{\lambda^*}{\lambda},\ Ra_d = \frac{dU}{\nu}$$
$$R = \frac{16T_\infty^2 \sigma}{3\nu k^*},\ Ec = \frac{\nu U^2}{Cp\Delta T},\ Sc = \frac{\nu}{D},\ Sr = \frac{DK_T \Delta T}{\nu T_m \Delta C},\ Bi = \frac{a}{k_f}\sqrt{\frac{\nu}{U}}, \tag{12}$$

The nondimensional physical parameters are the skin friction coefficient, local Nusselt number Nu_x and local Sherwood number Sh_x are written as

$$Ra_x^{1/2}\ C_f = \left(1 + \frac{1}{\beta}\right) f''(0),\ Ra_x^{-1/2}\ Nu_x = -[1 + \gamma Ra_d f'(0)]\theta'(0),$$
$$Ra_x^{-1/2}\ Sh_x = -[1 + \zeta Ra_d f'(0)]\phi'(0), \tag{13}$$

3. Solution method

In this section we describe implementation of the bivariate quasi-linearization method (BQLM) which is based on the quasi-linearization method (QLM) which is described in detail in Motsa et al. ([14]) We apply the quasi-linearization method (QLM) first proposed by Bellman and Kalaba [15] to equations (8)-(10) which is based on the Taylor series expansion with the assumption that the differences $(f_{r+1} - f_r)$,$(\theta_{r+1} - \theta_r)$ and all its derivatives are small. We obtain the following equations

$$\left(1 + \frac{1}{\beta}\right) f'''_{r+1} + a_{1,r}(\eta,\xi) f''_{r+1} + a_{2,r}(\eta,\xi) f'_{r+1} + a_{3,r}(\eta,\xi) f_{r+1}$$
$$+ a_{4,r}(\eta,\xi)\frac{\partial f'_{r+1}}{\partial \xi} + a_{5,r}(\eta,\xi)\frac{\partial f_{r+1}}{\partial \xi} = a_{6,r}(\eta,\xi), \tag{14}$$
$$b_{1,r}(\eta,\xi)\theta''_{r+1} + b_{2,r}(\eta,\xi)\theta'_{r+1} + b_{3,r}(\eta,\xi)\frac{\partial \theta_{r+1}}{\partial \xi} = b_{4,r}(\eta,\xi), \tag{15}$$
$$c_{1,r}(\eta,\xi)\phi''_{r+1} + c_{2,r}(\eta,\xi)\phi'_{r+1} + c_{3,r}(\eta,\xi)\phi_{r+1} + c_{4,r}(\eta,\xi)\frac{\partial \phi_{r+1}}{\partial \xi} = c_{5,r}(\eta,\xi). \tag{16}$$

Where

$$a_{1,r} = \frac{1}{2} f_r + \xi \frac{\partial f_r}{\partial \xi}, \tag{17}$$

$$a_{2,r} = -\xi \frac{\partial f'_r}{\partial \xi}, \tag{18}$$

$$a_{3,r} = \frac{1}{2} f''_r, \tag{19}$$

$$a_{4,r} = -\xi f'_r, \tag{20}$$

$$a_{5,r} = \xi f''_r, \tag{21}$$

$$a_{6,r} = \frac{1}{2} f_r f''_r - \lambda \xi \left(\theta_r + N\phi\right) - \xi \left(\frac{\partial f'_r}{\partial \xi} - f''_r \frac{\partial f_r}{\partial \xi}\right), \tag{22}$$

$$b_{1,r} = \frac{1}{Pr} + R + \gamma Ra_d f'_r, \tag{23}$$

$$b_{2,r} = \frac{1}{2} f_r + \xi \frac{\partial f_r}{\partial \xi} + \gamma Ra_d f''_r. \tag{24}$$

$$b_{3,r} = -\xi f'_r, \tag{25}$$

$$b_{4,r} = -Ec(1 + \frac{1}{\beta})(f''_r)^2, \tag{26}$$

$$c_{1,r} = \frac{1}{Sc} + \zeta Ra_d f'_r, \tag{27}$$

$$c_{2,r} = \frac{1}{2} f_r \tag{28}$$

$$c_{3,r} = \xi \frac{\partial f_r}{\partial \xi} + \zeta Ra_d f''_r, \tag{29}$$

$$c_{4,r} = -\xi f'_r, \tag{30}$$

$$c_{5,r} = -Sr\theta''_r. \tag{31}$$

The solution for the now linear partial differential equations (14)-(16) is obtained by approximating the exact solutions of $f(\eta, \xi)$, $\theta(\eta, \xi)$ and $\phi(\eta, \xi)$ by the Lagrange form of polynomial $F(\eta, \xi)$, $\Theta(\eta, \xi)$ and $\Phi(\eta, \xi)$ at the selected collocation points

$$0 = \xi_0 < \xi_1 < \xi_2 < \cdots < \xi_{N_\xi} = 1$$

The approximation for $f(\eta, \xi)$ and $\theta(\eta, \xi)$ has the form

$$f(\eta,\xi) \approx \sum_{j=0}^{N_\xi} F(\eta,\xi)L_j(\xi) = \sum_{j=0}^{N_\xi} F_j(\eta)L_j(\xi), \tag{32}$$

$$\theta(\eta,\xi) \approx \sum_{j=0}^{N_\xi} \Theta(\eta,\xi)L_j(\xi) = \sum_{j=0}^{N_\xi} \Theta_j(\eta)L_j(\xi), \tag{33}$$

$$\phi(\eta,\xi) \approx \sum_{j=0}^{N_\xi} \Phi(\eta,\xi)L_j(\xi) = \sum_{j=0}^{N_\xi} \Phi_j(\eta)L_j(\xi). \tag{34}$$

where $F_j(\eta) = F(\eta,\xi)$, $\Theta_j(\eta) = \Theta(\eta,\xi)$ and $\Phi_j(\eta) = \Phi(\eta,\xi)$, L_j is the characteristic Lagrange cardinal polynomial defined as

$$L_j(\xi) = \prod_{k=0,k\neq j}^{M} \frac{\xi - \xi_k}{\xi_j - \xi_k}, \tag{35}$$

that obey the Kronecker delta equation

$$L_j(\xi_k) = \delta_{jk} = \begin{cases} 0 & \text{if} \quad j \neq k \\ 1 & \text{if} \quad j = k \end{cases} \tag{36}$$

The equations for the solution of $F_j(\eta)$, $\Theta_j(\eta)$ and $\Phi_j(\eta)$ are obtained by substituting (32)-(34) into (14)-(16) and letting the equations be satisfied at the points $\xi_i, i = 0, 1, 2, \ldots, N_\xi$. To compute the derivatives of the Lagrange polynomial analytically we transform $\xi \in [0, L_\xi]$ to $\zeta \in [-1, 1]$ then choose Chebyshev-Gauss-Lobatto points $\zeta_i = \cos\frac{i\pi}{N_\xi}$. After using linear transformation $\xi = L_\xi(\zeta + 1)/2$, the derivatives of f' with respect to the collocation points ζ_j is computed as

$$\left.\frac{\partial f'}{\partial \xi}\right|_{\xi=\xi_i} = 2\sum_{j=0}^{N_\xi} F'_j(\eta)\frac{dL_j}{d\zeta}(\zeta_i) = \sum_{j=0}^{N_\xi} \mathbf{d}_{i,j}F'_j(\eta), i = 0, 1, 2, \ldots, N_\xi, \tag{37}$$

where $\mathbf{d}_{i,j} = \frac{dL_j}{d\zeta}(\zeta_i)(i = 0, 1, \ldots, N_\xi)$ are entries of the standard Chebyshev differentiation matrix, $\mathbf{d} = \frac{2}{L_\xi}d$. We now apply the collocation (η, ξ_i) in (14)-(16) we obtain

$$\left(1+\frac{1}{\beta}\right)F'''_{r+1,i}(\eta)+a^{(i)}_{1,r}F''_{r+1,i}(\eta)+a^{(i)}_{2,r}F'_{r+1,i}(\eta)+a^{(i)}_{3,r}F_{r+1,i}(\eta)$$
$$+a^{(i)}_{4,r}\sum_{j=0}^{N_\xi}\mathbf{d}_{i,j}F'_{r+1,i}(\eta)+a^{(i)}_{5,r}\sum_{j=0}^{N_\xi}\mathbf{d}_{i,j}F_{r+1,i}(\eta)=a^{(i)}_{6,r}, \tag{38}$$

$$b^{(i)}_{1,r}\Theta''_{r+1,i}(\eta)+b^{(i)}_{2,r}\Theta'_{r+1,i}(\eta)+b^{(i)}_{3,r}\sum_{j=0}^{N_\xi}\mathbf{d}_{i,j}\Theta_{r+1,i}(\eta)=b^{(i)}_{4,r}, \tag{39}$$

$$c^{(i)}_{1,r}\Phi''_{r+1,i}(\eta)+c^{(i)}_{2,r}\Phi'_{r+1,i}(\eta)+c^{(i)}_{3,r}\Phi_{r+1,i}(\eta)+c^{(i)}_{4,r}\sum_{j=0}^{N_\xi}\mathbf{d}_{i,j}\Phi_{r+1,i}(\eta)=c^{(i)}_{5,r} \tag{40}$$

where $a^{(i)}_{k,r}=a_{k,r}(\eta,\xi_i)\quad(k=1,2,3,4,5,6)$, $b^{(i)}_{k,r}=b_{k,r}(\eta,\xi_i)\quad(k=1,2,3,4)$ and $c^{(i)}_{k,r}=c_{k,r}(\eta,\xi_i)\quad(k=1,2,3,4,5)$. Since the solution at $\xi=0(\zeta=\zeta_{N_\xi})$ is known, we evaluate (38)-(40) for $i=0,1,\ldots,N_\xi-1$ the system becomes

$$\left(1+\frac{1}{\beta}\right)F'''_{r+1,i}+a^{(i)}_{1,r}F''_{r+1,i}+a^{(i)}_{2,r}F'_{r+1,i}+a^{(i)}_{3,r}F_{r+1,i}+a^{(i)}_{4,r}\sum_{j=0}^{N_\xi-1}\mathbf{d}_{i,j}F'_{r+1,i}$$
$$+a^{(i)}_{5,r}\sum_{j=0}^{N_\xi-1}\mathbf{d}_{i,j}F_{r+1,i}=a^{(i)}_{6,r}-a^{(i)}_{4,r}\mathbf{d}_{i,N_\xi}F'_{r+1,N_\xi}-a^{(i)}_{5,r}\mathbf{d}_{i,N_\xi}F_{r+1,N_\xi}, \tag{41}$$

$$b^{(i)}_{1,r}\Theta''_{r+1,i}+b^{(i)}_{2,r}\Theta'_{r+1,i}+b^{(i)}_{3,r}\sum_{j=0}^{N_\xi-1}\mathbf{d}_{i,j}\Theta_{r+1,i}=b^{(i)}_{4,r}-b^{(i)}_{3,r}\mathbf{d}_{i,N_\xi}\Theta_{r+1,N_\xi}, \tag{42}$$

$$c^{(i)}_{1,r}\Phi''_{r+1,i}+c^{(i)}_{2,r}\Phi'_{r+1,i}+c^{(i)}_{3,r}\Phi_{r+1,i}+c^{(i)}_{4,r}\sum_{j=0}^{N_\xi-1}\mathbf{d}_{i,j}\Phi_{r+1,i}=c^{(i)}_{5,r}-c^{(i)}_{4,r}\mathbf{d}_{i,N_\xi}\Phi_{r+1,N_\xi}. \tag{43}$$

For each ξ_i, the equation (41)-(42) forms a system of linear ordinary differential equations with variable coefficients. In this system we apply the Chebyshev spectral collocation independently in the η direction by choosing $N_\eta+1$ Chebyshev-Gauss-Lobatto points $0=\eta_0<\eta_1<\eta_2<\cdots<\eta_{N_\eta}=\eta_e$, where η_e is a finite value that is chosen to be adequately large to approximate the conditions at ∞. We now implement the collocation in the interval $[0,\eta_e]$ on the $\eta-$ axis which is then transformed into the interval $[-1,1]$ using a linear transformation $\eta=\eta_e(\tau+1)/2$. The collocation points are chosen as $\tau_j=\cos\frac{j\pi}{N_\eta}$. The derivatives with respect to η are defined in terms of the Chebyshev differentiation matrix as

$$\left.\frac{d^p F'_{r+1,i}}{d\eta^p}\right|_{\eta=\eta_j} = \left(\frac{2}{\eta_e}\right)^p \sum_{k=0}^{N_\eta} D^p_{j,k} F_{r+1,i}(\tau_k) = \left[\mathbf{D}^p \mathbf{F}_{r+1,i}\right]_j \tag{44}$$

where p is the order of the derivative, $\mathbf{D} = \frac{2}{\eta_e} D, (j,k = 0,1,2,\ldots,N_\eta)$ with D being an $(N_\eta+1)\times(N_\eta+1)$ Chebyshev derivative matrix, and the vector $\mathbf{F}_{r+1,i}$ is defined as

$$\mathbf{F}_{r+1,i} = [F_{r+1,1}(\tau_0), F_{r+1,1}(\tau_1), \ldots, F_{r+1,1}(\tau_{N_\eta})]^T, \tag{45}$$

$$\Theta_{r+1,i} = [\Theta_{r+1,i}(\tau_0), \Theta_{r+1,i}(\tau_1), \ldots, \Theta_{r+1,i}(\tau_{N_\eta})]^T, \tag{46}$$

$$\Phi_{r+1,i} = [\Phi_{r+1,i}(\tau_0), \Phi_{r+1,i}(\tau_1), \ldots, \Phi_{r+1,i}(\tau_{N_\eta})]^T. \tag{47}$$

substituting (44) into (41) we get

$$\mathbf{A}^{(i)}\mathbf{F}_{r+1,i} + \mathbf{a}^{(i)}_{4,r} \sum_{j=0}^{N_\xi - 1} d_{i,j}\mathbf{D}\mathbf{F}_{r+1,j} + \mathbf{a}^{(i)}_{5,r} \sum_{j=0}^{N_\xi - 1} d_{i,j}\mathbf{F}_{r+1,j} = R^{(i)}_1. \tag{48}$$

$$\mathbf{A}^{(i)} = (1+\frac{1}{\beta})\mathbf{D}^3 + \mathbf{a}^{(i)}_{1,r}\mathbf{D}^2 + a^{(i)}_{2,r}\mathbf{D} + \mathbf{a}^{(i)}_{2,r}, \tag{49}$$

$$\mathbf{R}^{(i)}_1 = \mathbf{a}^{(i)}_{6,r} - \mathbf{a}^{(i)}_{4,r} d_{i,N_\xi}\mathbf{D}\mathbf{F}_{r+1,N_\xi} - \mathbf{a}^{(i)}_{5,r} d_{i,N_\xi}\mathbf{F}_{r+1,N_\xi} \tag{50}$$

$$\mathbf{B}^{(i)}\Theta_{r+1,i} + \mathbf{b}^{(i)}_{2,r} \sum_{j=0}^{N_\xi - 1} d_{i,j}\Theta_{r+1,j} = R^{(i)}_2, \tag{51}$$

$$\mathbf{B}^{(i)} = \frac{1}{Pr}(1+\frac{4}{3}K)\mathbf{D}^2 + \mathbf{b}^{(i)}_{1,r}\mathbf{D}, \tag{52}$$

$$\mathbf{R}^{(i)}_2 = \mathbf{b}^{(i)}_{3,r} - \mathbf{b}^{(i)}_{2,r} d_{i,N_\xi}\Theta_{r+1,N_\xi}, \tag{53}$$

$$\mathbf{C}^{(i)}\Phi_{r+1,i} + \mathbf{b}^{(i)}_{2,r} \sum_{j=0}^{N_\xi - 1} d_{i,j}\Phi_{r+1,j} = R^{(i)}_3, \tag{54}$$

$$\mathbf{C}^{(i)} = \frac{1}{Pr}(1+\frac{4}{3}K)\mathbf{D}^2 + \mathbf{c}^{(i)}_{1,r}\mathbf{D}, \tag{55}$$

$$\mathbf{R}^{(i)}_3 = \mathbf{c}^{(i)}_{3,r} - \mathbf{c}^{(i)}_{2,r} d_{i,N_\xi}\Phi_{r+1,N_\xi}. \tag{56}$$

$\mathbf{a}_{k,r}(k=1,2,3,4,5,6)$, $\mathbf{b}_{k,r}(k=1,2,3)$ and $\mathbf{c}_{k,r}(k=1,2,3)$ are the diagonal matrix with vector $[a_{k,r}(\tau_0), a_{k,r}(\tau_1), \ldots, a_{k,r}(\tau_{N_x})]^T$, $[b_{k,r}(\tau_0), b_{k,r}(\tau_1), \ldots, b_{k,r}(\tau_{N_x})]^T$ and $[c_{k,r}(\tau_0), c_{k,r}(\tau_1), \ldots, c_{k,r}(\tau_{N_x})]^T$. We then impose boundary conditions and a matrix system is formed as follows.

$$\mathbf{AA} = \left(\begin{array}{c|c|c} A_{0,0}\dots A_{0,N_\xi-1} & 0\dots 0 & 0\dots 0 \\ \vdots \ddots \vdots & \vdots \ddots \vdots & \vdots \ddots \vdots \\ A_{N_\xi-1,0}\dots A_{N_\xi-1,N_\xi-1} & 0\dots 0 & 0\dots 0 \\ \hline 0\dots 0 & B_{0,0}\dots B_{0,N_\xi-1} & 0\dots 0 \\ \vdots \ddots \vdots & \vdots \ddots \vdots & \vdots \ddots \vdots \\ 0\dots 0 & B_{N_\xi-1,0}\dots B_{N_\xi-1,N_\xi-1} & 0\dots 0 \\ \hline 0\dots 0 & 0\dots 0 & C_{0,0}\dots C_{0,N_\xi-1} \\ \vdots \ddots \vdots & \vdots \ddots \vdots & \vdots \ddots \vdots \\ 0\dots 0 & 0\dots 0 & C_{N_\xi-1,0}\dots C_{N_\xi-1,N_\xi-1} \end{array}\right)$$

$$\mathbf{FF} = \left(\begin{array}{c} \mathbf{F}_{r+1,0} \\ \mathbf{F}_{r+1,1} \\ \vdots \\ \mathbf{F}_{r+1,N_\xi-1} \\ \hline \Theta_{r+1,0} \\ \Theta_{r+1,1} \\ \vdots \\ \Theta_{r+1,N_\xi-1} \\ \hline \Phi_{r+1,0} \\ \Phi_{r+1,1} \\ \vdots \\ \Phi_{r+1,N_\xi-1} \end{array}\right), \mathbf{RR} = \left(\begin{array}{c} R_1^{(0)} \\ R_1^{(1)} \\ \vdots \\ R_1^{(N_\xi-1)} \\ \hline R_2^{(0)} \\ R_2^{(1)} \\ \vdots \\ R_2^{(N_\xi-1)} \\ \hline R_3^{(0)} \\ R_3^{(1)} \\ \vdots \\ R_3^{(N_\xi-1)} \end{array}\right)$$

The above system is then solved as

$$\mathbf{FF} = \mathbf{AA}^{-1}\mathbf{RR}. \tag{57}$$

$$A_{i,i} = \mathbf{A}^{(i)} + a_{4,r}^{(i)} d_{i,i}\mathbf{D} + a_{5,r}^{(i)} d_{i,i},$$

$$B_{i,i} = \mathbf{B}^{(i)} + b_{2,r}^{(i)} d_{i,i} \quad i = 0, 1, \ldots, N_\xi - 1 \tag{58}$$

$$C_{i,i} = \mathbf{B}^{(i)} + b_{2,r}^{(i)} d_{i,i} \quad i = 0, 1, \ldots, N_\xi - 1 \tag{59}$$

$$A_{i,j} = a_{4,r}^{(i)} d_{i,j}\mathbf{D} + a_{5,r}^{(i)} d_{i,j}, \quad i \neq j$$

$$B_{i,j} = b_{2,r}^{(i)} d_{i,j} \quad i \neq j \tag{60}$$

$$C_{i,j} = b_{2,r}^{(i)} d_{i,j} \quad i \neq j \tag{61}$$

4. Results and discussion

In Table 1, we compare the results of the bivariate quasi-linearization method (BQLM) to the successive linearization method (SLM) and Matlab **bvp4c** method. The results of the BQLM are in excellent agreement with these two methods to seven decimal places showing the accuracy of this method.

Table 1: Comparison of the values of $f''(0)$ and $-\theta'(0)$ obtained by BQLM with those of bvp4c for $Pr = 5, 1/\beta \to 0, N = \xi = K = Ec = Ra_d = \gamma_0 = \zeta_0 = 0$

	Yih (1999)		bvp4c		BQLM	
Pr	$f''(0)$	$-\theta'(0)$	$f''(0)$	$-\theta'(0)$	$f''(0)$	$-\theta'(0)$
1	0.332057	0.332057	0.33205935	0.33205935	0.33205935	0.33205935
10	-	-	0.3305935	0.72814593	0.3305935	0.72814593

In order to get the physical insight, the system of ordinary differential Eqs. (9) - (11) along the boundary condition Eq. (12) by means of the Matlab **bvp4c** ODE solver. In this section a representative set of graphical results for the dimensional velocity, temperature, and solutal concentration as well as the local heat and mass transfer coefficient is presented and discussed for some parametric conditions.

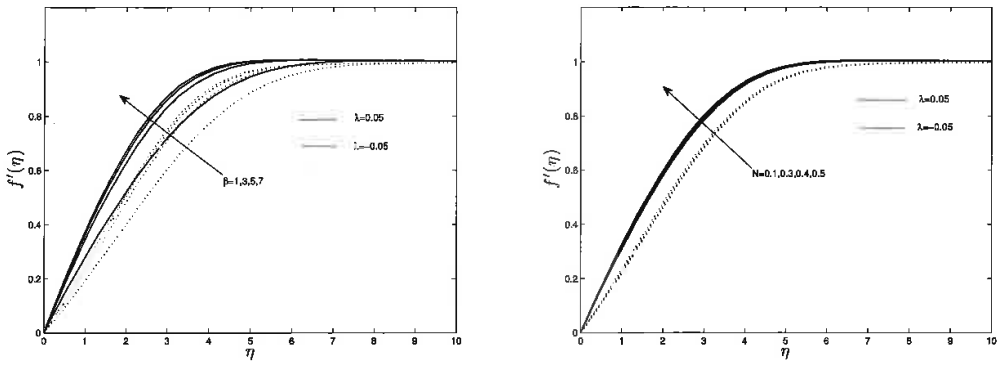

(a) (b)

Figure 2: Effects of (a) Casson parameter β and (b) buoyancy parameter N on velocity profiles

The influence of the Casson parameter and the buoyancy parameter at different values of the thermal convection parameter λ on the velocity profiles is shown in Figure 2. It is evident from Figure 3(a) that the velocity of the fluid increases with increase of the Casson parameter as the yield stress is inversely proportional to Casson parameter and so with increase of the Casson parameter, the yield stress decreases which reduce the friction between the fluid and surface and increase the velocity of the fluid. For higher value of β (i.e., $\beta \to \infty$), the fluid behaves as a Newtonian fluid hence, we may conclude that in general, the velocity of the Casson fluid is less than that of a Newtonian fluid. In Figure 3(b), the velocity of the fluid decelerate at the surface with increase of the buoyancy parameter which decreases the momentum boundary layer thickness as N increases.

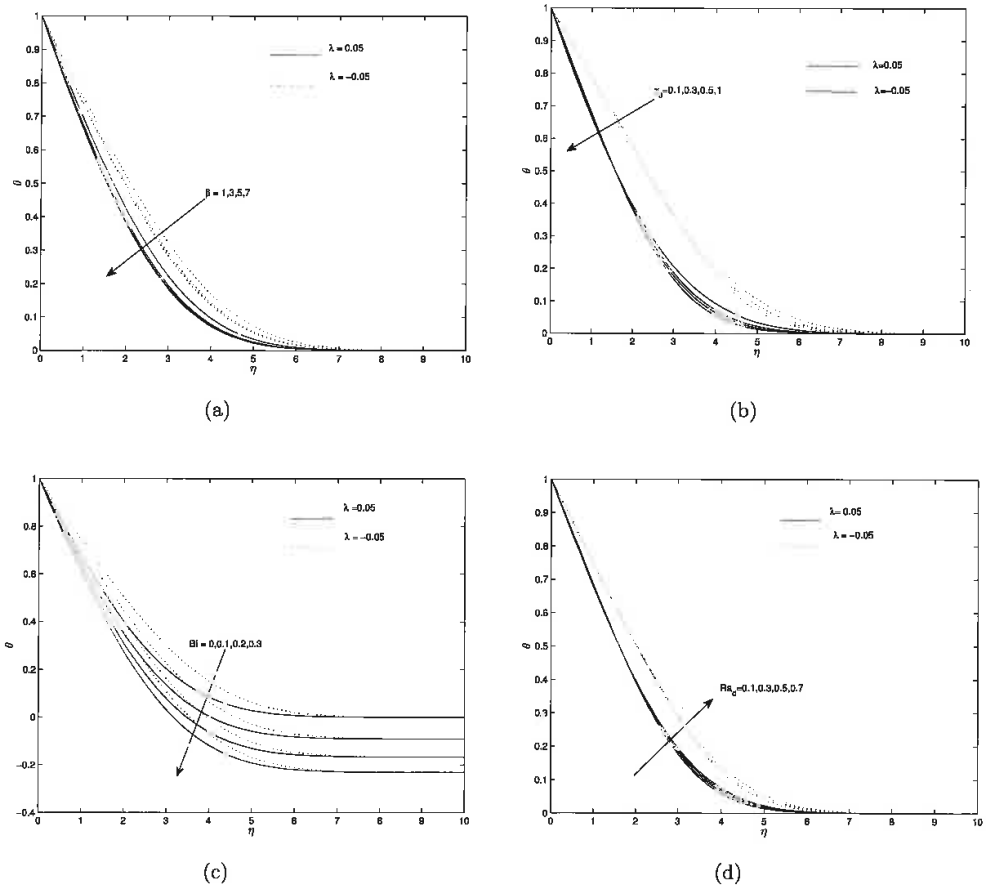

Figure 3: Effect of (a) Casson parameter β, (b) thermal diffusion constant γ_0, (c) Biot number Bi and (d) stratification parameter Ra_d on temperature profiles.

The effects of Casson parameter β, mechanical thermal-dispersion coefficient γ_0, Biot number Bi and stratification parameter Ra_d on temperature profiles is shown in Figures 3(a) - (d). It evident from Figure 3(a) that the thermal boundary layer thickness decreases with increase of the Casson parameter β in both aiding ($\lambda = 0.05$) and opposing flows ($\lambda = -0.05$). In Figure 3(b), increasing the mechanical thermal-dispersion coefficient γ_0 increases the thermal boundary layer thickness as the fluid moves away from the surface due to enhanced of γ_0 in both aiding ($\lambda = 0.05$) and opposing flows ($\lambda = -0.05$). In Figure 4(c), increasing the Biot

number highly influence the temperature of the fluid as it is directly related with the convective boundary condition. Increasing the Biot number result in the increase in convective heat transfer which reduce the thermal boundary layer thickness in both aiding ($\lambda = 0.05$) and opposing flows ($\lambda = -0.05$). In Figure 3(d), the thermal boundary layer thickness increases with increase stratification parameter. This is happens because when thermal stratification is introduced in the system, it reduces the effective temperature difference between the plate and the ambient fluid.

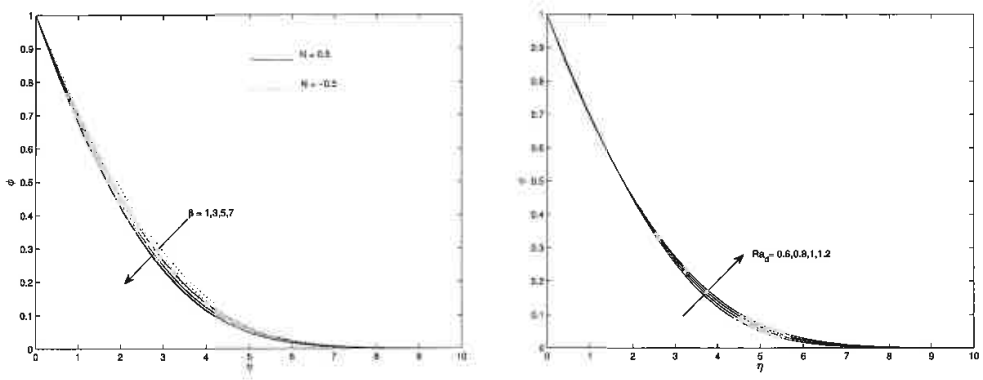

(a) (b)

Figure 4: Effects of (a) Casson parameter β and (b) Stratification parameter Ra_d on the concentration profiles.

In Figure 4, the influence of the Casson parameter β and stratification parameter parameter Ra_d on concentration parameters profiles is shown. The Casson parameter causes for the retardation in the fluid motion which decrease the concentration boundary layer thickness. This is more effective for the aiding buoyancy than the opposing buoyancy as shown in Figure 4(a). Stratification parameter increase the solute concentration near the surface which increase the boundary layer thickness as shown in Figure 4(b).

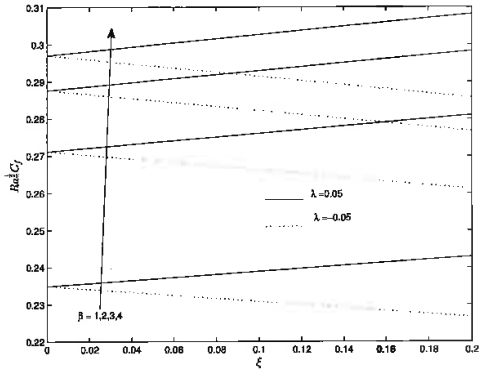

Figure 5: Plot of the skin friction coefficient $f''(0)$ against transverse coordinate ξ for different values of the Casson parameter β

Figure 5 shows the plot of skin friction coefficient $f''(0)$ against the transverse coordinate ξ for different values of the Casson parameter β for both aiding and opposing thermal convection. It can be seen from the graph that increasing the Casson parameter β result in the decrease in the skin friction coefficient. The increase in the Casson parameter has an effect of reducing the shear stress on the vertical surface thereby reducing skin friction coefficient. The skin friction coefficient increases with increasing ξ for the aiding case ($\lambda = 0.05$) and decreases with increasing ξ for the opposing case ($\lambda = -0.05$).

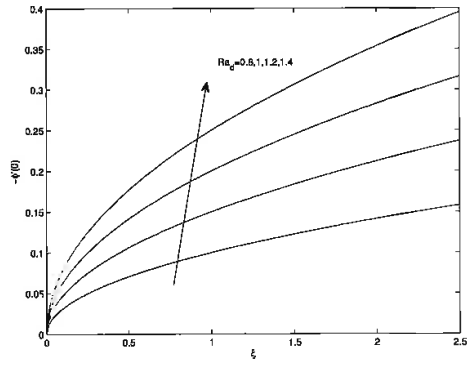

Figure 6: Plot of mass transfer coefficient against ξ for different values of the stratification parameter Ra_d

In Figure 7, the plot of the mass transfer coefficient against the transverse coordinate for different values of the stratification paramcter Ra_d is shown. Increasing the stratification parameter result in the decrease in the mass transfer coefficient. The increase in the stratification parameter has an effect of reducing the temperature gradient thereby reducing the solute transport from the surface of the vertical wall. The mass transfer coefficient decrease with increasing ξ.

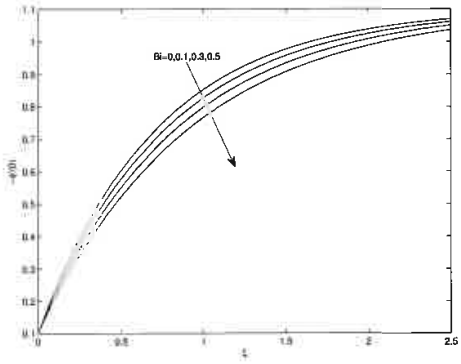

Figure 7: Plot of the mass transfer coefficient $-\phi'(0)$ against transverse coordinate ξ for different values of the Biot number Bi

In Figure 7, it can be seen that increasing the Biot number result in the decrease in the mass transfer coefficient. Increasing the Biot number would have an effect of increasing the heat resistance in the solid boundary thereby reducing mass transfer caused by heat transfer. The mass transfer coefficient increases with increasing transverse coordinate ξ.

5. Conclusion

The influence of the double dispersion on the double diffusion convection Casson fluid flow over a vertical plate have been studied. It shows that the double dispersion plays a vital role in the effectively act on the system. Thermal stratification decreases the heat transfer coefficient at the surface and increase mass transfer coefficient, temperature and concentration profiles. This study is very useful to study the dispersion in blood vessels and transportation of nanoparticles. Increasing the Casson parameter increase velocity profiles, skin friction coefficient and reduce both temperature and concentration profiles. Increasing the Biot number

reduce both temperature profiles and mass transfer coefficient. In this study we used the bivariate quasi-linearization method (BQLM) to solve the governing system of differential equations The accuracy of the method was compared to previously published results and the Matlab `bvp4c`.

[1] P.A. Lakshmi Narayana, P.V.S.N. Murthy,Free convective heat and mass transfer in a doubly stratified non-Darcy porous medium, Transactions of the ASME - J of Heat Transf., 128 (2006) 12041212.

[2] R.R. Kairi, P.V.S.N. Murthy, Free convection in a thermally stratified non-Darcy porous medium, Int. J of Fluid Mech. Res., 36 (2009) 414423.

[3] D. Srinivasacharya, Ch. RamReddy, Effect of Double Stratification on Free Convection in a Micropolar Fluid, Transactions of the ASME - Journal of Heat Transf., 133 (2011) 122502 (7 Pages)

[4] P.V.S.N. Murthy, Ch. RamReddy, A.J. Chamkha, A.M. Rashad, Magnetic effect on thermally stratified nanofluid saturated non-Darcy porous medium under convective boundary condition, Int. Commun. in Heat and Mass Transf., 47 (2013) 41-48.

[5] PK Kameswaran, P Sibanda, Thermal dispersion effects on convective heat and mass transfer in an Ostwald de Waele nanofluid flow in porous media, Boundary Value Problems 2013 (1), 243

[6] N. Casson, A flow equation for pigment-oil suspensions of the printing ink type. In: Mill, C.C. (ed.), Rheology of Disperse System. Pergamon Press, Newyork, Oxford (1959) 84-104.

[7] G.V. Vinogradov, A.Y. Malkin, Rheology of polymers, Mir Publisher, Moscow, 1979.

[8] D.A. McDonald, Blood flows in Arteries, 2nd Edition, Chap. 2., Arnold, London, 1974.

[9] S. Shaw, R.S.R. Gorla, P.V.S.N. Murthy, C.O. Ng., Pulsatile Casson fluid flow through a stenosed bifurcated artery, Int. J. Fluid Mech. Res., 36 (2009) 43-63.

[10] J. Zueco Jordan, Network Simulation Method Applied to Radiation and Dissipation Effects on MHD Unsteady Free Convection over Vertical Porous Plate. Appl. Math.Modelling, 31 (2007) 2019-2033.

[11] Suneetha, S., Bhaskar Reddy, N., Ramachandra Prasad, V., Radiation and mass transfer effects on MHD free convection flow past an impulsively started isothermal vertical plate with dissipation. Thermal Science, 13 (2009) 71-181.

[12] PK Kameswaran, M Narayana, P Sibanda, P Murthy, Hydromagnetic nanofluid flow due to a stretching or shrinking sheet with viscous dissipation and chemical reaction effects, Int. J of heat and mass trans., 55 (2012) 7587-7595.

[13] M. Nakamura, T. Sawada, Numerical study on the flow of a non-Newtonian fluid through an axisymmetric stenosis, J. Biomech Eng., 110 (1988) 137-143.

[14] Motsa, S. S., Magagula, V. M, Sibanda, P. (2014) A bivarate Chebyshev spectral collocation quasilinearization method for nonlinear evolution parabolic equations, *The Scientific World Journal*, **2014**, Article ID 581987, 13 pages, **doi**: 10.1155/2014/581987

[15] Bellman, R. E, Kalaba, R. E. (1965) *Quasilinearization and nonlinear boundary value problems*, Elsevier, New York

References

Aasaraai, A. (2011) Analytic solution for Newell-Whitehead-Segel equation by differential transform method, *Middle-East Journal of Scientific Research*, **10**, 270-273

Abbas, Z., Hayat, T., Pop I. (2008) Unsteady flow of a second grade fluid film over an unsteady stretching sheet, *Mathematical and Computer Modelling*, **48**, 518-526.

Abbasbandy, S. (2012) Numerical study on gas flow through a micro-nano porous media, *Acta Physica Polonica A*, **121**, 581-585

Abbasbandy, S., Naz, R., Hayat, T., Alsaedi, A. (2014) Numerical and analytical solutions for Falken-Skan flow of MHD Maxwell fluid, *Applied Mathematics and Computation*, **242**, 569-575

Abel, M. S., Joshi, A., Sonth, R. M. (2001) Heat transfer in MHD viscoelastic fluid flow over a stretching surface, *Journal of Applied Mathematics and Mechanics*, **81**, 691-698

Abel, M. S., Mahesha, N. (2008) Heat transfer in MHD viscoelastic fluid flow over a stretching sheet with variable thermal conductivity, non-uniform heat source and radiation, *Applied Mathematical Modelling*, **32**, 1965-1983

Abel, M. S., Mahesha, N., Tawade, J. (2009a) Heat Transfer in a liquid film over an unsteady stretching surface with viscous dissipation in the presence of external magnetic field, *Applied Mathematical Modelling*, **33**, 3430-3441

Abel, M. S., Sanjayanand, E., Nandeppanavar, M. M. (2008) Viscoelastic MHD flow and heat transfer over a stretching sheet with viscous and Ohmic dissipation, *Communications in Nonlinear Science and Numerical Simulations*, **13**, 1808-1821.

Abel, M. S., Siddheshwar, P. G., Mahesha, N. (2009b) Effects of thermal buoyancy and variable thermal conductivity on the MHD flow and heat transfer in a power law

fluid past a vertical stretching sheet in the presence of a non-uniform heat source, *International Journal of Nonlinear Mechanics*, **44**, 1-12

Abramowitz, M., Stegun, L. A. (1972) *Handbook of mathematical functions*, National Bureau of Standards, Applied Mathematics Series, **55**

Adomian, G. (1988) A review of the decomposition method in applied mathematics, *Journal of Mathematical Analysis and Applications*, **135**, 501-544

Agarwal, R., Rakich, J. V. (1982) Hypersonic laminar viscous flow past spinning cones at angle of attack, *The American Institute of Aeronautics and Astronautics*, **20**, 479-487

Ahmed, K., Nazar, R. (2011) Magnetohydrodynamic three dimensional flow and heat transfer over a stretching surface in a viscoelastic fluid, *Journal of Science and Technology*, **3**, 33-46

Ahmed, S. U., Ranganathan, P., Pandey, A., Sivaraman, S. (2010) Computational fluid dynamics modeling of gas dispersion in multi impeller bioreactor, *Journal of Bioscience and Bioengineering*, **109**, 588-597

Alaidarous, E. S., Ullah, M. Z., Ahmad, F, Al-Fhaid, A. S. (2013) An efficient higher-order quasilinearization method for solving nonlinear BVPs, *Journal of Applied Mathematics*, **2013**, Article ID 259371, 11 pages, **doi**: 10.1155/2013/259371

Alam, M. S., Ferdows, M., Ota, M., Maleque, M. A. (2006) Dufour and Soret effects on steady free convection and mass transfer flow past a semi-infinite vertical porous plate in a porous medium, *International Journal of Applied Mechanics and Engineering*, **3**, 535-545

Al-Amr, M. O. (2014) New applications of reduced differential transform method, *Alexandria Engineering Journal*, **53**, 243-247

Ali, A. H., Al-Saif, A. S. J. (2008) Adomian decomposition method for solving some models of nonlinear partial differential equations, *Barash Journal of Science*, **26**, 1-11

Alim, M. A., Alam, M. Md., Chowdhury, M. K. (2006) Pressure work effect on natural convection flow from a vertical circular cone with suction and non-uniform surface

temperature, *Journal of Mechanical Engineering*, **36**, 6-11

Aljoufi, M. D. (2013) New applications for a combined differential transform method with Adomian polynomials in astrophysics. In A. Zaharim, G. Bognar, Y. Bao, D. Anderson, M. K., Jha (ed), *Recent Advances in Mathematics of the Proceedings of the 7th International Conference on Applied Mathematics, Simulation, Modelling (ASM'13)*, WSEAS Press, **ISBN**: 978-1-61804-158-6, 63-67

Al-Mdallal, Q. M., Siam, M. I., Anwar, N. M. (2010) A collocation-shooting method for solving fractional boundary value problems, *Communications in Nonlinear Science and Numerical Simulations*, **15**, 3814-3822

Al-Shibani, F. S., Ismail, F. S., Md, Abdullah, F. A. (2012) The Implicit Keller Box Method for the one dimensional time fractional diffusion equation, *Journal of Applied Mathematics and Bioinfomatics*, **2**, 69-84

Alves, P. D., Barros, F. B., Pitangueira, R. L. S. (2013) An object oriented approach to the generalized finite element method, *Advances in Engineering Software*, **59**, 1-18

Andersson, H. I. (1992) MHD flow of a viscoelastic fluid past a stretching surface, *Acta Mechanica*, **95**, 227-230

Andersson, H. I., Bech, K. H., Dandapat, B.S. (1992) Magnetohydrodynamic flow of a power-law fluid over a stretching sheet, *International Journal of Nonlinear Mechanics*, **27**, 929-936

Anilkumar, D., Roy, S. (2004) Unsteady mixed convection flow on a rotating cone in a rotating fluid, *Applied Mathematics and Computation*, **155**, 545-561.

Anwar, I., Amin, N., Pop, I. (2008) Mixed convection boundary layer flow of a viscoelastic fluid over a horizontal circular cylinder, *International Journal of Nonlinear Mechanics*, **43**, 814-821.

Awad, F. G., Sibanda, P., Motsa, S. S., Makinde, O. D. (2011) Convection from an inverted cone in a porous medium with cross diffusion effects, *Computers and Mathematics with Applications*, **61**, 1431-1441.

Bakr, A. A. (2011) Effects of chemical reaction on MHD free convection and mass

transfer flow of a micropolar fluid with oscillatory plate velocity and constant heat source in a rotating frame of reference, *Communications in Nonlinear Science and Numerical Simulation*, **16**, 698-710

Bar-Meir, G. (2009) *Basics of fluid mechanics*, Orange Grove Texts Plus, Gainesville, Florida, U.S.A, **ISBN**-13: 978-1-61610-094-0

Belkhouche, F., Belkhouche. B. (2004) Successive linearization of second order multidimensional time-invariant systems, *Computer Physics Communication*, **162**, 79-88

Bellman, R. E, Kalaba, R. E. (1965) *Quasilinearization and nonlinear boundary value problems*, Elsevier, New York

Bellman, R. E., Kalaba, R. E.(2005) Solving ODEs and DDEs with residual control, *Applied Numerical Mathematics*, **52**, 113-127

Biazar, J., Babolian, E., Islam, R. (2004) Solution of the system of ordinary differential equations by Adomian decomposition method, *Applied Mathematics and Computation*, **147**, 713-719

Biazar, J., Mohammadi, F. (2010) Application of differential transform method to the generalized Burgers-Huxley equation, *Applications and Applied Mathematics*, **5**, 1726-1740

Bidin, B., Nazar, R. (2009) Numerical solution of the boundary layer flow over an exponentially stretching sheet with thermal radiation, *European Journal of Scientific Research*, **33**, 710-717

Blanco-Cocom, L., Estrella, A. G., Avilla-Vales, E. (2013) Solution of the Black-Scholes equation via the Adomian decomposition method, *International Journal of Computation Applied Mathematics and Research*, **2**, 486-494

Bodnar, T., Benes, L., Fraunie, Ph., Kozel, K. (2012) Applications of compact finite-difference schemes to simulations of stably stratified fluid flows, *Applied Mathematics and Computation*, **219**, 3336-3353

Bogacki, P., Shampine, L. F. (1996) An efficient Runge-Kutta (4,5) pair, *Computers Mathematics and Applications*, **32**, 15-28

Boivin, S., Cayre, F., Herard, J. M. (2000) A finite volume method to solve the Navier-Stokes equations for incompressible flows on structured meshes, *International Journal of Thermal Science*, **39**, 806-825

Botta, N., Klein, R., Langenberg, S., Lutzenkirchen, S. (2004) Well balanced finite volume methods for nearly hydrostatic flows, *Journal of Computational Physics*, **196**, 539-565

Budd, C., Koch, O., Weinmuller, E. (2006) From nonlinear PDEs to singular ODEs. *Applied Numerical Mathematics*, **56**, 413-422

Butcher, J. C. (1996) The history of the Runge-Kutta methods, *Applied Numerical Mathematics*, **20**, 247-260

Butcher, J. C. (2009) On fifth and sixth order explicit Runge-Kutta methods: order conditions and order barriers, *Canadian Applied Mathematics Quarterly*, **17**, 433-445

Butt, A. S., Munawar, S., Mehmood, A., Ali, A. (2012) Effects of viscoelasticity on entropy generation in a porous medium over a stretching plate, *World applied Sciences journal*, **17**, 516-523.

Butt, R. (2007) *Introduction to numerical analysis using MATLAB*, Jones and Bartlert Publishers, Canada, **ISBN**: 978-0-7637-7376-2

Cash, J. R., Singhal, A. (1982) Higher order methods for the numerical solution of two-point boundary value problems, *BIT Numerical Mathematics*, **22**, 184-199

Casson, N. (1959) A flow equation for pigment-oil suspensions of the printing ink type. In: Mill, C.C. (ed.), *Rheology of Disperse System*, Pergamon Press, New York, Oxford, 84-104.

Cebeci, T., Bradshaw, P. (1988) *Physical and computational aspects of convective heat transfer*, New York, Springer

Cebeci, T., Smith, A.M.O. (1974) *Analysis of turbulent boundary layers*, Academic Press Inc., U.S.A, **ISBN**: 0-12-164650-5

Cen, Z., Le, A., Xu, A. (2013) Finite difference scheme with a moving mesh for pricing

Asian options, *Applied Mathematics and Computation*, **219**, 8667-8675

Chakrabarti, A., Gupta, A.S. (1979) Hydromagnetic flow and heat transfer over a stretching sheet, *Quarterly Applied Mathematics*, **37**, 73-78

Chamkha, A. J., Aly, A. M., Mansour, M. A. (2010) Similarity solutions for unsteady heat and mass transfer from a stretching surface embedded in a porous medium with suction/injection and chemical reaction effects, *Chemical Engineering Communications*, **197**, 846-858.

Chamkha, A. J, Mujtaba, M., Quadri, A., Issa, C. (2003) Thermal radiation effects on MHD forced convection flow adjacent to a non-isothermal wedge in the presence of a heat source or sink, *Heat and Mass Transfer*, **39**, 305-312.

Chamkha, A. J., Rashad, A. M. (2012) Natural convection from a vertical permeable cone in a nanofluid saturated porous media for uniform heat and nanoparticles volume fraction fluxes, *International Journal of Numerical Methods for Heat & Fluid Flow*, **22**, 1073-1085.

Chang, J. R., Liu, C. S., Chang, C. W. (2007) A new shooting method for quasi-boundary regularization of backward heat conduction problems, *International Journal of Heat and Mass Transfer*, **50**, 2325-2332

Chang, S. H. (2010) Numerical solution of Troesch's problem by simple shooting method, *Applied Mathematics and Computation*, **216**, 3303-3306

Chen, C. H. (2004) Combined heat and mass transfer in MHD free convection from a vertical surface with Ohmic heating and viscous dissipation, *International Journal of Engineering Science*, **42**, 699-713

Chen, C. H. (2010) On the analytic solution of MHD flow and heat transfer for two types of viscoelastic fluids over a stretching sheet with energy dissipation, internal heat source and thermal radiation, *International Journal of Heat and Mass Transfer*, **53**, 4264-4273

Chen, C. K., Char, M.I, (1988) Heat transfer of a continuous stretching surface with suction or blowing, *Journal of Mathematical Analysis and Applications*, **135**, 568-580

Chen, Y. L., Li, L. X. (2015) An improved numerical manifold method and its application, *Engineering Analysis with Boundary Elements*, **52**, 120-129

Cheng, C. Y. (2009) Natural convection heat transfer of Non-Newtonian fluids in a porous media from a vertical cone under mixed boundary conditions, *International Communications in Heat and Mass Transfer*, **36**, 693-697

Cheng, C. Y. (2010) Soret and Dufour's effects on free convection boundary layer over a vertical cylinder in a saturated porous medium, *International communications in Heat and Mass Transfer*, **37**, 796-800.

Cheng, C. Y. (2011a) Soret and Dufour effects on natural convection boundary layer flow over a vertical cone in a porous medium with constant wall heat and mass fluxes, *International Communications in Heat and Mass Transfer*, **38**, 44-48

Cheng, C. Y. (2011b) Natural convection boundary layer flow in a micropolar fluid over a vertical permeable cone with variable wall temperature, *International Communications in Heat and Mass Transfer*, **38**, 429-433

Cheniguel, A., Ayadi, A. (2011) Solving Heat Equation by the Adomian Decomposition Method. *Proceedings of the World Congress on Engineering* **1**, London, United Kingdom

Christou, M. A., Papanicolaou, N. C. (2014) Kawahara solutions in Boussinesq equations using a robust Christov-Galerkin spectral method, *Applied Mathematics and Computation*, **243**, 245-257

Chu, H. P., Chen, C. L. (2008) Hybrid differential transform and finite difference method to solve the nonlinear heat conduction problem. *Communications in Nonlinear Science and Numerical Simulation*, **13**, 1605-1614

Chung, T. J. (2002) *Computational fluid dynamics*, Cambridge University Press, Cambridge, UK, **ISBN**:0-521-59416-2,

Cortell, R. (2006a) A note on flow and heat transfer of a viscoelastic fluid over a stretching sheet, *International Journal of Nonlinear Mechanics*, **41**, 78-85.

Cortell, R. (2006b) Flow and heat transfer of an electrically conducing fluid of second

grade over a stretching sheet subject to suction and to a transverse magnetic field, *International Journal of Heat and Mass Transfer*, **49**, 1851-1856

Cortell, R. (2011) Suction, viscous dissipation and thermal radiation effects on the flow and heat transfer of a power law fluid past an infinite porous plate, *Chemical Engineering Research and Design*, **89**, 85-93

Coudiere, Y., Pierre, C. (2006) Stability and convergence of a finite volume method for two systems of reaction-diffusion equations in electro-cardiology, *Nonlinear Analysis: Real World Applications*, **7**, 916-935

Crane, L. J. (1970) Flow past a stretching plate, *Zeitscrift fur Angewandte Mathematik und Physik*, **21**, 645-647

Damseh, R. A., Shatnawi, A. S., Chamkha, A. J., Duwairi, H. M. (2008) Transient mixed convection flow of a second grade visco-elastic fluid over a vertical surface, *Nonlinear Analysis: Modelling and Control*, **13**, 169-179

Das, K. (2011) Effect of chemical reaction and thermal radiation on heat and mass transfer flow of MHD micropolar fluid in a rotating frame of reference, *International Journal of Heat and Mass Transfer*, **54**, 3505-3513

Das, K. (2012) Slip effects on MHD mixed convection stagnation point flow of a micropolar fluid towards a shrinking vertical sheet, *Computers and Mathematics with Applications*, **63**, 255-267

Das, B., Batra, R. L.(1993) Secondary flow of a Casson fluid in a slightly curved tube, *International Journal of Nonlinear Mechanics*, **5**, 567-577

Dash, R. K., Mehta, K. N., Jayaraman, G. (1996) Casson fluid flow in a pipe filled with a homogeneous porous medium, *International Journal of Engineering Science*, **34**, 1145-1156.

Datta, S. K. (1964) The boundary layer flow of a Reiner-Rivlin fluid near a spinning cone, *Applied Scientific Research*, **13**, 194-202.

Deka, R. K., Paul, A., Chaliha, A. (2014) Transient free convection flow past an accelerated vertical cylinder in a rotating fluid, *Ain Shams Engineering Journal*, **5**,

505-513.

Dinarvand, S., Saber, M., Abulhasansari, M. (2014) Micropolar fluid flow and heat transfer about a spinning cone with Hall current and Ohmic heating, *Journal of Mechanical Engineering Science*, **5**, 505-513, **doi**: 10.1177/0954406213512628

Dlamini, P. G., Khumalo, M., Motsa, S. S. (2014) A Note on the multi-stage spectral relaxation method for chaos control and synchronization, *International Journal of Nonlinear Sciences and Numerical Simulation*, **15**, 289-298

Dlamini, P. G., Motsa, S. S., Khumalo, M. (2013) On the comparison between compact finite difference and pseudospectral approaches for solving similarity boundary layer problems, *Mathematical Problems in Engineering*, **2013**, Article ID 746489, 15 pages, **doi**: 10.1155/2013/746489

Diaz, M. J. C., Cheng, C. Y., Chertock, A., Kurganov, A. (2014) Solving two-mode shallow water wave equations using finite volume methods, *Communications in Computational Physics*, **16**, 1323-1354

Dimitrov, D. T., Kojouharov, H. V. (2008) Nonstandard finite-difference methods for predator-prey models with general functional response, *Mathematics and Computers in Simulation*, **78**, 1-11

Duan, J. S., Rach, R., Baleam, D., Wazwaz, A. M. (2012) A review of the Adomian decomposition method and its applications to fractional differential equations, *Computations in Fractional Calculus*, **3**, 73-99

Dutta, B. K, Gupta, A. S. (1987) Cooling of a stretching sheet in a various flows, *Industrial and Engineering Chemistry Research*, **26**, 333-336

Ebaid, A., El-Arabawy, H. A., Elazem, N. Y. A. (2013) An Improvement of the differential transform method and its application for boundary layer flow of a nanofluid, *International Journal of Differential Equations*, **2013**, Article ID 865464, 11 pages, **doi**: 10.1155/2013/865464

Ece, C. M. (2005) Free convection about a cone under mixed thermal boundary conditions and a magnetic field, *Applied Mathematical Modelling*, **29**, 1121-1134.

El-Amin, M. F., Aissa, W. A., Salama, A. (2008) Effects of chemical reaction and double dispersion on non-Darcy free convection heat and mass transfer, *Transport in Porous Media*, **75**, 39-109, **doi**: 10.1007/s11242-008-9213-0

El-Aziz, M. A. (2013) Mixed convection flow of a micropolar fluid from an unsteady stretching surface with viscous dissipation, *Journal of 1the Egyptian Mathematical Society*, **21**, 385-394.

Elbashbeshy, E. M. A. (2001) Heat transfer over an exponentially stretching continuous surface with suction, *Archives Mechanics*, **53**, 643-651

Elbashbeshy, E. M. A., Dimian, M. F. (2002) Effect of radiation on the flow and heat transfer over a wedge with variable viscosity, *Applied Mathematics and Computation*, **132**, 445-454

Eldabe, N. T. M., Ouaf, M. E. M. (2006) Chebyshev finite difference method for heat and mass transfer in a hydromagnetic flow of a micropolar fluid past a stretching surface with Ohmic heating and viscous dissipation, *Applied Mathematics and Computation*, **177**, 561-571

Eldabe, N. T. M., Sallam, S. M., Abou-Zeid, M. Y., (2012) Numerical study of viscous dissipation effect on free convection heat and mass transfer of MHD non-Newtonian fluid flow through a porous medium, *Journal of the Egyptian Mathematical Society*, **20**, 139-151

El-Gebeily, M. A., O'Regan, D. (2007) A quasilinearization method for a class of second order singular nonlinear differential equations with nonlinear boundary conditions, *Nonlinear-Analysis: Real World Applications*, **8**, 174-186

El-Kabeir, S. M. M, El-Sayed, E. A. (2012) Effects of thermal radiation and viscous dissipation on MHD viscoelastic free convection past a vertical isothermal cone surface with chemical reaction *International Journal of Energy and Technology*, **4**, 1-7

Esfahanian, V., Torabi, F. (2006) Numerical simulation of lead-acid batteries using Keller-Box method. *Journal of Power Sources*, **158**, 949-952

Evans, G., Blackledge, J., Yardley, P. (2000) *Numerical methods for partial differential*

equations, Springer-Verlag, London **ISBN**: 978-1-4471-0377-6, **doi**: 10.1007/978-1-4471-0377-6

Eymard, R., Gallouet, T., Herbin, R. (2000) The Finite Volume Method. In P.G. Ciarlet and J. L. Lions (Eds) *Handbook of Numerical Analysis Vol VII 713-1018*, North Holland, Amsterdam

Fakhar-Izadi, F., Dehghan, M. (2011) Spectral methods for parabolic Volterra integro-differential equations, *Journal of Computation and Applied Mathematics*, **235**, 4032-4046

Fazio, R., Jannelli, A. (2013) Numerical methods for a nonlinear BVP arising in physical oceanography, **arXiv**: 1310.2075v1 [math.NA], http://mat521.unime.it/fazio, downloaded:1/04/2015

Fereidoon, A., Ghadimi, M., Kaliji, H. D., Eftari, M., Alinia, S. (2010) Variational iteration method for nonlinear vibration of systems with linear and nonlinear stiffness, *International Journal of Research and Reviews in Applied Sciences*, **5**, 260-263

Ferreira, R. B., Falcao, D. S., Oliveira, V. B., Pinto, A. M. F. R. (2015) Numerical simulations of two phase flow in proton exchange membrane fuel cells using the volume of fluid method - A review, *Journal of Power Sources*, **277**, 329-342

Gajewski, J., Sadowski, T. (2014) Sensitivity analysis of crack propagation in pavement bituminous layered structures using a hybrid system integrating artificial neutral networks and finite element method, *Computational Materials Science*, **82**, 114-117

Gao, J., Zhang, Y. (2013) Staggered - grid finite difference method with variable - order accuracy for porous media, *Mathematical Problems in Engineering*, **2013**, Article ID 157071, 10 pages, **doi**: 10.1155/2013/157071

Ganji, D. D., Nourollari, M., Rostamian, M. (2007) A Comparison of variational iteration method with Adomian's decomposition method in some highly nonlinear equations, *International Journal of Science and Technology*, **2**, 179-188

Gebhart, B. (1962) Effect of viscous dissipation in natural convection, *Journal of Fluid Mechanics*, **14**, 225-232

Gebhart, B., Mollendorf, J. (1969) Viscous dissipation in external natural convection flows, *Journal of Fluid Mechanics*, **38**, 97-107

Geiger, S., Roberts, S., Matthai, S. K., Zoppou, C., Burri, A. (2004) Combining finite element and finite volume methods for efficient multiphase flow simulations in highly heterogeneous and structurally complex geologic media, *Geofluids*, **4**, 284-299

Geng, F. (2010) Variational iteration method for a class of singular boundary value problems, *Mathematical Sciences*, **4**, 359-370

Geng, F. (2012) A note on an improved variational iteration method for nonlinear equations arising in heat transfer, *International Review of Chemical Engineering*, **4**, 498-500

Gökhan, F. S. (2011) Effect of the guess function & continuation method on the run time of MATLAB BVP Solvers by. In C. M. Ionescu (Ed) *MATLAB - A ubiquitous tool for the Practical Engineer*, 3-22. InTech. url: downloaded: 13/10/2011, **doi**: 10.5772/820 **ISBN**: 978-953-307-907-3

Goncalves, F. F., Grossinho, M. R. (2014) Spatial approximation of Non-divergent type parabolic PDEs with unbounded coefficients related to finance, *Abstracts and Applied Analysis*, **2014**, Article ID 801059, 11 pages, **doi**: 10.1155/2014/801059

Gong, C., Bao, W., Tang, G., Jiang, Y., Liu, J. (2014) Computational challenge of fractional differential equations and the potential solutions: A survey, *Mathematical Problems in Engineering*, **2014**, Article ID 258265, 13 pages, **doi**: 10.1155/2014/258265

Gottlieb, D., Hesthaven, J. S. (2001) Spectral methods for hyperbolic problems. *Journal of Computation and Applied Mathematics*, **128**, 83-131

Gottlieb, D., Orszag, S. A. (1977) *Numerical analysis of spectral methods: Theory and applications*, Capital City Press, Montpelier, Vermont, USA

Griffiths, D. F., Higham, D. J. (2010) *Numerical methods for ordinary differential equations: Initial value problems*, Springer-Verlag, London, **ISBN**: 978-0-85729-148-6

Grubka, L. J., Bobba, K. M. (1985) Heat transfer characteristics of a continuous stretching surface with variable temperature, *ASME Journal of Heat Transfer*, **107**, 248-250.

Gupta, P. S., Gupta, A. S. (1977) Heat and mass transfer on a stretching sheet with suction or blowing, *Canadian Journal of Chemical Engineering*, **55**, 744-746

Ha, S. N. (2001) A nonlinear shooting method for two-point boundary value problems, *Computer and Mathematical Applications*, **42**, 1411-1420

Hajipour, M., Dehkordi, A. M. (2012) Transient behaviour of fluid flow and heat transfer in vertical channels partially filled with porous medium: Effects of inertial term and viscous dissipation, *Energy Conversion and Management*, **61**, 1-7

Hale, N., Moore, D. R. (2008) A sixth order extension of the Matlab package bvp4c of J.Kierzenka and L Shampine, *Technical Report NA-08/04*, Oxford University Computing Laboratory

Hamzah, N., Alias, N., Amin, N. S. (2008) The parallelization of the Keller box method on heterogeneous cluster of workstations, *Journal of Fundamental Science*, **4**, 253-259

Handlovicova, A., Mikula, K. (2002) Variational numerical methods for solving nonlinear diffusion equations arising in image processing, *Journal of Visual Communication in Image Representation*, **13**, 217-237

Haque, M. A. (2010) Numerical method in two dimensional boundary layer theory for Incompressible viscous fluid, *Journal of Science*, **38**, 61-73

Hassan, I. H. A. H. (2008) Application to differential transform method for solving systems of differential equations, *Journal of Applied Mathematical Modelling*, **32**, 2552-2559

Hattim, T. A. K. (2013) Variational iteration method for solving two-dimensional reaction diffusion Brusselator system, *Journal of Basrah Researches (Sciences)*, **39**, 67-80

Hayat, T., Abbas, Z., Pop, I. (2008) Mixed convection in a stagnation point flow adjacent to a vertical surface in a viscoelastic fluid, *International Journal of Heat and Mass Transfer*, **51**, 3200-3206.

Hayat, T., Abbas, Z., Sajid, M., Asghar, S. (2007) The Influence of thermal radiation on MHD flow of a second grade fluid, *International Journal of Heat and Mass Transfer*,

50, 931-941

Hayat, T., Mustafa, M., Pop, I. (2010) Heat and mass transfer for Soret and Dufour's effect on mixed convection boundary layer flow over a stretching vertical surface in a porous medium filled with viscoelastic fluid, *Communications in Nonlinear Science and Numerical Simulations*, **15**, 1183-1196

Hendi, F. A., Bakodah, H. O., Almazmumy, M., Alzumi, A. (2012) A simple program for solving nonlinear initial value problem using Adomian decomposition method, *International Journal of Research and Reviews in Applied Sciences*, **12**, 397-406

Hieu, T. N. (2003) Remarks on the shooting method for nonlinear two-point boundary-value problems, *Journal of Science, Vietnam National University*, **3**, 18-25

Higueras, I., Happenhofer, N., Koch, O., Kupka, F. (2014) Optimized strong stability preserving IMEX Runge-Kutta methods, *Journal of Computational and Applied Mathematics*, **272**, 116-140

Holsapple, R., Venkataraman, R., Doman, D.B. (2003) A new, fast numerical method for solving two-point boundary-value problems, *Journal of Guidance, Control and Dynamics*, **27**, 1-17

Householder, A. S. (1953) *Principles of numerical analysis*, Mcgraw Hill Book Co. Inc., New York

Hsiao, K. L. (2011) MHD mixed convection for viscoelastic fluid past a porous wedge, *International Journal of Nonlinear Mechanics*, **46**, 1-8

Hsiao, K. L. (2012) Multimedia physical feature for unsteady MHD mixed convection viscoelastic fluid over a vertical stretching sheet with viscous dissipation, *International Journal of the Physical Sciences*, **7**, 2515-2524

Hsiao, C. Y., Chang, W. J., Char, M. I., Tai, B. C. (2014) Influence of thermophoretic particle deposition on MHD free convection flow of non-Newtonian fluids from a vertical plate embedded in porous media considering Soret and Dufour effects, *Applied Mathematics and Computation*, **244**, 390-397

Hu, D., Lin, C., Liu, L., Li, S., Zhao, Y. (2012) Preparation, characterization, and in

vitro release investigation of lutein/zein nanoparticles via solution enhanced dispersion by supercritical fluids, *Journal of Food Engineering*, **109**, 545-552

Hussin, C. H. C., Killicman, A., Mandangan, A. (2010) General differential transform method for higher order of linear boundary value problems, *Borneo Science*, **27**, 35-46

Hysing, S. (2012) Mixed finite element FEM level set method for numerical simulation of immiscible fluids, *Journal of Computational Physics*, **231**, 2449-2465

Ibijola, E. A., Adegboyegun, B. J. (2012) A comparison of the Adomian's decomposition method and Picard Iterations method in solving nonlinear differential equations, *Global Journal of Science Frontier Research Mathematics and Decision Sciences*, **12**, 2249-4626

Idress, M., Mabood, F., Ali, A., Zaman, G. (2013) Exact solutions for a class of stiff systems by differential transform method, *Journal of Applied Mathematics Statistics and Informatics*, **4**, 440-444

Ion, S., Ion, A.V. (2011) A finite volume method for solving generalized Navier-Stokes equations, *Annals of the Academy of Romanian Scientists: Series on Mathematics and its Applications*, **3**, 145-163

Ishak, A. (2011) MHD boundary layer flow due to an exponentially stretching sheet with radiation effect, *Sains Malaysiana*, **40**, 391-395

Islam, S. H. R. (2012) Solving boundary value problems of shooting and finite difference method using Matlab, *Journal of Science and Technology*, **7**, 18-23

Jafari, H., Alipour, M., Tajadodi, H. (2010) Two-dimensional differential transform method for solving nonlinear partial differential equations, *International Journal of Research and Reviews in Applied Sciences*, **2**, 2076-7366

Jafari, H., Sadeghi, S., Biswas, A. (2012) The differential transform method for solving multidimensional partial differential equations, *Indian Journal of Science Technology*, **5**, 2009-2012

Jambal, O., Shigechi, T., Davaa, G., Momoki, S. (2005) Effects of viscous dissipation and fluid axial heat conduction on heat transfer for non-Newtonian fluids in ducts with

uniform wall temperature, *International Communications in Heat and mass transfer*, **32**, 1165-1173

Jankowski, T. (2003) Extensions of the quasilinearization method for differential equations with Integral boundary conditions. *Mathematical and Computer Modelling*, **37**, 155-165

Jeon, Y., Park, E. J., Sheenc, D. (2014) A hybridized finite element method for the Stokes problem, *Computers and Mathematics with Applications*, **68**, 2222-2232

Jha B. K., Ajibade, A. O. (2012) Effect of viscous dissipation on natural convection flow between vertical parallel plates with time-periodic boundary conditions, *Communications in Nonlinear Science and Numerical Simulation*, **17**, 1576-1587

Jovanovic, R., Kais, S., Alharbi, F. H. (2014) Spectral method for solving the nonlinear Thomas-Fermi equation based on exponential functions, *Journal of Applied Mathematics*, **2014**, Article ID 168568, 8 pages, **doi**: 10.1155/2014/168568

Kabir, K. H., Alim, M. A., Andallah, L. S. (2013) Effects of viscous dissipation on MHD natural convection flow along a vertical wavy surface, *Journal of Theoretical and Applied Physics*, **7**, 8 pages, **doi**: www.jtaphys.com/content/7/1/31

Kadem, A. (2006) Analytical solutions for the neutron transport using the spectral methods, *International Journal of Mathematical Science*, **2006**, Article ID 16214, 11 pages, **doi**:10.1155/IJMMS/2006/16214

Kairi R. R., Murthy, P. V. S. N. (2009) Free convection in a thermally stratified non-Darcy porous medium, *International Journal of Fluid Mechanics Research*, **36**, 414-423.

Kairi, R. R., Murthy, P. V. S. N. (2011) Effect of viscous dissipation on natural convection heat and mass transfer from vertical cone in a non-Newtonian fluid saturated non-Darcy porous medium, *Applied Mathematics and Computation*, **217**, 8100-8114.

Kameswaran, P. K., Narayana, M., Makanda, G., Sibanda, P. (2012a) On radiation effects on hydromagnetic Newtonian liquid flow due to an exponential stretching sheet, *Boundary Value Problems*, **2012**, **doi**: 10.1186/1687-2770-2012-105

Kameswaran, P. K., Shaw, S., Sibanda, P., Murthy, P. V. S. N. (2013a) Homogeneous-Heterogeneous reactions in a nanofluid flow due to a porous stretching sheet, *International Journal of Heat and Mass Transfer*, **57**, 465-472.

Kameswaran, P. K., Narayana, M., Sibanda, P., Murthy P. V. S. N. (2012b) Hydromagnetic nanofluid flow due to a stretching or shrinking sheet with viscous dissipation and chemical reaction effects, *International Journal of Heat and Mass Transfer*, **55**, 7587-7595

Kameswaran, P. K., Sibanda, P. (2013) Thermal dispersion effects on convective heat and mass transfer in an Ostwald de Waele nanofluid flow in porous media, *Boundary Value Problems*, **2013**, **doi**:10.1186/1687-2770-2013-243

Kameswaran, P. K., Sibanda, P., Motsa, S. (2013b) A spectral relaxation method for thermal dispersion and radiation effects in a nanofluid flow, *Boundary Value Problems*, **242**, 6-18, **doi**: www.boundaryvalueproblems.com/content/2013/242

Kasim, A. R. M., Admon, M. A., Shafie, S. (2011) Free convection boundary layer flow of a viscoelastic fluid in the presence of heat generation, *World Academy of Science, Engineering and Technology*, **5**, 3-29

Keller, H. B., Cebeci, T. (1972) Accurate numerical methods for boundary-layer flows: II Two-dimensional turbulent flows, *American Institute of Aeronautics and Aeronautics Journal*, **10**, 1193-1199

Khalid, A., Khan, I., Khan, A., Shafie, S. (2015) Unsteady MHD free convection flow of Casson fluid past over an oscillating vertical plate embedded in porous medium, *Engineering Science and Technology, an International Journal*, **2**, 1-9

Khan, S. K. (2006) Boundary layer viscoelastic fluid flow over an exponentially stretching sheet. *International Journal of Applied Mechanics and Engineering*, **11**, 321-335

Kierzenka, J., Shampine, L. F. (2001) A BVP solver based on residual control and the MATLAB pse, *ACM, Transactions on Mathematical Software*, **27**, 299-316

Kiymaz, O., Centinkaya, A. (2010) Variational iteration method for a class of nonlinear differential equations. *International Journal of Computational Mathematical Sciences*,

5, 1819-1826

Kozar, I., Malic N. T. (2013) Spectral method in realistic modelling of bridges under moving vehicles, *Engineering Structures*, **50**, 149-157

Kudryavtsev, O. (2013) Finite difference methods for option pricing under Levy processes: Wiener-Hopf factorization approach, *The Scientific World Journal*, **2013**, Article ID 963625, 12 pages, **doi**: 10.1155/2013/963625

Kumar, M. (2003) A second order spline finite difference method for singular two-point boundary value problems, *Applied Mathematics Computation*, **142**, 283-290

Kumar, M., Sivaraj, R. (2012) MHD viscoelastic fluid non-Darcy flow along a moving vertical cone, *International Journal of Applied Mathematics and Mechanics*, **8**, 69-81

Kwong, M. K. (2006) The shooting method and multiple solutions of two/multi-point BVPs of second-order ODE, *Journal of Qualitative Theory of Differential Equations*, **6**, 1-14

Laburta, M. P., Montijano, J. I., Randez. L., Calvo, M. (2015) Numerical methods for non-conservative perturbations of conservative problems, *Computer Physics Communications*, **187**, 72-82

Laha, M. K., Gupta, P.S., Gupta, A. S. (1989) Heat transfer characteristics of the flow of an incompressible viscous fluid over a stretching sheet, *Warme-undstoffubertrag*, **24**, 151-153

Lakshmikantham, V., Shahzad, N. (1994) Further generalization of generalized quasilinearization method, *Journal of Applied Mathematics and Stochastic Analysis*, **7**, 545-552

Langtangen, H. P. (2003) *Computational differential equations, numerical methods: Second Edition*, Springer-Verlag, Berlin Hiedelberg, **ISBN**: 3-540-43416

Lawrence, P. S., Rao, B. N. (1995) The non-uniqueness of the MHD flow of a viscoelastic fluid past a stretching sheet, *Acta Mechanica*, **112**, 223-228

Lehtikangas, O., Tarvainen, T., Kim, A. D., Arridge, S. R. (2015) Finite element ap-

proximation of the radiative transport equation in a medium with piecewise constant refractive index. *Journal of Computational Physics*, **282**, 345-359

LeVeque, R. (2002) *Finite volume methods for hyperbolic problems*, Cambridge University Press, Cambridge, UK, **ISBN**: 0 521 81087 6

Liu, Y., Sen, M. K., (2009) A new time-space domain high-order finite difference method for the acoustic wave equation, *Journal of Computational Physics*, **228**, 8779-8806

Loh, K. C., Vusadevan, V. (2013) Hydrodynamic and dispersion behavior in a non-porous silica monolith through fluid dynamic study of a computational mimic reconstructed from sub-micro-tomographic scans, *Journal of Chromatography A*, **1274**, 65-76

Magyari, E., Keller, B. (1999) Heat and mass transfer in the boundary layers on an exponentially stretching continuous surface, *Journal of Physics D: Applied Physics*, **32**, 577-585

Makanda, G., Makinde, O. D., Sibanda, P. (2013) Natural convection of viscoelastic fluid from a cone embedded in a porous medium with viscous dissipation, *Mathematical Problems in Engineering*, **2013**, Article ID 934712, 11 pages, **doi**: 10.1155/2013/934712

Makanda, G., Shaw, S., Sibanda, P. (2015a) Diffusion of chemically reactive species in Casson fluid over an unsteady stretching surface in porous medium with viscous dissipation, *Mathematical Problems in Engineering*, **2014**, Article ID 724596, 10 pages, **doi**: 10.1155/2014/724596

Makanda, G., Shaw, S., Sibanda, P. (2015b) Effects of radiation on MHD free convection of Casson fluid from a horizontal circular cylinder with partial slip in non-Darcy porous medium with viscous dissipation, *Boundary Value Problems*, **2015**, **doi**:1186/s13661/015/0333/5

Makanda, G., Shaw, S., Sibanda, P. (2015c) Effects of radiation on free convection from a spinning cone with partial slip in non-Darcy porous medium with cross diffusion and viscous dissipation, *Manuscript under review*

Makinde, O. D. (2009) On thermal stability of a reactive third grade fluid in a channel with convective cooling walls, *Applied Mathematics and Computation*, **213**, 170-176.

Makukula, Z.G., Sibanda, P., Motsa, S. S. (2010) A novel numerical technique for two-dimensional laminar flow between two moving porous walls, *Mathematical Problems in Engineering*, **2010**, Article ID 528956, 15 pages, **doi**: 10.1155/2010/528956

Maleknejad, K., Nouri, K., Torkzadeh, L. (2011) Comparison projection method with Adomian decomposition method for solving systems of Integral equations, *Bulletin of the Malaysian Mathematical Sciences Society*, **34**, 379-388

Mandal, I. C., Mukhopadhyay, S. (2013) Heat transfer analysis for fluid flow over an exponentially stretching porous sheet with surface heat flux in porous medium *Ain Shams Engineering Journal*, **4**, 103-110

Manzini, G., Russo, A. (2008) A finite volume method for advection-diffusion problems in convective-dominated regimes, *Computer Methods in Applied Mechanics and Engineering*, **197**, 1242-1261

Massoudi, M., Vaidya, A., Wulandana, R. (2008) Natural convection flow of a generalized second grade fluid between two vertical walls, *Nonlinear Analysis: Real World Applications*, **9**, 80-93

Matinfar, M., Fereidoon, A., Aliasghartoyeh, A., Ghanbari, M. (2009) Variational iteration method for solving nonlinear WBK equations, *International Journal of Nonlinear Science*, **8**, 419-423

Matinfar, M., Ghasemi, M. (2013) Solving BVPs with shooting method and VIMHP, *Journal of Egyptian Mathematical Society*, **21**, 354-360

McDonald, D. A. (1974) Blood flows in Arteries, 2nd Edition. In *Experimental physiology, Quarterly Journal of the Experimental Physiology and Cognate Medical Sciences*, Edward Arnold, London, **doi**: 10.1113/expphysiol.1975.sp002291/date downloaded: 1/04/2015

Md Ali, F., Nazar, R., Arifin, N. M. (2010) Numerical solutions of unsteady boundary layer flow due to an impulsively stretching surface, *Journal of Applied Computer*

Science and Mathematics, **8**, 25-30

Melton, T. G., Vatsala, A. S. (2008) Improved generalized quasilinearization method and rapid convergence for reaction diffusion equations, *Applied Mathematics and Computation*, **203**, 563-572

Merdan, M., Gokdogan, A., Erturk, V. S. (2011) On solving Coullet system by differential transform method, *Cankaya University Journal of Science Engineering*, **8**, 111-121

Mernone, A. V., Mazumdar, J. N., Lucas, S. K. (2002) A Mathematical study of peristaltic transport of Casson Fluid, *Mathematical and Computer Modeling*, **35**, 895-912.

Miansari, M. O., Miansari, M. E., Barari, A., Ganji, D. D. (2009) Application of He's variational iteration method to nonlinear Helmoltz and fifth-order KDV equations, *Journal of Applied Mathematics Statistics and Informatics*, **5**, 5-20

Milne, W. E. (1950) Note on the Runge-Kutta method, *Journal of Research for the National Bureau of Standards*, **44**, 549-550

Mirzaee, F. (2011) Differential transform method for solving linear and nonlinear systems of ordinary differential equations, *Applied Mathematical Science*, **5**, 3465-3472

Mishra, K. H.(2012) A comparative study of variational iteration method and He-Laplace method. *Applied Mathematics*, **3**, 1193-1201

Mitsoulis, E., Galazoulas, S. (2009) Simulation of viscoplastic flow past cylinders in tubes, *Journal of Non-Newtonian Fluid Mechanics*, **158**, 132-141

Mohyud-Din, S. T., Noor, M. A., Noor, K. I. (2009) Modified variational iteration method for solving Sine-Gordon equations, *World Applied Sciences Journal*, **6**, 999-1004

Molla, M. M., Saha, S. C., Khan, M. A. I., Hossain, M. A. (2011) Radiation effects on natural convection laminar flow from a horizontal circular cylinder, *Desalination and Water Treatment*, **30**, 89-97

Molliq, R. Y., Noorani, M. S. M., Hashin, I. (2009) Variational iteration method for

fractional heat-and wave-like equations, *Nonlinear Analysis: Real World Applications*, **10**, 1854-1869

Motsa, S., Shateyi, S. (2012) A successive linearization method approach to solve Lane-Emdem type of equations, *Mathematical Problems in Engineering*, **2012**, Article ID 280702, 14 pages, **doi**: 10.1155/2012/280702

Motsa, S., Sibanda, P. (2012) A note on the solutions of the Van der Pol and Duffing equations using a linearization method, *Mathematical Problems in Engineering*, **2012**, Article ID 693453, 10 pages, **doi**: 10.1155/2012/693453

Motsa, S., Sibanda, P. (2013) On extending the quasilinearization method to higher order convergent hybrid schemes using the spectral homotopy analysis method, *Journal of Applied Mathematics*, **2013**, Article ID 879195, 9 pages **doi**: 10.1155/2013/879195

Motsa, S. S. (2013) A new spectral local linearization method for nonlinear boundary layer flow problems, *Journal of Applied Mathematics*, **2013**, Article ID 423628, 15 pages, **doi**: 10.1155/2013/423628

Motsa, S. S. (2014) A new spectral relaxation method for similarity variable nonlinear boundary layer flow systems, *Chemical Engineering Communications*, **201**, 241-256

Motsa, S.S., Hayat, T., Aldossary, O. M. (2012a) MHD flow of upper-convected Maxwell fluid over porous stretching sheet using successive Taylor series linearization method, *Applied Mathematics and Mechanics (English Edition)*, **33**, 975-990

Motsa, S. S., Khan, Y., Shateyi, S. (2012b) A numerical solution of Maxwell fluid over a shrinking sheet in the region of a stagnation point, *Mathematical Problems in Engineering*, **2012**, Article ID 290615, 11 pages **doi**: 10.1155/2012/290615

Motsa, S. S., Magagula, V. M, Sibanda, P. (2014) A bivarate Chebyshev spectral collocation quasilinearization method for nonlinear evolution parabolic equations, *The Scientific World Journal*, **2014**, Article ID 581987, 13 pages, **doi**: 10.1155/2014/581987

Motsa, S. S., Makukula, Z. G. (2013) On spectral relaxation method approach for steady Von Karman flow of a Riner-Rivlin fluid with Joule heating, viscous dissipation and suction/injection, *Central European Journal of Physics*, **11**, 363-374

Motsa, S. S., Makukula, Z. G., Shateyi, S. (2013) Spectral local linearization approach for natural convection boundary layer flow, *Mathematical Problems in Engineering*, **2013**, Article ID 765013, 7 pages, **doi**: 10.1155/2013/765013

Motsa, S. S., Shateyi, S. (2010) A new approach for the solution of three dimensional magnetohydrodynamic rotating flow over a shrinking sheet, *Mathematical Problems in Engineering*, **2010**, Article ID 586340, 15 pages, **doi**: 10.1155/2010/586340

Moulla, R., Lefevre, L., Maschke, B. (2012) Pseudo-spectral methods for the spatial sympletic reduction of open systems of conservation laws, *Journal of Computational Physics*, **231**, 1272-1292

Mukherjee, S., Roy, B. (2012) Solution of Riccati equation with variable co-efficient by differential transform method, *International Journal of Nonlinear Science*, **14**, 251-256

Mukhopadhyay, S. (2013) MHD boundary layer flow and heat transfer over an exponentially stretching sheet embedded in thermally stratified medium *Alexandria Engineering Journal*, **52**, 259-265

Mukhopadhyay, S., De, P. R., Bhattacharyya, K., Layek, G.C. (2013) Casson fluid flow over an unsteady stretching surface, *Ain Shams Engineering Journal*, **4**, 933-938

Mukhopadhyay, S., Vajravelu, K. (2013) Diffusion of chemically reactive species in Casson fluid flow over an unsteady permeable stretching surface, *Journal of Hydrodynamics*, **25**, 591-598.

Murthy, P. V. S. N., RamReddy, C. H., Chamkha, A. J., Rashad, A. M. (2013) Magnetic effect on thermally stratified nanofluid saturated non-Darcy porous medium under convective boundary condition, *International Communications in Heat and Mass Transfer*, **47**, 41-48

Mustafa, M., Mushtaq, A., Hayat, T., Alsaedi, A. (2015) Radiation effects in three-dimensional flow over a bi-directional exponentially stretching sheet, *Journal of the Taiwan Institute of Chemical Engineers*, **47**, 43-49

Nadeem, S., Ul Haq, R., Akbar, N. S., Khan, Z. H. (2013) MHD three-dimensional Cas-

son fluid flow pas a porous linearly stretching sheet, *Alexandria Engineering Journal*, **52**, 577-582

Nadeem, S., Ul Haq, R., Khan, Z. H. (2014) Numerical study of MHD boundary layer flow of a Maxwell fluid past a stretching sheet in the presence of nanoparticles, *Journal of the Taiwan Institute of Chemical Engineers*, **45**, 121-126.

Nadeem, S., Ul Haq, R., Lee, C. (2012) MHD flow of a Casson fluid over an exponentially stretching sheet, *Scientia Iranica B*, **19**, 1550-1553.

Nakamura, M., Sawada, T. (1988) Numerical study on the flow of a non-Newtonian fluid through an axisymmetric stenosis, *Journal of Biomechanical Engineering*, **110**, 137-143

Nakashima, M. (1984) *Implicit Pseudo-Runge-Kutta processes*, Research Institute Mathematical Sciences, Kyoto University, Japan, **20**, 39-56

Narayana, M., Awad, F. G., Sibanda, P. (2013) Free magnetohydrodynamic flow and convection from a vertical spinning cone with cross diffusion effects, *Applied Mathematical Modelling*, **37**, 2662-2678.

Narayana, L. P. A., Murthy, P. V. S. N. (2006) Free convective heat and mass transfer in a doubly stratified non-Darcy porous medium, *Transactions of the ASME - Journal of Heat Transfer*, **128**, 120-121

Narayana, M., Sibanda, P. (2012) On the solution of double diffusive convective flow due to a cone by a linearization method, *Journal of Applied Mathematics*, **2012**, Article ID 587357, 19 pages, **doi**: 10.1155/2012/587357

Nasab, A. K., Kiliman, A., Pashazadeh Atabakan, Z., Abbasbandy, S. (2013) Chebyshev wavelet finite difference method: A new approach for solving initial and boundary value problems of fractional order, *Abstract and Applied Analysis*, **2013**, Article ID 916456, 15 pages, **doi**: 10.1155/2013/916456

Nawaz, Y. (2011) Variational iteration method and homotopy perturbation method for fourth-order fractional integro-differential equations, *Computers and Mathematics with Application*, **61**, 2330-2341

Ng, C. O. (2013) Combined pressure-driven and electro-osmotic flow of a Casson fluid through a slit microchannel, *Journal of Non-Newtonian Fluid Mechanics*, **198**, 1-9.

Noor, M. A., Mohyud-Din, S. T. (2009) Modified variational iteration method for a boundary layer problem in unbounded domain, *International Journal of Nonlinear Science*, **7**, 426-430

Oderinu, R. A., Aregbesola, Y. A. S. (2014) Shooting Method via Taylor series for solving two-point boundary value problems on an infinte interval, *General Mathematics Notes*, **24**, 74-83

Olajuwon, B. I. (2011) Convective heat and mass transfer in a hydromagnetic flow of a second grade fluid in the presence of thermal radiation and thermal diffusion, *International Communications in Heat and Mass Transfer*, **38**, 377-382

Orel, B., Perne, A. (2014) Chebyshev-Fourier spectral methods for nonperiodic boundary value problems. *Journal of Applied Mathematics*, **2014**, Article ID 572694, 10 pages, **doi**: 10.1155/2014/572694

Pal, D., Mandal, G. (2015) Mixed convection-radiation on stagnation point flow of nanofluids over a stretching/shrinking sheet in a porous medium with heat generation and viscous dissipation *Journal of Petroleum Science and Engineering*, **126**, 16-25

Pal, D., Shivakumara, I. S. (2006) Mixed convection heat transfer from a vertical plate embedded in a sparsely packed porous medium, *International Journal of Applied Mechanical Engineering*, **11**, 929-939

Papageorgiou, G., Tsitouras, Ch. (1996) Continuous Runge-Kutta(-Nystrom) methods with reduced phase-errors. *Journal of Computation and Applied Mathematics*, **69**, 1-11

Partha, M. K., Murthy, P. V .S. N., Rajasekhar, G. P. (2005) Effect of viscous dissipation on the mixed convection heat transfer from an exponentially stretching surface. *Heat and Mass Transfer*, **41**, 360-366

Patel, S. A., Chhabra, R. P. (2013) Steady flow of Bingham plastic fluids past an elliptical cylinder *Journal of Non-Newtonian fluid mechanics*, **165**, 32-53

Pavithra, G. M., Gireesha, B. J. (2014) Unsteady flow and heat transfer of a fluid of a fluid-particle suspension over an exponentially stretching sheet *Ain Shams Engineering Journal*, **5**, 613-624

Pavlov, K. B. (1974) Magnetohydromagnetic flow of an incompressible viscous fluid caused by deformation of a surface, *Magneto Hydro Dynamics*, **4**, 146-147

Pei, M., Chang, S. K. (2008) A quasilinearization method for second-order four-point boundary value problems. *Applied Mathematics Computation*, **202**, 54-66

Perot, J. B., Subramanian, V. (2007) A discrete calculus analysis of the Keller Box scheme and a generalization of the method of arbitrary meshes, *Journal of Computational Physics*, **226**, 494-508

Poochinapan, K.H., Wongsaijai, B., Disyadej, T. (2014) Efficiency of high-order accurate difference schemes for the Korteweg-de Vries equation, *Mathematical Problems in Engineering*, **2014**, Article ID 862403, 8 pages, **doi**: 10.1155/2014/862403

Pop, I., Takhar, H.S., Kumari, M. (1998) Free convection about a vertical wavy surface with prescribed surface heat flux in a micropolar Fluid,*Technishe Mechanik*, **4**, 229-237

Porshokouhi, M. G., Ghanbari, B., Porshokouhi, M.G. (2010) He's variational iteration method for solving differential equations of the fifth order, *General Mathematics Notes*, **1**, 153-158

Pozrikidis, C. (2006) A spectral collocation method with triangular boundary elements, *Engineering Analysis with Boundary Elements*, **30**, 315-324

Prabhakara, S., Deshpande, M. D. (2004) The no-slip boundary condition in fluid mechanics, *Resonance*, **9**, 50-60

Prakash, D., Muthtamilselvan, M. (2014) Effect of radiation on transient MHD flow of micropolar fluid between porous vertical channel with boundary conditions of the third kind *Ain Shams Engineering Journal*, **5**, 1277-1286

Pramanik, S. (2013) Casson fluid flow and heat transfer past an exponentially porous stretching surface in the presence of thermal radiation, *Ain Shams Engineering Jour-*

nal, **5**, 205-212

Pue-On, P., Viriyapong, N. (2012) Modified Adomian decomposition method for solving particular third-order ordinary differential equations. *Applied Mathematical Sciences*, **6**, 1463-1469

Ramachandra Prasad, V., Subba Rao, A., Anwar Beg, O. (2013a) Flow and heat transfer of Casson fluid from a horizontal cylinder with partial slip in non-Darcy porous medium, *Applied and Computational Mathematics*, **2**, article(2)

Ramachandra Prasad, V. R., Subba Rao, A., Reddy, N. B., Anwar Beg, O. (2013b) Modelling laminar transport phenomena in a Casson rheological fluid from an isothermal sphere with partial slip in a non-Darcy porous medium, *Theoretical and Applied Mechanics*, **40**, 469-510

Raptis, A. (1999) Radiation and viscoelastic flow, *International Communications of Heat and Mass Transfer*, **26**, 889-895

Raptis, A., Perdikis, C. (1998) Viscoelastic flow by the presence of radiation, *ZAMM: Journal of Applied Mathematics and Mechanics*, **78**, 277-279

Raptis, A., Perdikis, C., Takhar, H. S. (2004) Effect of thermal radiation on MHD flow, *International Journal of Heat and Mass Transfer*, **153**, 645-649

Rashad, A. M., Abbasbandy, S., Chamkha, A. J. (2012) Mixed convection flow of a micropolar fluid over a continuously moving vertical surface immersed in a thermally and solutally stratified medium with chemical reaction, *Journal of the Taiwan Institute of Chemical Engineers*, **45**, 2163-2169

Rashid, A., Abbas, M., Ismail, A.I., Md Majid, A. A. (2014) Numerical solution of the coupled viscous Burgers equations by Chebyshev-Legendre-Legendre pseudo-spectral method, *Applied Mathematics and Computation*, **245**, 372-381

Reddy, B. A., Reddy, P. B. N. (2011) Thermal radiation effects on hydromagnetic flow due to an exponentially stretching sheet, *International Journal of Applied Mathematics and Computation*, **3**, 300-306

Reddy, B. A., Reddy P. B. N., Suneetha, S. (2012) Radiation effects on MHD flow past

an exponentially accelerated isothermal vertical plate with uniform mass diffusion in the presence of heat source, *Journal of Applied Fluid Mechanics*, **5**, 119-126

Ribeiro, V. M., Coelo, P. M., Pinho, F. T., Alves, M. A. (2014) Viscoelastic flow past a confined cylinder: three dimensional effects and stability, *Chemical Engineering Science*, **111**, 364-380.

Rivertz, H. J. (2013) On those differential equations that are solved exactly by the improved Euler method, *Archivum Mathematicum (BRNO)*, **49**, 29-34

Rohlf, K., Tenti, G. (2001) The role of Womerseley number in pulsatile blood flow a theoretical study of the Casson model, *Journal of Biomechanics*, **34**, 141-148.

Saeed, U., ur Rehman, M. (2014) Wavelet-Galerkin quasilinearization method for nonlinear boundary value problems, *Applied and Applied Analysis*, **2014**, Article ID 868934, 10 pages, **doi**: 10.1155/2014/868934

Sahoo, B. (2009) Effects of partial slip, viscous dissipation and Joule heating on Von Krmn flow and heat transfer of an electrically conducting non-Newtonian fluid, *Communications in Nonlinear Science and Numerical Simulation*, **14**, 2982-2998

Sajid, M., Hayat, T. (2008) Influence of thermal radiation on the boundary layer flow due to an exponentially stretching sheet, *International Communications in Heat and Mass Transfer*, **35**, 347-356

Sajid, M., Pop, I., Hayat, T. (2010) Fully developed mixed convection flow of a viscoelastic fluid between permeable parallel vertical plates, *Computers and Mathematics with Applications*, **59**, 493-498

Saleh, M. A. (2005) A numerical study of natural convection heat transfer with variable viscosity and thermal radiation from a cone and wedge in porous media, *Applied Mathematics and Computation*, **170**, 64-75

Salehpoor, E., Jafari, H., Afrapoli, M. A. (2010) Revised Variational Iteration Method for solving systems of ordinary differential equations, *Applications and Applied Mathematics*, **1**, 110-121

Salehpoor, E. Jafari, E. (2011) Variational iteration method: A tool for solving partial

differential equations, *Journal of Mathematics and Computer Science*, **2**, 388-393

Sanjayanand, E., Khan, S. K. (2006) On heat and mass transfer in a viscoelastic boundary layer flow over an exponentially stretching sheet, *International Journal of Thermal Science*, **45**, 819-828

Sankar, D. S., Lee, U. (2008) Two-fluid nonlinear model for flow in catheterized blood vessels, *Communications in Nonlinear Science and Numerical Simulation*, **43**, 622-631

Sankar, D. S., Lee, U. (2010) Two-fluid Casson model for pulsatile blood flow through stenosed arteries: A theoretical model, *Communications in Nonlinear Science and Numerical Simulation*, **15**, 2086-2097

Sarif, N. M., Salleh, M. Z., Nazar, R. (2013) Numerical Solution of flow and Heat Transfer over a Stretching Sheet with Newtonian Heating using the Keller-box method, *Procedia Engineering*, **53**, 542-554

Sarpakaya, T. (1961) Flow of non-Newtonian fluids in a magnetic field, *American Institute of Chemical Engineers Journal*, **7**, 324-328

Seibold, B. (2008) Minimal positive stencils in mesh-free finite difference methods for the Poisson equation, *Computational Methods of Applied Mechanical Engineering*, **198**, 592-601

Shampine, L. F. (2003) Singular boundary value problems for ODEs, *Applied Mathematical Computation*, **138**, 99-112

Shampine, L. F. (2005) Solving ODEs and DDEs with residual control, *Applied Numerical Mathematics*, **52**, 113-127

Shampine, L. F., Muir, P. H. (2004) Estimating conditioning of Bvps for ODEs, *Mathematical and Computational Modelling*, **40**, 1309-1321

Shampine, L. F., Reichelt, M. W. (1997) The MATLAB ODE suite, *SIAM Journal of Scientific Computing*, **18**, 1-22

Sharidan, S., Mahmood, T., Pop, I. (2006) Similarity solutions for the unsteady boundary layer flow and heat transfer due to a stretching sheet, *International Journal of*

Applied Mechanical Engineering, **11**, 674 54

Sharma, R., Ishak, A., Pop, I. (2013) Partial slip flow heat transfer over a stretching sheet in a nanofluid, *Mathematical Problems in Engineering*, **2013**, Article ID 724547, 7 pages, **doi**: 10.1155/2013/724547

Shateyi, S. (2013) On spectral relaxation method for an MHD flow and heat transfer of Maxwell fluid, *International Conference on Mechanics, Heat and Mass Transfer*, **ISBN**: 978-1-61804-220-0, 102-106

Shateyi, S., Marewo, G. T. (2014) "Numerical analysis of MHD stagnation point flow of Casson fluid, heat and mass transfer over a stretching sheet" In Balicki, J. (Ed) *Advances in Applied and Pure Mathematics, WSEAS, Proceedings of the 7th international conference on finite differences, finite elements, finite volumes, boundary elements (F-and-B'14)*, Gdansk, Poland, 128-132, **ISBN**: 978-960-474-380-3

Shateyi, S., Motsa, S. S., Sibanda, P. (2010) The effects of thermal radiation, hall currents, Soret, and Dufour on MHD flow by mixed convection over a vertical surface in porous media, **2010**, Article ID 627475, 20 pages, *Mathematical Problems in Engineering*, **doi**:10.155/2010/627475

Shaw, S., Gorla, R. S. R., Murthy, P. V. S. N., Ng, C. O. (2009) Pulsatile Casson fluid flow through stenosed bifurcated artery, *International Journal of Fluid Mechanics Research*, **36**, 43-63

Shaw, S., Kameswaran, P. K., Sibanda, P., Murthy, P. V. S. N. (2013) Homogeneous-Heterogeneous reactions in a nanofluid flow due to a porous stretching or shrinking sheet in a porous medium, *Boundary Value Problems*, **2013**, **doi**: 10.1186/1687-2770-2013-77

Shaw, S., Makanda, G., Sibanda, P. (2014) Effects of double dispersion on Casson fluid flow with viscous dissipation and convective boundary condition, *Manuscript under review*

Shokouhmand, M., Soleimani, M. (2011) The effect of viscous dissipation on temperature profile of a power-law fluid flow over a moving surface with arbitrary injection/suction,

Energy Conversion and Management, **52**, 171-179

Shu, J. J, Wilks, G. (1995) An accurate numerical method for systems of differentio-integral equations associated with multiphase flow, *Computational Fluids*, **24**, 625-652

Sibanda, P., Khidir, A. B., Awad, F. G. (2012) On cross diffusion effects on flow over a vertical surface using linearization method, *Boundary Value Problems*, **25**, 1-15

Siddappa, B., Abel, M. S. (1985) Non-Newtonian flow past a stretching plate, *Zeitschrift fur Angewandte Mathematik Physik*, **36**, 47-54

Siddheshwar, P. G., Mahabaleswar, U. S. (2005) Effects of radiation and heat source on MHD flow of a viscoelastic liquid and heat transfer over a stretching sheet, *International Journal of Nonlinear Mechanics*, **40**, 807-820

Siddiqa, S., Hossain, M. A., Gorla, R. S. R. (2012) Conduction-Radiation effects on periodic magnetohydrodynamic natural convection boundary layer flow along a vertical surface, *International Journal of Thermal Sciences*, **53**, 119-129

Singh, V., Agarwal, S. (2012) Heat transfer in a second grade fluid over an exponentially stretching sheet through porous medium with thermal radiation and elastic deformation under the effect of magnetic field, *International Journal of Applied Mathematics and Mechanics*, **8**, 41-63

Sivaraj, R., Kumar, B. R. (2012) Unsteady MHD dusty viscoelastic fluid Couette flow in an irregular channel with varying mass diffusion, *International Journal of Heat and Mass Transfer*, **55**, 3076-3089

Soltanalizadeh, B. (2012) Application of the differential transform method for solving a fourth order parabolic partial differential equations, *International Journal of Pure and Applied Mathematics*, **78**, 299-308

Somali, S., Gokmen, G. (2007) Adomian decomposition method fot nonlinear Sturm-Liouville problems. *Surveys in Mathematics and its Applications*, **2**, 11-20

Spijker, M. N. (1996) Error propagation in Runge-Kutta methods, *Applied Numerical Mathematics*, **22**, 309-325

Srinivasacharya, D., RamReddy, Ch. (2011) Effect of double stratification on free convection in a micropolar fluid, *Transactions of the ASME - Journal of Heat Transfer*, **133**, 122-129

Stockie, J. M., Promislow, K., Wetton, B. R. (2003) A finite volume method for multicomponent gas transport in a porous fuel cell electrode, *International Journal of Numerical Methods in Fluids*, **41**, 577-599

Sugiyama, K., Ii, S., Takeuchi, S., Takagi, S., Matsumoto, Y. (2011) A full Eulerian finite difference approach for solving fluid-structure coupling problems, *Journal of Computational Physics*, **230**, 596-627

Suli, E., Mayers, D. F. (2003) *An introduction to numerical analysis*, Cambridge University Press, Cambridge, UK, **ISBN**: 0-521-81026-4

Suneetha, S., Bhaskar Reddy, N., Ramachandra Prasad, V. (2009) Radiation and mass transfer effects on MHD free convection flow past an impulsively started isothermal vertical plate with dissipation, *Thermal Science*, **13**, 71-181

Sungu, I. C., Demir, H. (2014) A new approach and solution technique to solve time fractional nonlinear reaction-diffusion equation, *Mathematical Problems in Engineering*, **2014**, Article ID 457013, 13 pages, **doi**: 10.1155/2014/457013

Takhar, H. S., Beg, O. A., Kumari, M. (1998) Computational analysis of coupled radiation-convection dissipative non-gray gas flow in a non-Darcy porous medium using the Keller-box implicit difference scheme, *International Journal of Energy Research*, **22**, 141-159.

Takhar, H. S., Rama, S. B., Williams, R. S. (1988) Free convection boundary layer flow of a micropolar fluid past a slender cone, *Mechanics Research Communications*, **15**, 167-176.

Tatari, M., Haghighi, M. (2014) A generalized Laguerre spectral collocation method for solving initial-boundary value problems, *Applied Mathematical Modelling*, **38**, 1351-1364

Thongmoon, M., Pusjuso, S. (2010) The numerical solutions of differential transform

method and the Laplace transform method for a system of differential equations, *Nonlinear Analysis: Hybrid Systems*, **4**, 425-431

Tonks, L. (1939) Theory of magnetic effects in the plasma of an Arc, *Physical Review*, **56**, 360-373

Toolabi, M., Fallah, A. S., Baiz, P. M., Louca, L. A. (2013) Dynamic analysis of a viscoelastic orthotropic cracked body using the extended finite element method, *Engineering Fracture Mechanics*, **109**, 17-32

Tripathi, D. (2013) Study of transient peristaltic heat flow through a finite porous channel, *Mathematical and Computer Modeling*, **57**, 1270-1283.

Vajravelu, K., Hadjinicolaou, A. (1993) Heat transfer in a viscous fluid over a stretching sheet with viscous dissipation and internal heat generation, *International Communications in Heat and Mass Transfer*, **20**, 417-430

Van der Houwen, Messina, E. (1997) Parallel linear system solvers for Runge-Kutta-Nystrom methods, *Journal of Computational Applied Mathematics*, **82**, 407-422

Veress, A., Rohacs, J. (2012) *Application of finite volume method - powerful means of Engineering Design*, Chapter 1, InTech, Janeza Trdine 9, 51000 Rijeka, Croatia, **ISBN**: 978-953-510445-2

Vilhena, M. T., Barichello, L. B., Zabadal, J. R., Segatto, C. F., Cardona, A. V., Pazos, R. P. (1999) Solutions to the multidimensional linear transport equation by the spectral method, *Progress in Nuclear Energy*, **35**, 275-291

Vinogradov, G. V., Malkin, A. Y. (1979) *Rheology of polymers*, Mir Publisher, Moscow

Voss, D. A., Muir, P. H.(1999) Mono-implicit Runge-Kutta schemes for the parallel solution of initial value ODEs, *Journal of Computational Applied Mathematics*, **102**, 235-252

Wang, H. W., Zhou, H. W., Ji, H. W., Zhang, X. C. (2014) Application of extended finite element method in damage progress simulation of fibre reinforced composites, *Materials and Design*, **55**, 191-196

Wang, P., Kong, T. (2013) Quasilinearization for the boundary value problem of second order singular differential system, *Abstract and Applied Analysis*, **2013**, Article ID 308413, 7 pages, **doi**:101155/2013/308413

Wang, Q., Zhan, H. (2015) On different numerical inverse Laplace methods for solute transport problems, *Advances in Water Resources*, **75**, 80-92

Wang, T. (2004) A mixed finite element method based on rectangular mesh for biharmonic equations. *Journal of Computational Applied Mathematics*, **172**, 117-130

Wang, W., Xu, C. (2014) Spectral methods based on new formulations of coupled Stokes and Darcy equations, *Journal of Computational Physics*, **257**, 126-142

Wen, J., He, Y. (2014) Convergence analysis of a new multi-scale finite element method for stationary Navier-Stokes problem, *Computers and Mathematics Applications*, **67**, 1-25

Wu, G. C., Baleanu, D. (2013) New applications of the variational iteration method - from differential equations to q-fractional difference equations, *Advances in Differential Equations*, **21**, 1-16

Wu, G. C., Shi, Y. G., Wu, K. T. (2011) Adomian decomposition method and non-analytical solutions of fractional differential equations, *Romanian Journal of Physics*, **56**, 873-880

Wu, W., Feng, X., Liu, D. (2013) The local discontinuous Galerkin finite element method for a class of convection-diffusion equations, *Nonlinear Analysis: Real World Applications*, **14**, 734-752

Yakar, C., Yakar, A. (2010) A refinement of quasilinearization method for Caputo's sense fractional order differential equations, *Abstract and Applied Analysis*, **2010**, Article ID 704367, 15 pages, **doi**: 10.1155/2010/704367

Yang, M. (2008) Analysis of second order finite volume element methods for pseudo-parabolic equations in three spatial dimensions, *Applied Mathematics and Computation*, **196**, 94-104

Yang, X. J., Baleanu, D., Khan, Y., Mohyud-Din, S. T. (2014) Local fractional vari-

ational iteration method for diffusion and wave equations on cantor sets, *Romanian Journal of Physics*, **59**, 36-48

Yih, K. A. (1999) MHD forced convection flow adjacent to a non-isothermal wedge, *International Communications in Heat and Mass Transfer*, **26**, 819-827

Zaimi, W. M. K. A. W., Bidin, B., Abu Bakar, N. A., Hamid, R. A. (2012) Applications of Runge-Kutta-Fehlberg method and shooting technique for solving Blasius equation, *World Applied Sciences Journal*, **17**, 10-15

Zak, A., Krawczuk, M. (2011) Certain numerical issues of wave propagation modelling in rods by the spectral finite element method, *Finite Elements in Analysis and Design*, **47**, 1036-1046

Zhang, Q., Johansen, H., Colella, P. (2012) A Fourth-Order accurate finite volume method with structured adaptive mesh refinement for solving the advection-diffusion equation, *SIAM Journal of Scientific Computation*, **34**, B179-B201

Zhao, J., Corless, R. M. (2006) Compact finite difference method for integro-differential equations. *Applied Mathematics and Computation*, **177**, 271-288

Zheng, H., Liu, F., Li, C. (2015) Primal mixed solution to unconfined seepage flow in porous media with numerical manifold method, *Applied Mathematical Modelling*, **39**, 794-808

Zhou, J. (2014) The constants in a posteriori error indicator for state-constrained optimal control problems with spectral methods, *Abstracts and Applied Analysis*, **2014**, Article ID 946026, 8 pages, **doi**: 10.1155/2014/946026

Zhou, J. K. (1986) *Differential transform and its applications for electrical circuits*, Huazhong University Press, Wuhan, China

Zou, S., Yuan, X. F., Yang, X., Yi, W., Xu, X. (2014) An integrated lattice Boltzmann and finite volume method for the simulation of viscoelastic fluids, *Journal of Non-Newtonian Fluid Mechanics*, **211**, 99-113

Zueco, J. (2007) Network simulation method applied to radiation and dissipation effects on MHD unsteady free convection over vertical porous plate, *Applied Mathematical*

Modelling, **31**, 2019-2033